Hold your horses!

Terra, H.

2020

document version
Publisher's PDF, also known as Version of record

HOLD YOUR HORSES!

CONTROLLING BEHAVIOR
WITH PREFRONTAL
TO SUBCORTICAL TARGETS
PROJECTION NEURONS

HUUB TERRA

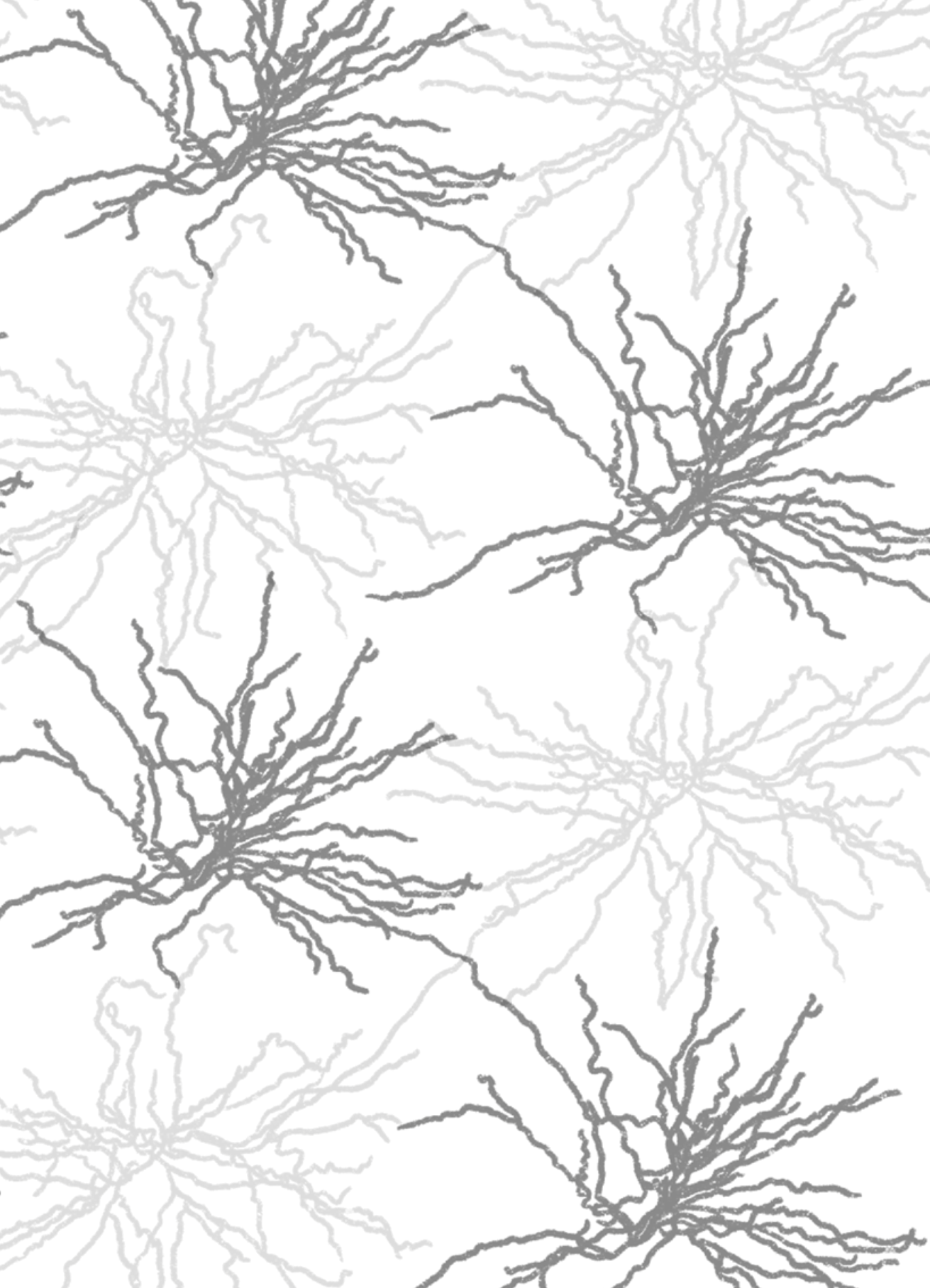

Experiments were carried out at the department of
Integrative Neurophysiology, Center for Neurogenomics
and Cognitive Research, Neuroscience Campus Amsterdam,
Vrije Universiteit, the Netherlands.

ISBN: 978-94-6421-016-3

Cover design and layout: Emma Terra | www.emmaterra.nl

The cover shows an anthropomorphic rat waiting for a traffic light while commuting to work. To do this successfully he has to exert cognitive control (i.e. inhibit behavior and pay attention) over his behavior.

VRIJE UNIVERSITEIT

Hold your horses!
Controlling behavior with prefrontal to subcortical targets projection neurons

ACADEMISCH PROEFSCHRIFT

ter verkrijging van de graad Doctor aan
de Vrije Universiteit Amsterdam,
op gezag van de rector magnificus
prof.dr. V. Subramaniam,
in het openbaar te verdedigen
ten overstaan van de promotiecommissie
van de Faculteit der Bètawetenschappen
op woensdag 18 november 2020 om 13.45 uur
in de aula van de universiteit,
De Boelelaan 1105

door
Huub Terra
geboren te Zaandam

promotor:	prof.dr. H.D. Mansvelder
copromotor:	dr. T. Pattij

Personal contribution

This thesis is a product of close collaboration between different members of the lab, but mostly with Bastiaan Bruinsma and Sybren de Kloet. While each member has greatly contributed to the final result, I will here provide a narrative for each experimental chapter with emphasis on my personal contribution.

CHAPTER 2 While starting my PhD, this line of experiments was already started by Antonio Luchicchi. Over the course of experiments I gained essential experience in optogenetics, in the 5-choice serial reaction time task, in confocal microscopy, in stereotaxic surgery and in rat handling. I contributed to this chapter with overall support in training and testing of rats, stereotaxic surgery, conceptual input and commenting on writing.

CHAPTER 3 Within this chapter I collaborated with Bastiaan and Sybren on the development of the CombiCages and training and testing of rats. I provided input to the manuscript, which was written by Bastiaan.

CHAPTER 4 In this chapter I continued the collaboration with Bastiaan and Sybren. I strongly contributed to the design of the experiments, did the stereotactic surgeries, virus injections, and led the patch-clamp experiments of thalamic and striatal neurons, which I designed, executed (together with Tim Heistek), analyzed and wrote in to a part of the manuscript. Moreover, early on I provided general support for the DREADD experiments. Finally, I provided input in to writing of the manuscript.

CHAPTER 5 Throughout my PhD I designed, built and tested a set-up for wireless single-unit electrophysiology, combined with optogenetic identification for freely moving rats, resulting in this chapter. I designed, executed and analyzed all single-unit data and behavioral data, and wrote the manuscript with input from other authors. DREADD experiments were performed and analyzed by Bastiaan.

Table of contents

CHAPTER 1

Introduction

COGNITIVE CONTROL

What do taking a sip of that tasty coffee, driving your car and listening to your favorite neuroscience professor in class have in common? These are all behaviors with a future goal in mind, from tasting the caramel flavored goodness to the excitement about learning novel things! We therefore collectively call this goal-directed behavior. This type of behavior requires cognitive effort, or cognitive control, as opposed to reflexive behavior which is purely driven by sensory input. For example, drinking hot coffee requires us to restrain our urge to drink it too early and risk burning ourselves, or driving requires a steady focus on the cars ahead of us to prevent a collision. More specifically, cognitive control allows the tuning of lower level motor, sensory and memory systems so that they can optimally perform complex sequences of actions guided by your motivational state[1]. Within this thesis I will delve into the broader question: how are specific neural circuits able to exert cognitive control over our behavior? In the process I will largely ignore reflexive and stimulus driven forms of behavior. Having said that, I must note that in reality stimulus-driven and goal-directed behavior work closely together to continuously compare the expected stimuli with the presented stimuli to flexibly update one's expectations[2,3].

INHIBITORY CONTROL AND ATTENTION

Cognitive control is an umbrella term for many psychological constructs, including working memory, executive functioning, decision-making, cognitive flexibility, attention and proactive inhibitory control (henceforth referred to as inhibitory control)[1,4]. Within this thesis I will specifically focus on two cognitive constructs: inhibitory control and attention. Whereas all constructs under the umbrella 'cognitive control' serve different functionalities, they likely have considerable functional and neuronal circuit overlap that revolves around ability to attend to information that is kept in working memory[1,5–8]. Thus, knowledge about one cognitive control construct can sometimes be informative about others. Therefore, I will sometimes discuss cognitive control in a broader sense and sometimes talk specifically about inhibitory control and attention, depending on what is known in the literature. Inhibitory control is the ability to inhibit a prepotent response (e.g. impulse) until the correct environmental circumstances are presented. In

everyday life impaired inhibitory control could for example result in aggressive behavior in response to social feedback[9], is associated with substance abuse and can severely impact the quality of life[10]. Attentional processing allows the brain to prioritize which streams of information are important to process at that moment while being in a higher state of vigilance. For example when driving your car around the Avenue des Champs-Élysées, you focus on the unpredictable traffic around you while filtering out the noise of arguing kids in the back seat. Many forms of attention have been described that focus on processing of different sensory domains[11], I will here focus on sustained visual spatial attention, which includes an increased attentional level over a sustained timescale of seconds in order to process expected visual stimuli in an unknown location in space or time[12]. Both inhibitory control and attention are affected in disorders of the brain, such as schizophrenia[13], mood disorders[14,15] and attention deficit hyperactivity disorder[16]. A thorough understanding of the underlying pathophysiology of these disorders can potentially result in the development of circuit-based therapeutic interventions.

MEASURING INHIBITORY CONTROL AND ATTENTION

Inhibitory control and visuospatial attention can both be measured in rodents using translational paradigms, in which subjects are trained to respond to spatially and/or temporally unpredictable sensory events (**Figure 1**). Within this thesis I will be using the so-called 5-choice serial reaction time task (5-CSRTT)[17]. In the 5-CSRTT, food deprived rats learn to pay attention to five apertures and inhibit a nose poke response during a seconds long delay period until a cue light is presented randomly in one of the five apertures. Making a nose poke response into the illuminated aperture is a correct response, after which the rat receives a food reward. A failure to inhibit the urge to make an 'exploratory' nose poke response before the stimulus cue onset is called a premature response and is a measure of inhibitory control. The ratio between correct and incorrect responses or number of omissions of responses are seen as an attentional measures, while response latency measures control for motivational and motor deficits. Although the 5-CSRTT has successfully been used over several decades, there are aspects that can still be improved. Traditionally, training times can exceed months before animals can be tested, which includes extensive manual work. This makes the task very

time-inefficient, precluding high-throughput testing of experimental groups and testing of the same animal on different protocols[18]. Likely as a consequence of the high manual labor, the number of trials often does not exceed 100 per session[19–21]. A higher number of trials would increase the statistical power, especially for trial types with sparser behavior, such as premature, incorrect and omissions of responses. Moreover, the typically used rapid automatic continuous cycle of trials can cause carry-over effects (e.g. consumption of a food reward), to the next trial and thereby preclude a clear readout of neural activity within the subsequent delay period[19,21]. Semi-automatic, self-paced, home-cage based systems to assess mouse behavior have increasingly been used in the last years[22,23], providing an elegant solution to the aforementioned issues. In chapter 3 we describe the development of such a rapid self-paced homecage-based 5-CSRTT for rats, adopted from the mouse CombiCage[23]. This CombiCage paradigm is used throughout chapter 3, 4 and 5, whereas the conventional 5-CSRTT is used for chapter 2.

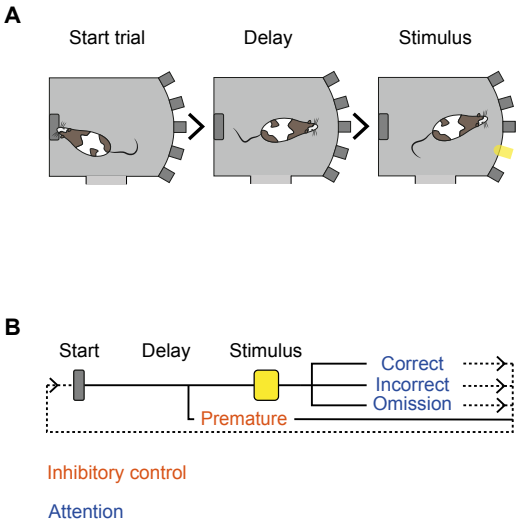

Figure 1. *General inhibitory control and attention task structure.*
(**A**) Schematic of the general task structure of an inhibitory control and attention paradigm, exemplified using the rodent 5-CSRTT. In general there are three main phases of the task: the start of the trial, a delay period and a presentation of a stimulus to which an animal has to respond. (**B**) After starting a trial an animal has to wait during a delay period for the presentation of an expected sensory stimulus. This stimulus-free delay period is regarded as the period where both inhibitory control and attention are engaged in order to prepare for a response to an upcoming stimulus. A correct response to the stimulus is rewarded with a rewarding substance. A premature response is seen as a failure of inhibitory control. The ability to detect the presentation of the stimulus, measured in amount and balance between correct, incorrect and omissions of responses, can be used as readout of attention.

THE PREFRONTAL CORTEX – A KEY BRAIN REGION FOR COGNITIVE CONTROL

The prefrontal cortex (PFC), a higher order brain area all the way in the front of the neocortex, holds a key role in cognitive control (**Figure 2**)[1,24–26]. The PFC learns to predict what the best course of action is to achieve your goal - i.e. "the rules of the game" or action-outcome contingencies - based on the current context, including sensory input and your internal drive[1,2]. The ensembles of neurons that represent "the rules of the game" in the PFC, in turn instruct downstream brain areas on how to process information and execute behavior, including inhibitory control and how much attention is required for processing of the upcoming event[2]. I will specifically focus on the medial section of the rodent PFC (mPFC), as this is the region of the PFC often linked to inhibitory control and attention, and because we use a rat animal model within this thesis. I will briefly discuss the human and non-human primate dorsolateral PFC (dlPFC) and medial mPFC homologue, as the cross-species homology is a matter of debate and outside the scope of this thesis[27–29]. Nonetheless, human and non-human primate research has greatly contributed, and still contributes, to our understanding of the role of the PFC in cognitive control and will thus be discussed in light of rodent research. A wealth of lesion, pharmacological, optogenetic, chemogenetic, imaging and electrophysiological studies have given much insight on how the mPFC regulates inhibitory control and attention. These will be extensively discussed in this introduction. First, I will introduce the functional organization of the mPFC in support of inhibitory control and attention.

Figure 2. *The prefrontal cortex.* Structural MRI images of the human (top) and rat (bottom) brain. The rodent (bottom) medial prefrontal cortex and human homologue (top), the dorsolateral prefrontal cortex and medial prefrontal cortex, are indicated with a red circle, sagittal view. Human MRI courtesy of the Oxford Centre for Functional MRI of the Brain, rat MRI adapted from Rumple et al. (2013).

COGNITIVE CONTROL ALONG THE DORSOVENTRAL AXIS OF THE MEDIAL PREFRONTAL CORTEX

The role of the mPFC in inhibitory control and attention is supported by a range of studies performing lesion or pharmacological interventions in rats performing the 5-CSRTT, 3-CSRTT or simpler cue detection tasks. Nearly all reported interventions resulted in decreased accuracy of responding, increased omissions and increased impulse responses[30–36]. Together this provides compelling evidence for the role of the mPFC as a whole in inhibitory control and attention.

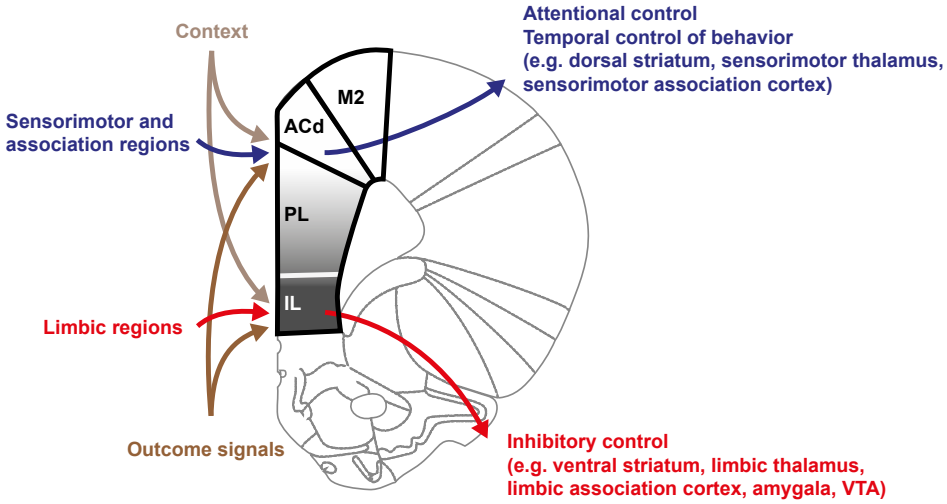

Figure 3. *Integrative properties of the mPFC in support of cognitive control*
Schematic of the integrative function of the rodent mPFC. Coronal view of a unilateral sections of the rodent mPFC. Premotor cortex (M2), Dorsal Anterior cingulate (ACd), prelimbic (PL), infralimbic (IL), color gradient indicates dorsoventral axis of the mPFC. Figure adapted from Euston et al. (2012).

The mPFC can be divided along a functional and anatomical dorsoventral axis[37] (**Figure 3**). The dorsal mPFC contains the dorsal prelimbic (PL), dorsal anterior cingulate cortex (ACd), and the secondary motor cortex (M2), although different definitions have been used throughout literature[29]. The ventral mPFC arguably contains the ventral prelimbic and infralimbic cortex. The dorsal and ventral mPFC are interconnected with different brain regions. The dorsal mPFC receives input from and projects to more sensorimotor association-related brain regions, and

the ventral mPFC receives input from and projects to more limbic brain regions[2]. This dorsoventral gradient in connectivity is also reflected in the proposed functionality of these brain regions. Lesion, pharmacological, optogenetic and chemogenetic studies indicate that the dorsal mPFC is more involved in attention and temporal control over behavior[7]. Lesioning or perturbation of neural activity in the dorsal mPFC results in a decrease in accuracy or increase of omissions in the 5-CSRTT[20,31,32,38–40]. It is important to note that the role of the dorsal mPFC is not exclusive to attention, as inhibitory control deficits in the form of premature responses have also been reported after dorsal mPFC lesions in the 5-CSRTT[31], 3-CSRTT[40] and other stimulus detection tasks[41]. Targeted lesion and neuronal activity manipulations to the ventral mPFC indicate that this region is involved in inhibitory control, resulting in increased premature responses in the 5-CSRTT[38,42]. However, similar to the dorsal mPFC, the role of the ventral mPFC is also not exclusive to inhibitory control, as a role for attention has also been observed[42]. Taken together, the mPFC can roughly be divided along a functional dorsoventral axis, however, the division is not clear as functions overlap. This might depend on the used paradigm[43,44].

NEURAL CODES OF COGNITIVE CONTROL

Cognitive control, including inhibitory control and attention, requires neuronal activity within the PFC to bridge a stimulus-free delay period. In-vivo electrophysiological and calcium imaging studies have provided insight in to how neurons within the mPFC are able to exert cognitive control. A long-standing hypothesis is that neurons do this by persistent changes in firing rate during the delay period (**Figure 4A**)[45,46]. Importantly, this persistent change in activity has also been associated with inhibitory control and attention[19–21,41]. Alternatively and not mutually exclusive, populations of PFC neurons, displaying sequential bouts of activity throughout the delay period, have been proposed to encode cognitive control, including working memory, attention and temporal organization of behavior (**Figure 4B**)[47–51].

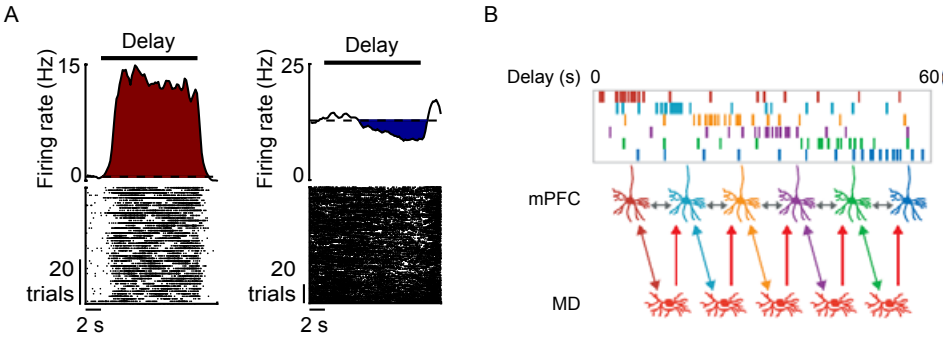

Figure 4. *Suggested encoding mechanisms for cognitive control.*
(**A**) Persistent changes in firing rate. Activity of two example putative pyramidal mPFC neurons that are persistently activated (red) or silenced (blue) during a stimulus free delay period. Top, peri-event time histogram, bottom, raster plot. (**B**) Sequential firing rate. Sequential activity of synaptically connected mPFC pyramidal neurons, sustained through reciprocal connectivity with relay neurons in the mediodorsal thalamus (MD). Figure adapted from Parnaudeau et al., 2017.

In the next section, I will discuss how persistent changes in firing rate and sequential firing rate of mPFC neurons are linked to cognitive control. I will focus on persistent changes as they have most extensively been linked to inhibitory control and attention. Although it is known that PFC neurons use both rate coding and temporal coding mechanisms[52], I will focus on rate coding. This means that within my thesis I assume that information in neural activity is represented in firing frequency, while leaving open the possibility that information is also encoded when neurons are active.

DELAY PERIOD ACTIVITY – BRIDGING THE STIMULUS FREE GAP

Persistent changes in firing rate

Persistent changes in firing activity of PFC neurons have been extensively linked to inhibitory control and attention[19–21,41,53–55]. Persistent changes in neuronal activity have been proposed to represent goals and how to achieve them, biasing information processing in downstream brain areas in support of this goal[1]. Importantly, mPFC neurons showing persistent changes in activity are also present during the delay period in the 5-CSRTT[19–21], and other cue detection tasks[41,43,53], in which inhibitory control and attention are required. Neurons showing persistent changes are roughly equally divided in activation and silencing of activity[19,21]. This balanced activation and silencing of mPFC neurons could reflect activation of ensembles that represent beneficial rules while inhibiting unwanted rules[5]. The amplitude of persistent changes in firing rate has been linked to trial outcome, in which both failed inhibitory control and attention correlate to a lower amplitude of change in persistent activity in the mPFC[19,20,41]. This suggests that persistent changes in activity are required to sustain task-relevant information, such that lower changes in activity can disrupt information transfer strength to downstream brain areas and result in impaired inhibitory control and attention.

In support of a functional dorsal-ventral gradient in mPFC neuronal recruitment during cognitive control, different neuronal activity dynamics have also been observed. Dorsal mPFC neurons show a more consistent delay-period pattern[41,43] of activity with roughly an equal number of persistently activated and persistently silenced neurons[19,20] whereas ventral mPFC neurons show a mixed activity pattern[41] and a higher fraction of persistently silenced neurons[43]. Moreover, in premature response trials, subgroups of neurons in the dorsal mPFC show a reduced firing activity and in the ventral mPFC neurons showed increased activityy[41].

Sequential firing rate

Sequential periods of activity are also observed within the mPFC neuronal population during cognitive control, when each neuron is activated sequentially during a specific epoch, together spanning the entire delay period[45]. This is (not exclusively) explained by the synaptic chain model (or synfire chain model), that

describes ensembles of synaptically-connected pyramidal neurons that represent a task-rule (i.e. 'attend to visual cue'), where sequential activity can be achieved through reciprocal connectivity to the thalamus[45,56,57]. A lower peak firing rate and reduced synaptic connectivity strength have both been associated with a failure to retain task-information online in a divided attention task or working memory task, in which animals were required to maintain a task rule in working memory over a short delay[56,57]. While sequential activity of PFC neurons is suggested to encode working memory, attention[49,51] and temporal organization of behavior[50], persistent changes in firing rate have more often been linked to motor control[45,58,59]. Nonetheless, it remains unclear to what extent the synaptic chain model accounts for inhibitory control and attention behavior within the 5-CSRTT, especially after short training times and under unpredictable task conditions which might rely on motor preparation and working memory[8]. Moreover, whether and how this encoding mechanism is present throughout the dorsoventral axis of the mPFC remains to be explored.

Taken together, there are different proposed encoding mechanisms for inhibitory control and attention that allow the online maintenance of rule information during a stimulus free delay period. Moreover, there are indications that cognitive control is differentially encoded along the dorsoventral axis of the mPFC. Response preparation during the delay period consists of a non-uniform balance between withholding and executing a response, with the right amount of attention to detect an upcoming cue, likely with the earlier delay period relying more on proactive control and the period around the cue detection relying on reactive control[41]. When exactly dorsal and ventral mPFC neurons are required during seconds of response preparation and the subsequent execution of a response remains poorly understood. In chapter 2 we address this question using the conventional 5-CSRTT and optogenetic inhibition of pyramidal neurons, during defined epochs around the delay period in either the dorsal or ventral mPFC.

SUBCORTICAL PROJECTIONS IN COGNITIVE CONTROL

The high level of interconnectivity between the PFC and other cortical and subcortical brain areas places the PFC in an ideal position to bias neuronal processing throughout the brain in favor of the current behavioral goal[1]. Two brain areas that receive dense topographical innervation from PFC neurons are the mediodorsal nucleus of the thalamus (MD) and striatum[60,61]. The MD and striatum have both been implicated in cognitive control, including inhibitory control and attention[5,10,62,63]. Based on their classical roles in sensory and behavioral processing, the thalamus may be more involved in bottom-up attention, whereas the striatum is more tuned to top-down regulation of behavioral output. Recent work has demonstrated that projection-specific neurons within the mPFC serve differential roles in cognitive control[64–68]. However, the role of topographically organized MD and striatum-projecting PFC neurons in inhibitory control and attention is poorly understood. Within this thesis, I will focus on the role of dorsal and ventral mPFC projection neurons to corresponding dorsomedial (DMS) and ventromedial (VMS) striatal and lateral (MDL) and medial (MDM) MD subregions in inhibitory control and attention (**Figure 5**). In the next sections, I will discuss the role of subregions of the MD, striatum and corresponding topographical mPFC input in cognitive control, including inhibitory control and attention.

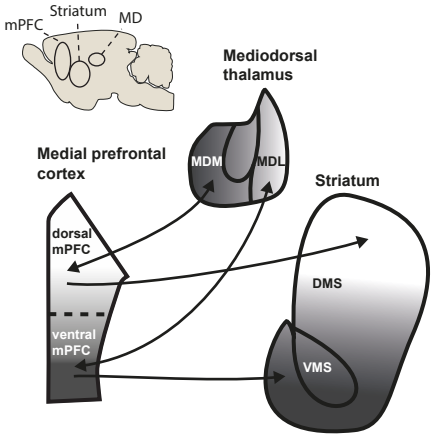

Figure 5. *Macroscale anatomical connectivity between the medial prefrontal cortex (mPFC) to the medial dorsal thalamus (MD) and striatum.*
Simplified schematic of the topographical macroscale connections between the dorsal and ventral mPFC and the lateral MD (MDL), medial MD (MDM), dorsomedial striatum (DMS) and ventromedial striatum (VMS). Arrows indicate direction of afferent and efferent connections. Color gradient indicates respective connectivity with the mPFC.

THE PREFRONTAL – MEDIODORSAL THALAMUS LOOP

The MD is a higher order thalamic nucleus, meaning that it mostly receives its glutamatergic input from association cortices, in this case the PFC[69]. In turn, many MD neurons, consisting mostly of glutamatergic thalamic relay neurons in rodents (but also local inhibitory interneurons in primates[69]), project directly back to the PFC, forming reciprocal cortico-thalamo-cortico loops[56,57,70–72]. It is therefore not surprising that the function of the MD is closely linked to that of the PFC[73]. Below I will discuss evidence for the involvement of the PFC-MD loop in several cognitive control functions. Additionally, I will argue that more research is needed in to the role of subregion-specific connectivity of the mPFC to the MD in cognitive control.

Functional connectivity between the PFC and MD

Similar to the PFC, MD lesions, disease-induced MD impairments, chemogenetic or optogenetic manipulations of the MD are associated with broad deficits in cognitive control, including cognitive flexibility[57,74–78], working memory[79,80], inhibitory control as measured in the 5-CSRTT[77] and attention[56]. Likewise, in disorders affecting cognitive control, such as alcohol use disorder, Korsakoff's syndrome and schizophrenia, the MD has shrunk or PFC-MD connectivity is impaired[62,81]. Taken together, the similarity in PFC and MD functionality and dense connectivity suggests a crucial role for PFC-MD interactions in cognitive control.

The role of PFC-MD interactions in cognitive control is further supported by projection-specific experiments that directly demonstrated the complementary, but partly dissociable, roles of PFC-MD and MD-PFC projections. Using projection-specific optogenetic inhibition in a delayed nonmatching-to-sample (DNMS) working memory task, in which rats learned to sample one side of a T-maze, remember the sampled location, and in the next trial to go to the nonmatching side to receive a reward, Bolkan et al. (2017) showed that both the mPFC-MD and MD-PFC pathway are required for task-performance. However, temporally precise optogenetic interference in discrete phases of the task showed that specifically mPFC-MD projection neurons are required for the choice execution phase of the task, whereas the complete mPFC-MD reciprocal loop is required for maintenance of the working memory trace (or task-relevant information) throughout

the delay period[57]. Moreover, using projection-specific chemogenetic inhibition in a goal-directed outcome devaluation task, Alcaraz et al. (2018) showed that the complete mPFC-MD loop is required for updating reward-value, whereas only the MD-mPFC pathway is required for updating action-outcome associations. Together these recent findings are starting to indicate a role for the prefrontal-MD loop in cognitive control, with direction-dependent dissociable functions. However, whether the prefrontal-to-MD projection neurons are required for inhibitory control and attention remains unknown.

Sustaining mPFC task-relevant information by innervation from the MD

An important hypothesis about how mPFC-MD connectivity supports cognitive control is through retaining task-relevant information in the mPFC. How the PFC-MD loop is able to sustain task-relevant information was demonstrated by Schmitt et al. (2017). Using combined optogenetic perturbations and in-vivo single-unit recordings in the mPFC and MD, they showed that PFC-MD reciprocity is required for maintaining delay activity within the mPFC and task performance in a divided attention task in which mice had to maintain task-rule information online during a short delay period. Importantly, MD activity was required for increasing the synaptic strength between mPFC neuronal ensembles that represent task-rule information with sequential activation during a delay period[56]. While this experiment was not projection-specific, thereby allowing multi-synaptic pathways as a confounding factor, it strongly suggests an active role for PFC-innervated MD neurons in sustaining task-relevant information in the PFC. Taken together, PFC-MD connectivity is required for sustaining delay period activity of PFC neurons in order to maintain task-relevant information online and updating reward value.

The mediolateral axis of the MD

Similar to the dorsoventral axis of the mPFC, the MD can also be divided along a mediolateral axis that receives topographically organized mPFC input. The MDL is interconnected with the dorsal mPFC and sensorimotor related brain regions, whereas the MDM is interconnected with the ventral mPFC and other limbic brain areas[37,61,70,72,90]. This differential pattern of innervation of the MDL

and MDM strongly suggests a differential function of these regions. Studies investigating mPFC-MD interactions have generally focused on the dorsal mPFC connections with the MDL, or alternatively did not focus on subregion[56,57,76]. Moreover, morphological and connectivity differences over the mediolateral axis of the MD indicate that these MD relay neurons can differentially process information streams. Moreover, the limited studies on the nature of interaction between the mPFC and MD have mostly been done in paradigms which test the ability to retain information in working memory or action-outcome contingencies in goal-directed behavior[56,57,76]. It therefore remains unknown how topographically organized connectivity between the mPFC and MD contribute to inhibitory control and attention.

Synaptic connectivity between the mPFC and MD

The synaptic connectivity characteristics of the mPFC-MD reciprocal loop play an important role in the regulation of cognitive control (**Figure 6**). MD relay neurons receive glutamatergic input from L5 and L6 pyramidal neurons. Sparse L5 PFC pyramidal neurons give strong synaptic depressing 'driver' input with high release probability. The more abundant L6 PFC pyramidal neurons are considered modulatory and give weaker synaptic facilitating input with lower initial release probability, but together these neurons are still able to exert strong driver-like input and are suggested to play an important to in maintaining delay period activity of mPFC neurons[70,82]. In turn, cortically innervated MD relay neurons strongly innervate PFC L2/3 cortico-cortical pyramidal neurons, but also fast-spiking basket cells expressing parvalbumin (PV), reciprocal corticothalamic L5 and L6 pyramidal neurons and cortico-cortical L5 pyramidal neurons, using glutamatergic depressing synapses[70,80,83,84]. Together these characteristics are determinants in how the mPFC-MD loop is able to exert cognitive control.

Electrophysiological properties of MD relay neurons

Thalamic relay neurons, including MD neurons, show some distinct electrophysiological properties that contribute to integration of synaptic input. They can shift between an hyperpolarized burst firing mode and a depolarized tonic firing mode[69] (**Figure 7**). The burst firing mode has been suggested to support high information

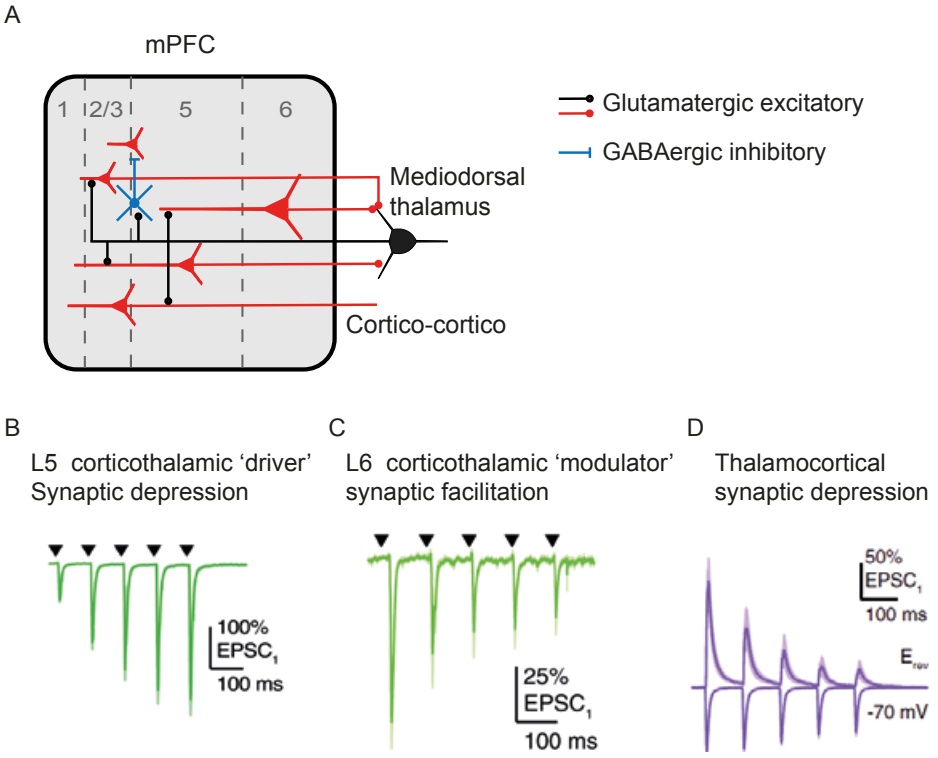

Figure 6. *Synaptic connectivity properties between the mPFC and MD.*
(**A**) Schematic of the synaptic connectivity properties between the mPFC pyramidal neurons (red), fast-spiking interneurons (blue) and MD relay neurons (black). Estimated proportion of projection neurons per cortical layer indicated in relative soma size. Relative synaptic input strength not depicted. (**B and C**) Example optogenetics-evoked excitatory postsynaptic current (EPSC) recorded in a reciprocally connected MD relay neuron, evoked by optogenetic stimulation (triangles, 10 Hz LED stimulation train) of axons of a L5 (**B**) or L6 (**C**) mPFC neuron. Recorded at -60 mV in voltage clamp. (**D**) Example of optogenetics-evoked excitatory and inhibitory postsynaptic current recorded in a cortico-cortico L2/3 pyramidal neuron, evoked by optogenetic stimulation (triangles, 10 Hz LED stimulation train) of axons of a MD relay neuron. Recorded at -70 mV and excitatory reversal potential (E_{rev}) in voltage clamp. Recording normalized to first peak amplitude of the first pulse. (B-D) Adapted from Collins et al. (2018).

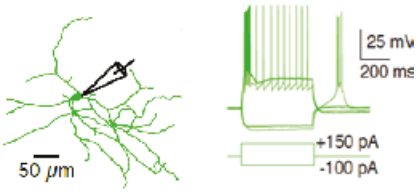

Figure 7. *Electrophysiological properties of MD relay neurons.*
Example current clamp response (right) of a MD relay neuron (left) in response to positive and negative current steps, recorded at depolarized -50 mV (light trace, tonic firing mode, right) and hyperpolarized resting membrane potential (dark trace, burst firing mode, right). Figure adapted from Collins et al. (2018).

transfer, with the ability to track low frequency synaptic input, acting as a 'wake-up call' to the cortex and the tonic firing mode supports low information transfer but with the ability to track high frequency inputs[88,89]. Which state a relay neuron is in and how information is processed depends on the interplay between its active and inactive currents, including an important hyperpolarization activated Ih-current or 'sag' current[88]. Whether relay neurons across the mediolateral axis of the MD show similar electrophysiological properties remains, however, unknown[63].

Morphological features of MD relay neurons

Relay neurons within the MD are a relatively homogeneous population of neurons, however some different types have been reported that could contribute to differential functionality and information processing. Detailed anatomical work has shown that rat MD relay neurons consist of two major types: stellate-shaped and fusiform-shaped neurons as well as a third smaller group of spindle-shaped neurons that are thought to represent an intermediate form[85]. These neurons do not show differences along the anterior-posterior axis but mediolateral differences have been reported. Roughly speaking stellate-shaped cells are found equally in the medial and lateral MD, but predominantly in the central MD[85]. Fusiform cells are reported throughout the medial and lateral MD, with a preferential distribution in the lateral MD. The distinction in cell types is, however, not clear cut as they form a continuous distribution[85]. Further complicating cell typing of thalamic relay neurons is the different nomenclature throughout literature. For example, X and Y type relay neurons are often reported that correspond to bushy and radiate type relay neurons[69]. Regional and species differences further complicate cell typing[63,69,86]. Therefore, a general classification framework is required in order to overcome the regional, species and nomenclature discrepancies[87]. Thus, there are indications that subtypes of relay neurons are differentially spread across the mediolateral axis of the MD, however further investigation is needed.

Combined, these studies indicate a clear role for dorsal mPFC-MDL interactions in support of retaining task-relevant information in the PFC and executing PFC-dependent behavior. However, the role of subregion-specific PFC-MD communication in inhibitory control and attention remains unknown. In chapter

4 we investigate the contribution MDL and MDM-projecting dorsal and ventral mPFC neurons, in inhibitory control and attention. We do this at the behavioral and pre- and post-synaptic neuronal level using the CombiCage 5-CSRTT, chemogenetics, fiber photometry and patch-clamp electrophysiology.

THE PREFRONTAL – STRIATAL PATHWAY

The striatum is the main input region of the basal ganglia, and is important for motor learning and motor execution. It integrates various types of information streams including sensorimotor control, attentional function, motivation, value and emotion, ultimately leading to proper control of behavior[91]. The striatum is densely innervated by the mPFC, supporting cognitive control of striatal output[60,92]. Comparable to the dorsoventral axis of the mPFC, the striatum can also be divided along a functional and anatomical dorsoventral axis. The dorsal striatal region predominantly receives sensorimotor information, including input from the dorsal mPFC, whereas the ventral striatal area receives limbic, emotion and motivational information, including input from the ventral mPFC[60,93]. Specifically, the dorsomedial (DMS) and ventromedial (VMS) region of the striatum have been implicated in cognitive aspects of motor control, including attention and inhibitory control.

Functional connectivity between the mPFC and striatum

Lesions of the DMS and VMS in rats performing the 5-CSRTT indicate separate roles in inhibitory control and attention. DMS lesions resulted in prominent attentional deficits, indicated by a decrease in accuracy of responding, but also deficits in inhibitory control, indicated by an increase in premature responding[94]. VMS lesions resulted in an increase of premature responses, while no effects on accuracy were observed[95]. The regulatory role of the mPFC on the striatum in support of inhibitory control and attention is indicated through disconnection studies. Disconnecting the mPFC from the DMS resulted in deficits in accuracy and inhibitory control[96], whereas disconnecting the mPFC and VMS resulted in inhibitory control deficits[95].

Neuronal activity recordings in both the mPFC and striatum further support the functional frontostriatal connectivity in inhibitory control and attention. Single-unit recordings within the dorsal mPFC and DMS show that both areas display similar activity patterns, with sustained activation or silencing of neuronal activity measured during a task in which rats had to hold down a lever and withhold from prematurely releasing until an estimated time interval had elapsed[53]. Similar delay-period persistent activation and silencing were found in mPFC and VMS neurons in rats performing the 5-CSRTT[21]. This suggests that striatal-projecting mPFC neurons regulate inhibitory control and attention through persistent activation and silencing of firing rates.

Signal integration in the striatum

An important component of the dorsal and ventral frontostriatal pathways are GABAergic medium spiny neurons (MSNs) of the striatum, which receive dense innervation from the mPFC[60] (**Figure 8**). MSNs are the main output neurons of the striatum, comprise about 90% of striatal neurons and are supported by cholinergic and GABAergic interneurons[97]. Single MSNs receive synapses from many brain areas and are relatively hyperpolarized, requiring a barrage of synaptic input in order to fire an action potential[91]. These properties are in line with the strong integrative function of MSNs. MSNs can roughly be divided in to type 1 (D1) and type 2 (D2) dopamine receptor containing subtypes, of the direct and indirect pathways, respectively[91]. D1 MSNs provide inhibitory input to the globus pallidus interna and substantia nigra and D2 MSNs provide inhibitory input on to the globus pallidus externa. D1 MSNs are part of the direct pathway and promote action execution and D2 MSNs are part of the indirect pathway and inhibit action execution[98–101]. The combined activity of D1 and D2 neuronal ensembles that represent different actions are thought to control behavior[91]. A strong driver of MSN activity is the mPFC, which is thought to provide contextual input (i.e. when to inhibit or execute an action or how much attention is required) for action execution[5,91]. Both D1 and D2 MSNs receive equal amounts of mPFC input[102,103]. It has been suggested that the activity balance between D1 and D2 MSNs can be resolved by mPFC input[104]. Where MSNs are classically seen as homogenous across the striatum, recent findings suggest that there are differences between the dorsal and ventral regions, which could indicate the presence of differential integration

mechanisms. Kupchik et al. (2015) showed that the dorsal and ventral striatum MSNs differ in their projection pathway, with the ventral striatum D1 and D2 MSN showing more convergent input on to downstream brain areas than the dorsal striatum. Moreover, the nature of synaptic input on to MSNs is also variable along the dorsoventral axis showing both paired-pulse depression as well as facilitation, with paired-pulse depression and facilitation for dorsal mPFC or cortical input to medial dorsal striatal MSNs[92,105,106] and paired pulse depression for ventral mPFC to ventral striatum[107]. Additionally it has been suggested that differences in basic electrophysiological properties between the dorsal and ventral striatal MSNs exist, which could contribute to differential integration of information, but a direct comparison is missing[108].

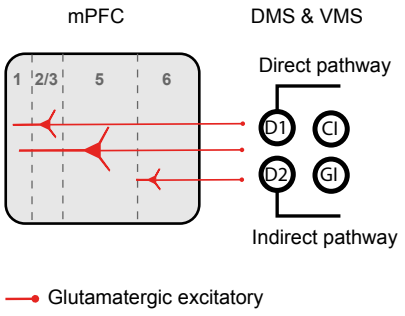

Figure 8. *Synaptic connectivity properties between the mPFC and the striatum.*
Schematic of the synaptic connectivity properties between the mPFC projection neurons (red) and striatal MSNs (D1 MSN and D2 MSN), cholinergic interneuron (CI) and GABAergic interneuron (GI). Estimated proportion of mPFC-striatum projection neurons per cortical layer indicated in relative soma size. Relative synaptic input strength not depicted. Most mPFC-striatal synapses are glutamatergic, although GABAergic input has also been reported.

Taken together, the VMS and DMS have been implicated in inhibitory control and attention. Topographical input along the dorsoventral axis of the mPFC on to striatal MSNs of the DMS and VMs, respectively, has been suggested to exert cognitive control over behavior, including inhibitory control and attention[5,10] with persistent activation and silencing in activity as possible encoding mechanism[19–21,53]. Moreover, MSNs across the dorsoventral axis of the striatum show differences in connectivity and electrophysiological properties, but a direct comparison is missing. In chapter 4 and 5 we investigated the role of the dorsal and ventral frontostriatal pathways in inhibitory control and attention at the behavioral, presynaptic and postsynaptic neuronal level using the CombiCage 5-CSRTT, fiber photometry, patch-clamp electrophysiology and wireless singe-unit electrophysiology combined with optogenetic identification.

OUTLINE OF THESIS

Neurons in the mPFC are crucially involved in a wide variety of cognitive control functions, including inhibitory control and attention. Projection-specific pyramidal neurons within the mPFC have differential functions in cognitive control. Two major projection areas of the mPFC that receive topographically organized input are the MD and striatum. Whether and how these MD and striatal-projecting mPFC neurons regulate inhibitory control and attention is poorly understood. We therefore set out to investigate the role of pyramidal projection neurons along the dorsoventral axis of the mPFC in inhibitory control and attention in rats, with a specific focus on projection neurons to the MD and striatum. Here, I will briefly introduce each chapter of my thesis.

CHAPTER 2 *When are pyramidal neurons along the dorsoventral axis of the mPFC required for inhibitory control and attention?*

We start by investigating how pyramidal neurons along the dorsoventral axis of the mPFC are temporally and functionally involved in inhibitory control and attention. We do this by using optogenetic inhibition of pyramidal neurons during different epochs around the delay and cue presentation period, during which inhibitory control and attention are most needed, in rats trained to perform the conventional 5-CSRTT.

CHAPTER 3 *Can we improve on the conventional 5-CSRTT task design?*

Next, we set out to improve several limitations of the conventional 5-CSRTT. This resulted in the establishment of a CombiCage approach for rats, based on the CombiCage for mice: a rapid, self-paced, homecage-based version of the 5-CSRTT. Most importantly, we were able to greatly reduce training time, reduce experimenter time investment and increase the number of trials per session. The CombiCage was subsequently used for the experiments in chapter 4 and chapter 5.

CHAPTER 4 *What is the role of topographically-projecting MD and striatum neurons, along the dorsoventral axis of the mPFC, in inhibitory control and attention?*

We continue with investigating the role of four different groups of projection neurons to subcortical brain areas receiving dense innervation along the dorsoventral axis of the mPFC in inhibitory control and attention. Specifically I will focus on topograph-

ical mPFC projections to the lateral and medial MD and dorsomedial and ventromedial striatum. We use projection-specific DREADD-mediated inhibition in the CombiCage to investigate their requirement in attention and inhibitory control. Next, I show how these projections are task-involved with population calcium imaging using fiber photometry. Finally, we investigate if these four pathways are part of different functional networks by recording the synaptic input to and the passive and active electrophysiological properties of the post-synaptic MD and striatal neurons using patch-clamp electrophysiology in brain slice preparations.

CHAPTER 5 *How do individual dorsomedial striatum-projecting mPFC neurons encode inhibitory control and attention?*
Finally, I focus on if and how individual dorsal mPFC neurons, projecting to the dorsomedial striatum, encode inhibitory control and attention. We do this using DREADD-mediated inhibition and wireless single-unit electrophysiology combined with optogenetic identification in the CombiCage.

Throughout my thesis I use different techniques to record and manipulate from specific groups of neurons, both in living animals and ex-vivo in slice preparations. In **figure 9** I have provided an infographic about the most prominent techniques. Furthermore, the definitions of a few key concepts used throughout this thesis are explained in **box 1**.

Box 1.
Important concepts as used throughout this thesis

COGNITIVE CONTROL
An umbrella term for many cognitive constructs that are involved in the preparation, execution and updating of goal-directed behavior. This includes inhibitory control and attention.

THE PREFRONTAL CORTEX (PFC)
A brain area highly involved in cognitive control. Specifically, the rodent medial PFC and the primate homologue, dorsolateral and medial PFC.

INHIBITORY CONTROL
The ability to proactively suppress a behavioral response.

ATTENTION
The ability to detect spatially or temporally unpredictable visual cues. This is dependent on the vigilance state of the animal as well as the ability to filter out important spatial and temporal information.

PERSISTENT ACTIVITY
Sustained, ramping like, change in neuronal activity during a stimulus free delay period before the presentation of an expected stimulus. The neuron can be either activated or silenced.

COMBICAGE
The combination of a home-cage and operant chamber. This allows rapid, semi-automatic, self-paced, training and testing of rodents in the 5-CSRTT.

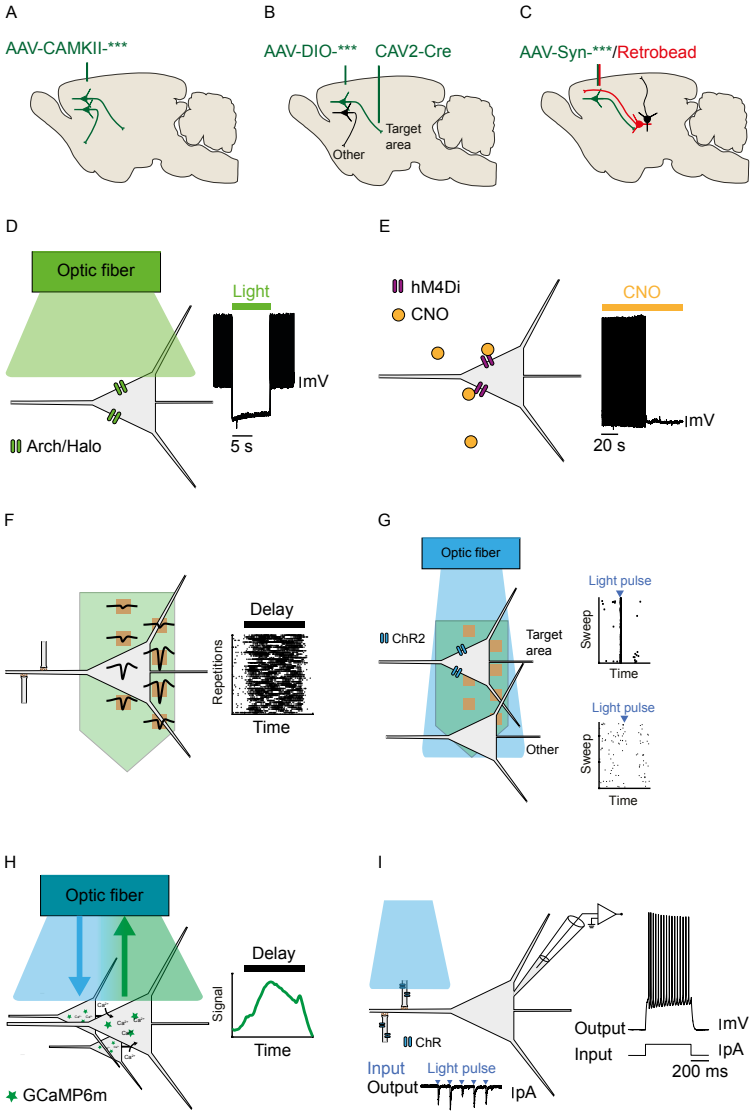

Figure 9. *Schematic of neuronal recording and manipulation techniques.*
(**A–C**). Targeting of pyramidal neurons (**A**), projection-specific neurons (**B**) or reciprocal neuronal loops (**C**) using viral and retrobead techniques. (**D** and **E**) Manipulation of neuronal activity using optogenetic inhibition (**D**) or DREADD-mediated silencing (**E**). (**F–I**) Recording of neuronal activity using: in-vivo single-unit electrophysiology (**F**) combined with optogenetic identification (**G**), fiber photometry (**H**) or patch-clamp electrophysiology in ex-vivo brain slices (**I**) with optogenetic pre-synaptic axonal stimulation (left) or input-output characteristics (right).

Antonio Luchicchi
Ouissame Mnie-Filali[1], **Huub Terra**[1], Bastiaan Bruinsma[1], Sybren F. de Kloet[1]
Joshua Obermayer
Tim S. Heistek
Roel de Haan
Christiaan P. J. de Kock
Karl Deisseroth
Tommy Pattij[#] and Huibert D. Mansvelder[#]

[1]shared second authorship

[#]shared senior authorship

PUBLISHED AS

Luchicchi, A., Mnie-Filali, O.*, **Terra, H.***, Bruinsma, B.*, de Kloet, S.F.*, Obermayer, J., Heistek, T.S., de Haan, R., de Kock, C.P.J., Deisseroth, K., et al. (2016). Sustained attentional states require distinct temporal involvement of the dorsal and ventral medial prefrontal cortex. Front. Neural Circuits 10, 70.

CHAPTER 2

Sustained attentional states require distinct temporal involvement of the dorsal and ventral medial prefrontal cortex

ABSTRACT

Attending the sensory environment for cue detection is a cognitive operation that occurs on a time scale of seconds. The dorsal and ventral medial prefrontal cortex (mPFC) contribute to separate aspects of attentional processing. Pyramidal neurons in different parts of the mPFC are active during cognitive behavior, yet whether this activity is causally underlying attentional processing is not known. We aimed to determine the precise temporal requirements for activation of the mPFC subregions during the seconds prior to cue detection. To test this, we used optogenetic silencing of dorsal or ventral mPFC pyramidal neurons at defined time windows during a sustained attentional state. We find that the requirement of ventral mPFC pyramidal neuron activity is strictly time-locked to stimulus detection. Inhibiting the ventral mPFC 2 s before or during cue presentation reduces response accuracy and hampers behavioral inhibition. The requirement for dorsal mPFC activity on the other hand is temporally more loosely related to a preparatory attentional state, and short lapses in pyramidal neuron activity in dorsal mPFC do not affect performance. This only occurs when the dorsal mPFC is inhibited during the entire preparatory period. Together, our results reveal that a dissociable temporal recruitment of ventral and dorsal mPFC is required during attentional processing.

INTRODUCTION

The medial prefrontal cortex (mPFC) plays a crucial role in several cognitive functions, among which attentional processes[7]. Pharmacological and lesion studies in rodents performing in different visual attention probing paradigms, including the 5-choice serial reaction time task (5-CSRTT)[30,31,109–112], have shown that deactivation of the mPFC impairs rodent performance[31]. Furthermore, more detailed investigations have pointed toward a functional diversity in the management of various visuospatial attention-related functions by different mPFC areas[7,32]. Along the dorsomedial-ventromedial axis of the PFC, the most dorsal subregions (including anterior cingulated cortex, ACg) might more prominently participate in sustained attentional states, controlling accuracy of responding to light cues as well as omission rates[7,32], whereas the ventral stations (prelimbic and infralimbic cortices) might be more involved in executive functions such as inhibition of inappropriate responses and behavioral flexibility[32,38,113].

Pharmacological interventions and lesions of brain regions interfere with brain function on a time scale of hours to weeks, thereby exceeding the time scale of attentional processing. When an organism pays attention to its sensory environment for accurate detection of sensory cues in demanding tasks, attention-related neuronal activity typically occurs on a time scale of seconds[19–21,114]. During these seconds of changed neuronal activity, both the ACg and the ventral regions of the mPFC process information to prepare the organism to respond to a stimulus[19]. It was shown recently that activity of fast-spiking parvalbumin-containing interneurons in the mPFC is required for attentional processing, since optogenetic inhibition of these neurons on a seconds time-scale increases errors in performance. In addition, it has been reported that mPFC GABA interneurons might be crucially involved in the modulation of executive functions[115]. Despite this, it is unknown how activity of pyramidal neurons in specific subcompartments of the mPFC is causally related to attentional processing in the seconds that precede the cue presentation as well as in the actual period of instrumental action, when rodents have to produce an adaptive response to the stimulus.

Pyramidal neurons represent 80–90% of cells in the mPFC[116] and their laminar organization renders their role in complex cognitive functions difficult to disentangle. For example, it has been shown that while superficial layer pyramidal neurons send their projections mainly intracortically, deep layer cells (among which those residing in layer V-VI) send efferent connection to subcortical and limbic structures[117]. Notably, layer V-VI cells in the mPFC are also strongly interconnected with the mediodorsal thalamus[60], a crucial region for the modulation of cognitive flexibility[118] and attention-related functions[77].

Due to the importance of pyramidal neurons in attentional processing, we addressed here the temporal requirements for activation of pyramidal neurons in the dorsomedial PFC (DmPFC, encompassing the ACg and the dorsal portion of the PL) and ventromedial PFC (VmPFC, centered in the border between the ventral part of PL and the dorsal IL) in rats performing in the 5-CSRTT. Since attention is a multi-dimensional construct, this task assesses aspects of a sustained visuospatial attentive state by testing the ability to monitor 5 different spatial locations over an extensive amount of trials. In addition, the task also provides information on other behavioral functions such as motivation, motor behavior, inhibitory control, decision-making strategies and timing (see for review Robbins et al., (2002)). Using the 5-CRSTT, we tested whether the involvement of DmPFC and VmPFC excitatory cells was required during specific phases of preparatory attentional states, or whether these two sub compartments modulate this function at different time-scales and epochs. By optogenetic silencing of either DmPFC or VmPFC pyramidal neurons[119] at defined time windows of a few seconds prior and during cue detection, we find that pyramidal neuron activity in DmPFC and VmPFC shows distinct temporal requirements during early and late phases of preparatory sustained attentional states, and during cue detection/instrumental action. These findings help to better disentangle the intricate network activity of the mPFC during complex cognitive tasks, providing a temporal view on mPFC activity requirements for adaptive and maladaptive behaviors.

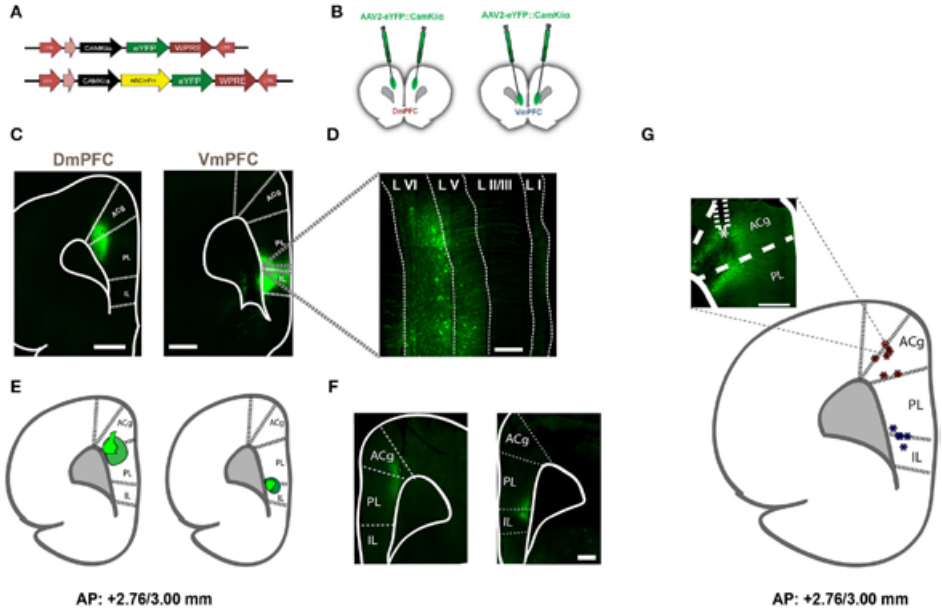

Figure 1. *Viral expression in rats injected with AAV2-eYFP, AAV2-eNPHR3.0, and AAV2-eARCH3.0 and optical fiber location to achieve selective illumination of either dmPFC or vmPFC.*
(**A**) Schematic representation of the viruses used to achieve expression of inhibitory opsins and eYFP in either dmPFC or vmPFC. (**B**) Graphic representation of the injections made in either the dmPFC or the vmPFC to test the spread of transfection of the virus in both regions (**C**) Overview (zoom 10×) of injection location in both the dmPFC (left panel) and the vmPFC (right panel). In this figure animals were injected with AAV2-eYFP::CamkIIα. Scale bar is 1 mm for both pictures. (**D**) Magnified (zoom 40×) confocal picture reporting an example of the transfected neurons by using the same viral plasmid used for the behavioral experiments. White dotted lines illustrate the empirical differentiation between the different mPFC layers, indicating that the majority of the transfected cells were in the deep layers with a reduced amount in the upper layers. Scale bar is 200 μm. Also in this example viral infusions were made using AAV2-eYFP::CamkIIα. (**E**) Visual identification of the virus spread in a sample of rats previously used to perform behavioral experiments and injected with either AAV2-eNPHR3.0-eYFP::CamkIIα or AAV2-eARCH3.0-eYFP::CamkIIα. Dark green wider circles represent the maximal expression achieved, while light green small shapes report the smallest expression detected (n = 10 in total). Confocal pictures of exemplificative images in this batch are reported in (**F**) (scale bar is 500 μm for both images). In this examples rats were injected with AAV2-eNPHR3.0-eYFP::CamkIIα. (**G**) Visual identification of fiber placement in a sample of rats previously used for 5-CSRTT experiments and injected with either AAV2-eNPHR3.0-eYFP::CamkIIα or AAV2-eARCH3.0-eYFP::CamkIIα. Inset reports an example of the fiber location in the mPFC (scale bar is 500 μm) in a rat injected with AAV2-eARCH3.0-eYFP::CamkIIα. Blue asterisks are referred to optic fibers located to achieve regional inhibition in the vmPFC, while red asterisks report the same fiber placement in the dmPFC (n = 12 in total).

RESULTS

To express inhibitory opsins in excitatory pyramidal neurons of either DmPFC or VmPFC, we used an AAV2 plasmid containing the CamkIIα promoter driving expression of either archaerhodopsin (eARCH3.0) or halorhodopsin (eNPHR3.0) and eYFP[119]. For the control group we injected the same virus with eYFP only (**Figure 1A**). Injections in the DmPFC targeted the border between the ventral part of the pregenual anterior cingulated cortex (ACg) and the dorsal part of the prelimbic cortex (PL), whereas VmPFC viral infusions transfected neurons in the ventral PL and the dorsal infralimbic cortex (IL) (**Figures 1B,C**). In both cases AAV2 injections primarily targeted the deep layers (layer V-VI) of the mPFC (**Figure 1D**). Same pattern was revealed in rats dissected after 5-CSRTT experiments (**Figures 1E** and **1F**), where also fiber placement in both the Dm- and the VmPFC was mainly located in the area ranging from layer V to layer VI (**Figure 1G**). Whole-cell patch clamp recordings performed in rats that previously were tested in the 5-CSRTT, confirmed the correct expression of the inhibitory opsins eNPHr3.0 or eARCH3.0 in pyramidal cells. Brief light pulses of similar length as used for the behavioral experiments (1 or 5 s; 530 nm) triggered after 50 consecutive repetitions a marked hyperpolarization response in the recorded cells (**Figures 2A–D**). Hyperpolarization remained stable across the different trials (**Figures 2C** and **2D**), with a slight reduction (about 20%) when light was consecutively delivered at the duration of 5 s (**Figure 2D**). In addition, input/output curves confirmed that: (a) light manipulation of pyramidal neurons was intensity-dependent, with stronger hyperpolarization following higher light intensity and that (b) also the lowest light intensity (1.3 mW) produced a sustained hyperpolarization of the cells (**Figure 2E**). We did not observe rebound action potentials following light-induced inhibition.

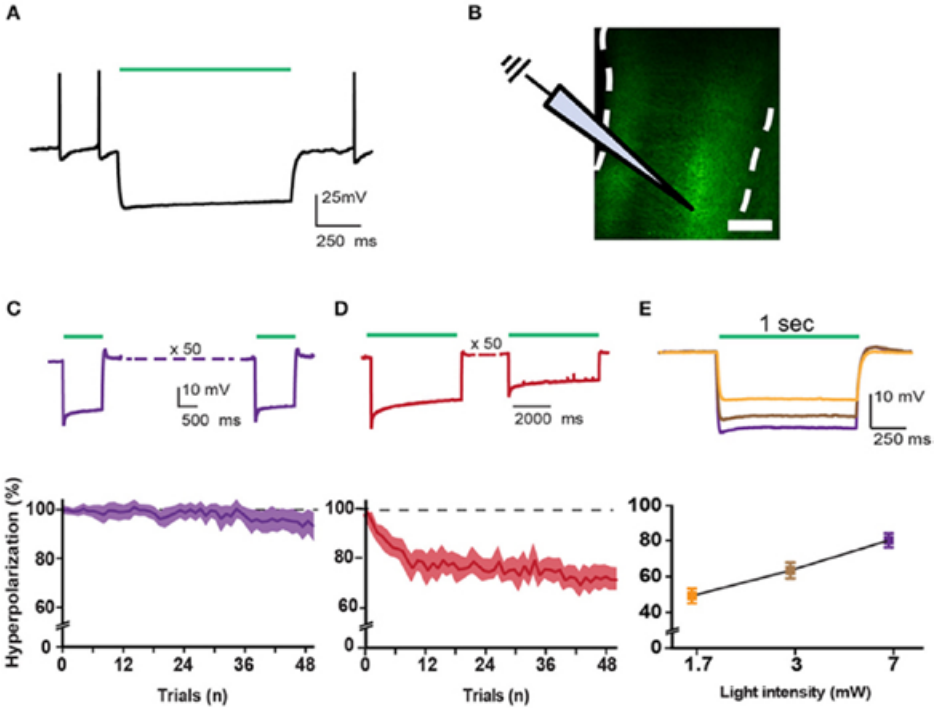

Figure 2. *Correct incorporation of inhibitory opsins in pyramidal cells.*
(**A**) Trace showing a typical eARCH3.0-mediated voltage waveform in a L5 pyramidal neuron in response to green light (530 nm, 1 s, 7 mW). (**B**) Schematic representation of recording configuration in mPFC coronal slices of a rat. White dotted lines represent the borders of the mPFC. Scale bar is 200 μm. (**C**) Top panel shows characteristic voltage waveforms monitored in response to one green light pulse (1 s duration: n = 14) in a L6 pyramidal neuron transfected with the AAV2-eARCH3.0::eYFP. Bottom panel graph reports the normalized hyperpolarization amplitude of each trial (50 trials, 1 s light pulse, repeated each 10 s, 7 mW light intensity). All responses were normalized to the maximal amplitude of the first response (graph report values as mean ± S.E.M.). (**D**) Top and bottom panels report the same example and analysis showed in (C) with a longer light pulse (5 s; n = 13). (**E**) Example traces show that pyramidal neurons responded to light pulses in an intensity-dependent fashion, with more pronounced hyperpolarization following higher light intensities (top panel). Bottom panel shows an input/output curve for different light intensities (n = 11 neurons, data are reported as mean ± S.E.M.). Percentage of hyperpolarization: 1.7 mW = 49.3 ± 4.1%; 3 mW = 63.4 ± 4.4%; 7 mW = 80.1 ± 3.8%, Data are normalized in each cell to the maximal response (evoked by a 17 mW light pulse). Average amplitude at 17 mW light pulses is −23.5 ± 3.4 mV (n = 22; data are reported as mean ± S.E.M.).

TRANSIENT MPFC INHIBITION IMMEDIATELY BEFORE AND DURING CUE PRESENTATION

To address whether a reversible inactivation of pyramidal neuron activity in either Dm or VmPFC affects rodent performance at specific time points during a preparatory attentional state, we trained rats in the 5-CSRTT (**Figure 3A**) and tested the effect of subregion-specific deactivation during precise time-windows in the task (see methods). Neither training [two-way ANOVA, effect of interaction group x protocol: $F(12, 156) = 0.992$; $p = 0.452$; effect of group: $F(2, 26) = 0.684$; $p = 0.513$; **Figure 3B**], nor baseline performance differed between groups [Accuracy: one-way ANOVA: $F(2, 28) = 1.607$; $p = 0.220$; omissions: one-way ANOVA: $F(2, 28) = 0.117$; $p = 0.893$; **Figure 3C**]. During the preparatory period, when the animal is actively attending the cue-holes, single-units in the ACg and PL area show a transient pre-cue increase in firing rate[19]. However, it is not known whether this activity causally drives a sustained attentional state. To test whether increased activity during this period in either DmPFC or VmPFC is required for proper performance, pyramidal neurons in either of these subregions were inhibited by light for 2 s prior to cue presentation (**Figure 4A**), during the time window that represents the actual period when the rat orients and actively awaits the upcoming stimulus, before it is required to produce a response to the cue[114]. Only inhibition of VmPFC pyramidal neurons resulted in a reduction of accuracy of responding [two-way repeated measures ANOVA: effect of light x virus interaction: $F(2, 26) = 5.984$; $p = 0.007$; effect of virus: $F(2, 26) = 6.154$; $p = 0.006$; effect of light: $F(1, 26) = 4.175$; $p = 0.051$; Sidak's multiple comparison test OFF vs. ON: CTRL: $p = 0.965$; DmPFC: $p = 0.854$; VmPFC: $p = 0.001$; **Figure 4B**]. This effect was primarily due to an increase in the percentage of incorrect responses [two-way repeated measures ANOVA: effect of light x virus interaction: $F(2, 26) = 4.115$; $p = 0.028$; Sidak's multiple comparison test OFF vs. ON: CTRL: $p = 0.952$; DmPFC: $p = 0.999$; VmPFC: $p = 0.002$; **Figure 4C**], and accompanied by an increase in premature responses (Wilcoxon matched-pairs signed rank test; $p = 0.008$; **Figure 4D**). Inhibition of pyramidal neurons in the DmPFC 2 s prior to cue presentation did not affect any parameter of performance in the 5-CSRTT (**Figure 4B, Table 1**). These results suggest that a reduction in accurate responding might be due to the reduced ability to control inappropriate responses when VmPFC activity is inhibited for 2 s before cue presentation.

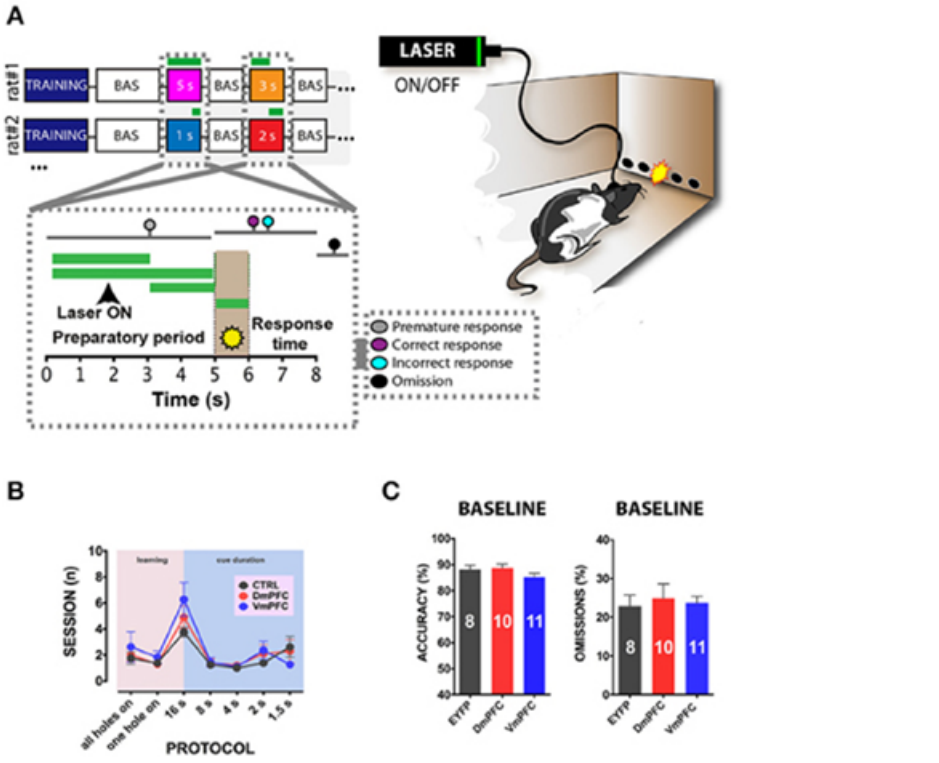

***Figure 3**. 5-CSRTT: protocols, training and baseline performance.*
(**A**) After stable baseline performance (BAS) for three consecutive sessions rats were assigned to the testing phase. Colored squares in the top-right panel represent the different light epochs of stimulation used. Numbers represent the length of the stimulation per session. White squares in between the stimulation days represent a baseline session when no light was delivered in the brain. Bottom-right panel represents a schematic picture of a single trial of the task. The first 5 s reported in the x axis shows the preparatory period of sustained attentional state, the light brown period (5th to 6th s in the x axis) refers to the presentation of the cue, and the last 2 s represent the limited hold period. Colored dots represent the possible responses that were recorded during the session. Responses before cue presentation were considered as premature and punished with a 5 s time-out period. Correct responses were rewarded with a food pellet, whereas incorrect pokes were punished with a time-out period. If a response did not occur within the limited hold period, an omitted trial was recorded. Green lines represent the different light epochs (see methods). Left panel reports a representative illustration of a rat performing in the 5-CSRTT. Rats are bilaterally connected via patch cables to a laser, which delivers (ON) or does not deliver (OFF) light in the desired epoch. The percentage of trials with light ON and OFF was approximately fifty for both options. (**B**) Illustration of the number of sessions within each training phase and stimulus duration of the task for the three different groups of rats included in the study (CTRL: n = 8; dmPFC: n = 10; vmPFC: n = 11; data are expressed as mean ± S.E.M.). (**C**) Graphs illustrating the averaged baseline with cables in accuracy and omissions for the 3 groups. Results are expressed as mean ± S.E.M.

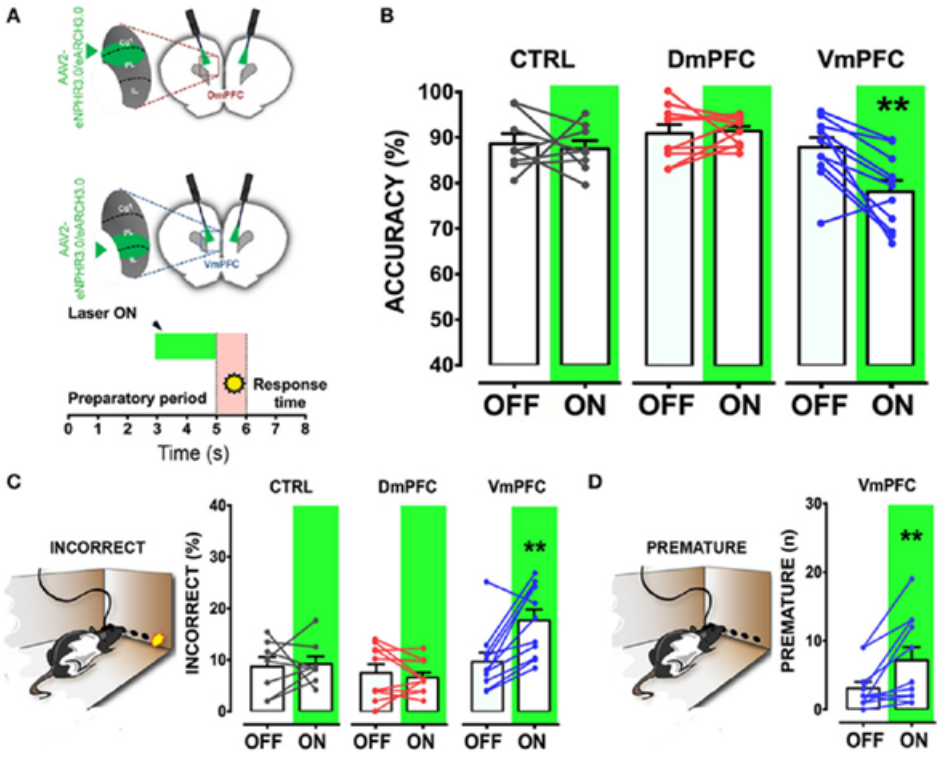

***Figure 4**. VmPFC inhibition affects sustained attentional state seconds before cue presentation.*
(**A**) Top panel shows a schematic representation of the optogenetic inhibition of either the dmPFC or the vmPFC. Optic fibers were placed 200–300 µm above the viral infusion location. Insets represent the target area in the two subregions. Bottom panel shows a graphical representation of the light protocol used to achieve the mPFC inhibition 2 s before cue presentation. (**B**) Accuracy of performance in controls (CTRL; n = 8), dmPFC (n = 10), and vmPFC (n = 11) injected animals (**C**) Percent of incorrect responses and (**D**) number of premature responses in the different groups. Asterisks indicate the result of the post-hoc multiple comparison Sidak's test. **p < 0.01. All numbers and statistical results are available in Table 5.1.

We next tested whether pyramidal neuron activity of the VmPFC or DmPFC is necessary during cue presentation for a proper sustained attentional state. Inhibition of VmPFC pyramidal neurons during cue presentation resulted in a reduction of the accuracy of responding [two-way repeated measures ANOVA: effect of light x virus interaction: $F(2, 14) = 4.393$; $p = 0.033$; effect of virus: $F(2, 14) = 1.864$; $p = 0.192$; effect of light: $F(1, 14) = 6.273$; $p = 0.025$; Sidak's multiple comparison test OFF vs. ON: CTRL: $p = 0.270$; DmPFC: $p = 0.826$; VmPFC: $p = 0.014$; **Figures 5A** and **5B**]. This effect was due to an increase of incorrect

responses and a decrease in correct responses [two-way repeated measures ANOVA: effect of interaction light x virus correct: $F(2, 14) = 5.535$; $p = 0.017$; Sidak's multiple comparison test OFF vs. ON: CTRL: $p = 0.494$; DmPFC: $p = 0.524$; VmPFC: $p = 0.013$; incorrect: effect of interaction light x virus: $F(2, 14) = 3.809$; $p = 0.048$; Sidak's multiple comparison test OFF vs. ON: CTRL: $p = 0.304$; DmPFC: $p = 0.714$; VmPFC: $p = 0.044$; **Figures 5C** and **5D**]. Also in this case, inhibition of DmPFC pyramidal neurons during cue presentation did not affect any parameter of performance (**Figure 5B**, **Table 1**). Thus, pyramidal neuron activity in the VmPFC is required during the preparatory phase, 2 s before cue presentation as well as during cue presentation itself, when rats are requested to prepare cue detection and to translate this into an instrumental response.

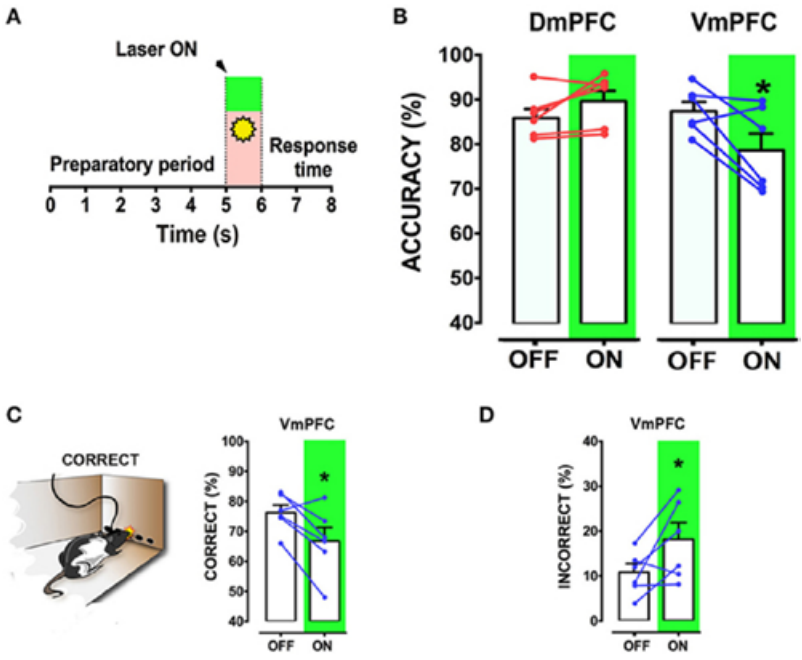

***Figure 5**. VmPFC inhibition affects sustained attentional state during cue presentation.*
(**A**) Graphical representation of the protocol used to optically inhibit mPFC neurons during cue presentation (CTRL: n = 5; dmPFC: n = 6; vmPFC: n = 6). (**B**) Accuracy of performance in dmPFC and vmPFC injected animals in light ON and light OFF trials. (**C** and **D**) Graphs showing the effect of the vmPFC inactivation on percent of correct and incorrect responses. Bar graphs are expressed as mean ± S.E.M.; lines report the performance per subject in the 2 different light conditions (ON vs. OFF). Asterisks indicate the result of the post-hoc multiple comparison Sidak's test. *p < 0.05.

SUSTAINED INHIBITION OF MPFC DURING A PREPARATORY SUSTAINED ATTENTIONAL STATE

Is the DmPFC causally involved in a sustained attentional state at these second time scales[7,19,38]? To test whether activity of the VmPFC or DmPFC is required earlier in the task to guide a sustained attentional state, we inhibited pyramidal neurons in either the dorsal or the ventral mPFC for 3 s starting 5 s before cue presentation during the early phases of the preparatory sustained attentional state (**Figure 6A**). Optogenetic inhibition of VmPFC or DmPFC pyramidal neurons during this period did not affect any of the behavioral parameters in the task [two-way repeated measures ANOVA; effect of light x virus interaction: $F(2, 14) = 0.827$; $p = 0.457$; effect of virus: $F(2, 14) = 0.514$; $p = 0.609$; effect of light: $F(1, 14) = 1.238$; $p = 0.285$, **Figure 6B, Table 1**]. In contrast, a sustained inhibition of the DmPFC for 5 s during the entire preparatory sustained attentional state (**Figure 7A**) did significantly affect the rodent accuracy of responding in the 5-CSRTT [two-way repeated measures ANOVA: effect of light x virus interaction $F(2, 22) = 11.760$; $p = 0.0003$; effect of virus: $F(2, 22) = 0.849$; $p = 0.441$; effect of light: $F(1, 22) = 0.856$; $p = 0.365$; Sidak's multiple comparison test OFF vs. ON: CTRL: $p = 0.194$; DmPFC: $p = 0.005$; **Figure 7B**]. This effect was explained by a reduction in the percentage of correct responses, as well as an increase in the percentage of incorrect responses [two-way repeated measures ANOVA correct: effect of interaction $F(2, 22) = 14.790$; $p = 0.0001$; Sidak's multiple comparison test OFF vs. ON: CTRL: $p = 0.991$; DmPFC: $p = 0.0001$; incorrect: $F(2, 22) = 9.199$; $p = 0.001$; Sidak's multiple comparison test OFF vs. ON: CTRL: $p = 0.268$; DmPFC: $p = 0.021$; **Figure 7C**]. In addition, the response latencies for incorrect responses was significantly longer during ON trials, when compared to OFF trials (OFF vs. ON = 1.30 ± 0.16 s vs. 1.51 ± 0.18 s; paired t-test: $p = 0.021$) suggesting that prolonged inhibition of the DmPFC may interfere with responding to a cue.

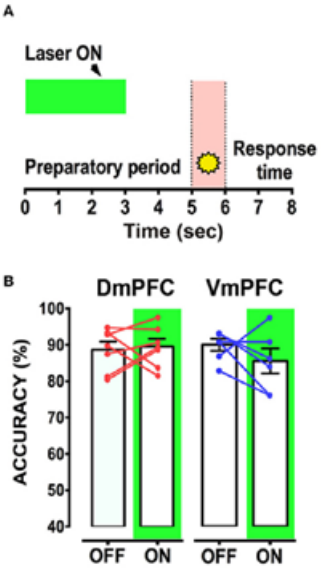

***Figure 6**. mPFC inhibition during the first 3 s from trial onset does not affect sustained attentional state.*
(**A**) Schematic representation of the protocol used to inhibit either dmPFC or vmPFC pyramidal cells in the first 3 s of the trial. (CTRL: n = 4; dmPFC: n = 7; vmPFC: n = 6); (**B**) Performance is not affected by the optogenetic manipulation of the mPFC in either Dm or vmPFC rats during the first 3 s of the trial, suggesting that optical inhibition in this epoch does not suffice to influence sustained attentional state.

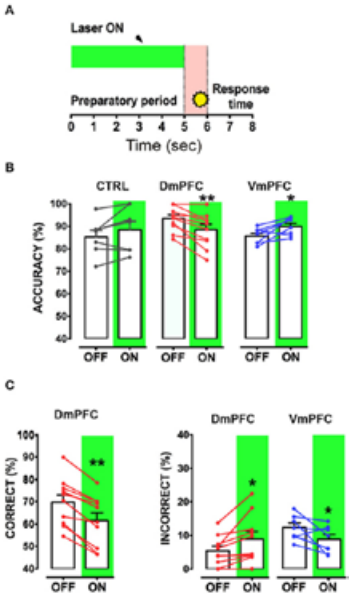

***Figure 7**. Inhibition of dmPFC during the entire preparatory period reduces sustained attentional state.*
(**A**) Graphical representation of the light protocol used, indicating that the laser was ON for half of the trials for 5 s before cue presentation. (**B**) Accuracy of performance in controls, dmPFC (n = 10), and vmPFC (n = 8) injected animals in light ON and light OFF trials. (**C**) Percentage of correct responses and incorrect responses that were significantly altered in the light ON condition. *p < 0.05, **p < 0.01.

Optical inhibition of the VmPFC during the entire 5 s of preparatory phase did not reduce control over a sustained attentional state, but to our surprise, slightly improved accurate responding, by decreasing the percentage of incorrect responses (Sidak's multiple comparison test OFF vs. ON accuracy: p = 0.037; % incorrect: p = 0.045; **Figures 7B** and **7C**) while not affecting reaction latencies for both correct and incorrect responses (Correct response latency, OFF vs. ON: 0.62 ± 0.04 vs. 0.61 ± 0.04; paired t-test: p = 0.749; incorrect response latency, OFF vs. ON: 1.11 ± 0.18 vs. 1.14 ± 0.10; paired t-test: p = 0.863). Nevertheless, taken together, these results show that the requirements for neuronal activity in the DmPFC and VmPFC during a sustained attentional state are temporally dissociated.

	CTRL		DmPFC		VmPFC	
	OFF	ON	OFF	ON	OFF	ON
ACCURACY (%)						
2 s before cue	88.78 ± 2.21	87.61 ± 1.83	90.69 ± 1.91	91.18 ± 1.00	87.6 ± 2.11	77.93 ± 2.44*
1 s during cue	87.54 ± 3.79	82.21 ± 5.14	86.41 ± 2.04	90.19 ± 2.39	87.99 ± 2.10	79.09 ± 3.85*
First 3 s of the trial	86.88 ± 3.02	84.24 ± 4.79	88.55 ± 2.19	89.38 ± 2.12	89.68 ± 1.64	85.23 ± 3.43
5 s before cue	85.39 ± 3.04	88.58 ± 3.81	93.21 ± 1.65	88.26 ± 2.41*	85.76 ± 1.19	90.01 ± 1.38*
OMISSIONS (%)						
2 s before cue	22.07 ± 2.98	23.45 ± 5.55	21.37 ± 2.91	27.35 ± 5.14	21.32 ± 2.7	19.85 ± 3.91
1 s during cue	15.69 ± 2.19	15.13 ± 2.86	18.4 ± 3.66	16.7 ± 7.45	13.2 ± 2.73	15.5 ± 4.61
First 3 s of the trial	14.19 ± 1.04	12.37 ± 1.7	13.3 ± 3.15	19.72 ± 5.44	11.75 ± 1.1	14.54 ± 1.02
5 s before cue	19.65 ± 4.99	22.56 ± 6.43	24.67 ± 3.95	29.45 ± 4.82	15.84 ± 2.79	16.35 ± 3.27
CORRECT (%)						
2 s before cue	69.18 ± 3.16	67.34 ± 5.54	71.07 ± 2.37	66.23 ± 4.55	69.00 ± 3.16	62.52 ± 3.94
1 s during cue	73.50 ± 3.87	69.74 ± 4.49	76.53 ± 2.40	71.92 ± 5.22	76.29 ± 2.53	66.76 ± 4.55*
First 3 s of the trial	74.63 ± 3.33	73.74 ± 4.19	76.34 ± 2.51	72.13 ± 5.22	79.21 ± 2.28	72.99 ± 3.72
5 s before cue	68.54 ± 4.91	68.08 ± 5.86	69.93 ± 3.36	61.79 ± 3.58*	72.05 ± 2.00	75.27 ± 2.32
INCORRECT (%)						
2 s before cue	8.74 ± 1.79	9.21 ± 1.47	7.55 ± 1.65	6.62 ± 1.00	9.66 ± 1.76	17.62 ± 2.1*
1 s during cue	10.4 ± 3.04	15.21 ± 4.38	10.16 ± 2.19	8.36 ± 1.63	10.51 ± 1.93	17.73 ± 3.59*
First 3 s of the trial	11.18 ± 2.5	13.83 ± 4.12	10.11 ± 2.16	8.39 ± 1.64	9.04 ± 1.32	12.46 ± 2.78
5 s before cue	11.81 ± 2.73	9.37 ± 3.16	5.39 ± 1.38	8.95 ± 2.29*	12.11 ± 1.28	8.63 ± 1.41*
PREMATURE (N)						
2 s before cue	3.37 ± 1.12	5.62 ± 1.67	2.2 ± 0.42	2.8 ± 0.63	3.09 ± 0.94	7.18 ± 1.89*
1 s during cue	6.6 ± 2.2	7 ± 2.53	3.67 ± 0.67	4.67 ± 1.93	5.16 ± 3.00	5.67 ± 1.43
First 3 s of the trial	4.75 ± 2.01	3.5 ± 1.94	2.57 ± 0.89	2.00 ± 0.95	4.17 ± 1.35	4.5 ± 0.92
5 s before cue	4.57 ± 1.7	4.28 ± 1.64	3.4 ± 1.27	3.6 ± 1.45	3.37 ± 0.96	5.12 ± 1.27
RESPONSE TIME CORRECT (S)						
2 s before cue	0.68 ± 0.04	0.69 ± 0.04	0.71 ± 0.05	0.69 ± 0.05	0.78 ± 0.07	0.87 ± 0.15
1 s during cue	0.62 ± 0.03	0.66 ± 0.01	0.66 ± 0.04	0.64 ± 0.04	0.62 ± 0.03	0.66 ± 0.05
First 3 s of the trial	0.63 ± 0.04	0.65 ± 0.07	0.64 ± 0.04	0.64 ± 0.02	0.61 ± 0.06	0.61 ± 0.05
5 s before cue	0.66 ± 0.05	0.67 ± 0.05	0.69 ± 0.04	0.72 ± 0.06	0.62 ± 0.04	0.61 ± 0.04

RESPONSE TIME INCORRECT (S)						
2 s before cue	1.03 ± 0.18	1.13 ± 0.12	1.38 ± 0.18	1.57 ± 0.23	1.09 ± 0.15	1.15 ± 0.1
1 s during cue	0.81 ± 0.13	1.04 ± 0.1	0.91 ± 0.20	1.08 ± 0.28	0.78 ± 0.18	1.14 ± 0.17
First 3 s of the trial	1.12 ± 0.09	1.44 ± 0.29	1.2 ± 0.22	0.97 ± 0.19	1.35 ± 0.25	1.18 ± 0.26
5 s before cue	1.00 ± 0.24	0.96 ± 0.14	1.30 ± 0.16	1.51 ± 0.18*	1.11 ± 0.18	1.14 ± 0.1
MAGAZINE LATENCY (S)						
2 s before cue	2.02 ± 0.4	2.07 ± 0.35	1.98 ± 0.14	1.98 ± 0.12	1.85 ± 0.16	1.92 ± 0.25
1 s during cue	1.68 ± 0.31	1.94 ± 0.41	1.79 ± 0.13	1.81 ± 0.16	2.37 ± 0.38	2.46 ± 0.55
First 3 s of the trial	1.27 ± 0.22	1.25 ± 0.2	1.91 ± 0.22	2.16 ± 0.29	2.58 ± 0.58	2.12 ± 0.45
5 s before cue	2.05 ± 0.22	1.94 ± 0.28	2.63 ± 0.57	2.05 ± 0.29	2.03 ± 0.17	1.87 ± 0.18
PERSEVERATIVE RESPONSES ON TARGET (%)						
2 s before cue	0.07 ± 0.02	0.05 ± 0.01	0.05 ± 0.02	0.07 ± 0.02	0.1 ± 0.03	0.07 ± 0.02
1 s during cue	0.01 ± 0.01	0.04 ± 0.04	0.04 ± 0.02	0.05 ± 0.03	0.06 ± 0.02	0.08 ± 0.04
First 3 s of the trial	0.06 ± 0.01	0.02 ± 0.01	0.03 ± 0.01	0.05 ± 0.02	0.02 ± 0.004	0.05 ± 0.02
5 s before cue	0.08 ± 0.03	0.01 ± 0.01	0.05 ± 0.02	0.06 ± 0.02	0.07 ± 0.01	0.04 ± 0.01
PERSEVERATIVE RESP OFF TARGET (%)						
2 s before cue	0.02 ± 0.01	0.03 ± 0.02	0.03 ± 0.01	0.02 ± 0.01	0.01 ± 0.01	0.004 ± 0.004
1 s during cue	0.08 ± 0.06	0.08 ± 0.07	0.004 ± 0.004	0.02 ± 0.02	0.03 ± 0.02	0.004 ± 0.004
First 3 s of the trial	0.02 ± 0.01	0.02 ± 0.01	0.01 ± 0.01	0.03 ± 0.01	0.04 ± 0.02	0.03 ± 0.01
5 s before cue	0.08 ± 0.04	0.04 ± 0.03	0.01 ± 0.01	0.02 ± 0.01	0.04 ± 0.02	0.01 ± 0.01

***Table 1**. Complete overview of the different parameters analyzed in the 5CSRTT under the four different light epochs.*
Data are expressed as mean ± S.E.M. and asterisks represent significant differences between the light OFF vs. light ON condition in the same protocol.

DISCUSSION

In this study we found that pyramidal neurons in the DmPFC and VmPFC require distinct temporal activation profiles during a preparatory sustained attentional state. In particular, we found that the VmPFC plays an important role in the seconds that immediately precede and coincide with cue presentation. Transient inhibition of VmPFC pyramidal neurons during these seconds impairs visuospatial sustained attentional states as measured in the 5-CSRTT task and affects various parameters, including premature responses. In contrast, the visuospatial sustained attentional state is less sensitive to short inactivation of the DmPFC. Only when the DmPFC is inhibited for the entire preparatory phase before stimulus presentation and cue detection, a reduction in the sustained attentional state was observed. Since response latencies and errors of omission were not altered by optogenetic silencing, the observed findings were not secondary to changes in motor performance.

Even though a functional distinct role of different mPFC areas in cognitive functions has been previously shown, most of this evidence was obtained using tools that affect mPFC function on time scales far beyond the time scale for attentional processing[32,37,38,120]. As a result, a causal understanding of the temporal requirements of ventral and dorsal mPFC pyramidal neuron activity during different phases of attentional processing was lacking. In addition, due to the relatively low selectivity of these tools, previous studies have inactivated large portions of mPFC tissue hampering the understanding of the role of subregions in cognitive processes.

In fact, it is well known that the distribution of pyramidal neurons in the mPFC, as in the rest of the cortex, follows a laminar organization where different layers receive and send projections to different cortical and subcortical structures[37]. For example while superficial layers of the mPFC (layer I and II/III) receive afferent projections from limbic and other cortical regions[121], organize granular cortico-cortical communication[117], and send compact projections to subcortical regions involved in impulse control[122,123], deep layers (V and VI) might represent a crucial pathway for complex cognitive functions due to the relations with the mediodorsal thalamus[60,124,125] and due to their ability to integrate highly processed

information from cortico-cortical and thalamic-projecting neurons[125,126]. In our study, we only inhibited the deep layers of the mPFC thereby sparing layer II/III pyramidal cells to provide further insights into activity of subclasses of cells within different mPFC subregions.

Optogenetic inhibition of the VmPFC in the seconds that precede cue presentation, as well as during cue presentation, revealed the driving role of this region in a sustained attentional state when a cue detection is required to produce an adaptive response. This provides additional evidence to support previous findings over the role of the prelimbic and infralimbic cortices in preparatory activity[19,46,127].

In line with previous studies that induced prolonged inactivation of more ventral sub compartments of the mPFC by lesions or pharmacological inhibition[32], we observed that transient and reversible optical inhibition of short epochs and during cue presentation resulted in a reduced suppression of undesired responses, i.e. increase in incorrect responding and increase in premature responding. Other studies have also shown that selective lesions of the PL/IL mantle, sparing ACg, are able to impair the preparatory processes in the condition movements triggered by the stimulus, affecting both the rate of correct responses and premature responses in a reaction time task[128], suggesting that VmPFC inhibition might also influence the instrumental response per se. Interestingly, we observed that the effect on undesired responses was primarily present when the manipulation immediately preceded stimulus presentation, and not observed when inhibitions were prolonged during the whole preparatory period, suggesting that pyramidal neuron-dependent withholding of non-desired responses might be a process that occurs late in the inter-trial interval. This is also in line with studies performed in the rodent PFC during visual and cross-modal attention tasks and auditory stimulus selection task that showed that this region might enhance neural representation of the target stimulus suppressing representation of other distractor stimuli[1,129–131]. In particular, optogenetic perturbation of the PFC in mice performing a visual/auditory cognitive task reported impairment in the ability to select between conflicting sensory cues[131]. As a consequence, it is then possible that our findings in the VmPFC might also be due to alterations in top-down control

of a sustained attentional state that this subregion might exert on sensory regions before stimulus presentation.

We found that only short lapses of inhibition of ventromedial subregions affect performance in the 5-CSRTT. This may be explained by the fact that PL/IL have been regarded as pivotal players in representing the association between cue and response[19] and that IL cortex has been shown to be crucial in the modulation of habitual behaviors[132,133]. Thus, inhibition of the VmPFC in the seconds around stimulus presentation may primarily affect the planning of entering the illuminated port, also impairing the pattern of habitual responses which may be present in well-trained rodents[19], leading to more inappropriate response (e.g., too early as in the case of premature responses, or in a poorly adequate manner as in the case of incorrect nose-pokes).

It was previously found that rats with vast lesions of the PL/IL cortices or pharmacological inhibition of the mPFC showed increases in perseverative responses[32,42,113,134]. We did not observe an increase in perseverative responding in our study, which may be explained by various reasons. First, the time-scale of our inhibition protocols was much smaller than the time scales from hours to week achieved with lesions or pharmacological agents. To increase perseveration may require longer mPFC inhibition for a behaviorally manifestation thereof. Second, since in our experiments opsins were expressed in the deep layers of the mPFC, it is possible that cognitive modules that suppress perseveration reside in upper layers rather than deeper layers of the mPFC. This is in line with evidence on a compact layer II/III projection to impulse-related subcortical regions, such as the core of the nucleus accumbens pyramidal neurons in deep layers have been reported to exert a pivotal function in modulating[122,123]. Therefore, since we did not inhibit layers II/III of the VmPFC, this might explain the difference in findings on perseverative responding. Finally, the earlier studies inactivated the PL and IL cortices in their entirety, whereas in our study only the ventral part of the PL cortex and the dorsal part of the IL cortex were affected by optical manipulation. As a consequence, our protocols of inhibition may not have been targeted to a sufficiently large area to exert a sustained effect on perseveration in our animals.

Future studies will have to clarify the specific temporal requirements and exact mPFC regions that control impulsive and compulsive responses.

Deactivation of the DmPFC during the entire preparatory period reduced the sustained attentional state, whereas transient inhibition of the DmPFC for only 3 s at the start of the preparatory phase or immediately preceding cue presentation and during cue presentation, had no effect on the sustained attentional state. This suggests that the ACg and dorsal PL have an active role in preparatory processing, but the timing of DmPFC activity is not strictly time-locked to the cue. As long as the DmPFC was not inhibited during the entire preparatory phase, 5-CSRTT performance was unaffected. Neuronal activity in the ACg is increased during a preparatory sustained attentional state[19], and relatively long-lasting chemogenetic inhibition of this area reduced attention-related performance in mice. The DmPFC is interconnected with a number of cortical and subcortical regions among which the sensorimotor areas[135] and the visual cortex[39,135,136] and recent electrophysiological observations have shown that afferents from the mediodorsal thalamus promote feed-forward inhibition of ACg pyramidal cells via recruitment of parvalbumin-containing interneurons modulating the network activity that is crucial to maintain adaptive behaviors[83]. Therefore, it is likely that long-lasting inhibition might have hampered the communication between DmPFC and other brain regions that hold and manipulate the sensory representation of the imminent cue, and/or might have dysregulated the delicate excitation/inhibition balance that is maintained functional by inhibitory parvalbumin-positive interneurons. This may suggest that the DmPFC plays a role in cognitive and sensory flexible representation of the rule to respond into the illuminated port.

Other studies have indeed shown that the ACg/DmPFC is involved in representing the task-rules in a set-shifting performance task[137], may be sequencing temporally ordered behaviors in a go/no-go task[138], and is able to maintain the task-rule across delay periods before a response in a win-shift radial arm maze task[139].

Notably, the mPFC is also involved in a number of other behavioral functions that may be interrelated with attentional processing. For example, it has been shown

that PL and IL cortices exert opposing roles in the expression and extinction of fear responses[140] and that silencing of IL projections to the basomedial amygdala causes increase in anxiety[141]. Moreover, whereas the IL seems more crucial for habitual behaviors, the PL compartment might be more influential in developing goal-directed behaviors[140]. Future work is warranted to unravel as to what extent these other behavioral functions relate to the current findings.

Surprisingly, we also observed that sustained inhibition of the VmPFC during the entire preparatory phase of a sustained attentional state slightly improved accuracy of responding, in contrast to the short inhibition protocols. It is at this point not clear how the 5 s inhibition of deep layers of the VmPFC led to improvement of performance. Possibly, the inhibition of the deep layers was compensated for by activation of other PFC regions, since PFC subregions are anatomically and functionally interconnected[19,42,60,142,143]. Alternatively, the 5-s long inhibition of the VmPFC may have resulted in circuit re-modulation and change in functionality. Recordings of unit activity within the medial PFC during a visuospatial task showed that neurons can change their activity in opposite directions, either increasing or decreasing their activity[19,123]. Optogenetic inhibition of pyramidal neuron activity as we did here may favor neurons that reduce their activity during the preparatory period of a sustained attentional state. How this translates into behavioral performance is not understood.

Our findings reveal that pyramidal neurons in the VmPFC and DmPFC require distinct temporal activation profiles during a sustained attentional state. Albeit effect sizes on performance were in the order of 5–10% (from baseline levels of approximately 85%) and as such may seem modest, they were very consistent across rats. Given the strong connectivity that the mPFC has with other cortical and subcortical structures, and the relative quick optical manipulations we used it is also possible that changes we observed in some of our parameters may result at least in part from propagated network activity in afferent/efferent structures rather than a direct engagement of pyramidal cells.

Activity in the VmPFC is strictly time-locked to cue onset and is required shortly before and during cue presentation, whereas activity of DmPFC is temporally more loosely associated with cue onset, but is required during the preparatory phase of sustained attentional states. Thus, our results show that a dissociable temporal recruitment of VmPFC and DmPFC in cognitive functions exists during sustained attentional states as measured by the 5-CSRTT. During the preparatory sustained attentional state, the VmPFC controls behavior by withholding inappropriate responses and by processing the imminent stimulus presentation[32,42,144], whereas the DmPFC may integrate temporal and visuospatial information[135] to temporally organize task-related responding (e.g., rule to enter the illuminated port) (**Figure 8**). It is interesting to note that studies employing prefronto-cortical electrophysiological recordings during selective attention tasks in macaque, and other non-human primates also underscored a functional dissociation between the activity of the ACg and the VmPFC. In this regard, it has been observed that while confined clusters of neurons in the macaque VmPFC transfer stimulus information values during task performance, ACg neurons predict the stimulus location to allow shifts in attentive state[145]. Moreover, whereas ventrolateral regions of the PFC might maintain internal stimulus representations, more dorsal PFC regions might manipulate this information for task-relevant aspects[146].

To conclude, our interventions may reveal the timing requirements to modulate cortical and subcortical areas to set up control over attentional processing in the context of reward expectation[19,147] and prepare the organism to integrate cognitive and sensory inputs to produce adaptive responses to achieve a goal.

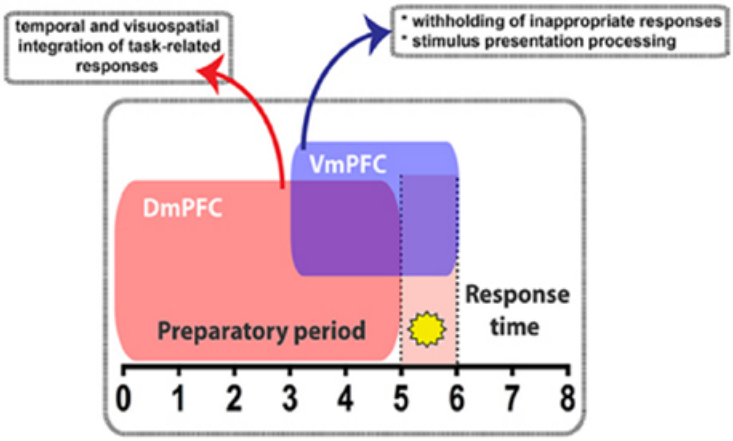

***Figure 8**. Diagram summarizing the main findings of this study.*
During the 5-CSRTT performance, temporally segregated manipulation of pyramidal neuron activity in either the Dm- or the VmPFC exert differential effect. VmPFC activity is necessary in the seconds that precede and coincide with the stimulus presentation (yellow star) where it might play a role in withholding the unwanted responses and process the information of the stimulus. DmPFC is required throughout the whole preparatory period to likely integrate the temporal and visuospatial aspect related to the task.

METHODS

ANIMALS

All experimental procedures were in accordance with European and Dutch law and approved by the animal ethical care committee of the VU University and VU University Medical Center. Male Long Evans wild-type rats (Janvier Labs, France; 8–10 weeks old at the start of the experiments) were used for all the experiments. Rats were individually housed on a 12 h light/dark reversed cycle (lights OFF: 7 a.m.). Only when assigned to behavioral experiments rats were food deprived. Food restriction began 1 week before the initiation of operant training in order to achieve and maintain about 85–90% of the free-feeding body weight. Water was provided ad libitum. In total 31 rats were included in this study (29 for behavioral testing and 2 for structural imaging).

OPSIN VIRUS DELIVERY AND IMPLANTATION OF OPTIC FIBERS

CaMKIIα promoter-driven opsin pAAV-enhanced halorhodopsin (eNPHR3.0)::eYFP, pAAV-enhanced archaerhodopsin (eARCH3.0)::eYFP and pAAV::eYFP were packaged as AAV serotype 2 virus (titer 1.0–6.0 × 1012). Rats were anesthetized with isoflurane (2.5%) and then mounted in a stereotaxic frame (Kopf instruments, Tujunga, USA). The skin of the scalp was retracted and 2 holes were drilled at the level of the medial prefrontal cortex (mPFC). Stainless steel micro-needles connected to a syringe (Hamilton, USA) were inserted at the desired coordinates to deliver the virus in the brain. For the DmPFC group, injections were made at AP +2.76 mm; ML ±1.49 mm; DV −2.94 and −2.84 mm from bregma (infusion angle 10°), while for the VmPFC group at AP +2.76 mm; ML ±1.45 mm; DV −4.87 and −4.77 mm from skull (10° infusion angle) (Paxinos and Watson, 2007). One microliter virus was injected per hemisphere in two steps of 500 nL at an infusion rate of 6 μL/h. A total of 8 rats were injected with AAV2-eNPhR3.0::EYFP, 13 with AAV2-eARCH3.0::EYFP and 8 with AAV2::EYFP. 14 rats in total were injected in the DmPFC and 15 rats were injected in the VmPFC (including control rats).

Then, 2 guide screws and 2 chronic implantable glass fibers (200 μm diameter, 0.20 numerical aperture, ThorLabs, Newton, NJ, USA) mounted in a sleeve (1.25 mm diameter; ThorLabs, Newton, NJ, USA) were placed in the rat brain. The

fibers were implanted right on top of the viral injection location (200–300 μm on average). Finally, a double component dental cement (Pulpdent©, Watertown, USA) mixed with black carbon powder (Sigma Aldrich, USA) was used in order to secure the optic fibers. All the surgical manipulations were performed before the behavioral training and testing.

BEHAVIORAL PROCEDURES

After 1 week of recovery from surgery and 1 week of habituation in the reverted light/dark cycle, rats started training in the 5-CSRTT in operant cages (Med Associates Inc., St. Albans, VT, USA). Training consisted of a period during which rats learned to respond to a brief visual cue that was randomly lit in one out of the five apertures of the operant cage[17]. To associate cue with the delivery of reward rats were first trained with all the apertures illuminated (all holes on, **Figure 3B**) in order to learn that a nose-poke returns a food pellet and subsequently with only one aperture constantly illuminated (one hole on, **Figure 3B**) to learn responding into this illuminated aperture is associated with reward delivery. After the learning phase, titration of shortening the stimulus duration was based on individual performance of each rat, and was reduced from 16 to 1 s. Criteria to move to a shortened stimulus duration were the percentage of accuracy (> 80%) and omitted trials (< 20%). Finally, when rats met the criteria at 1 s stimulus duration they were moved to the pretesting phase. In the pretesting phase, a green custom-made LED replaced the normal house-light of the operant cages, (< 1 mW intensity) to mask reflections by the laser light used for the experiments. The LED house-light did not affect performance when compared to normal house-light.

After three consecutive sessions during which rats performed according to the aforementioned criteria with the LED on, additional baseline sessions were conducted (3 consecutive sessions). During these sessions subjects were connected to the patch-cable (Doric Lenses, Quebec city, Canada) used to deliver the light into the brain. In this condition, accuracy was typically above 80%. However, they often did not show less than 20% omissions. This was most likely due to the fact that the animals were connected to the optic fiber patch cable and therefore less free to move in combination with the short time window for the

animal to respond (i.e. within 2 s after the cue light went off). This parameter makes the paradigm more demanding than other versions of the 5-CSRTT in which response time is usually set to 5 s[32]. Therefore, the omission criterion was increased to less than 40% omissions.

After acquisition of baseline rats were assigned to the testing phase where the task comprised 100 consecutive trials with a random assignment to the condition of laser ON or laser OFF (see below). In the whole text we refer to completed trials (correct, incorrect, omissions) while in the 100 trials premature responses are left apart from the count.

To light-activate the opsins in vivo, we used a diode-pumped laser (532 nm, Shanghai Laser and Optics Century Co, China) directly connected to the rat optic glass fiber implant. Light was delivered at 9–12 mW for experiments performed with eNPhR3.0 and at 7–8 mW for experiments carried out with eARCH3.0. These stimulation regimens are able to produce a theoretical irradiance which ranges between 9.76 and 13.01 mW/mm^2 500 μm from the fiber tip for the eNPhR3.0 experiments (corresponding to the center of the viral transfection) and ranging between 7.59 and 8.68 mW/mm^2 for eARCH3.0 experiments (http://web.stanford.edu/group/dlab/cgi-bin/graph/chart.php).

Light was delivered according to scheduled epochs by a stimulator (master 9, AMPI Jerusalem, Israel) connected to the computer interface.

For the testing phase, the following parameters have been acquired and analyzed through a box-computer interface (Med-PC, USA) and custom written MATLAB scripts (Mathworks): accuracy on responding to cues (ratio between the number of correct responses per session over the sum between correct and incorrect hits, expressed as percentage); absolute and percentage of correct, incorrect responses and errors of omission; correct or incorrect response latency; latency to collect reward; number of premature and perseverative responses. Percent of correct, incorrect and omissions were calculated based on the number of started trials[148]. In line with previous studies[149], no differences were found in behavioral effects

of eARCH3.0 and eNPhR3.0 injected animals (data not shown). Therefore, data from eARCH3.0 and eNPhR3.0 injected animals were pooled.

OPTICAL INHIBITION PROTOCOLS

Rats were randomly assigned to different stimulation protocols and received different optical inhibition epochs. Optical inhibition sessions were done 2–3 times a week with a baseline session in between to control for potential carry-over effects. Rats were tested according to the following optical inhibition protocols: (a) 3 s at the trial onset, (b) 2 s at the end of the preparatory period of a sustained attentional state, (c) 5 s throughout the whole preparatory period, (d) 1 s during light cue presentation. During a session, animals received only one light stimulation protocol. We chose these light regimens to make a clear distinction between prestimulus period and stimulus presentation/instrumental response period[123] (protocol a, b, and c vs. protocol d) and to differentiate between the whole pre-cue period and the period which consists in the actual orienting activity of the rat toward the task ports[19,21,123] (protocol c vs. protocol b). Light-ON and light-OFF trials were assigned semi-randomly with approximately 50% ON trials and 50% OFF trials. The majority of animals (28 out of 29) completed 100 trials within the first 20–25 min. One animal did not complete 100 trials before the time cut off of 60 min. Whereas animals were tested in all four different optical inhibition protocols, in some rats due to fiber loss not all protocols could be completed. Moreover, reported data for the majority of rats refer to the first optical inhibition session after establishment of stable baseline performance. In some cases, as described below, rats were retested in the same optical inhibition session.

EXCLUSION CRITERIA

Single sessions were excluded from analysis when technical problems (i.e. patch-cables disconnected during the task) made the results unreliable. In all these cases, we repeated the same protocol after re-acquisition of baseline criteria and used data from these sessions.

HISTOLOGICAL VERIFICATION

After behavioral testing, brains were checked for fiber placement and viral expression. For this, rats were anesthetized with isoflurane and a mix of ketamine (200 mg/kg *i.p.*) and dormitol (100 mg/kg *i.p.*) and then transcardially perfused (50–100 mL NaCl and 200–400 mL PFA 4%). Brains were removed and maintained in 4% PFA for at least 24 h. After that, brains were sliced with a vibratome (Leica Biosystem, Germany) into 50–100 μm coronal sections and mPFC slices were mounted on glass slides covered by 2% Mowiol and anti-fading mounting covers. Images were taken with a confocal microscope (LSM 510 Meta; Zeiss, Germany) with excitation wavelength of 514 nm bandpass filtered between 530 and 600 nm, and further analyzed using ImageJ (NIH, USA).

IN VITRO PHYSIOLOGICAL RECORDINGS

Following behavioral testing, five rats (by that time 8–10 months old) were used for electrophysiological recordings. Animals were anesthetized with 5% isoflurane and an *i.p.* injection of 0.1 ml/g Pentobarbital and subsequently perfused with 35 ml of ice-cold N-Methyl-D-glucamin solution (NMDG solution; in mM: NMDG 93, KCl 2.5, NaH_2PO_4 1.2, $NaHCO_3$ 30, HEPES 20, Glucose 25, NAC 12, Sodium ascorbate 5, Sodium pyruvate 3, $MgSO_4$ 10, $CaCl_2$ 0.5, at pH 7.4 adjusted with 10M HCl). After decapitation the brain was removed and incubated for 10 min in ice-cold NMDG solution. Coronal mPFC slices (350 μm) were made in ice-cold NMDG solution and incubated afterwards for 3 min in 34°C NMDG solution. Slices were maintained in an incubation chamber for at least 1 h before recordings were conducted at room temperature in oxygenated holding solution containing the following (Holding solution; in mM): NaCl 92, KCl 2.5, NaH_2PO_4 1.2, $NaHCO_3$ 30, HEPES 20, Glucose 25, NAC 1, Sodium ascorbate 5, Sodium pyruvate 3, $MgSO_4$ 0.5, $CaCl_2$ 1M.

Whole-cell recordings from pyramidal neurons were made at 32°C in oxygenated artificial cerebrospinal fluid (ACSF; in mM: NaCl 125, KCl 3, NaH_2PO_4 1.25, $MgSO_4$ 1, $CaCl_2$ 2, $NaHCO_3$ 26, Glucose 10). For recordings a potassium-based internal solution was used (in mM: K-gluconate 135, NaCl 4, Hepes 10, Mg-ATP 2, K_2Phos 10, GTP 0.3, EGTA 0.2) with patch-pipettes that had a resistance of 3–6 MΩ. Recorded neurons were kept at a holding potential close to –70 mV.

For recordings Multiclamp 700/B amplifiers (Molecular Devices) were used and data was collected with a sampling rate of 10 kHz and low-pass filtering at 3 kHz (Axon Digidata 1440A and pClamp 10 software; Molecular Devices).

OPTOGENETIC SLICE STIMULATION

To optically activate opsins, green light (530 nm) was applied to the slices. Light pulses were evoked by using a DC4100 4-channel LED-driver (Thorlabs, Newton, NJ) or a Fluorescence lamp (X-Cite Series 120q, Lumen Dynamics). During recordings fifty sweeps, each 10 s apart were applied. One sweep consists of a single light pulse with a duration of 1 or 5 s. These pulse regimes represent the shortest and the longest stimulation protocol used for behavioral experiments, respectively. The intensity of the light source was adjusted to 1.7, 3, 7, or 17 mW. For recording the in/output curves 1 s light pulse with all different stimulation intensities were applied for five sweeps with an interval of 10 s.

STATISTICAL ANALYSES FOR BEHAVIORAL EXPERIMENTS

To evaluate the main behavioral data between the opsin group and eYFP control group, two-way ANOVAs for repeated measures were performed. Corrected values for multiple comparison with Sidak's test were used when interaction between light and virus was significant. In all cases, the ANOVAs were preceded by the Kolmogorov-Smirnov (KS) test for normal distribution. In cases when the KS p-value was > 0.05, factorial analysis was performed on the raw data per parameter. In the other cases, raw data were first transformed with square-root or arcsin transformation.

Data were analyzed by MATLAB 2014a (Mathworks), Microsoft Excel (Office) and graphs were plotted by GraphPad Prism. In all cases the significance level was $p < 0.05$.

Bastiaan Bruinsma[1], **Huub Terra[1]**, Sybren F. de Kloet[1]
Antonio Luchicchi
Jaap Timmerman
Esther Remmelink
Maarten Loos
Tommy Pattij[#] and Huibert D. Mansvelder[#]

[1]shared first authorship

[#]shared senior authorship

PUBLISHED AS

Bruinsma, B.*, **Terra, H.***, de Kloet, S.F.*, Luchicchi, A., Timmerman, A.J., Remmelink, E., Loos, M., Pattij, T., and Mansvelder, H.D. (2019). An automated home-cage-based 5-choice serial reaction time task for rapid assessment of attention and impulsivity in rats. Psychopharmacology (Berl). 236, 2015-2026.

CHAPTER 3

An automated home-cage-based 5-choice serial reaction time task for rapid assessment of attention and impulsivity in rats

ABSTRACT

The 5-choice serial reaction time task (5-CSRTT) is a widely used operant task for measuring attention and motor impulsivity in rodents. Training animals in this task requires an extensive period of daily operant sessions. Recently, a self-paced, automated version of this task has been developed for mice, which substantially reduces training time. Whether a similar approach is effective for rats is currently unknown. Here, we tested whether attention and impulsivity can be assessed in rats with a self-paced version of the 5-CSRTT. Operant boxes were connected to home-cages with tunnels. Two groups of rats self-paced their training by means of an automated script. The first group of animals was allowed unlimited access (UA) to start trials in the task; for the second group, trial availability was restricted to the first 2.5 h of the dark cycle (TR). Task parameter manipulations, such as variable inter-trial intervals and stimulus durations as well as pharmacological challenges with scopolamine, were tested to validate the task. Self-paced training took less than 1 week. Animals in the UA group showed higher levels of omissions compared with the TR group. In both protocols, variable inter-trial intervals increased impulsivity, and variable stimulus durations decreased attentional performance. Scopolamine affected cognitive performance in the TR group only. In conclusion, home-cage-based training of the 5-CSRTT in rats, especially the TR protocol, presents a valid and fast alternative for measuring attention and impulsivity.

INTRODUCTION

Animal models of executive functioning are pivotal to understanding the neurobiology of psychiatric illness. Executive function domains, such as attention and impulse control, are affected in several psychiatric disorders, including schizophrenia and attention-deficit hyperactivity disorder (ADHD)[150,151,111,152]. In this task, animals are trained to scan a horizontal array of 5 apertures for the onset of a visual stimulus and withhold responding until its appearance. After a stimulus presentation in one of the pseudo-randomly chosen apertures, the animal must make a response in the form of a nose poke within a limited time window. From typically 60 to 100 repetitions of these trials, attentional performance is deduced from the ratio of the number of correct and incorrect responses. Levels of motor impulsivity can be assessed from the number of premature responses before the onset of the visual cue. Importantly, possible non-specific effects of pharmacological or neuronal circuit interventions can be controlled for by assessing motor effects via different response latencies[17,111].

Before animals can perform this task reliably with a stimulus duration (SD) of typically 0.5 s to 1.0 s, weeks to months of operant training are required[17,153]. Not only is this labor-intensive, the long periods of food deprivation can add to the cumulative discomfort of animals during the experiment. Besides animal discomfort, idiosyncratic handling by the experimenter has been shown to alter behavioral outcomes in rats, such as learning and memory[154]. Additionally, experimenter-induced interventions can increase corticosterone concentrations[155,156], which in turn could affect executive functioning[157].

A previous study asserted the efficacy of a self-paced variant of the 5-CSRTT (SP-5-CSRTT) in mice. In that study, home-cages of animals were connected to operant 5-CSRTT chambers (the so-called CombiCage), and mice could self-pace task progression with minimal interference by experimenters[23]. This adaptation of the 5-CSRTT led to a marked reduction in time that animals took to learn the task. Although the researchers reported slight differences in baseline performance at a SD of 1 s between animals trained in the SP-5-CSRTT and a conventional 5-CSRTT protocol, effects of behavioral challenges on attention and impulse control were

similar. Additionally, the use of the SP-5-CSRTT for drug testing was shown by a dose-dependent effect of scopolamine, an acetylcholine muscarinic receptor antagonist, on attentive behavior[23]. Whether this approach could be applied to testing attention and impulse control in rats is unknown. Additionally, whether task availability in the home-cage setting is an important factor for learning speed and performance is still unknown.

Here, we tested a modified version of the CombiCage SP-5-CSRTT, which was adjusted for rats. We measured training time and baseline performance and validated the SP-5-CSRTT by randomly varying behavioral parameters and quantifying effects on attention and impulsivity. Finally, we tested the effects of scopolamine, a muscarinic acetylcholine receptor antagonist, which has been shown to impact attention and impulsivity in rats in the conventional 5-CSRTT[111].

RESULTS

TRAINING TIME IS LESS THAN 1 WEEK IN SP-5-CSRTT

To test whether attention and impulsivity in rats can be assessed using an automated, self-paced task, as previously described for mice[23], we trained two groups of rats in an automated, modified home-cage version of the 5-CSRTT. Briefly, the home-cage of the animals was connected to an operant cage with a tunnel creating a CombiCage (**Figure 1**). To test whether limited trial availability would increase motivation and affect learning speed and performance of animals, two protocols were tested that differed solely in trial availability. In the first protocol, the UA group could start trials throughout light and dark cycles for 24 h, whereas in the second protocol, the TR group could only start trials during the first 2.5 h of the dark cycle. Additionally, we have included data from a group of rats conventionally trained in the 5-CSRTT, by means of daily 30-min training sessions[158]. This data was included to show training and baseline performance of animals that were trained in a conventional 5-CSRTT in our lab.

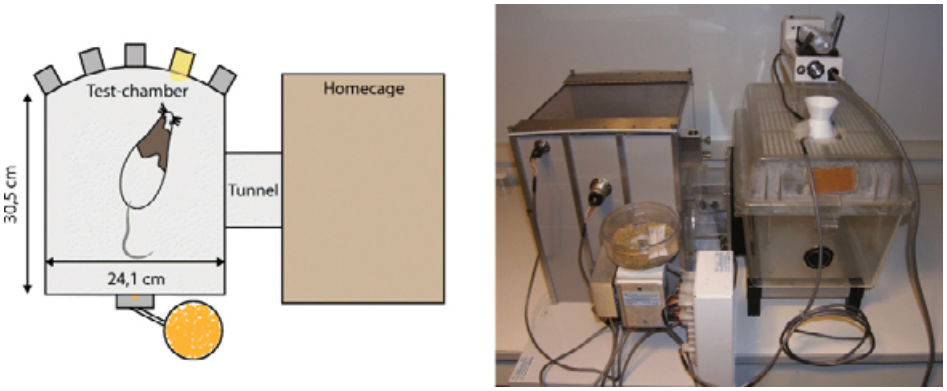

***Figure 1**. Schematic overview of the rat CombiCage.*
A standard macrolon home-cage is connected to a Med-Associates operant box by a polymer connection tube (diameter 10 cm). The operant box is equipped with a food magazine connected to a pellet dispenser. On the opposite wall, five equally spaced cue holes are positioned with yellow LEDs. Each cue hole is equipped with an infrared response detector to measure nose-poke responses.

Animals in both the UA and TR group were trained to SD 1 criterion in less than 7 days (**Table 1, Figure 2a**). In particular, rats in the UA group finished training in less than 3.5 days and were quicker than the TR group (**Figure 2a**; Wilcoxon rank-sum test, $p < 0.01$). However, the total number of trials that was required to finish SD1 to stable baseline performance criterion was less for the TR group (**Figure 2b**; t test, $p < 0.01$). Closer inspection of the number of trials required per stage of the task did reveal differences in learning between the groups (**Figure 2c**; group × stage: $F\,[5,110] = 4.26$, $p < 0.01$). Specifically, learning of the final stage, SD1, required less trials for the TR group compared with the UA protocol (**Figure 2c**; FDR-corrected Wilcoxon rank-sum test, $p < 0.01$).

TRAINING	UNLIMITED ACCESS	TIME-RESTRICT	CONVENTIONAL TRAINING
Number of rats	312	12	14
Days to finish SD1 criterion	3.29 ± 0.76	6.55 ± 2.99	23.21 ± 6.13
Number of trials to SD1 criterion	1499 ± 522	1023 ± 717	1347 ± 409
Weight difference (% start vs end training)	+2 ± 2.8	+1 ± 1.9	NA
Earned pellets / day	282 ± 41	268 ± 29	60.71 ± 7.97
Punishment after error	TO + HL on	TO + HL on	TO + HL off
Eat-interval (s)	5	5	0
PERFORMANCE AT SD1			
Started trials per session / day (#)	832 ± 182	390 ± 60	100 ± 0
Accuracy (%)	83.11 ± 8.12	84.63 ± 4.32	84.61 ± 5.84
Omissions (%)	49.52 ± 8.14	20.03 ± 8.31	17.46 ± 7.65
Premature responses (%)	0.12 ± 0.08	0.32 ± 0.26	10.90 ± 5.14
Correct response latency (s)	1.66 ± 0.29	1.41 ± 0.30	0.66 ± 0.36
Magazine latency (s)	2.21 ± 0.47	2.05 ± 0.41	1.51 ± 0.48
FIRST 100 TRIALS SD1 SESSION			
Accuracy (%)	80.33 ± 11.69	83.55 ± 5.72	84.61 ± 5.84
Omissions (%)	51 ± 10.28	16.33 ± 8.42	17.46 ± 7.65
Premature responses (%)	0.33 ± 0.49	1.17 ± 1.53	10.90 ± 5.14
Correct response latency (s)	1.67 ± 0.27	1.45 ± 0.34	0.66 ± 0.36
Magazine latency (s)	2.09 ± 0.42	2.11 ± 0.44	1.51 ± 0.48

***Table 1**. Summary of training variables and performance for conventional training and both the unlimited access and time-restricted home-cage 5CSRTT groups.*
TO = 5 s time-out; HL = houselight. Data are expressed as mean ± SD.

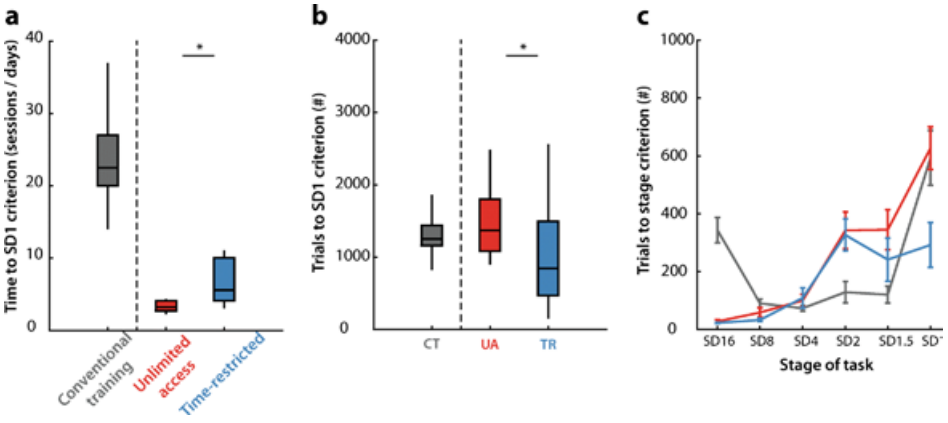

***Figure 2**. Training time to SD1 criterion performance is less than 1 week in home-cage 5CSRTT protocols.* **a.** Number of training sessions (conventional protocol) or training days (home-cage protocol) to SD1 criterion in the task. **b.** Total number of trials to reach SD1 criterion. CT, conventional training; UA, unlimited access; TR, time-restricted. **c.** Number of trials to reach criterion performance during each learning stage of the task for the different protocols. Data are expressed as mean ± SEM. n = 14 for conventional training (CT), n = 12 for both the unlimited access (UA), and time-restricted group (TR). * $p < 0.01$ Wilcoxon rank-sum test or t test between UA and TR protocol. Conventional training separated by vertical dashed line.

STABLE BASELINE PERFORMANCE IN THE SP-5-CSRTT

Similar to mice[23], in rats, the UA group also started significantly more trials during the dark phase of day-night cycles (91.1% of total) than during the light phase (**Figure 3a**, $p < 0.001$). In addition, accurate responding was higher during the dark phase (**Figure 3b**, $p < 0.001$), and omissions were lower, compared with the light phase (**Figure 3c**, $p = 0.018$). Surprisingly, the percentage of premature responses, a measure for motor impulsivity, was below 1% of the number of trials. Levels of premature responding did not differ between the light or dark phase (**Figure 3d**, $p = 0.097$). Since animals started trials almost exclusively during the dark phase and because of differences in task performance during the light and dark phase, we will henceforth only report behavioral parameters analyzed for trials started during the dark phase.

Next, we analyzed baseline SD1 performance across behavioral parameters and compared them between protocols (**Table 1**). The UA group rats started more than 800 trials per day on average, whereas the TR group started close to 400 trials (**Figure 4a**). Accuracy, the measure for attention, did not differ between protocols (**Figure 4b**, t test, $p = 0.64$), with rats in all groups reaching levels of approximately 85% correct choice at SD1. Interestingly, the percentage of omitted trials markedly differed between protocols (**Figure 4c**, t test, $p < 0.001$). UA group rats showed almost three times more omissions than the TR group. Premature responding was reduced in the UA group compared with the TR protocol (**Figure 4d**, t test, $p < 0.05$). Finally, whereas correct-response latencies were slightly elevated in the UA group compared with the TR protocol **(Figure 4e,** t test, $p = 0.04$), magazine latencies were comparable (**Figure 4f**, t test, $p = 0.35$). When we compared the first 100 trials of the UA and TR session, we only found significant differences in the percentage of omissions between the protocols (**Table 1**, Wilcoxon rank-sum test, $p < 0.0001$).

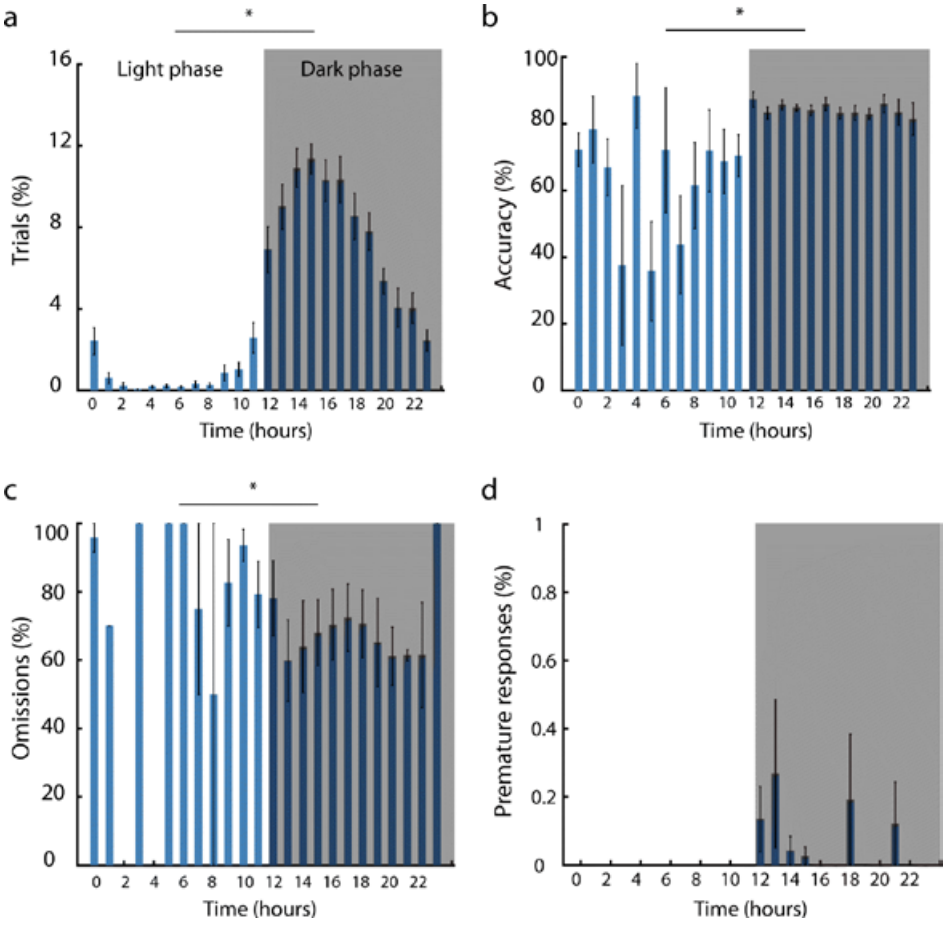

***Figure 3**. Behavioral performance over the light/dark cycle in the unlimited access group.*
a–d. Performance in home-cage 5C unlimited protocol distributed over the day. Time is indicated as hour of the day, and time bins in shading represent the dark phase of the day. * $p < 0.05$ paired t test light vs dark phase. n = 12. Data are expressed as mean ± SEM.

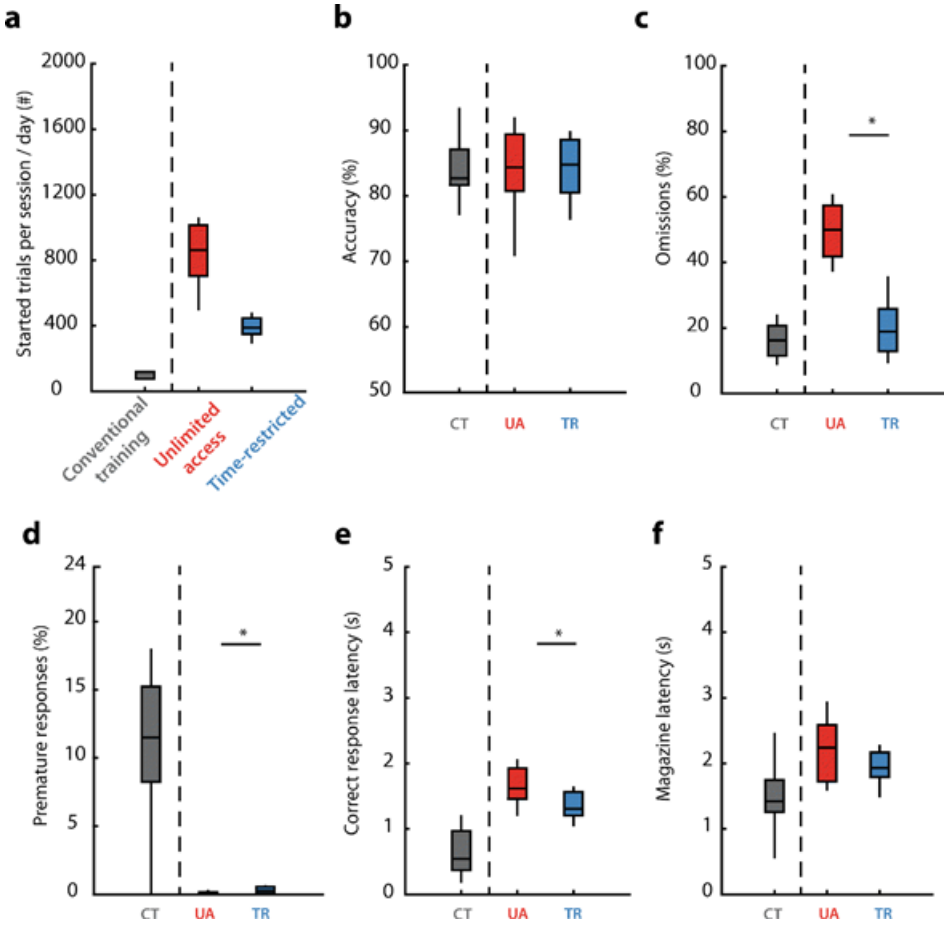

***Figure 4**. Behavioral performance at SD1 in the conventional 5CSRTT task and home-cage 5CSRTT protocols.* **a**. Number of started trials per session (conventional 5C) or per day (home-cage protocols). **b-f**. Performance at SD1, data displayed for the measured task parameters. * $p < 0.05$ t test between UA and TR protocol. Conventional training separated by vertical dashed line. CT, conventional training; UA, unlimited access; TR, time-restricted. n = 14 for conventional training, n = 12 for each home-cage 5C group.

SP-5-CSRTT PERFORMANCE IS MODULATED BY VARIABLE ITI AND SD MANIPULATIONS

Since we observed differences in baseline performance in the SP-5-CSRTT compared with the conventional 5-CSRTT, we asked whether behavioral challenges would affect performance equally in the different protocols. For this, we subjected rats from the UA and TR group to days with either a variable ITI or a variable SD. Randomly varying the ITI between 5, 7.5, and 12.5 s affected accuracy to the same extent in both groups (**Figure 5a**, ITI: $F[2,42] = 5.18$, $p < 0.01$; group × ITI: $F[2,22] = 1.97$, $p = 0.15$). However, post hoc testing revealed no significant differences in accuracy between trials with different ITI durations. The percentage of omitted trials was significantly decreased for the UA group on trials with the longest ITI (**Figure 5b**, ITI: $F[2,42] = 6.57$, $p < 0.01$; group × ITI: $F[2,22] = 10.08$, $p < 0.001$). Premature responses were significantly and differentially increased in the UA and TR group (**Figure 5c**, ITI: $F[2,42] = 23.42$, $p < 0.001$; group × ITI: $F[2,22] = 8.3$, $p < 0.001$), with the TR group showing the strongest increase in premature responding at the longest ITI.

Variable SDs between 1, 0.5, and 0.2 s significantly affected accuracy to the same extent in both protocols, with a decrease at shorter SDs (**Figure 5d**, SD: $F[2,42] = 68.45$, $p < 0.001$; group × SD: $F[2,22]$, $p = 0.3$). Omissions were differentially increased in the groups, with increments in the UA group at 0.5 and 0.2 s, whereas only the shortest SD increased omissions in the TR group (**Figure 5e**, SD: $F[2,42] = 81.34$, $p < 0.001$; SD × group: $F[2,22] = 7.14$, $p < 0.001$). Premature responses were not affected in either group by varying the SD (**Figure 5f**, SD: $F[2,42] = 0.57$, $p = 0.57$; SD × group: $F[2,22] = 0.42$, $p = 0.66$). Taken together, these data show that varying ITIs mainly affected premature responding in both groups, with subtle effects on omissions in the UA group, whereas variable SD conditions caused decrements in accuracy and increments in omissions in both UA and TR group, similar to what has been reported previously in the conventional 5-CSRTT[17,111].

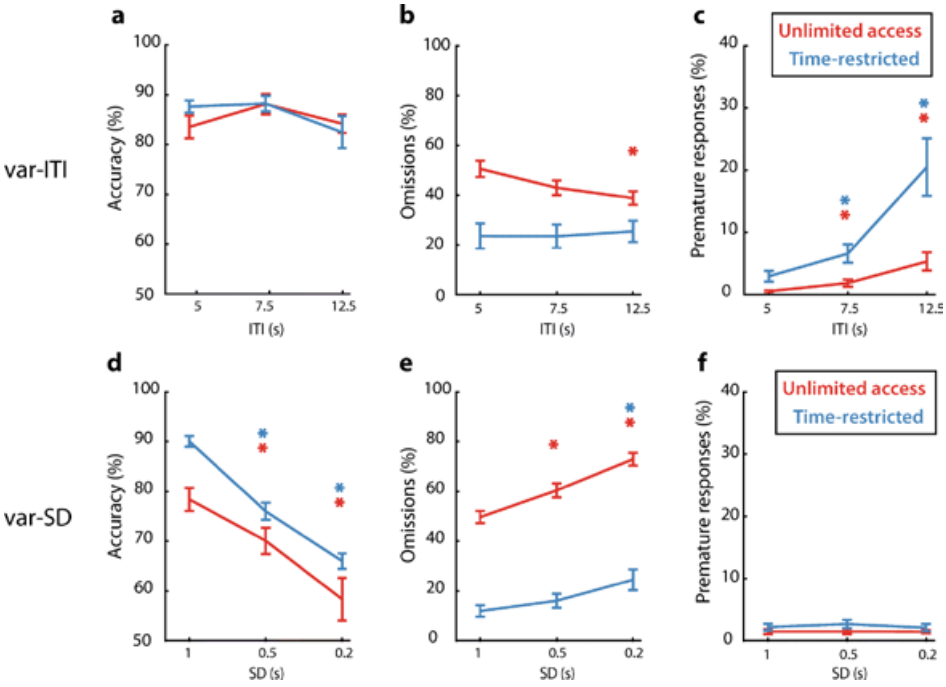

***Figure 5**. Behavioral performance in home-cage 5C is affected by varying SD and ITI.*
a–c. Effect of varying the inter-trial interval (var-ITI) on selected task parameters. * $p < 0.05$ FDR-corrected paired t test vs ITI = 5 s. The color of the asterisk depicts in which group the difference is detected. **d–f**. Effect of varying the stimulus duration (var-SD) on selected task parameters. * $p < 0.05$ FDR-corrected paired t test vs SD = 1 s. The color of the asterisk depicts which group the difference is detected. UA, unlimited access (n = 12); TR, time-restricted protocol (n = 11). Data are expressed as mean ± SEM.

EFFECTS OF SCOPOLAMINE ON BEHAVIORAL PERFORMANCE

During the scopolamine experiments, one animal in the TR group and one animal in the UA group did not start trials after the high dose (0.3 mg/kg) and were therefore excluded from analyses. For further pharmacological validation of the SP-5-CSRTT protocols, we used scopolamine, a muscarinic acetylcholine receptor antagonist. Scopolamine has previously been shown to affect multiple aspects of executive functioning in both the conventional 5-CSRTT in rats, as well as the automated home-cage 5-CSRTT in mice[23,159,160]. The 2.5-h session of the TR group was analyzed in five 30-min blocks considering the short half-life of scopolamine in rats[161]. For the UA group, we analyzed the first 2.5 h in 30-min blocks.

In the TR SP-5-CSRTT protocol, scopolamine decreased the number of started trials throughout the 2.5-h session and to a similar extent across the 30-min blocks. The number of started trials also decreased over time in a session (**Figure 6a**, dose: $F[2,9] = 18.44$, $p < 0.001$, time: $F[4,9] = 5.37$, $p < 0.01$, dose × time: $F[8,9] = 1.06$, $p = 0.4$). The high dose of scopolamine, 0.3 mg/kg, decreased accuracy of responding in the first and last half hour block of the session (**Figure 6b**, dose: $F[2,9] = 4.88$, $p < 0.05$, time: $F[4,9] = 5.59$, $p < 0.01$, dose × time: $F[8,9] = 2.56$, $p < 0.05$). Omissions were dose-dependently increased by scopolamine throughout the entire session (**Figure 6c**, dose: $F[2,9] = 13.59$, $p < 0.001$, time: $F[4,9] = 4.06$, $p < 0.01$, dose × time: $F[8,9] = 1.65$, $p = 0.13$). Scopolamine specifically increased premature responses during the first half hour block at the highest dose, and overall premature responding decreased over time (Figure 6d, dose: $F[2,9] = 2.25$, $p = 0.13$, time: $F[4,9] = 9.26$, $p < 0.001$, dose × time: $F[8,9] = 2.5$, $p < 0.05$). Correct-response latencies were increased by scopolamine throughout the session (**Figure 6e**, dose: $F[2,9] = 6.72$, $p < 0.01$, time: $F[4,9] = 2.87$, $p < 0.05$, dose × time: $F[8,9] = 1.87$, $p = 0.08$). Magazine latencies were not affected by administration of scopolamine, but increased over the half hour time blocks (**Figure 6f**, dose: $F[2,9] = 1.71$, $p = 0.21$, time: $F[4,9] = 10.2$, $p < 0.001$, dose × time: $F[8,9] = 1.09$, $p = 0.38$). In conclusion, scopolamine affected attention and impulse control performance in the TR SP-5-CSRTT similarly as has been reported previously for the conventional 5-CSRTT and SP-5-CSRTT in mice[23,159,160].

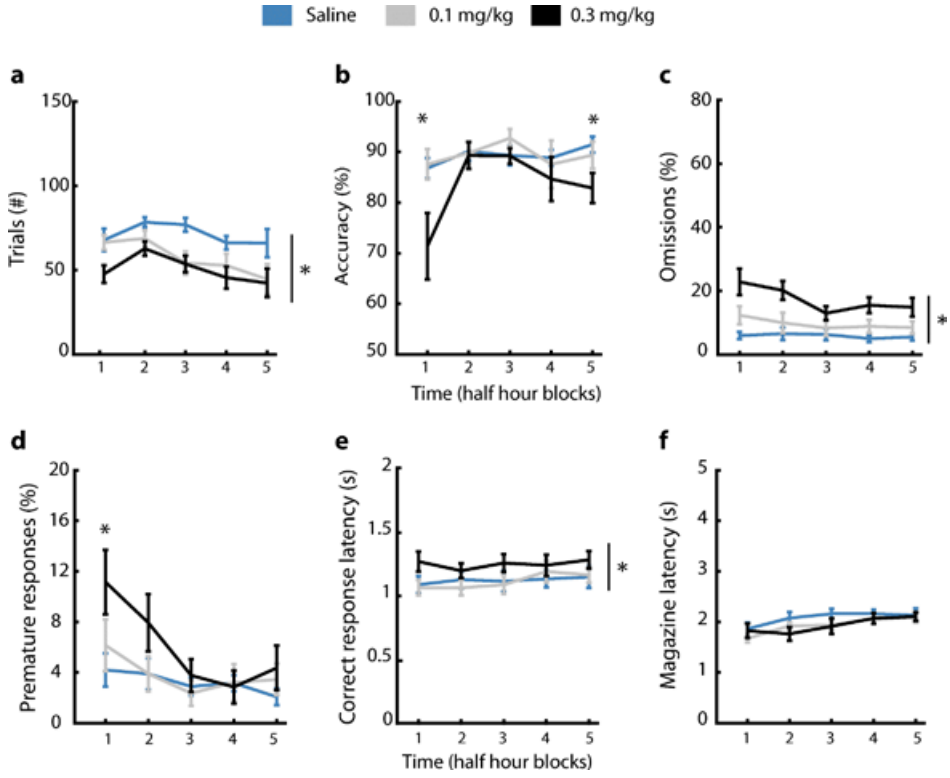

***Figure 6**. Scopolamine affects cognitive parameters in time-restricted (TR) home-cage 5C task.*
a. Scopolamine decreased the number of started trials over the session. * $p < 0.05$ main effect dose repeated-measures ANOVA. **b.** Accuracy was reduced by the highest dose of scopolamine in the first and fifth time block. * $p < 0.05$ FDR-corrected Wilcoxon signed-rank test 0.3 mg/kg vs saline. **c.** Scopolamine increased the percentage of omitted trials over the session. * $p < 0.05$. **d.** Scopolamine increased the percentage of premature responses in the first time block of the session. *$p < 0.05$ FDR-corrected Wilcoxon signed-rank test 0.3 mg/kg vs saline. **e.** Correct-response latency was increased after scopolamine administration. * $p < 0.05$ main effect dose repeated-measures ANOVA. **f.** Scopolamine did not affect the magazine latency. $n = 10$. Data are expressed as mean ± SEM.

In the UA SP-5-CSRTT protocol, scopolamine did not affect the number of started trials, but this variable was affected by time (**Figure 7a**, dose: $F[2,10] = 1.33$, $p = 0.29$, time: $F[4,10] = 8.87$, $p < 0.001$, dose × time: $F[8,10] = 0.82$, $p = 0.59$). Accurate responding was not affected by scopolamine administration or by time (**Figure 7b**, dose: $F[2,10] = 0.11$, $p = 0.9$, time: $F[4,10] = 1.19$, $p = 0.33$, dose × time: $F[8,10] = 1.01$, $p = 0.43$). Scopolamine did not alter omissions in the task, which were affected by time (**Figure 7c**, dose: $F[2,10] = 2.13$, $p = 0.15$, time: $F[4,10] = 5.4$, $p < 0.01$, dose × time: $F[8,10] = 1.49$, $p = 0.18$). Premature responses were not affected by either scopolamine or time (**Figure 7d**, dose: $F[2,10] = 3.23$, $p = 0.06$, time: $F[4,10] = 0.94$, $p = 0.45$, dose × time: $F[8,10] = 0.77$, $p = 0.63$). Scopolamine increased correct-response latencies throughout the session (**Figure 7e**, dose: $F[2,10] = 4.31$, $p < 0.05$, time: $F[4,10] = 0.81$, dose × time: $F[8,10] = 1.17$, $p = 0.33$). Finally, magazine latencies were not altered by scopolamine administration (**Figure 7f**, dose: $F[2,10] = 1.51$, $p = 0.25$, time: $F[4,10] = 1.95$, $p = 0.13$, dose × time: $F[8,10] = 1$, $p = 0.44$). In summary, scopolamine failed to affect attention and inhibitory control in the UA SP-5-CSRTT protocol but increased correct-response latencies.

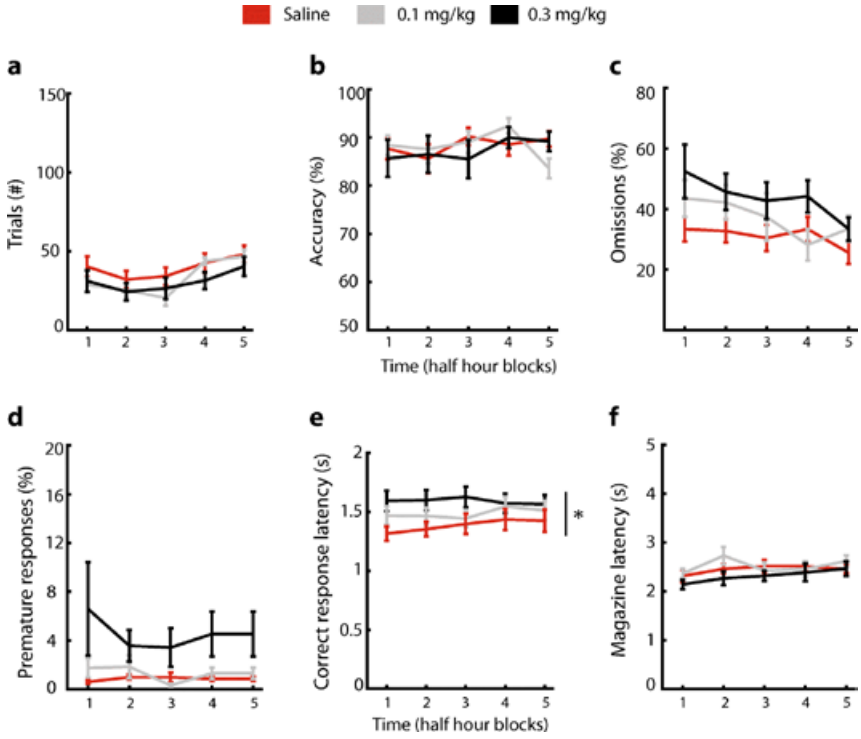

***Figure 7**. Scopolamine does not affect attention and inhibitory control in unlimited access (UA) home-cage 5C task.* **a–f.** Effect of scopolamine on selected task parameters. Scopolamine increased the correct-response latency but did not alter other parameters. * $p < 0.05$ main effect dose repeated-measures ANOVA. $n = 11$. Data are expressed as mean ± SEM.

DISCUSSION

We present an automated home-cage-based version of the 5-CSRTT for rats, as was previously developed for mice[23]. Our main findings are that in the SP-5-CSRTT, training time was less than 1 week and that animals gained weight during training without the necessity of prior food restriction. SP-5-CSRTT was sensitive to behavioral challenges in similar fashion as demonstrated in the conventional 5-CSRTT, whereas only in the TR-group, pharmacological interventions with scopolamine were effective.

Conventional 5-CSRTT requires long training periods[17,158,162,163]. Rats with UA to SP-5-CSRTT finished training in less than 4 days, while rats with TR access finished within 1 week. The training time reduction most likely results from the increased number of trials that rats performed each day. Interestingly, the total number of trials to reach SD1 criterion was reduced for the TR protocol. A closer look at the number of required trials per stage revealed that learning dynamics differed between protocols. Rats trained in the TR protocol required less trials to learn the final stage under SD1 conditions. One factor contributing to this different rate of learning could be the continuous food availability in the UA protocol. This might increase satiety and decrease motivation, possibly reflected by the increase in percentage omissions as discussed below.

Baseline performance in SP-5-CSRTT differed on several parameters between protocols. Rats in the UA group started trials preferably in the dark phase compared with the light phase[23,164,165]. Omissions were dramatically increased in the UA group, possibly resulting from reduced motivation or reduced salience of visual cues in light surroundings. Restriction of trial accessibility (TR) strongly reduced levels of omissions in the SP-5-CSRTT. In human subjects, similar observations have been made regarding time limits in motivation and task performance. When subjects were given twice the necessary amount of time needed for solving an addition task, it not only took longer to complete the task, but easier task goals were set[166]. To our knowledge, our study is the first to directly compare effects of time limits on task performance in rodents. In addition, levels of premature responding were lower in both home-cage 5-CSRTT protocols. In mice, no differences in

levels of premature responding or increases in omissions were reported between conventional training and home-cage 5-CSRTT[23]. This might be due to subtle differences in task design, such as a longer eat-ITI in the mouse SP-5-CSRTT protocol or to inherent differences in premature responding strategies between mice and rats as previously reported[167,168].

A potential caveat could be differences in signaling of response errors in the tasks. In the conventional 5-CSRTT, errors are punished by timeout periods signaled through house-light extinction[17]. In SP-5-CSRTT, time-out periods were signaled by turning on the house-light. Despite this, behavioral challenges, such as varying ITI or SD, resulted in similar effects to conventional 5-CSRTT[17,169,170]. Varying the ITI led to increased premature responding and decreased omissions. Increasing ITI durations has previously been reported to lower omissions in rats[170], yet increases in omissions have also been shown[33,169]. This may result from shorter limited hold periods urging faster responses following stimulus presentation. Shortening SDs decreased accurate choice as well as increased the percentage of omitted trials[17,171]. Thus in SP-5-CSRTT, variable ITIs mainly affected impulsive responding, while variable SDs mainly affected attentional performance. The validity of the SP-5-CSRTT for drug screening was demonstrated by scopolamine (muscarinic acetylcholine receptor antagonist) challenges, which have been well characterized in both mice and rats in conventional 5-CSRTT[23,159,160]. Reported effects of scopolamine on attention and inhibitory control were replicated in the TR protocol, but not in the UA protocol. Scopolamine decreased accuracy mainly in the first half hour block of the TR protocol. Additionally, premature responding was specifically increased in the first half hour, in line with plasma half-life of scopolamine[161]. In contrast, the number of started trials, correct-response latency, and omissions were affected throughout the entire session. Whereas in mice, scopolamine has been shown to robustly decrease accurate responding, in rats, results are inconsistent in literature[23,159]. Similar to our findings, decrements in accuracy have been reported[172,173]. In contrast, several other studies found no effect of scopolamine on accurate choice in rats[160,174,175]. Interestingly, effects of scopolamine on accurate choice were mainly found under more challenging conditions, such as white noise distraction[172], or by reducing SDs[173]. In the present study,

animals were tested with long, variable ITI sessions to increase task unpredictability. Possibly, scopolamine affects attentional parameters when the cognitive load is increased. Alternatively, scopolamine effects may be rat strain-dependent, similar to effects of nicotine in the 5-CSRTT[176].

In the TR protocol, scopolamine also increased omission rate and decreased number of started trials throughout the entire 2.5-h duration of the session, suggesting decreased motivation. This could indicate that scopolamine impacts cognitive functions for a short period after injection, whereas its effects on motivation are longer-lasting. Reduced motivation may also be the main effect of scopolamine in the UA protocol, where we only found an increase in correct-response latency and no effect on accurate choice and premature responding. This finding is in contrast with the results in the TR protocol in rats and findings in mice where scopolamine did affect impulsivity and attentional processes in the SP-5-CSRTT[23]. We hypothesize that the lower number of started trials in a specific time bin and the higher level of omissions in the UA protocol reflect diminished engagement in the task as mentioned above. This would make the UA protocol less valid for pharmacological testing than conventional 5-CSRTT or the TR protocol, especially for drugs with a short half-life like scopolamine. Careful consideration for the selection of training and testing protocol is thus necessary based on the research question.

One remaining question is how the SP-5-CSRTT contributes to habitual versus goal-directed responding in this task compared with conventional training. Learning of this task is based on reinforcement and continuation of similar task contingencies after reaching criterion performance results in stimulus-response habits or overtraining[177]. This habitual form of responding lacks signs of cognitive contributions and exhibits insensitivity to value of the outcome and to changes in action-outcome contingencies[178,179]. To our knowledge, the transition from goal-directed behavior to habitual responding has not directly been studied in the 5-CSRTT, by, for instance, changing action-outcome contingencies, i.e., by rewarding only 50% of correct responses and assess effects on performance. Since the SP-5-CRTT protocols allow the animals to perform more trials per day, they will potentially overtrain more quickly in the task. We therefore recommend that

testing of pharmacological compounds takes place in cognitively challenging sessions, which require the animal to break fixed response routines.

A potential caveat of the SP-5-CSRTT is that rats were housed individually in CombiCages. Social isolation in rats can lead to increased stress levels and altered neuroendocrine state, particularly during early weaning[180–182], which has been found to impact executive functions in rats[183,184]. Notably, these effects are most pronounced when social isolation occurs following early weaning, for instance starting at postnatal day 21. Our SP-5CSRTT training started when animals were at least 63 days old. It has recently been shown that prolonged individual housing of adult rats did not influence corticosterone concentration, hippocampal long-term potentiation measurements, and object place recognition[185]. Combined with the restricted amount of experimental time, self-paced training, and less food restriction, stress effects are most likely limited in SP-5CSRTT. Social housing and home-cage testing can be combined in rats[165] and are important points of improvement of the SP-5-CSRTT. Secondly, the accelerated learning rate and format of the task might influence the neurobiological correlates of behavioral performance when compared with the conventional 5-CSRTT. Nevertheless, home-cage-based training of rats in the SP-5-CSRTT provides a rapid and reliable alternative for conventional training in the task to measure attention and motor impulsivity. The short training time opens up new possibilities and allows, for instance, specific testing of young or adolescent rats, which in the conventional paradigm is not possible due to time constraints. Thereby, SP-5CSRTT is highly suited to address questions involving pharmacological challenges or to investigate the physiological mechanisms of attention and motor impulsivity during limited time windows.

METHODS

ANIMALS

For training and testing in CombiCages, 36 male Long Evans rats (Janvier Labs, France, 8 weeks old) were initially housed in pairs with food and water available ad libitum 1 week before the start of experiments. Next, animals were housed individually in CombiCages, and behavioral procedures were initiated. Rats were housed under a 12-h light/dark cycle (lights off at 12 PM). For the conventional 5-CSRTT training, 14 male Long Evans rats (Janvier Labs, France, 8 weeks old) were housed individually. Food restriction began 1 week prior to behavioral training to achieve and maintain 85–90% of free feeding weight. Animals were trained daily for 5 days per week (Monday-Friday) as described in Luchicchi et al. (2016). One animal in the time-restricted (TR) group became sick after training and variable-ITI sessions and was excluded for the variable-SD session and scopolamine experiments. All experimental procedures were in accordance with the European and Dutch law and approved by the animal ethical care committee of the VU University and VU University Medical Center.

SP-5-CSRTT TASK

For construction of CombiCages, a standard makrolon home-cage was connected to an operant box (Med-Associates Inc., St. Albans, VT, USA) with a custom-made polymer tube with a diameter of 10 cm. Operant chambers were on one side equipped with five cue holes, containing LED stimulus lights and infrared beam detectors. On the opposite wall, a food magazine, a red magazine light, and a yellow houselight were placed (**Figure 1**). Rats were placed in CombiCages 2 days before the experiment started, and food was available ad libitum. After the start of the task, animals earned their food in the form of pellets in the task (Dustless Precision Pellets, grain-based, F0165, 45 mg, Bio-Serve, USA). Animals were weighed each day before onset of the dark cycle. Animals were not food restricted prior to the start of the training. If rats did not earn enough pellets to gain weight according to an 85–90% food restriction regime, additional chow was given. In the present study, no additional chow was necessary during training, animals in the TR-group were fed extra chow after training to keep stable grow and performance during pharmacological testing.

For training in the SP-5-CSRTT, the same training stages were applied as in conventional 5-CSRTT training[23]. First, animals learned to associate pellet delivery with reward during magazine training, and during 50 trials, a pellet was delivered after a variable inter-trial interval (ITI) of 4, 8, 16, or 32 s. Reward availability in the task was signaled by the magazine light, and collection of pellets triggered the next trial start. In the subsequent training stage, all five stimulus lights were lit until a nose-poke response was made in one of them to earn a reward. After 50 trials, animals moved on to the next stage. Here, a nose-poke response in the food magazine started an ITI period of 5 s followed by presentation of randomly selected single stimulus light. A nose poke into the lit cue hole was rewarded with a pellet; incorrect nose pokes were not punished.

In the next stage, rats started trials with a nose poke in the food magazine, starting an ITI of 5 s. Subsequently, one of the 5 cue holes was lit for a certain SD. Initially, SDs were 16 s and were titrated down in five steps to 1 s for the final stage. Rats had to make a response in the lit stimulus hole during stimulus presentation or within a 2-s limited hold period after stimulus presentation. A lack of response was considered an omission and resulted in a time-out period of 5 s. Incorrect and premature responses, during the ITI, also resulted in a time-out period of 5 s. Additionally, these errors were signaled with the houselight that was switched on for the duration of the time-out period. Correct responses were rewarded with a food pellet. After reward collection in the food magazine, rats could start the next trial 5 s later with a subsequent nose poke in the food magazine. We refer to the period of reward collection before start of the next trial as the "eat-interval."

For the SP-5-CSRTT protocols, the performance criterion to reach a following stage with shorter SD was a minimum of 50 started trials with accuracy levels (ratio of correct and incorrect responses, see below) > 80% and either omissions < 20% or number of correct trials > 200 in the current stage. These parameters were calculated online during task performance using a sliding window of 20 trials on which accuracy levels and percentage omissions were calculated. This approach was based on recent work in mice[23]. If the animal passed the performance criterion in this block of 20 trials analyzed by the sliding window, the program automatically moved to the next stage[23].

Two different groups were trained in CombiCages with different trial availabilities. In the unlimited access (UA) protocol, animals could initiate trials 24 h per day, whereas in the TR protocol, rats could only start trials during the first 2.5 h of the dark cycle. To examine effects of manipulation of task parameters, both groups were subjected to a session with variable ITIs (5, 7.5, or 12.5 s) or variable SDs (0.2, 0.5, or 1 s). These sessions comprised of a block of 500 trials for the UA group and a 2.5-h session for the TR group.

In the conventional 5-CSRTT group, rats were trained in the same training stages as described for the home-cage protocols. The criterion to move on to the next stage was set at accuracy > 80% and omissions < 20%. Performance was calculated after each half-hour session.

DRUG ADMINISTRATION

Scopolamine hydrochloride (Sigma-Aldrich, St. Louis, MO, USA) was dissolved in 0.9% saline and injected intraperitoneally (i.p.) 20 min prior to the start of the dark phase. Scopolamine was freshly prepared on each test day, and doses were administered using a Latin square design on Monday, Wednesday, and Friday. Animals continued with training on Tuesday, Thursday, Saturday, and Sunday.

DATA ANALYSIS AND STATISTICS

All data were acquired with MED-PC software (Med-Associates, USA). Data analyses and statistics were done with custom-written scripts in MATLAB (Mathworks, USA). Accuracy was calculated a: (#correct) / ((#correct + #incorrect) * 100). Omissions and premature responses were expressed as percentage of the total number of trials. Correct-response latency was expressed as the time in seconds between stimulus onset and a correct response. Magazine latency was expressed as the time in seconds between the correct response and pellet collection. Trials with a magazine latency > 10 s were excluded from further analysis. Normality of the data was tested with the Shapiro-Wilk test.

For comparison of training time and the number of required trials per training stage in the different groups, a Wilcoxon rank-sum test and two-way mixed

repeated-measures ANOVA were used with group as between-subjects factor. Post hoc testing was performed using Wilcoxon rank-sum tests or t tests with Benjamin-Hochberg false discovery rate (FDR) to adjust p values for multiple comparisons[186].

To compare baseline performance between groups, a block of 500 trials at SD1 for the UA group after passing SD1 criterion was compared with a 2.5-h session of SD1 trials for the TR group. Additionally, we compared baseline performance of the first 100 trials of the dark cycle for the TR and UA protocol with the CT baseline session. For both analyses, t tests or Wilcoxon rank-sum tests were performed.

Behavioral challenges with variable ITI or SD were only performed in the SP-5-CSRTT protocols and were analyzed using two-way mixed repeated-measures ANOVAs. To test differences in the number of started trials, accuracy, premature responses, and omissions between the dark period and light period for the UA group, t tests on grand means were performed.

The effect of scopolamine was tested in 2.5-h variable-ITI sessions (TR group), or data from the first 2.5 h in the dark cycle was analyzed (UA group). 2.5-h sessions were split in 30-min blocks for analyses. For the different behavioral parameters, two-way mixed repeated-measures ANOVAs were employed with dose and time as within-subject factors. Post hoc testing was performed with FDR-controlled t tests or Wilcoxon rank-sum tests. In all cases, the significance level was set at $p < 0.05$.

Sybren F. de Kloet[1], Bastiaan Bruinsma[1], **Huub Terra**[1]
Tim S. Heistek
Emma M.J. Passchier
Alexandra R. van den Berg
Antonio Luchicchi
Rogier Min
Tommy Pattij
Huibert D. Mansvelder

[1]shared first authorship

IN PREPARATION AS

S.F. de Kloet, B. Bruinsma, **H. Terra**, T.S. Heistek, E.M.J. Passchier, A.S. van den Berg, A. Luchicchi, R. Min, T. Pattij, H.D. Mansvelder. Bi-directional command of cognitive control by distinct prefrontal cortical output neurons to thalamus and striatum.

CHAPTER 4

Bi-directional command of cognitive control by distinct prefrontal cortical output neurons to thalamus and striatum

ABSTRACT

Psychiatric disorders often involve dysfunctional top-down cognitive control of behavior. The medial prefrontal cortex (mPFC) steers goal-directed actions and withholds inappropriate behavior. Dorsal and ventral mPFC (dmPFC/vmPFC) circuits have distinct roles in cognitive control, but underlying mechanisms are poorly understood. In this study, we provide anatomical, behavioral, and neurophysiological evidence for distinct roles of four distinct prefrontal projection populations in behavior. We used neuroanatomical tracing techniques, chemogenetics, fiber photometry and in vitro electrophysiology to characterize dmPFC and vmPFC outputs to distinct thalamic and striatal subdomains and show that they have dissociable roles in cognitive control. We identify four spatially segregated projection neuron populations in the mPFC. Chemogenetic silencing shows that dmPFC and vmPFC projections to lateral and medial mediodorsal thalamus subregions oppositely regulate cognitive control. In addition, superficial and deep layer dmPFC neurons projecting to striatum and thalamus divergently regulate cognitive control. Using fiber photometry, we show that these projections distinctly encode behavior. Finally, we show that postsynaptic striatal and thalamic neurons differentially process synaptic inputs from dmPFC and vmPFC, highlighting mechanisms that potentially amplify distinct pathways underlying cognitive control of behavior. Collectively, we show that mPFC output circuits targeting anatomically and functionally distinct striatal and thalamic subregions encode bi-directional command of cognitive control.

INTRODUCTION

Cognitive control involves the ability to suppress undesirable actions and remain attentive to relevant stimuli. The medial prefrontal cortex (mPFC) is highly involved in these processes, as shown in lesion, pharmacological, optogenetic and chemogenetic experiments[20,38,39,158]. Distinct neuronal activation patterns across mPFC subregions, cell types, and behavioral subdomains often underlie cognitive control[20,41,123]. However, there is substantial heterogeneity in timing, location and origin of brain activity associated with behavior[187]. Cortical cells, including mPFC neurons, can be classified based on their projection target and transcriptomic profile[60,188,189]. Functional studies have established a role for projection-specific mPFC populations in goal-directed behavior[65,190]. This suggests that studying the function of projection-specific neurons may lead to better understanding of the role of specific neural populations and circuits in cognitive control.

Several downstream targets of the mPFC are associated with cognitive control. The mediodorsal thalamus (MD) contains lateral and medial subregions (MDL/MDM), which are reciprocally connected to the ventral mPFC (vmPFC) and dorsal mPFC (dmPFC), respectively. These circuits maintain activity during cognitive control[56,62,76,77,191]. Likewise, the dorsomedial and ventromedial striatum (DMS/VMS) have both been linked to impulse control and attention[10,192] and receive input from the dmPFC and vmPFC, respectively. Moreover, specific mPFC-DMS projections are linked to development of cognitive control and show ramping during preparatory attention[53,190], whereas mPFC-VMS projections are associated with anticipation and reward processing during cognitive control tasks[21,64,65]. This indicates that prefrontal populations can be separated based on projection target and that they are distinctly involved in behavior. However, the role and timing of activity of these projections in cognitive control is unknown.

We provide evidence for the existence of four distinct prefrontal projection populations. We used neuroanatomical tracers and retrograde viruses to identify corticothalamic and corticostriatal projection neurons. We then trained rats in a self-paced 5-choice serial reaction time task (SP-5-CSRTT[23]) and inhibited each projection population. In a separate group of rats, we investigated temporal

dynamics of brain activity during task performance. Finally, we measured post-synaptic responses to prefrontal stimulation in striatal and thalamic neurons. Based on literature, we expected differential involvement of two corticostriatal and two corticothalamic projection populations. Collectively, we here demonstrate a distinct role for each projection population in cognitive control.

RESULTS

DISTINCT DISTRIBUTION OF PREFRONTAL PROJECTION NEURONS

Pyramidal neurons projecting to the thalamus and striatum are located in the vmPFC and dmPFC[60,188]. However, whether these neurons have distinct targets is unclear. Therefore, we first expressed eYFP in the dmPFC or vmPFC and observed axonal eYFP expression in MD and striatum subdomains (**Figure S1A-D**). We next infused retrobeads in subdomains with a high degree of eYFP-positive axons. Quantification of labeled mPFC somata across three anterior-posterior-locations revealed a gradient of retrobead-positive neurons along the dorsoventral axis, as well as a gradient across cortical layers. We found that 90 ± 2.25% of MDL-projecting neurons were located in dmPFC areas, with the remaining cells located in the vmPFC (**Figure 1A**), and 81 ± 3.07% of all MDM-projecting neurons were found in the vmPFC with the remaining neurons situated in the dmPFC (**Figure 1B**). mPFC neurons projecting to the MD were primarily found in deep layers, while striatum-projecting mPFC neurons were located in superficial layers. 82 ± 1.6% of all DMS-projecting neurons were located in the dmPFC with the remaining part being in the vmPFC (**Figure 1C**), and 75 ± 1.98% of all VMS-projection neurons were located in the vmPFC with the remaining neurons located in the dmPFC (**Figure 1D**). Layer distributions of MDL- and DMS-projecting neurons in the dmPFC, and MDM- and VMS-projecting neurons in the vmPFC were significantly different (MDL/DMS: $p < 0.0001$; MDM/VMS: $p < 0.0001$). Neuron distribution revealed by retrobead labeling was confirmed by injection of retrograde CAV2-Cre in target areas combined with cre-dependent eYFP expression in the mPFC (**Figure S1E-H**).

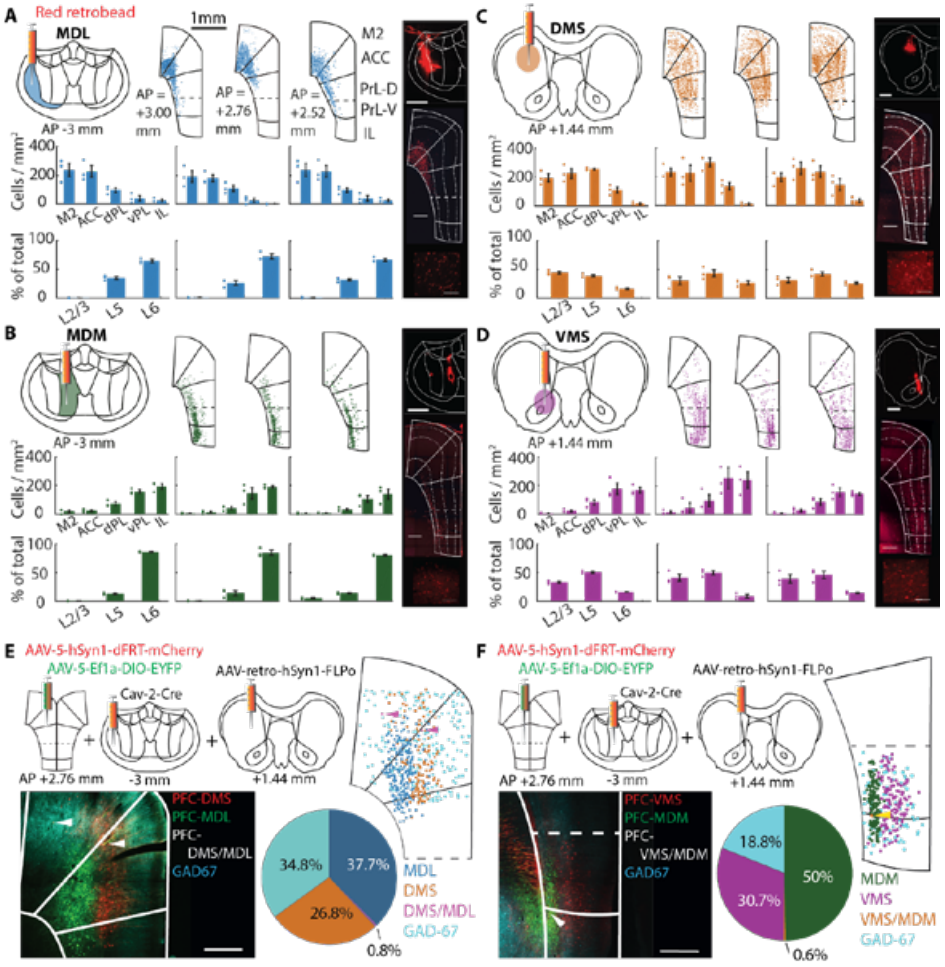

***Figure 1**. Distinct distribution of prefrontal projection neurons.*

(**A**) Distribution of MDL-projecting neurons at three mPFC locations (anterior-posterior (AP) locations relative to bregma. Top left: retrobead injection location at AP. Top middle: somata labeled by retrobeads injected in MDL. Middle row: Labeled neuron distribution across prefrontal areas. Bottom row: Neuron distribution across mPFC layers. Top right: retrobead labeling in MDL. Scale bar 500 µm. Middle right section: mPFC with labeled cells. Scale bar 500 µm. Bottom right: close-up of cell bodies in mPFC. Scale bar 200 µm. (**B-D**) Similar to (A), but for MDM-projecting neurons (**B**), DMS-projecting neurons (**C**), and VMS-projecting neurons (**D**). (**E**) Distribution of thalamus and striatum-projecting mPFC neurons in dmPFC. Top left: virus injection protocol. Bottom left: antibody staining for eYFP, mCherry and GAD67. Neurons that project to both target areas marked with arrow heads. Top right: distribution of labeled neurons in dmPFC. Arrow heads mark neurons expressing both eYFP and mCherry. Pie chart: quantification of projection neurons in dmPFC (blue: MDL-projecting neurons, purple: DMS + MDL-projecting neurons, orange: DMS-projecting neurons, blue: GAD67-positive neurons). Scale bar 500 µm. (**F**) Same as (E), but for vmPFC neurons projecting to VMS and MDM. Pie chart: quantification of projection neurons in mPFC (green: MDM-projecting neurons, orange: MDM + VMS-projecting neurons, purple: VMS-projecting neurons, blue: GAD67-positive neurons). Scale bar 500 µm. Dots represent individual cells; bar graphs represent mean ± SEM. N = 3 animals for groups in (A-D); n = 2 animals for groups in (E and F).

Cortical neurons can project to multiple target regions through axon collaterals[70,194]. Moreover, while projection neuron location was biased to layers, the layers did not exclusively contain neurons projecting to a single target area (**Figure 1A-D**). To test whether single neurons project to multiple regions, we separately injected CAV2-cre and retro-FLPo in the MD and striatum combined with cre-dependent eYFP expression and FLPo-dependent mCherry expression in the mPFC (**Figure 1E** and **1F**). Only a minority of dmPFC neurons (0.8%) and vmPFC neurons (0.6%) were positive for both mCherry and eYFP (**Figure 1E** and **1F**), suggesting that the vast majority of neurons specifically project to either thalamus or striatum. Additionally, no eYFP- or mCherry-positive neurons were positive for GAD67. Together, these data show that the majority of MD- and striatum-projecting mPFC neurons form distinct pyramidal neuron populations.

BI-DIRECTIONAL CONTROL OF IMPULSIVITY BY MPFC PROJECTION NEURONS

The mPFC, MD and striatum regulate cognitive control of behavior[10,76,77,158], but the role of specific mPFC projections to MD and striatal subdomains is incompletely understood. We expressed the inhibitory DREADD-receptor hM4D(Gi) in each projection population to test whether they are causally involved in cognitive control (**Figure 2A**). Clozapine-N-Oxide (CNO) elicited membrane potential hyperpolarization, increased rheobase, and decreased spike frequency under current step injections in acute mPFC brain slices of hM4D(Gi)-expressing animals (**Figure S2**). We then expressed hM4D(Gi) in each projection population and trained animals the SP-5-CSRTT[193]. Animals could earn food rewards by withholding responses until a visual cue appeared randomly in one of five cue holes (**Figure 2B**). Premature responses made before cue onset were used as a measure for inhibitory control, whereas the ratio of correct and incorrect responses, as well as omissions, were used as a measure for attention (**Figure 2B** and **2C**). On test days, we either randomly varied cue durations or delays between trial start and cue presentation, to increase cognitive load and avoid overtraining[17,193]. Animals performed over 400 trials per 2.5-hour session in these conditions (**Figure 2D**). Premature responding consistently increased with longer delay duration (**Figure 2E** and **2F, Table S1**), while trials with shorter cue duration decreased accuracy and increased omissions (**Figure S3A, Table S1**).

CNO-mediated inhibition of MDL-projecting mPFC neurons decreased premature responding, especially in trials with long delays (**Figure 2G**; values relative to saline condition). Additionally, we observed a delay-independent increase in omissions (**Figure 2H, Table S1**). To test whether CNO effects persisted the entire 2.5 h session, we analyzed sessions in five 30-minute blocks. The decrease in premature responses and increase in omissions were consistent (**Figure S3C** and **S3D**), indicating that CNO effects lasted throughout entire sessions. In contrast to inhibition of MDL-projecting neurons, perturbation of vmPFC-MDM projections dose-dependently increased premature responding, but we found no change in omissions (**Figure 2G** and **2H, Table S1**). CNO-mediated inhibition of MD-projecting neurons during variable cue duration sessions increased omissions, independent of cue duration, but did not affect accuracy or any other behavioral parameter (**Figure S3M-P, Table S1**). Parameters reflecting motivation or motor control were unaffected in all sessions (**Table S2**). Finally, no effect of CNO was observed in the eYFP control group (**Figure 2G** and **2H, Table S1**). Together, these data show that mPFC projections to thalamic subdomains have opposite roles in cognitive control: inhibition of vmPFC-MDM projections increases premature responses, whereas inhibition of dmPFC-MDL-projecting populations reduces premature responses.

Inhibition of DMS-projecting dmPFC neurons in the variable delay protocol increased premature responding, but did not affect omissions (**Figure 2I, Table S3**), while inhibition of vmPFC-VMS projections did not affect premature responses, omissions or any other behavioral parameter in the task (**Figure 2J, Table S3** and **S4**). During variable cue duration sessions, CNO had no effect on accuracy (**Figure S3, Table S3** and **S4**), and additional behavioral parameters such as premature responses, response latencies, and number of started trials were also unaffected (**Table S1** and **S2**), suggesting that inhibitory control, motivation and task engagement of animals were unaltered.

Altered premature responding can reflect changes in temporal strategies or perception[168]. However, we found no effect of CNO on the temporal distribution of premature response latencies in long delay trials (**Figure S3G-L**), suggesting

that temporal structure of responding was unaffected. Thus, while dmPFC projection neurons to MD and striatum bi-directionally regulate cognitive control, in the vmPFC only projection neurons that target the thalamus regulate cognitive control. Thereby, dmPFC and vmPFC can orchestrate response inhibition in opposite manners controlling distinct thalamic subregions. In addition, dmPFC neurons in superficial and deep layers can achieve this, through opposite control of thalamic and striatal regions.

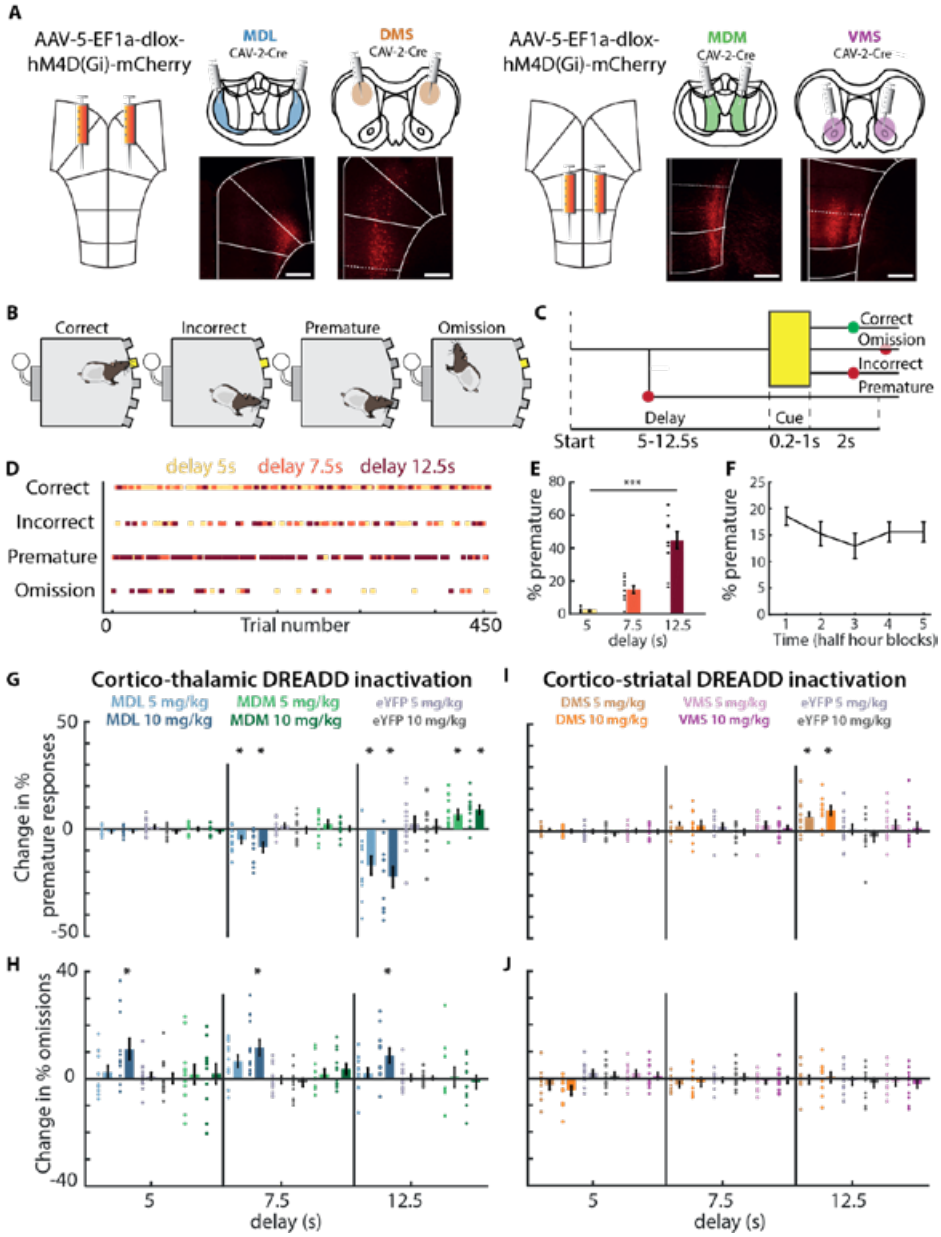

Figure 2. *Bi-directional control of impulsivity by mPFC projection neurons*

(**A**) Viral injection protocol for hM4D(Gi) expression in distinct projection neurons. Bottom right: examples of mCherry-expression in the mPFC for each group. (**B**) visual 5-CSRTT overview with all possible trial outcomes. (**C**) schematic representation of possible trial outcomes. Green dot = rewarded trial outcome, red dot = timeout. Delay period was randomly varied between 5, 7.5 and 12.5 s in variable delay sessions. Cue duration

was randomly varied between 1, 0.5 and 0.2 s in variable cue duration sessions. (**D**) Example of behavior in a typical variable delay session. Darker colors indicate outcomes of long delay trials. (**E**) Percentage of premature responses in variable delay sessions. *** main effect one-way ANOVA: $F[2,20] = 51.13$, $p < 0.001$. (**F**) Distribution of premature responses after saline and CNO injections in 2.5-hour variable delay session, divided into 30-minute blocks. (**G**) Change in premature responding of animals expressing either hM4D(Gi) in frontothalamic neurons (MDL and MDM) with different CNO doses in 5-CSRTT-sessions with variable delay times. eYFP controls also shown. FDR-corrected paired t test vs saline. MDL: group x dose x delay: $F[8,128] = 9.31$, $p < 0.001$. MDM: group x dose x delay: $F[8,128] = 9.31$, $p < 0.001$. Group sizes: MDL n = 11, MDM n = 11, eYFP n = 13. (**H**) same as (G), but for animals expressing hM4D(Gi) receptors in corticostriatal neurons (DMS and VMS), as well as eYFP control groups. MDL: group x dose: $F[4,64] = 4.25$, $p < 0.01$, group x dose x delay: $F[8,128] = 1.22$, $p = 0.29$. MDM: group x dose: $F[4,64] = 4.25$, $p < 0.01$, group x dose x delay: $F[8,128] = 1.22$, $p = 0.29$. (**I**) Change in omissions in corticothalamic populations and eYFP control groups. DMS: group x dose x delay: $F[8,124] = 2.72$, $p < 0.01$. Group size: DMS n = 10, VMS n = 12, eYFP n = 12. (**J**) same as (I), but for corticostriatal populations. Dots represent individual animals; bar graphs represent mean ± SEM.

MPFC PROJECTIONS SHOW DISTINCT ACTIVATION DURING IMPULSE CONTROL

Prefrontal neurons show various activity patterns during 5-CSRTT trails with distinct behavioral outcomes[20,21,123,192]. To determine the activation profiles of the projection populations targeting the MD and striatum during 5-CSRTT trials, we expressed GCaMP6m in each population (**Figure 3A-C**). Using fiber photometry, we recorded GCaMP6m fluorescence in several behavioral sessions, during which animals started up to 400 trials per session (**Figure 3D** and **3E, Figure S4**). Animals increased premature responding during long delay duration trials (**Figure 3F, S4**). Fluorescence changes reflecting neuronal activation recorded during behavioral trials closely followed delay period duration, with fluorescence signal elevation lasting longer during longer delay trials (**Figure 3E-G**). The area under the curve (AUC) of fluorescence between trial start and cue presentation was significantly larger in long delay-trials in all populations, indicating that increased activity was strictly related to periods of cognitive control over behavior (**Figure 3G** and **3H**). Dorsal mPFC projections showed stronger activation in the first second following trial start than vmPFC projection populations (**Figure 3I**). Ventral mPFC-VMS neurons showed little activation compared to other projection neuron populations. dmPFC neuron populations targeting thalamus (MDL) and dorsal striatum (DMS) reached peak fluorescence, defined as the first local maximum above 20% of overall peak fluorescence, faster than vmPFC projection neurons targeting the VMS (**Figure 3J**). dmPFC projection neuron populations

targeting MDL and DMS were also activated longer and for a greater portion of the delay period (**Figure 3K**), and reached higher overall fluorescence values than vmPFC neuron populations (**Figure 3L**). These results show that dorsal and ventral mPFC projection neuron populations to thalamus and striatum show distinct activation profiles during cognitive control.

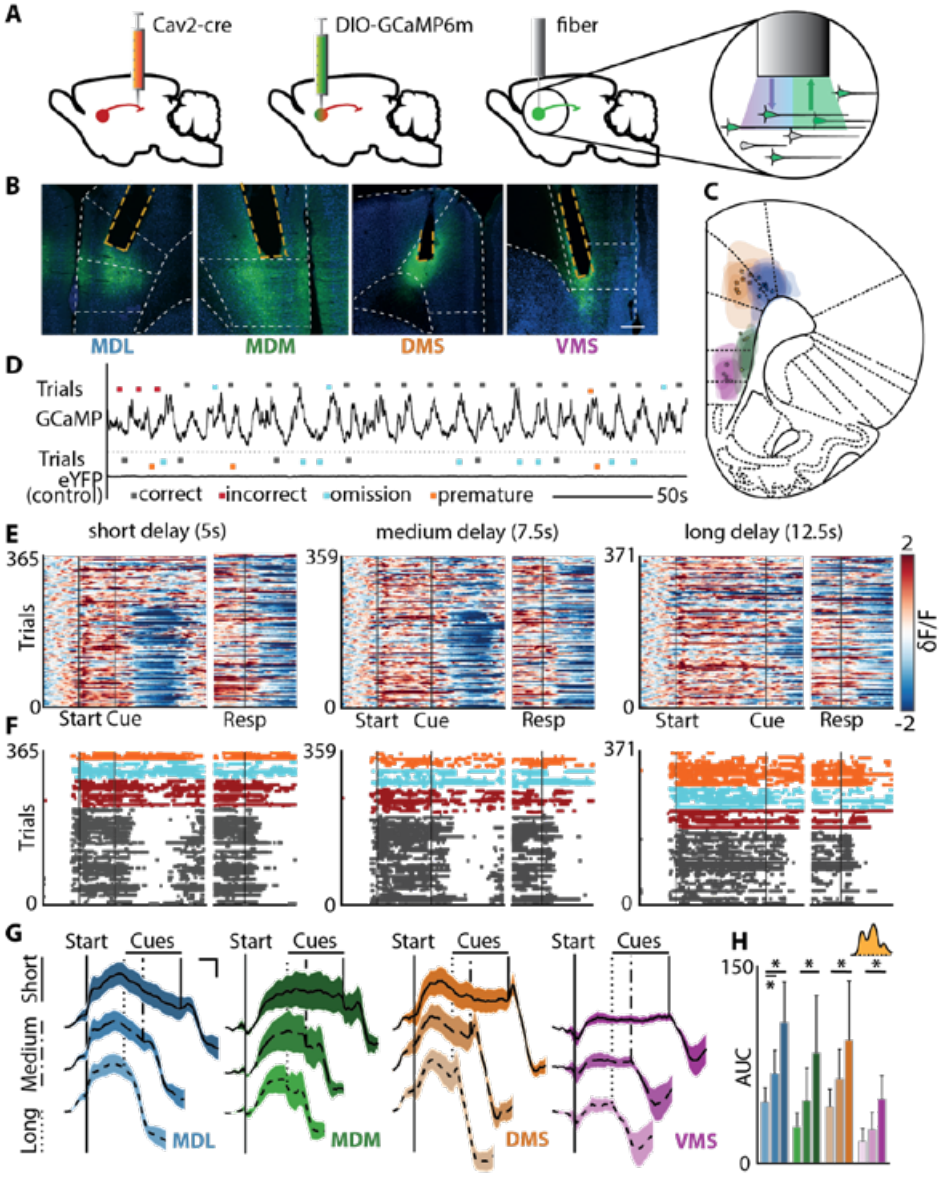

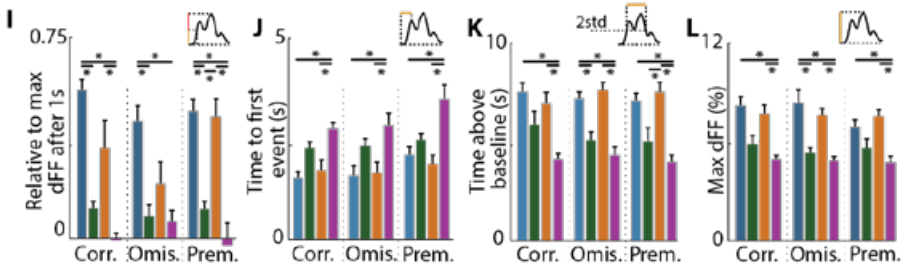

Figure 3. *mPFC projections show distinct activation during impulse control.*
(**A**) Viral injection and fiber placement protocol. (**B**) Examples of GCaMP6m-expression and fiber placement. Scale bar 400 µm. (**C**) Expression and fiber placement at AP + 2.76 mm. Shaded areas represent area of GCaMP6-expression. Stars represent fiber tip location. (**D**) Fluorescence traces from a GCaMP6m-expressing rat (top) and eYFP-expressing rat (bottom). Dots represent trial starts. (**E**) Trial traces of a variable delay session from one rat, sorted by trial outcome. Left two plots: 5 s delay trials, synchronized on trial start (left) or response (right). Middle plots: same for 7.5 s delay trials. Right plots: same for 12.5 s delay trials. δF/F is z-scored for each trial relative to baseline (5 s-1 s before each trial start). (**F**) Same as (E), but color coded based on outcome. Colors correspond to those in (D). (**G**) Average fluorescence during correct trials in each population, separated by delay duration. Shades indicate SEM. (**H**) AUC during delay for correct trials after different delays in each population. * $p < 0.01$ Dunn-Sidak multiple comparison test. * $p < 0.05$ Dunn-Sidak multiple comparison test. MDL: $\chi^2 = 9$, $p < 0.05$, delayshort vs delaylong $p < 0.01$; MDM: $\chi^2 = 8$, $p < 0.05$, delayshort vs delaylong $p < 0.05$; DMS: $\chi^2 = 12.29$, $p < 0.01$, delayshort vs delaylong $p < 0.01$; VMS: $\chi^2 = 12$, $p < 0.01$, delayshort vs delaylong $p < 0.01$. (I-L) Comparisons of signal parameters in projection populations. (**I**) Fluorescence rise kinetics during first second after trial start, expressed as fraction of peak fluorescence. Main group effect: Correct: $\chi^2[3] = 14.13$, $p < 0.001$; Omission: $\chi^2[3] = 7.18$, $p < 0.001$; Premature: $\chi^2[3] = 15.93$, $p < 0.001$. (**J**) Time to first large synchronous event after trial start (fluorescence increases to at least 20% of peak fluorescence). Main group effect: Correct: $\chi^2[3] = 6.97$, $p < 0.001$; Omission: $\chi^2[3] = 4.25$, $p < 0.01$; Premature: $\chi^2[3] = 9.25$, $p < 0.001$. (**K**) Total time fluorescence remains at least two std above baseline. Main group effect: Correct: $\chi^2[3] = 6.41$, $p < 0.001$; Omission: $\chi^2[3] = 8.07$, $p < 0.01$; Premature: $\chi^2[3] = 7.24$, $p < 0.01$. (**L**) Peak fluorescence during delay. Main group effect: Correct: $\chi^2[3] = 6.81$, $p < 0.001$; Omission: $\chi^2[3] = 12.16$, $p < 0.01$; Premature: $\chi^2[3] = 5.43$, $p < 0.001$. Group size: MDL n = 8, MDM n = 4, DMS n = 7, VMS n = 6. Bar graphs represent mean ± SEM.

ACTIVITY OF MPFC PROJECTION NEURONS ENCODES BEHAVIORAL TRIAL OUTCOME

To test whether activity patterns of specific mPFC projection neuron populations encode trial outcome, mean population fluorescence traces, synchronized z-scored δF/F traces to task-relevant events, were bootstrapped to determine periods of elevated activation during trials (**Figure 4A-C**, upper panel). MDL-, MDM-, and DMS-projecting populations each showed specific temporal windows of activation, in particular early in the delay period following trial start and before a response. vmPFC-VMS projection neurons showed no elevated fluorescence. We then tested whether the activation patterns differed between projection populations using permutation tests (**Figure 4C**, lower panel). Projection populations significantly differed in activity during several temporal windows, in particular compared to VMS-projecting neurons. Thalamus-projecting populations (dmPFC-MDL and vmPFC-MDM) showed differences in activation during the delay period in correct, omission and premature response trials, whereas dmPFC populations projecting to thalamus or striatum did not show differences in activation. vmPFC populations projecting to striatum and vmPFC-MDM neurons showed distinct activation during the delay period in omission and premature response trials. These data show that three of four mPFC projection neuron populations were activated during cognitive control of behavior with projection-specific activity dynamics.

We then asked whether these projection population-specific activation profiles contain predictive information on behavioral trial outcomes. We compared activation dynamics within each population during trials with different behavioral outcomes (**Figure 4D**), and bootstrapped differences between activity windows (**Figure 4E**, upper panel). Projection populations showed distinct windows of elevated activation during correct, omission and premature response trials during the delay period and around task-relevant events. Statistical comparison using permutation tests (**Figure 4E**, lower panel) showed that dmPFC-MDL neurons were more active during the delay in correct trials compared to premature responses, indicating that this population is associated with trial outcome. In contrast, ventral mPFC neurons projecting to the MDM showed reduced activation both during omission trials and premature response trials compared to correct

trials. Dorsal mPFC neurons projecting to the striatum showed brief predictive windows during the delay period when comparing correct response and omission trials. Together, these results show that three out of four projection populations are involved in cognitive control of behavior and they each contain predictive information to predict trial outcome.

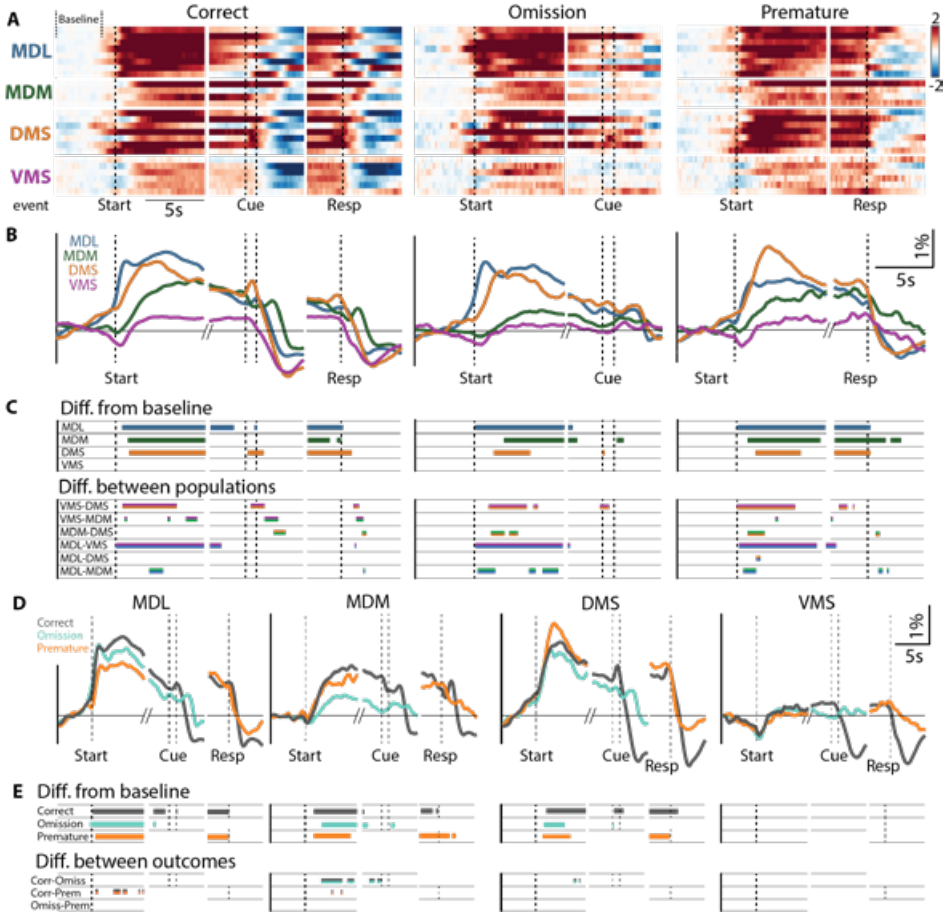

Figure 4. *Activity of mPFC projection neurons encodes behavioral trial outcome.*
(**A**) Average GCaMP6 fluorescence of each mPFC projection neuron population in individual rats during correct response, omission and premature response trials (z-scored on single-trial level relative to baseline between 5 to 1s before trial start). Plot is capped at -2 and 2 z-scores. Baseline window marked in top left. (**B**) Group average activity for each projection population during behavioral trials. (**C**) Upper: windows of significantly increased

activity during delay and around cue and response, for each projection population. Bootstrap parameters: 5000 iterations, $\alpha = 0.001$. Lower: windows with significant difference in activity between activity in the indicated mPFC projection populations. Bars represent significant permutation test results. (see Supplemental Methods for permutation test procedures). Double colored bars represent populations that were compared. Iterations: 5000, $\alpha < 0.01$. (**D**) Average activity during different trial outcomes in each projection population. (**E**) Statistical evaluation of activity. Upper: time windows with significant elevated activity during delay, and around cue and response. Bootstrap parameters same as in (C), see Supplemental Methods section for detailed procedure. Lower: windows with significant difference between activity during different behavioral trial outcomes. Bars represent significant permutation test results. Permutation test parameters same as in (C). Singleton significant data frames were discarded. Double colored bars as in (C). Group size: MDL n = 8, MDM n = 4, DMS n = 7, VMS n = 6.

DISTINCT FUNCTIONAL PROPERTIES OF MPFC OUTPUT PATHWAYS

Since prefrontal output neurons have distinct roles and activation profiles during behavior, we next asked whether striatal and thalamic target neurons also showed differential synaptic input properties and passive and active electrophysiological properties that could support differential integration of incoming information. We performed whole-cell recordings in acute thalamic slices from animals injected with AAV9-Syn-Chronos-GFP and red retrobeads in dmPFC or vmPFC, or in acute striatal slices from animals AAV9-Syn-Chronos-GFP in dmPFC or vmPFC (**Figure 5A-C**). In the thalamus, we targeted retrobead-positive, reciprocally connected neurons and recorded light-evoked postsynaptic currents. To prevent overstimulation, we adjusted light intensity of the first pulse to an intensity that resulted in half maximum peak amplitude. Excitatory inputs from both dmPFC and vmPFC neurons to thalamic neurons showed pronounced paired pulse facilitation, (**Figure 5B**). In the striatum, we targeted medium spiny neurons and recorded light-evoked postsynaptic currents. Excitatory inputs from vmPFC to VMS showed paired pulse depression, while the overall mean of dmPFC to DMS synaptic inputs showed no facilitation (**Figure 5D**).

Next, we compared passive and active electrophysiological properties of the same postsynaptic neurons in thalamus and striatum. Input resistance, membrane time constant (tau), capacitance and sag ratio were determined using hyperpolarizing steps from -70mV in current-clamp configuration. MDM neurons that were reciprocally connected to the vmPFC showed larger input resistance and larger membrane time constant compared to MDL neurons, while capacitance and sag

ratio were similar (**Figure 5E-F, Figure S5A-B**). DMS and VMS neurons showed no differences in passive and active electrophysiological properties (**Figure 5G-H, Figure S5C-D**). The input-output relationship was tested using depolarizing steps from -70mV in current-clamp configuration. In correspondence with their higher input resistance, MDM neurons showed an increased steady state action potential firing rate in response to depolarizing current steps, but no change in burst firing, compared to MDL neurons (**Figure 5I**). Both dorsal and ventral striatal neurons showed a similar increase in depolarizing current-evoked firing rates (**Figure 5J**).

These data show that synaptic inputs of prefrontal projections are processed differentially in striatal and thalamic target areas. In the thalamus, input-output properties of MDM and MDL neurons differ. Synaptic input current from the vmPFC generates larger AP frequency output of MDM neurons than dmPFC input to MDL neurons. dmPFC and vmPFC input to dorsal and ventral striatum show differences in short-term plasticity, and a similar series of synaptic inputs depresses ventral striatum neurons, but not dorsal striatum neurons. These differences in processing of dmPFC and vmPFC inputs to the thalamus and the striatum could amplify differences in activation profiles of the different mPFC output pathways during trials with distinct behavioral outcomes.

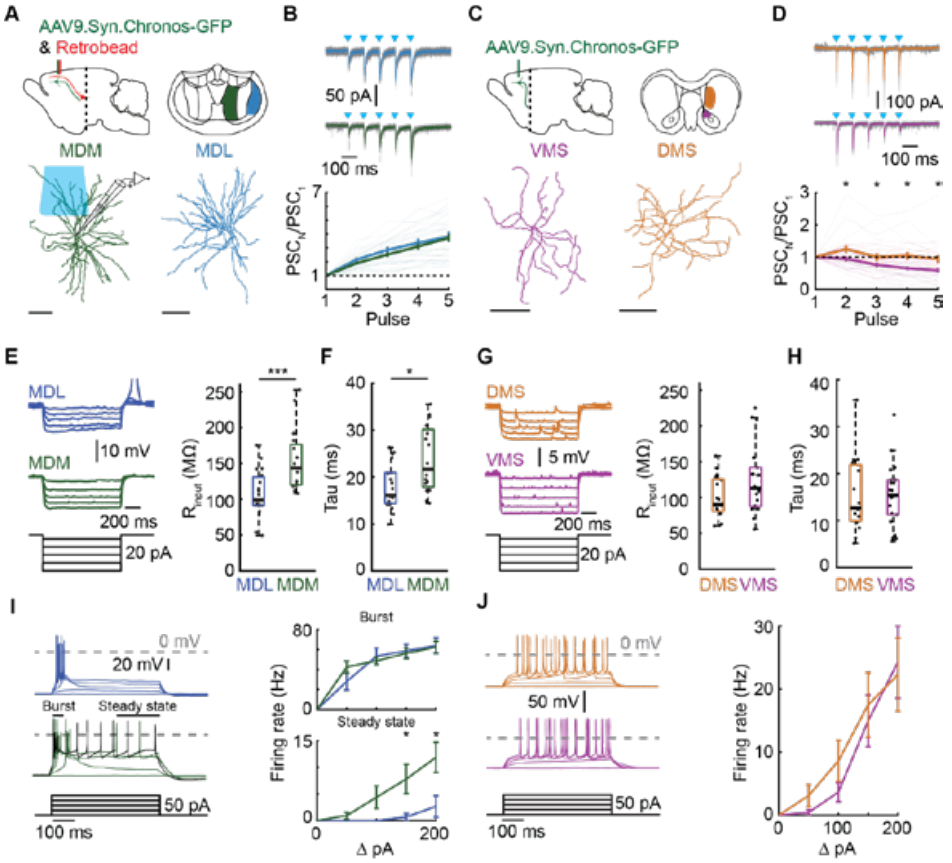

Figure 5. *Distinct functional properties of mPFC output pathways.*
(**A-D**) Synaptic input from mPFC to reciprocally-connected thalamic relay neurons and striatal medium spiny neurons. (**A and C**) Top: Schematic of virus and/or retrobead injection locations and experimental configuration. Green, MDM (18 cells, 6 rats), blue, MDL (19 cells, 7 rats). Purple, DMS (21 cells, 6 rats), orange, VMS (23 cells, 7 rats). Bottom: Digital reconstruction of recorded relay and medium spiny neurons. Scale bar 100µm. (**B and D**) Top: Example PSCs in response to blue-light-induced Chronos activation (blue squares). Grey trace, individual sweeps, solid trace, median. Stimulation protocol: 5 pulses, 10Hz, 1ms. Bottom: Summary plot of paired pulse ratios. Main pulse effect MDL: $\chi^2[4] = 62.44$, $p < 0.0001$, Main pulse effect MDM: $\chi^2[4] = 66.57$, $p < 0.0001$; PSC_1 vs. PSC_3 to PSC_5, $p < 0.05$. Main pulse effect DMS: $\chi^2[4] = 15.70$, $p = 0.0035$; PSC_1 vs. PSC_n, $p > 0.05$, Main pulse effect VMS: $\chi^2[4] = 44.90$, $p < 0.0001$, PSC_1 vs. PSC_3 to 5, $p < 0.05$; VMS vs. DMS, stim2-5, $p < 0.05$. (**E and G**) Input resistance (R_{input}). Left: example traces. Right: summary plot (MDL = 99.00 MΩ, MDM = 143.90 MΩ, U = 51.00, p = 0.0005).(**F and H**) Membrane time constant (Tau, MDL = 16.09 ms, MDM = 21.65 ms, U = 77, p = 0.0120). (**I and J**) Action potential firing profiles in response to 0 to 200 pA current steps. Left: example traces. Burst, 50 ms after first spike, Steady state, last 200 ms of pulse. Right: Summary plot for burst. Main effect MDL (burst): $\chi^2[4] = 36.95$, $p < 0.0001$, main effect MDM (burst): $\chi^2[4] = 47.32$, $p < 0.0001$; Main effect MDL (steady

state): $\chi^2[4] = 7.077$, $p = 0.1319$, main effect MDM (steady state): $\chi^2[4] = 30.01$, $p < 0.0001$; MDL vs. MDM, 150 pA: U=187, p=0.0192, 200 pA: U = 182, p = 0.0192. Main effect DMS: $\chi^2[4] = 44.39$, $p < 0.0001$, Main effect VMS: $\chi^2[4] = 69.54$, $p < 0.0001$. (B, D, I, J) Friedman test with Dunn's post-hoc and Mann-Whitney U test with Benjamini-Hochberg false discovery rate correction, * $p < 0.05$, *** $p < 0.001$. Data presented as mean ± SEM. Boxplots: center line, median; box edges, 1st and 3th quartile; whiskers, data range without outliers.

DISCUSSION

In this study, we provide anatomical, behavioral, and neurophysiological evidence for distinct roles of four distinct prefrontal projection populations in behavior. Projection neuron populations are spatially segregated in the mPFC, and inhibition of these projection neurons disrupts both cognitive control and attention. We show for the first time that mPFC projection neurons targeting distinct MD subregions have opposite roles in inhibitory control. We also show that thalamus and striatum-projecting mPFC neurons have distinct behavioral roles. Moreover, projection neuron populations showed distinct temporal dynamics that predicted behavioral trial outcome.

Prefrontal neurons are known to project to the striatum or thalamus[60,64,65] in a dorsal-to-ventral and layer-based distribution[188,190,195]. Our data further specifies prefrontal afferents into populations of excitatory neurons that specifically target subdomains of the thalamus and striatum. Additionally, inhibitory fronto-striatal projections have been reported in mice[196], we found no GAD-67 expression in projection populations. Possibly, inhibitory projections target more posterior regions of the caudate-putamen[197]. Projection-specific transcriptomic analysis of mPFC neurons[64,189,195] may resolve this issue in the future.

Superficial and deep neurons, as well as dorsal and ventral neurons within the mPFC show bi-directional effects on cognitive control during DREADD-mediated inhibition. Impulsive responding decreased after inhibition of MDL-projecting neurons, but increased after perturbation of DMS- and MDM-projection activity. Only inhibition of MDL projections increased omissions. Studies that globally perturbed mPFC function through lesions, chemogenetics, or optogenetics during 5-CSRTT generally affect attentional parameters[38,39,158]. Our results suggest that inhibiting specific projection neuron populations disentangles various aspects of cognitive control and attention behavior that are collectively affected when

manipulating large scale mPFC circuits in a non-specific manner.

Activation of mPFC neurons during the delay period of cue detection choice paradigms has frequently been reported, but timing and amplitude of activity varies between trial outcomes, target area, and task parameters[19–21,41,53]. In all projection populations, we observed that activity scaled with delay duration, indicating that each population was activated in support of cognitive control over behavior. We find that dorsal mPFC projection neurons were recruited faster than ventral-projecting neurons, and that dmPFC efferents were active for a larger proportion of the delay period. This is in line with previous findings of different activity kinetics between non-identified vmPFC and dmPFC units[41,158]. We also report differences in population activity between projection populations, and between activity levels during delay periods leading up to different trial outcomes.

Connections between the mPFC and MD are organized in recurrent loops, through which the MD can amplify local connectivity in the mPFC[56]. Both mPFC-MD projections and MD neurons have been associated with behavioral flexibility and working memory, and drive correct behavioral output in different paradigms[56,118,191]. Additionally, mPFC input to MDL neurons was shown to be required for proper rule encoding[75]. In this study, we show an opposite effect of manipulation of mPFC neurons projecting to MDL- or MDM when delay duration was unpredictable. Inhibiting mPFC to MDL neurons increased omissions. Possibly, inhibition of this projection affects rule encoding, which thereby reduces response readiness and manifests behaviorally with both a reduction of premature responses and increased omissions. Hence, activity in the MDL-projecting population could drive responsive action, while MDM-projecting mPFC neurons could relay a signal to withhold a response until a sensory event occurs.

Similar to other corticothalamic loops, MD neurons directly project back to the mPFC to maintain cortical activity[56,70,198]. We find that prefrontal input elicits a facilitating response in both MDL and MDM neurons, which may be a potential mechanism through which recurrent activity in corticothalamic circuits is maintained during a delay period, and through which these projections regulate rule

encoding[75,199]. We also find that MDL-projecting neurons are recruited earlier during the delay than MDM-projecting neurons, supporting earlier evidence that MD subregions likely have distinct roles and are part of distinct circuits. Our findings that MDL and MDM differ in basic electrophysiological features further support distinct roles in cognitive control. Additionally, we show differences between population activity before premature and correct responses in the MDL, and between omissions and correct responses in the MDM. This difference suggests that different levels of activity in this circuit can underlie distinct types of behavior.

Non-specific perturbation of both dmPFC and DMS results in increased premature responding[96], and the mPFC has been shown to exert top-down control over the DMS[53]. Our data support these findings and provides more evidence for the role of dmPFC-DMS projections in cognitive control. A potential mechanism could involve striatal dopamine. It was shown that optogenetic enhancement of mPFC excitability diminishes the striatal response to dopamine and suppresses reward seeking behavior[200], while infusions of both D1 and D2-like receptor agonists specifically in the DMS increase premature responding in the 5-CSRTT[201]. Thereby, dopamine in the DMS may increase reward seeking and impulsivity, which can be controlled by mPFC inputs in a top-down fashion.

Our results show an increase in population activity in DMS-projecting neurons during the delay period. Changes in firing rate have been reported in both mPFC and DMS during the delay before a response[21,123,202], as well as during cue presentation[190]. Premature responses have been associated with reduced amplitude of neuronal activity in the dmPFC[41]. Our data show that this population is active during the delay period and during the cue presentation before a correct response. While we did not see a reduced amplitude in the delay period before premature responses, we do see a shorter active window compared to correct responses. We also found a mixed synaptic input response in the DMS, which could be due to projection neurons differentially innervating D1- and D2-receptor expressing MSNs[102,203], or by specific topological innervation patterns seen in corticostriatal projection neurons[204].

We found no behavioral effect of inhibition of VMS-projection neurons. Previous functional disconnection studies targeting the mPFC and NAc shell, but not core, showed increased premature responding[205]. Additionally, mPFC and contralateral NAc lateral core lesions increased premature responses after an error in the 5-CSRTT, suggesting a role of this pathway in adaptive control[95]. However, we did not target a specific NAc subregion. Our neuroanatomical data shows axon terminals in the medial ventral caudate-putamen and NAc core. Additionally, the NAc core receives top-down glutamatergic inputs from several other brain regions, such as the ventral hippocampus or insula[206,207]. It has been shown that fast-spiking interneurons in the NAc core have different levels of activity leading up to correct and premature responses in the 5-CSRTT, indicating that this area is active during the task[192]. We also find that NAc neurons show a depressing response to vmPFC input, and VMS-projecting neurons do show delay-dependent kinetics of population activity, even though signal amplitude was not significantly increased from baseline. Hence, the vmPFC does project to the NAc, but it likely does not drive the behavior we studied. Whether mPFC projections to the NAc shell region are involved in cognitive control remains to be tested.

Together, our findings show a functional distinction between prefrontal projection populations, where MDL-projecting neurons represent a 'go'-signal, and MDM- and DMS-projections withhold responses during a delay period. The various projection neuron populations within the PFC can provide a combinatorial activity pattern that drives cognitive behavior and attention.

METHODS

ANIMALS

A total of 172 rats (Charles River, Den Bosch, The Netherlands; Janvier, Le Genest-Saint-Isle, France, control groups were vendor matched) were used across all experiments (overview in **Table 1**). For neuroanatomical tracing experiments, and ex-vivo electrophysiological validation, 29 male Long Evans rats (8 weeks old) were housed in pairs with food and water available ad libitum. For chemogenetic experiments, 84 male Long Evans rats (8 weeks old) were initially housed in pairs with food and water available ad libitum one to two weeks before surgeries, after which they were separated for training and testing in CombiCages[193]. Rats were housed under a 12h light/dark cycle (lights off at 12PM). For fiber photometry experiments, 29 male Long Evans rats were housed in pairs until surgery. After surgery for these experiments, animals were housed individually in CombiCages until finishing the testing protocol. For electrophysiology experiments, 26 male Long Evans rats were used, which underwent surgery at 8 weeks of age, and were then housed in pairs until the start of experiment. All experimental procedures were in accordance with European and Dutch law and approved by the central committee animal experiments and local animal ethical care committee of the VU University and VU University Medical Center (Amsterdam, Netherlands).

EXPERIMENT	GROUPS	NUMBER OF ANIMALS
Anterograde tracing	Dorsal / ventral mPFC	1
Retrograde tracing (Retrobeads)	MDL / MDM/ DMS / VMS	6 / 9 / 3 / 6
Double labeling	Dorsal mPFC + DMS + MDL / ventral mPFC + VMS + MDM	2 / 2
Ex-vivo electrophysiology	Dorsal mPFC + MDL	4
Chemogenetics (thalamus)	MDL / MDM / eYFP	16 / 16 / 14
Chemogenetics (striatum)	DMS / VMS / eYFP	12 / 14 / 12
Fiber photometry	MDL / MDM / DMS / VMS / eYFP	8 / 4 / 7 / 6 / 4
Slice electrophysiology	MDL / MDM / DMS / VMS	7 / 6 / 6 / 7
Total		**172**

Table 1. *Overview of all experimental groups and number of animals.*

VIRAL VECTORS AND TRACERS

For anterograde tracing of dorsal and ventral mPFC projections, we infused AAV2-CaMKIIα-eYFP (UPenn, USA, 0.483 µl, 4×10^{12} particles/ml). We used Red Retrobeads (0.138 µl, Lumafluor, USA) to anatomically label projection neurons in the mPFC. To retrogradely express Cre-recombinase in prefrontal projection neurons, CAV-2-Cre (IGMM, France) was infused in either DMS/VMS (0.483 µl, 1.25 × 1012 particles/ml) or in MDL/MDM (0.345 µl, 5×10^{12} particles /ml). For double labeling of projection populations, additional infusions with AAV-retro-EF1a-FLPo (0.483 µl, 1.25×10^{12} particles/ml, Addgene 55637) were performed in DMS/VMS. For double labeling with fluorophores in the mPFC, a mixture of 1µl containing AAV5-hSyn1-dFRT-mCherry (UZH, Switzerland, 3.4×10^{12} particles / ml) and AAV5-EF1α-DIO-eYFP (UPenn Vector Core, USA, 2.1×10^{12} particles / ml) was infused. The DREADD-receptor hM4D(Gi) was expressed in mPFC using AAV5-EF1α-DIO-hm4D(Gi)-mCherry (UZH, Switzerland, 0.483 µl, 3.6 × 1012 particles /ml). DREADD control animals were infused with AAV5-EF1α-DIO-eYFP (UPenn Vector, 4.2×10^{12} particles /ml). For fiber photometry, we unilaterally expressed GCaMP6m in the mPFC using AAV5-CAG-FLEX-GCaMP6m (UPenn Vector core, 0.483 µl, 4.7 x 10^{12} particles/ml). Fiber photometry control animals were infused with AAV5-EF1α-DIO-eYFP (UPenn Vector Core, 0.483 µl, 4.7 x 10^{12} particles/ml). For slice electrophysiology experiments, we unilaterally injected 278 nl AAV9-Syn-Chronos-GFP-WPRE-bGH (UPenn Vector Core, 1.13×10^{13} particles/ml) in the dorsal or ventral mPFC for DMS/VMS targeting and a mixture (~1:4, retrobead:virus) of red retrobeads and AAV9-Syn-Chronos-GFP-WPRE-bGH in the same dorsal and ventral mPFC locations for MDL/MDM experiments.

SURGERY

For all experiments, rats were anaesthetized with 2.5% isoflurane gas mixed with air and oxygen and delivered with a flow rate of 1.2 L / min. The rats were placed on a heating pad in a stereotaxic frame (Kopf, USA) and their skin of the scalp was retracted to expose the skull. A craniotomy was made at the location stated below and the virus/Retrobead infusion was done using a Nanoject II (Drummond Scientific, USA) via a glass micropipette. After the infusion, we held the pipette in place for 8 min to allow for diffusion, retracted it for 100 µm, waited 1 min,

repeated this procedure, and then finally slowly retracted the pipette to minimize virus/Retrobead leakage. The following infusion coordinates (from bregma), under a 10° angle unless otherwise indicated. DMS: Anteroposterior (AP): +1.44 mm; Mediolateral (ML): +/- 2.78 mm, Dorsoventral (DV): -4.47 mm. VMS: (AP +1.44 mm, ML +/- 2.59 mm, DV 7.41 mm + 6.8 mm). MDL: (AP -3 mm, ML +/- 2.32 mm, DV 5.89 mm). MDM: (AP -3 mm, ML 1.42 mm, DV 5.89 mm). Dorsal mPFC: (AP +2.76 mm, ML +/- 1.3 mm, DV -2.9 mm). Ventral mPFC: (AP +2.76 mm, ML +/- 1.47 mm, DV: -4.87 mm. Slice electrophysiology in MD and striatum at a 0° angle: Dorsal mPFC: (AP +2.76 mm, ML +/- 0.7 mm, DV -3.1 mm), Ventral mPFC: (AP +2.76 mm, ML +/- 0.5 mm, DV: -5.1). As indicated above in the VMS two infusions at different DV locations were made to cover the dorsal-ventral extent of this target region. Red Retrobeads and calcium indicators were infused unilaterally, whereas all other virus infusions were performed bilaterally. For the fiber photometry experiments, we implanted the fiber optic cannulas (pre-assembled from Doric lenses, NA 0.51, core diameter 400µm, fiber length 4.5mm for dmPFC targets, 5.5mm for vmPFC targets) directly after, at the same location as the virus infusions. Additionally, we attached stainless steel screws (0.7mm diameter, Jeveka) to the skull to improve headcap stability. Fibers were fixed to the skull using UV-cured dental cement (RelyX, 3M). To minimize suffering from surgeries, as an analgesic, Rimadyl (carprofen, 5 mg/kg), was administered a day before the surgery, on the day of the surgery and two days afterwards. Also, the analgesic temgesic (buprenorphine, 0.05 mg/kg) was administered once, 30-60 min before the surgery. During surgeries, lidocaine (xylocaine) was used as local anesthetic. Immediately after the surgery, before waking up, animals received 1 ml 0.9% saline.

HISTOLOGY AND IMMUNOFLUORESCENCE

Rats were anesthetized with Euthasol (AST Farma, The Netherlands) and perfused transcardially, first with 200 ml 0.9% saline followed by 300 ml of 4% paraformaldehyde. Brains were removed and kept in the same fixative for 24 h and were then transferred to PBS with 0.02% NaN_3. Coronal sections of 50 µm were cut on a vibratome. Sections from the Retrobead experiments were directly mounted on glass slides using 2% Mowiol. Immunofluorescent stainings were performed

for either NeuN, mCherry, GAD67, and GFP. We used the following antibodies: mouse anti-NeuN (Abcam, 1:1000) with Alexa Fluor 647 donkey anti-mouse (Thermo Fisher Scientific, 1:400), rabbit anti-RFP (Rockland, 1:1000) with Alexa Fluor 546 donkey anti-rabbit (Thermo Fisher Scientific, 1:400), mouse anti-GAD67 (Millipore, 1:1000) with Alexa Fluor 647 donkey anti-mouse (Thermo Fisher Scientific, 1:400), and rabbit anti-GFP (Abcam, 1:1000) with Alexa Fluor 488 donkey anti-rabbit (Thermo Fisher Scientific, 1:400). The sections were washed and permeabilized in PBS with 0.25% Triton X before being incubated for 3 h with blocking solution containing PBS, 0.3% Triton X and 5% normal goat serum. Next, sections were incubated overnight with primary antibodies in blocking solution at 4°C. The following day, the sections were rinsed with PBS and incubated with secondary antibodies in blocking solution for 2 h at room temperature. Images were acquired with a Nikon Eclipse Ti confocal microscope.

SP-5-CSRTT TASK

Elaborate descriptions of the self-paced (SP-5)-CSRTT have been described previously[193]. Briefly, we constructed CombiCages by connecting a macrolon home-cage to an operant chamber (Med Associates Inc., St. Albans, VT, USA) using a custom-made polymer tube with a diameter of 10 cm. Operant chambers were equipped with five cue holes containing LED stimulus lights and infrared beam detectors on one side. A food magazine, a red magazine light and a yellow house light were positioned on the opposite wall.

We placed the rats in the CombiCages[193] two days before the training in the task started. During training, animals earned their food in the form of precision pellets in the task (Dustless Precision Pellets, grain-based, F0165, 45mg, Bio-Serve, USA). To maintain the rats' weight to an 85-90% food restriction regime, we provided additional standard food chow.

Acquisition of SP-5-CSRTT performance was established by different training phases. First, animals learned to associate pellet delivery with reward. In this phase, for 50 trials a pellet was delivered after a variable delay. Reward was signaled by the magazine light, and a magazine response started the next trial.

In the subsequent phase, rats needed to nose poke in one of five illuminated cue holes to earn reward for 50 trials. Next, only one of the 5 cue holes was illuminated and responses into this hole after a delay of 5 s led to reward delivery. During this phase, incorrect or premature nose pokes were not punished. Animals needed to complete 100 trials in this stage.

In the final phase, the animals needed to respond to the cue after a fixed delay of 5 s. The cue hole was lit for a specific cue duration which was initially 16 s and was reduced to 1 s in five steps. The rats had to nose poke during the cue within a 2 s limited hold period after cue presentation. A lack of response was considered an omission and resulted in a timeout period of 5 s. Premature responses, nose pokes during the delay, or incorrect responses were also punished with a 5 s timeout period. Correct responses were always rewarded with a pellet.

After a correct response, animals could start the next trial 5 s after reward collection of the pellet. Importantly, animals could only initiate during the first 2.5 h of the dark cycle[193]. In this final phase, the performance criterion to reach a following stage with shorter SD was a minimum of 50 started trials, accuracy (ratio of correct and incorrect responses, see below) > 80% and either omissions < 20% or correct trials > 200 in the current stage. The program monitored these parameters online using a sliding window of 20 trials. If rats passed performance criterion, the program automatically moved to the next shorter cue duration[193].

Chemogenetic inactivation was performed in cognitively challenging sessions in which either the delay was randomly varied between 5, 7.5 or 12.5 s to test inhibitory control, or sessions in which the cue duration was varied between 0.2, 0.5 or 1 s to test attentional aspects of the task[17].

Fiber photometry sessions were performed in similarly cognitively challenging sessions. In addition, rats were also retrained to baseline performance in an operant cage without homecage attachment, which was more suited to tethered recordings.

DRUG ADMINISTRATION

Clozapine N-oxide (CNO) dihydrochloride (Hello Bio, UK) was dissolved in 0.9% saline and injected intraperitoneally 30 min prior to the start of the dark phase. Solutions were freshly prepared on each test day and doses were administered using a Latin square design. Animals received either 0, 5 or 10 mg/kg CNO, based on recent work in rats[194].

FIBER PHOTOMETRY

Rats used for fiber photometry were trained in CombiCages until baseline performance, and then recorded for 4-6 sessions, each lasting up to 150 minutes. We used a setup based on the one used by Lerner et al. 2015 (see **Figure S4B** for schematic overview), centered around a lock-in amplifier (RZ5P, Tucker-Davis Technologies, USA) that controls two excitation LEDs (405nm at 531Hz, and 490nm at 211Hz; Thor Labs M490F1 and M405F1). This setup allowed us to use the isosbestic wavelength of GFP as a control for motion-induced and other systemic noise, since the 405nm channel will contain all incoming signal except specifically GCaMP-emission. Light was then led through a filter cube (FMC4_AE(405)_E(460-490)_F(500-550)_S, Doric Lenses) into the fiber optic rotary joint. Rats were tethered to the recording setup with a patch cord (MFP_400/440/LWMJ-0.53.FC-ZF2.5, Doric Lenses) and a fiber optic rotary joint (FRJ_1x1_FC-FC, Doric Lenses). Emitted light from GCaMP6m was led back to the filter cube into a photodetector (Newport Femtowatt 2151), which then transmitted signal back to the lock-in amplifier which demodulated both incoming channels into separate signal traces. Data was then recorded on a dedicated recording PC using Synapse (Tucker-Davis Technologies). Incoming behavioral signals were also transmitted from the operant chamber to the lock-in amplifier using a Med-PC SuperPort card (DIG-726, Med Associates) and corresponding cable (CMF, Tucker-Davis Technologies). Using this system, we could reliably perform chronic recording experiments for over 3 months.

ACUTE BRAIN SLICE PREPARATION

Coronal slices of rat MD or striatum were prepared for electrophysiological recordings. Rats (4–6 months old) were anesthetized (5% isoflurane, *i.p.* injection of

0.1 ml/g pentobarbital) and perfused with ice-cold N-Methyl-D-glucamin (NMDG) solution containing (in mM): NMDG 93, KCl 2.5, NaH_2PO_4 1.2, $NaHCO_3$ 30, HEPES 20, Glucose 25, sodium ascorbate 5, sodium pyruvate 3, $MgSO_4*7H_2O$ 10, $CaCl_2*2H_2O$ 0.5, at pH 7.3 adjusted with 10 M HCl. Brains were removed and incubated in ice-cold NMDG solution. MD or striatum brain slices (250 µm thick) were cut in ice-cold NMDG solution and subsequently incubated for 15-30 min in 34°C. Before the start of experiments slices were allowed to recover for at least 1 hour at room temperature in carbogenated (95% O_2/5% CO_2) ACSF solution containing (in mM): NaCl 120, KCl 2.5, NaH_2PO_4 1.4, $NaHCO_3$ 25, Glucose 21, sodium ascorbate 0.4, sodium pyruvate 2, $CaCl_2*2H_2O$ 2, $MgCl*6H_2O$ 1[70]. All recordings were made between 31.1°C and 33.6°C.

ELECTROPHYSIOLOGY

After obtaining a stable giga seal, a ramp current was injected from 0 to 500pA to assess baseline rheobase current. Spike frequency was determined both by increasing steps of current injection and by constant supra-threshold current injection. ACSF with 10 µm CNO was washed in for at least 5 min before rheobase current and spike frequency were determined again.

For voltage- and current-clamp experiments borosilicate glass patch-pipettes (3–5 MΩ, resulting in access resistances typically between 7 and 12 MΩ) were used with a K-gluconate-based internal solution containing (in mM): K-gluconate[135], NaCl 4, MgATP 2, Phosphocreatine 10, GTP (sodium salt) 0.3, EGTA 0.2, HEPES 10 at a pH of 7.4. Reciprocally connected MD neurons were targeted using somatic expression of red retrobeads and striatal medium spiny neurons were targeted based on morphology. Data was sampled using a Multiclamp 700B amplifier (Axon Instruments) and pClamp software (Molecular Devices) at 20 kHz and low-pass filtered at 2 kHz. Neurons were filled with 2-4% biocytin for reconstruction.

Chronos-induced post-synaptic currents (PSCs) were recorded in voltage clamp at -60mV. Chronos was activated by blue light (470 nm, 10 sweeps, 10Hz, 5 pulses of 1 ms) using a DC4100 4-channel LED-driver (Thorlabs, Newton, NJ) as light source. The light source was directed as far away from the soma as possible (typi-

cally > 200 um) and the illumination area was limited using a diaphragm such that reliable but minimal activation was achieved. Light intensity was adjusted to elicit a half maximum amplitude (typically > 10 pA) of the first EPSC to prevent overstimulation of the axon boutons[70].

EXCLUSION CRITERIA

Animals with misplaced virus or retrobead infusions were excluded, as were rats for the chemogenetic experiments that had unilateral virus expression or that did not establish stable baseline performance. Additionally, for the photometry experiments, rats with misplaced fibers or no virus expression were excluded. For slice electrophysiology experiments, three outliers were removed, one had a capacitance above 500 pF, and two had a R_{input} above 340 MΩ, exclusion did not affect outcome.

CELLULAR QUANTIFICATION

For the Retrobead experiments, maximum intensity Z projections of 5 z-planes were made using ImageJ. Next, images were overlayed with a rat brain atlas at AP + 3.00 mm, +2.76 mm or +2.52 mm. Subregions of the mPFC were included as ROIs. Layers of the PFC were determined using the Swanson brain atlas and were validated with NeuN sections. Cells were counted manually using ImageJ per ROI and area of the ROIs was determined. For the double labeling experiments, composite images were created for signal from eYFP, GAD67 and mCherry. Cells were counted manually. For the DREADD experiments, the areas of virus expression were selected as a ROI in ImageJ. The area of the ROI was calculated and cells within the ROI were counted manually.

CHEMOGENETICS AND BEHAVIOR

Behavioral data were acquired with MED-PC software (Med-Associated, USA). All data analyses and statistics were done with custom written scripts in MATLAB (Mathworks, USA). We calculated the percentage accuracy as: #correct/ (#correct + #incorrect) * 100. Premature responses and omissions were expressed as a percentage of the total number of trials. All latencies were expressed in seconds. Trials with a magazine latency > 10 s were excluded from further analysis[193].

Normality of the data was tested with the Shapiro-Wilk test. Time-dependent effects of CNO were analyzed by splitting the 2.5 h session in five blocks of 30 minutes. Two-way mixed repeated measures ANOVAs were employed with time and dose as within-subject factors[193]. To compare the effects of CNO in the different projection groups, three-way mixed repeated-measured ANOVAs were employed with dose and delay or cue duration as within-subject factors and group as between-subjects factor. Additional parameters, such as number of started trials, were not dependent on delay or cue duration and effects of CNO were tested with two-way mixed repeated-measures ANOVAs with dose as within-subject factor and group as between-subject factor. Post hoc testing was done using Wilcoxon rank-sum tests or t tests with Benjamin-Hochberg false discovery rate (FDR) to adjust p values for multiple comparisons. For the neuroanatomical data, a Chi-Square independence test was used to test differences in mediolateral distributions between projection populations in dorsal and ventral mPFC. In the ex-vivo electrophysiological experiments, a non-parametric Mann-Whitney-U test was used to assess the effects of CNO on mCherry (putative DREADD)-positive cells versus control neurons. To test the effects of CNO on the distribution of premature responses, paired Kolmogorov-Smirnov tests were performed between the doses and p-values were corrected for multiple testing. In all cases, the significance level was set at $p < 0.05$. Data are presented as mean +/- SEM throughout the main text and figures and as mean +/- SD in the supplementary tables.

FIBER PHOTOMETRY

Fiber photometry data was analyzed using custom made MATLAB scripts. In short, raw data from the TDT RZ5P recording system was first corrected for motion and other systemic noise by fitting the 405nm-channel to the 470nm-channel and dividing, resulting in a raw δF/F (F being the adjusted 405nm-channel). We then lowpass filtered the signal on 1Hz and highpass filtered on 30Hz. We then performed a spectral analysis to correct for remaining low frequency noise. Finally, we down sampled the signal by a factor of 64, yielding a final frame rate of around 16Hz, which was our final δF/F. For all subsequent analyses, we used small time windows around the trial. To be able to standardize signals and look only for changes in population activity associated to the task, we aligned every

trace to a baseline period between -5 and -1 seconds before the start of each trial. Since we included a 10 second inter-trial interval after each trial where rats could not initiate a new trial, the baseline should not include any trial-related signals. To test differences in signal between delay periods, we only looked at signal between trial initiation and the cue presentation time of the longest delay (12.5s). We either used Friedman test (comparison between trial outcomes within group), or Kruskal Wallis one-way ANOVAs (comparison between groups), with post hoc Dunn-Sidak multiple comparison tests and Benjamini-Hochberg false discovery rate to adjust p values. Significance for ANOVAs was set on $p < 0.05$. To assess difference from baseline, we calculated bootstrapped confidence intervals with 5000 iterations and alpha of 0.001. In short, we randomly sampled combinations of signal traces for each outcome type for each rat and took the mean, and repeated 5000 times. We then took a confidence interval with an alpha of 0.001 of all 5000 mean traces of a given trial outcome, yielding an interval between the 99.9th and 0.01st percentile value for each data frame, which we considered as boundaries between which the signal could be. We then took averages of the upper and lower confidence interval bounds of all rats to construct the group confidence interval. To study differences between signal traces of two experimental groups or two outcomes, we performed permutation tests that compared distributions at every data point. For each data point, we considered the distributions significantly different if the alpha was < 0.01. For both the bootstrapping and permutation tests, singleton significant points (i.e. data points with no neighbors that were also significant) were filtered out of the data set. One data frame corresponded to approximately 125 ms.

ELECTROPHYSIOLOGY

Chronos-evoked PSCs were calculated by taking the median over 10 sweeps that were corrected for drift using a robust regression fit. Paired-pulse-ratios were calculated by dividing the peak of PSC_N by PSC_1. Chronos-evoked PSC latency was calculated as time to reach 80% of peak value from light onset. Input resistanc was calculated using the slope of the linear fit to the current-voltage curve using negative current steps between 0 and -100 pA (15 or 20 pA increments, 0.5 or 1 s duration), using the steady state voltage in the last 200 ms of the step. The membrane time constant tau determined by the median over fitting a first order exponential

function (only goodness of fit > 0.8 used) to the first 300 ms to the voltage trace in response to three negative current steps between 0 and 50 pA (15 or 20 pA increments, 0.5 or 1 s duration). Capacitance was calculated as input resistance over membrane time constant. Sag was calculated as the percentage difference between the Δ peak voltage and Δ steady state (last 1/5th of the step duration) from baseline in response to a negative step current (0.5 or 1 s) that elicited a Δ peak voltage closest to -20mV. Burst and steady state firing frequency were calculated based on the number APs (threshold at 0 mV) in the 50 ms after the first AP (burst) or the last 200 ms (steady state) of positive current steps between 0 and 200 pA (50 pA increments, 0.5 s duration). Some neurons were recorded with 15 pA increments, here steps with less than 5 pA difference from the 50 pA increments steps were used. Biocytin-filled neurons were reconstructed in Neuromantic software (V1.6.3) and plotted for illustrative purposes using the Neuroanatomy toolbox in ImageJ. Offline data analysis was performed in Graphpad Prism 6 and Matlab 2019a. No assumptions were made about the data distribution and all analyses were done using non-parametric Friedman with post-hoc Dunn's and Benjamini-Hochberg's false discovery rate corrected Mann-Whitney U-tests for repeated measures and Mann-Whitney U-tests for simple comparisons, significance set at $p < 0.05$.

SUPPLEMENTARY FIGURES

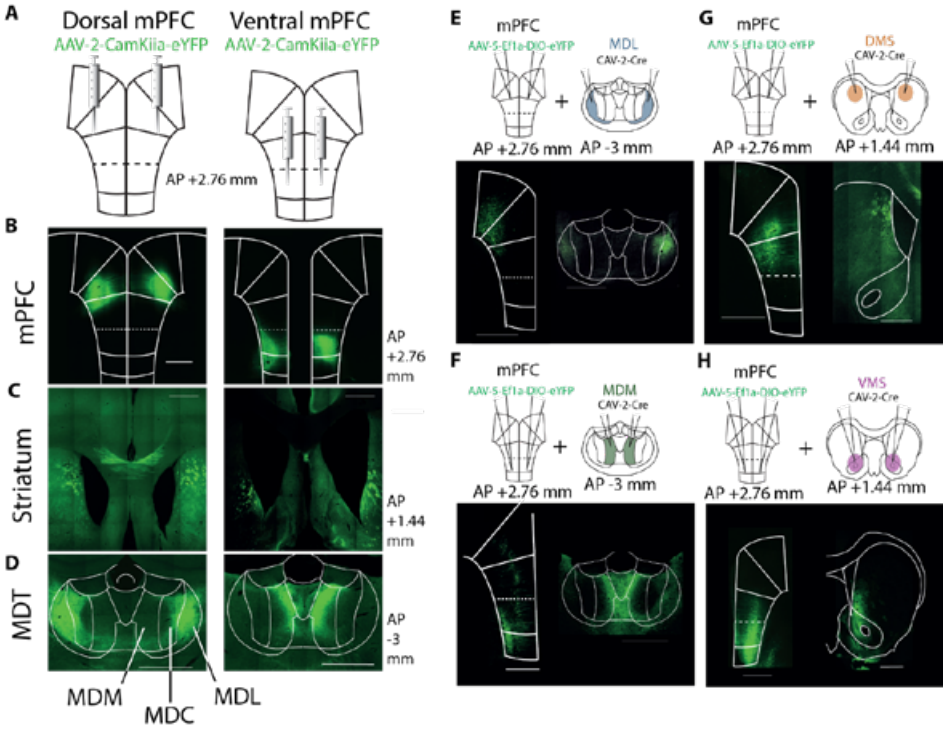

Figure S1. *Viral tracing in corticostriatal and corticothalamic projections.*
(**A**) AAV2-CaMKIIa injection protocol for anterograde tracing experiments. (**B**) Prefrontal cortex eYFP expression following dorsal (left) and ventral (right) virus injections. (**C**) eYFP expression in corticostriatal axon terminals. Left: Injections and expression of eYFP in dorsal mPFC result in eYFP positive axon terminals in dorsal striatum. Right: Ventral mPFC eYFP expression leads to eYFP positive axon terminal fields in ventral striatum. (**D**) eYFP expression in corticothalamic axon terminals. Left: In the MDT, lateral portions (MDL) show positive axon terminals following injections and expression of eYFP in dorsal mPFC. Right: Medial portions of MDT show positive axon terminals after virus injection and eYFP expression in ventral mPFC. (**E**) Top: Cav2-Cre injection protocol for retrograde tracing MDL-projecting neurons. Bottom left: eYFP expression in dmPFC. Bottom right: eYFP expression in MDL. (**F**) Same as (E), but for MDM-projecting neurons. (**G**) Same as (E), but for DMS-projecting neurons. (**H**) Same as (E), but for VMS-projecting neurons. Scale bars 1 mm.

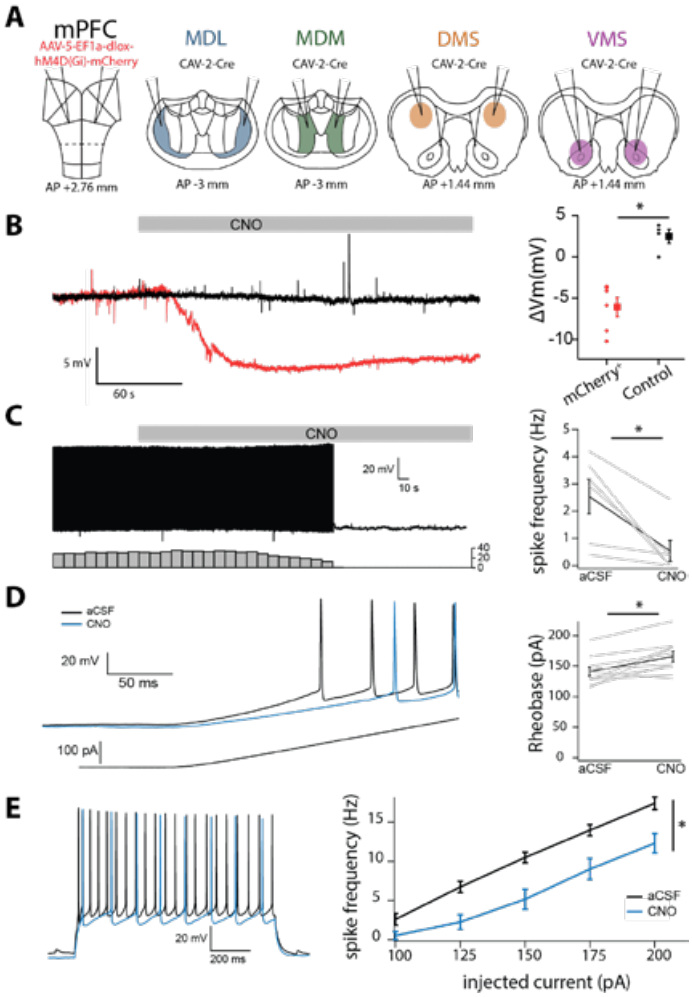

Figure S2. *DREADD-mediated hypofunction of specific PFC projection populations.*
(**A**) Experimental design for expression of hM4D(Gi) receptors with mCherry-tag in prefrontal projection populations. (**B**) Left: raw traces from a mCherry-positive and negative (control) neuron resting membrane potential before and during CNO bath application. Right: Quantification of CNO-induced resting membrane potential change. * $p < 0.05$ Mann-Whitney test. mCherry+ n = 6, control n = 4. (**C**) Left top: Raw trace from mCherry+ neuron. Left bottom: Spike frequencies in 10 s bins. Right: Quantification of spike frequency during aCSF or CNO application. * $p < 0.05$ Wilcoxon signed rank test, n = 6 cells. (**D**) Left: raw trace of mCherry+ neuron during aCSF (black) and CNO (blue) bath application. 100 pA ramp current injection. Right: rheobase quantification. * $p < 0.01$ paired t-test, n = 10 cells. (**E**) Spike frequency induced by different current steps. * $p < 0.01$ main effect bath application aCSF vs CNO, two-way ANOVA. n = 10 cells.

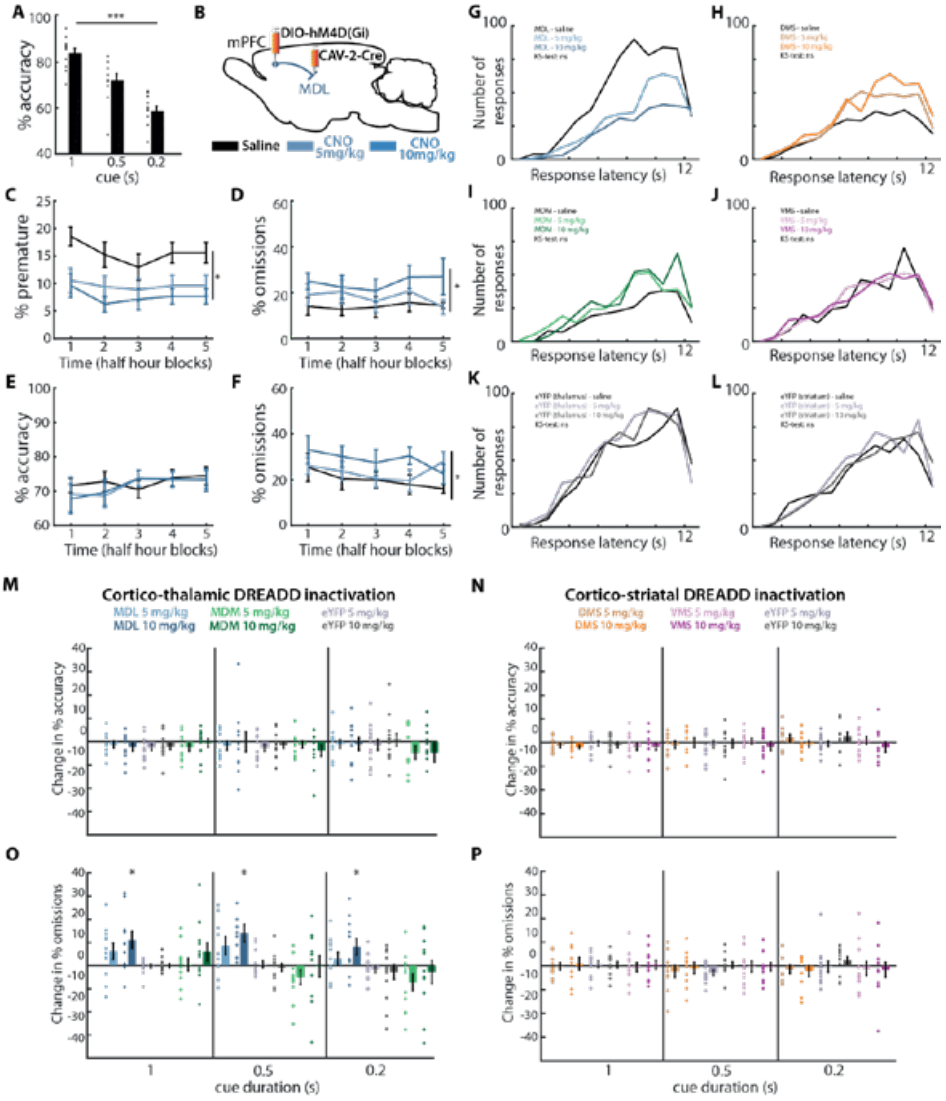
A
% accuracy
cue (s)
B
mPFC
DIO-hM4D(Gi)
CAV-2-Cre
MDL
Saline
CNO 5mg/kg
CNO 10mg/kg
C
% premature
Time (half hour blocks)
D
% omissions
Time (half hour blocks)
E
% accuracy
Time (half hour blocks)
F
% omissions
Time (half hour blocks)
G
Number of responses
Response latency (s)
H
Response latency (s)
I
Number of responses
Response latency (s)
J
Response latency (s)
K
Number of responses
Response latency (s)
L
Response latency (s)
M
Cortico-thalamic DREADD inactivation
MDL 5 mg/kg
MDM 5 mg/kg
eYFP 5 mg/kg
MDL 10 mg/kg
MDM 10 mg/kg
eYFP 10 mg/kg
Change in % accuracy
N
Cortico-striatal DREADD inactivation
DMS 5 mg/kg
VMS 5 mg/kg
eYFP 5 mg/kg
DMS 10 mg/kg
VMS 10 mg/kg
eYFP 10 mg/kg
Change in % accuracy
O
Change in % omissions
cue duration (s)
P
Change in % omissions
cue duration (s)

Figure S3. *Additional behavioral parameters after DREADD treatment duringSP-5-CSRTT.*
(**A**) Accuracy in variable cue duration sessions. ***p < 0.001, one-way ANOVA. Main effect: F[2,20] = 207.76, p < 0.001. (**B**) Virus injection protocol for expression of hM4D(Gi) receptor in MDL-projecting neurons. (**C**) Distribution of premature responses after saline and CNO injections in 2.5-hour variable delay sessions, divided into 30-minute blocks. * Main effect dose repeated measures ANOVA: F[2,20] = 11.20, p < 0.001, dose x time: F[8,80] = 1.57, p = 0.15. Only data for MDL-projecting neurons shown. (**D**) same as (C), for omissions in variable delay sessions. * F[2,20] = 8, p < 0.01, dose x time: F[8,80] = 0.92, p = 0.50. (**E**) same as (C), for accuracy in variable cue duration sessions. (**F**) same as (D), for omissions in variable cue duration sessions. (**G-L**) Cumulative premature responses displayed for the trials with a delay of 12.5 s. Number of premature responses are shown in 1 s bins. Group size: MDL n = 11, DMS n = 10, MDM n = 11, VMS n = 12, eYFP (thalamus) n = 13, eYFP (striatum) n = 12. (**M**) Difference in accuracy between CNO sessions and saline during variable cue duration sessions. Dose x group: F[4,64] = 0.26, p = 0.90, dose x group x cue duration: F[8,128]=0.79, p = 0.67. (**N**) Data from the cortico-striatal inactivation experiments, same as for B. DMS n = 10, VMS n = 12, eYFP n = 12. (**O** and **P**) Similar as panel B and C but for the change in omissions. MDL: Dose x group: F[4,64] = 3.71, p < 0.01, dose x group x cue duration: F[8,128] = 1.12, p = 0.36. Dots are individual datapoints, bar graphs represent mean ± SEM.

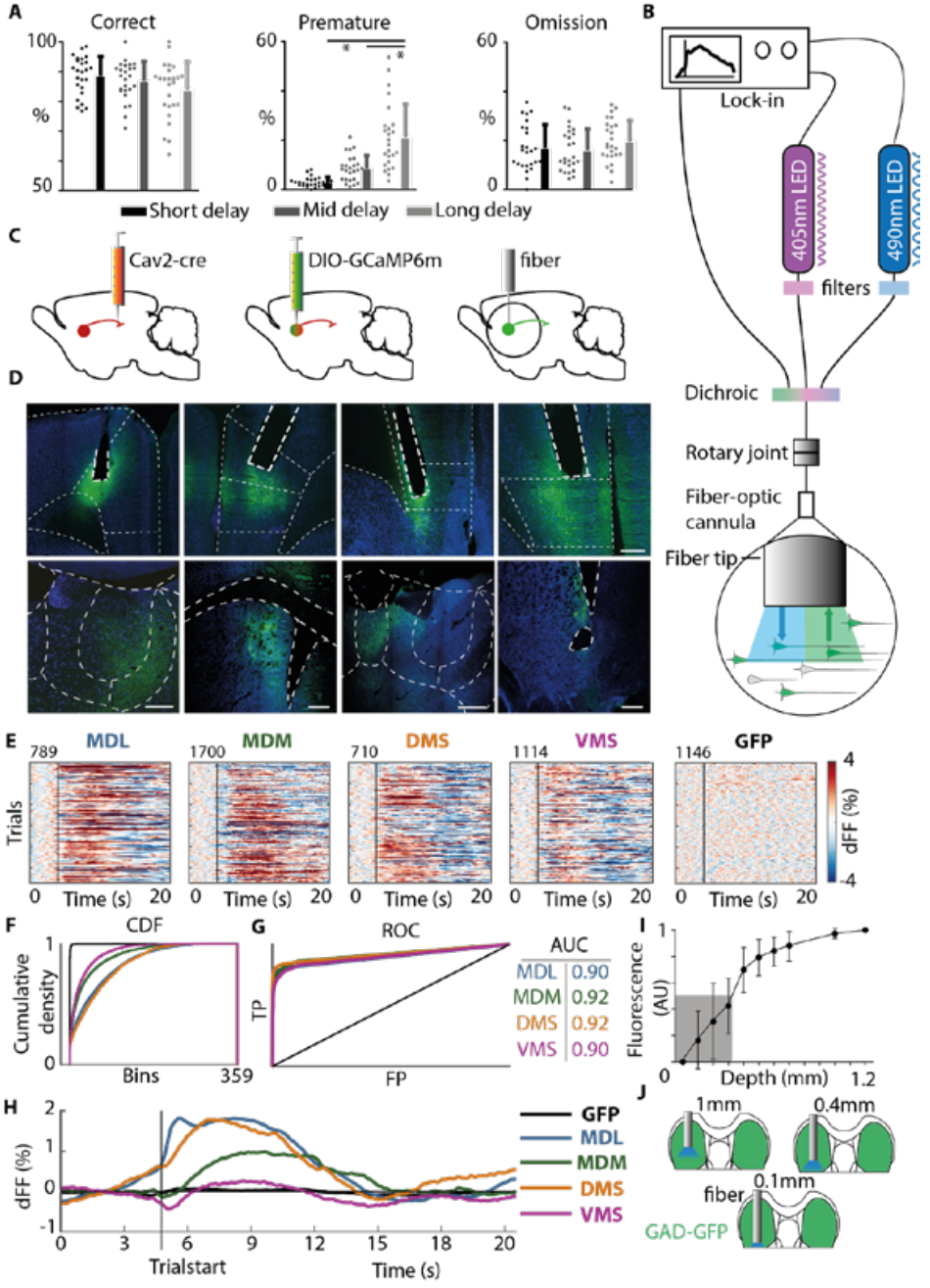
A
Correct
Premature
Omission
100
%
50
60
%
0
60
%
0
Short delay
Mid delay
Long delay
B
Lock-in
405nm LED
490nm LED
filters
Dichroic
Rotary joint
Fiber-optic cannula
Fiber tip
C
Cav2-cre
DIO-GCaMP6m
fiber
D
E
MDL
MDM
DMS
VMS
GFP
789
1700
710
1114
1146
Trials
Time (s)
0
20
4
dFF (%)
-4
F
CDF
Cumulative density
Bins
359
G
ROC
TP
FP
AUC
MDL 0.90
MDM 0.92
DMS 0.92
VMS 0.90
I
Fluorescence (AU)
Depth (mm)
1.2
H
dFF (%)
Trialstart
Time (s)
GFP
MDL
MDM
DMS
VMS
J
1mm
0.4mm
0.1mm
fiber
GAD-GFP

Figure S4. *Behavioral parameters, equipment, viral expression and signal dynamics during fiber photometry experiments.*
(**A**) 5-CSRTT performance parameters during fiber photometry recording sessions. Bars are mean +- SEM. Dots are sessions. * p < 0.01 one-way ANOVA. (**B**) Schematic representation of fiber photometry setup. (**C**) Experimental procedure for GCaMP6m expression in prefrontal projection populations. (**D**) Top: Examples of GCaMP6m expression in somata of prefrontal projection neurons. White dashed line: Brain atlas overlay. Yellow dashed lines: fiber tract. Scale bar 500µm. Bottom: Examples of GCaMP6m expression in axon terminals in target areas. White dashed lines: Brain atlas overlay. Scale bars: 500µm. (**E**) Example heatmaps for animals with either GFP (left), or GCaMP6m expressed in projection populations. Only sessions with variable delay, but all trial outcomes and delays have been pooled together. Data are z-scored to baseline (t-5 to t-1 from trial start). (**F**) Cumulative density plot for bins that are >2std above or below baseline. X axis is number of bins, Y axis is cumulative proportion of trials. (**G**) Receiver operator characteristic for trials made by GFP-expressing rats vs each projection population. AUC indicates area under curve for each population. (**H**) Population averages for GFP rats and projection populations. (**I**) Experimental procedure for determination of excitation light tissue coverage. (**J**) Proportion of fluorescence compared to maximum fluorescence measured in recording session. Grey area corresponds to 50% of maximum signal.

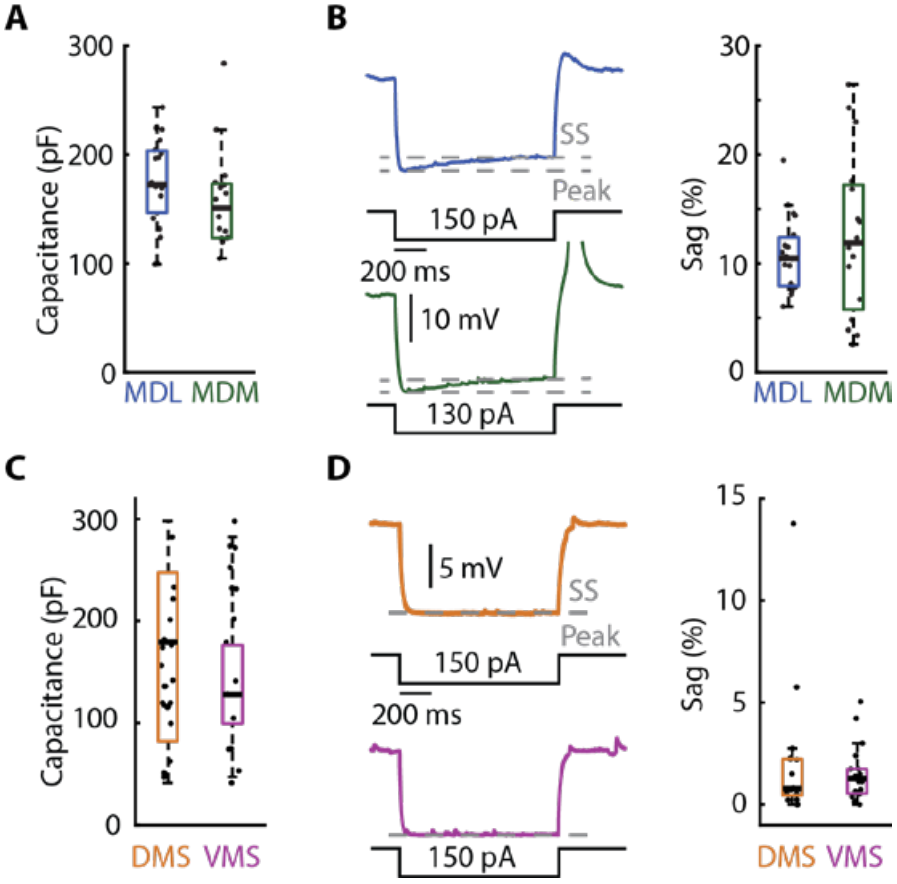

Figure S5. *Electrophysiological properties of dorsally and ventrally PFC-innervated MD and striatum neurons.*

(**A** and **C**) Capacitance. (**B** and **D**) Sag, calculated as percentage difference between Δ steady state (SS) and Δ peak from a hyperpolarizing current step resulting in a peak voltage change closest to -20mV. Left: example trace, right: summary plot. Boxplots: center line, median; box edges, 1st and 3rd quartile; whiskers, data range without outliers.

SUPPLEMENTARY TABLES

		MDL			MDM			EYFP		
	Delay/cue duration (s)	Saline	CNO 5 mg/kg	CNO 10 mg/kg	Saline	CNO 5 mg/kg	CNO 10 mg/kg	Saline	CNO 5 mg/kg	CNO 10 mg/kg
Accuracy (%)	5	86.6 ± 8.59	88.51 ± 6.22	90.88 ± 7.44	88.54 ± 9.13	85.27 ± 12.81	84.97 ± 11.59	91.45 ± 7.27	89.98 ± 6.57	89.72 ± 7.26
	7.5	85.4 ± 7.04	86.80 ± 6.18	87.07 ± 7.60	85.57 ± 11.11	83.21 ± 9.29	84.03 ± 11.33	87.29 ± 9.42	87.85 ± 7.83	86.23 ± 8.80
	12.5	80.46 ± 6.39	80.67 ± 7.57	81.61 ± 6.22	81.36 ± 12.58	78.52 ± 14.40	80.34 ± 13.35	85.09 ± 7.77	83.52 ± 9.86	82.08 ± 8.84
Premature responses (%)	5	2.38 ± 1.48	1.37 ± 1.35	1.81 ± 1.89	3.83 ± 3.85	4.01 ± 2.56	2.85 ± 3.48	4.17 ± 2.94	5.29 ± 3.96	3.12 ± 2.33
	7.5	14.70 ± 7.21	9.88 ± 6.16	6.35 ± 4.76	8.37 ± 5.95	10.90 ± 6.03	8.84 ± 6.10	12.20 ± 7.26	13.84 ± 7.46	11.87 ± 7.41
	12.5	44.78 ± 17.15	27.99 ± 16.67	22.63 ± 15.31	21.09 ± 7.93	28.02 ± 11.86	30.26 ± 10.28	31.76 ± 18.17	34.30 ± 18.94	33.26 ± 16.41
Omissions (%)	5	18.92 ± 14.55	21.48 ± 17.83	30.12 ± 19.30	27.66 ± 21.54	29.38 ± 19.24	29.63 ± 22.70	8.01 ± 5.41	9.06 ± 8.92	8.28 ± 7.58
	7.5	11.24 ± 8.82	17.90 ± 11.70	22.91 ± 14.59	20.13 ± 15.10	21.97 ± 15.15	23.88 ± 18.32	7.20 ± 5.79	7.02 ± 7.35	5.93 ± 4.23
	12.5	9.19 ± 5.76	11.28 ± 7.43	17.90 ± 11.22	15.60 ± 10.80	16.34 ± 13.44	14.41 ± 10.26	4.88 ± 3.91	5.37 ± 5.05	5.25 ± 3.52
Correct response latency (s)	5	1.06 ± 0.20	1.04 ± 0.17	1.12 ± 0.22	1.24 ± 0.38	1.22 ± 0.39	1.23 ± 0.38	0.80 ± 0.20	0.80 ± 0.19	0.80 ± 0.20
	7.5	0.98 ± 0.19	1.02 ± 0.19	1.06 ± 0.20	1.15 ± 0.34	1.09 ± 0.28	1.14 ± 0.30	0.78 ± 0.20	0.78 ± 0.18	0.79 ± 0.18
	12.5	0.96 ± 0.19	0.97 ± 0.16	1.02 ± 0.19	1.02 ± 0.29	1.00 ± 0.17	1.04 ± 0.24	0.81 ± 0.20	0.80 ± 0.19	0.78 ± 0.19

Premature response latency (s)	**5**	3.81 ± 0.41	4.20 ± 0.35	3.70 ± 0.69	3.83 ± 0.50	3.57 ± 0.76	3.76 ± 0.82	4.06 ± 0.43	3.84 ± 0.49	3.93 ± 0.40
	7.5	5.67 ± 0.48	5.76 ± 0.60	5.50 ± 0.65	5.72 ± 0.98	5.43 ± 0.62	5.41 ± 0.98	5.27 ± 0.59	5.49 ± 0.43	5.55 ± 0.64
	12.5	8.72 ± 0.47	9.22 ± 0.47	9.10 ± 1.09	8.71 ± 1.26	8.61 ± 1.40	8.90 ± 1.02	8.67 ± 0.70	8.27 ± 1.36	8.74 ± 0.66
Accuracy (%)	**1.0**	84.01 ± 7.00	82.70 ± 7.51	81.78 ± 8.98	82.24 ± 11.74	79.89 ± 8.35	81.75 ± 12.17	90.40 ± 6.35	88.02 ± 6.95	88.35 ± 6.32
	0.5	72.00 ± 9.52	70.20 ± 9.17	71.95 ± 9.83	72.17 ± 11.00	70.88 ± 9.88	68.29 ± 12.52	78.29 ± 9.76	75.76 ± 10.56	76.72 ± 10.92
	0.2	58.64 ± 6.79	57.65 ± 5.64	57.60 ± 12.32	61.70 ± 14.96	56.98 ± 8.45	57.03 ± 19.01	61.41 ± 6.6	60.07 ± 11.20	62.21 ± 10.56
Premature responses (%)	**1.0**	3.77 ± 3.39	3.38 ± 2.73	3.36 ± 1.80	5.53 ± 5.49	6.53 ± 4.27	7.42 ± 5.62	7.34 ± 5.59	7.32 ± 5.66	8.64 ± 6.16
	0.5	4.70 ± 4.19	4.13 ± 4.13	3.39 ± 2.35	5.24 ± 4.86	6.53 ± 3.98	5.34 ± 3.65	5.91 ± 3.54	6.91 ± 4.89	7.45 ± 5.60
	0.2	4.10 ± 3.68	4.81 ± 2.91	3.56 ± 1.73	5.17 ± 4.48	5.36 ± 3.05	5.77 ± 3.66	6.65 ± 4.26	7.39 ± 4.61	7.23 ± 5.99
Omissions (%)	**1.0**	19.28 ± 12.86	25.50 ± 14.40	30.32 ± 15.31	22.79 ± 18.69	23.21 ± 19.29	28.71 ± 24.95	6.27 ± 6.30	6.07 ± 4.47	6.26 ± 6.49
	0.5	25.93 ± 13.33	34.60 ± 16.90	39.97 ± 19.38	34.17 ± 22.06	29.09 ± 21.36	33.83 ± 25.03	11.51 ± 6.60	12.08 ± 9.01	10.75 ± 6.45
	0.2	40.39 ± 16.37	43.32 ± 15.93	48.58 ± 16.71	46.55 ± 25.77	39.28 ± 21.42	43.75 ± 27.09	22.52 ± 12.40	21.01 ± 9.44	19.72 ± 10.89
Correct response latency (s)	**1.0**	0.99 ± 0.22	1.04 ± 0.21	1.08 ± 0.27	1.14 ± 0.37	1.05 ± 0.29	1.09 ± 0.34	0.76 ± 0.17	0.76 ± 0.18	0.74 ± 0.20
	0.5	0.90 ± 0.21	0.92 ± 0.21	0.95 ± 0.21	0.98 ± 0.27	0.93 ± 0.25	0.95 ± 0.34	0.65 ± 0.13	0.67 ± 0.15	0.67 ± 0.15
	0.2	0.84 ± 0.17	0.91 ± 0.18	0.87 ± 0.18	0.86 ± 0.24	0.86 ± 0.23	0.86 ± 0.25	0.60 ± 0.17	0.59 ± 0.14	0.60 ± 0.15

Table S1. *Effects of chemogenetic cortico-thalamic inactivation on var delay and var SD parameters.*
Summary of behavioral parameters from variable delay and SD sessions shown per delay /SD. Green colored cells represent significant increases compared to saline after dose x group interaction. Red/green colored and underlined parameters reflect significant decreases/increases compared to saline respectively after dose x group x delay /SD interaction. Post-hoc tests are FDR-corrected for multiple testing. CNO5: CNO 5 mg/kg. CNO10: CNO 10 mg/kg injection. Data are expressed as mean ± SD.

		MDL			MDM			EYFP		
		Saline	CNO 5 mg/kg	CNO 10 mg/kg	Saline	CNO 5 mg/kg	CNO 10 mg/kg	Saline	CNO 5 mg/kg	CNO 10 mg/kg
Number of started trials	Var delay	349.91 ± 84.28	328.18 ± 78.36	304.36 ± 82.85	298.27 ± 72.78	306.18 ± 102.95	310.36 ± 94.32	363.31 ± 125.62	398.77 ± 93.44	396.08 ± 87.77
Magazine latency (s)	Var delay	2.37 ± 0.83	2.45 ± 0.96	2.47 ± 0.97	2.38 ± 0.39	2.20 ± 0.35	2.30 ± 0.39	2.23 ± 0.47	2.18 ± 0.47	2.20 ± 0.51
Perseverative responses on target (%)	Var delay	5.09 ± 3.01	5.27 ± 2.80	5.35 ± 3.38	5.69 ± 6.44	4.70 ± 5.09	5.67 ± 5.36	4.56 ± 3.05	4.34 ± 2.86	5.05 ± 2.69
Number of started trials	Var SD	382.36 ± 103.93	371.82 ± 108.20	346.18 ± 104.22	351.18 ± 108.78	381.00 ± 105.98	334.73 ± 103.48	462.54 ± 133.05	463.38 ± 134.72	449.46 ± 133.68
Magazine latency (s)	Var SD	2.53 ± 1.11	2.48 ± 1.24	2.42 ± 0.96	2.27 ± 0.34	2.17 ± 0.31	2.17 ± 0.41	2.10 ± 0.35	2.18 ± 0.50	2.22 ± 0.48
Perseverative responses on target (%)	Var SD	4.21 ± 2.16	3.66 ± 2.74	4.37 ± 3.55	4.26 ± 5.55	4.24 ± 5.41	3.51 ± 3.85	4.21 ± 2.82	4.01 ± 2.53	3.49 ± 2.20

Table S2. *Effects of chemogenetic cortico-thalamic inactivation on general task parameters.*
Summary of general behavioral parameters from variable DELAY and SD sessions. No significant differences compared to saline were found for any of the parameters. CNO5: CNO 5 mg/kg. CNO10: CNO 10 mg/kg injection. Data are expressed as mean ± SD.

		DMS			VMS			EYFP		
	Delay/cue duration (s)	Saline	CNO 5 mg/kg	CNO 10 mg/kg	Saline	CNO 5 mg/kg	CNO 10 mg/kg	Saline	CNO 5 mg/kg	CNO 10 mg/kg
Accuracy (%)	5	88.09 ± 2.56	89.38 ± 4.54	87.99 ± 5.44	89.82 ± 6.03	89.13 ± 5.56	91.65 ± 4.98	89.94 ± 6.17	89.13 ± 5.56	91.53 ± 4.85
	7.5	88.56 ± 3.62	86.46 ± 4.00	87.33 ± 5.39	89.04 ± 8.41	88.16 ± 7.39	88.43 ± 7.06	88.62 ± 8.05	88.16 ± 7.39	88.85 ± 7.49
	12.5	84.85 ± 6.80	82.84 ± 7.29	82.03 ± 6.94	81.59 ± 10.23	83.86 ± 9.13	82.67 ± 9.37	80.90 ± 9.80	83.86 ± 9.13	83.36 ± 9.69
Premature responses (%)	5	2.88 ± 1.91	3.47 ± 2.30	3.05 ± 1.92	3.63 ± 2.55	3.92 ± 2.20	3.46 ± 2.98	4.00 ± 2.92	3.92 ± 2.20	3.09 ± 2.54
	7.5	6.99 ± 4.69	9.40 ± 4.72	9.70 ± 6.06	8.30 ± 5.76	11.29 ± 5.53	9.79 ± 5.17	9.21 ± 6.80	11.29 ± 5.53	8.88 ± 3.85
	12.5	19.80 ± 12.07	26.38 ± 13.84	29.74 ± 12.64	25.22 ± 15.88	28.15 ± 14.38	26.82 ± 14.15	27.21 ± 16.29	28.15 ± 14.38	24.83 ± 13.62
Omissions (%)	5	12.35 ± 6.23	10.06 ± 5.97	7.97 ± 3.27	7.25 ± 3.96	9.25 ± 4.72	8.25 ± 5.43	7.18 ± 3.96	9.25 ± 4.72	8.31 ± 5.41
	7.5	8.54 ± 3.77	6.38 ± 4.37	7.22 ± 5.10	6.95 ± 3.34	5.97 ± 2.33	6.51 ± 5.03	6.46 ± 2.89	5.97 ± 2.32	6.99 ± 5.30
	12.5	9.13 ± 6.12	8.80 ± 4.56	9.71 ± 5.45	8.24 ± 5.65	7.11 ± 4.59	6.36 ± 2.87	8.05 ± 5.72	7.11 ± 4.59	6.54 ± 2.87
Correct response latency (s)	5	1.26 ± 0.16	1.21 ± 0.22	1.16 ± 0.12	1.12 ± 0.17	1.12 ± 0.18	1.10 ± 0.19	1.10 ± 0.15	1.12 ± 0.18	1.11 ± 0.20
	7.5	1.19 ± 0.17	1.13 ± 0.16	1.14 ± 0.12	1.09 ± 0.19	1.04 ± 0.17	1.03 ± 0.15	1.07 ± 0.18	1.04 ± 0.17	1.05 ± 0.17
	12.5	1.15 ± 0.14	1.13 ± 0.16	1.11 ± 0.12	1.08 ± 0.16	1.05 ± 0.18	1.01 ± 0.16	1.07 ± 0.15	1.05 ± 0.18	1.02 ± 0.17
Premature response latency (s)	5	3.64 ± 0.55	3.41 ± 0.51	3.51 ± 0.61	3.42 ± 0.58	3.75 ± 0.56	3.46 ± 0.46	3.50 ± 0.59	3.75 ± 0.56	3.37 ± 0.42
	7.5	5.51 ± 0.75	5.32 ± 0.53	5.52 ± 0.45	5.36 ± 0.46	5.41 ± 0.58	5.42 ± 0.50	5.39 ± 0.47	5.41 ± 0.58	5.39 ± 0.50
	12.5	8.18 ± 0.68	8.35 ± 0.71	8.62 ± 0.47	8.36 ± 0.64	8.32 ± 0.83	8.57 ± 0.85	8.33 ± 0.64	8.32 ± 0.83	8.61 ± 0.84

Accuracy (%)	1.0	87.38 ± 3.82	85.94 ± 5.06	84.97 ± 4.73	87.35 ± 5.66	85.30 ± 7.40	85.30 ± 6.79	90.02 ± 5.00	89.52 ± 6.11	88.78 ± 4.66
	0.5	70.94 ± 7.11	69.72 ± 6.91	70.89 ± 7.00	70.83 ± 6.68	71.48 ± 7.15	68.80 ± 10.92	78.13 ± 4.93	77.12 ± 6.05	77.60 ± 6.74
	0.2	60.73 ± 10.44	63.13 ± 12.06	60.02 ± 9.29	60.25 ± 9.74	61.24 ± 12.41	57.85 ± 11.92	65.13 ± 4.87	64.49 ± 6.43	68.24 ± 8.03
Premature responses (%)	1.0	3.12 ± 2.06	4.44 ± 1.42	3.81 ± 2.68	3.81 ± 4.49	4.30 ± 3.71	6.07 ± 6.83	4.24 ± 2.44	4.25 ± 3.85	4.00 ± 2.70
	0.5	3.49 ± 1.88	3.33 ± 3.29	2.92 ± 2.37	3.19 ± 4.05	4.04 ± 3.76	6.53 ± 8.13	4.03 ± 3.02	4.42 ± 3.56	4.66 ± 3.21
	0.2	3.50 ± 2.69	3.79 ± 2.56	3.99 ± 2.80	2.87 ± 2.04	4.20 ± 3.73	6.25 ± 7.84	4.51 ± 3.17	4.04 ± 3.59	3.03 ± 2.00
Omissions (%)	1.0	15.20 ± 6.41	15.07 ± 5.24	16.13 ± 5.91	14.41 ± 12.18	13.91 ± 13.38	14.86 ± 10.93	6.80 ± 4.56	7.54 ± 5.28	7.32 ± 3.55
	0.5	22.73 ± 9.42	20.42 ± 8.72	21.81 ± 8.90	21.33 ± 11.27	21.11 ± 14.85	21.02 ± 11.98	11.44 ± 6.77	8.55 ± 5.31	11.83 ± 6.07
	0.2	33.78 ± 11.88	32.41 ± 11.69	31.65 ± 7.55	33.00 ± 12.41	31.93 ± 18.42	31.33 ± 15.04	17.73 ± 6.37	17.42 ± 9.51	20.10 ± 7.15
Correct response latency (s)	1.0	1.32 ± 0.15	1.29 ± 0.16	1.27 ± 0.19	1.25 ± 0.32	1.23 ± 0.33	1.21 ± 0.32	1.09 ± 0.15	1.10 ± 0.14	1.10 ± 0.12
	0.5	1.09 ± 0.13	1.06 ± 0.14	1.08 ± 0.17	1.05 ± 0.26	1.07 ± 0.30	1.02 ± 0.23	0.94 ± 0.14	0.94 ± 0.09	0.96 ± 0.10
	0.2	0.99 ± 0.16	0.93 ± 0.15	0.94 ± 0.13	0.98 ± 0.22	0.95 ± 0.23	0.93 ± 0.26	0.86 ± 0.15	0.85 ± 0.12	0.89 ± 0.08

Table S3. *Effects of chemogenetic cortico-striatal inactivation on var delay and var SD parameters.*
Summary of behavioral parameters from variable delay and SD sessions shown per delay /SD. Red/green colored and underlined parameters reflect significant decreases/increases compared to saline respectively after dose x group x delay /SD interaction. Post-hoc tests are FDR-corrected for multiple testing. CNO5: CNO 5 mg/kg. CNO10: CNO 10 mg/kg injection. Data are expressed as mean ± SD.

		DMS			VMS			EYFP		
		Saline	CNO 5 mg/kg	CNO 10 mg/kg	Saline	CNO 5 mg/kg	CNO 10 mg/kg	Saline	CNO 5 mg/kg	CNO 10 mg/kg
Number of started trials	**Var delay**	400.20 ± 58.69	399.50 ± 79.56	416.60 ± 55.97	425.33 ± 55.99	442.10 ± 33.32	437.83 ± 42.50	433.08 ± 53.41	442.08 ± 33.32	430.08 ± 46.57
Magazine latency (s)	**Var delay**	2.15 ± 0.36	2.04 ± 0.38	2.03 ± 0.37	2.27 ± 0.33	2.28 ± 0.35	2.27 ± 0.30	2.24 ± 0.28	2.28 ± 0.35	2.30 ± 0.34
Perseverative responses on target (%)	**Var delay**	2.98 ± 2.21	2.91 ± 1.66	3.04 ± 1.11	3.24 ± 1.56	2.99 ± 1.48	2.70 ± 1.15	3.12 ± 1.55	2.99 ± 1.48	2.82 ± 1.22
Number of started trials	**Var SD**	432.3 ± 84.11	416 ± 107.95	431.7 ± 75.71	424.58 ± 103.31	415.67 ± 105.65	424.75 ± 123.73	517.25 ± 48.07	509.42 ± 37.65	505.25 ± 42.98
Magazine latency (s)	**Var SD**	2.17 ± 0.35	2.14 ± 0.34	2.21 ± 0.42	2.07 ± 0.34	2.04 ± 0.39	2.03 ± 0.33	2.46 ± 0.29	2.43 ± 0.31	2.54 ± 0.33
Perseverative responses on target (%)	**Var SD**	1.41 ± 0.75	2.22 ± 1.40	2.16 ± 1.38	2.73 ± 2.47	2.27 ± 1.13	2.57 ± 1.81	3.09 ± 1.50	2.89 ± 1.27	2.99 ± 0.81

Table S4. *Effects of chemogenetic cortico-striatal inactivation on general task parameters.*
Summary of general behavioral parameters from variable delay and SD sessions. No significant differences compared to saline were found for any of the parameters. CNO5: CNO 5 mg/kg. CNO10: CNO 10 mg/kg injection. Data are expressed as mean ± SD.

Huub Terra[1] and Bastiaan Bruinsma[1]
Sybren F. de Kloet
Marcel van der Roest
Tommy Pattij[#] and Huibert D. Mansvelder[#]

[1]shared first authorship

[#]shared senior authorship

PUBLISHED AS

Terra, H.*, Bruinsma, B.*, de Kloet, S.F., van der Roest, M., Pattij, T., and Mansvelder, H.D. (2020). Prefrontal cortical projection neurons targeting dorsomedial striatum control behavioral inhibition. Current Biology.

CHAPTER 5

Prefrontal cortical projection neurons targeting dorsomedial striatum control behavioral inhibition

ABSTRACT

A neural pathway from prefrontal cortex (PFC) to dorsal striatum (DS) has been suggested to mediate cognitive control of behavior, including proactive inhibitory control and attention. However, a direct causal demonstration thereof is lacking. Here, we show that selective chemogenetic silencing of corticostriatal PFC neurons in rats increases premature responses. Wireless single-unit electrophysiological recordings of optogenetically-identified corticostriatal PFC neurons revealed that the majority of these neurons encode behavioral trial outcome with persistent changes in firing rate. Attentional parameters were not affected by silencing corticostriatal PFC neurons, suggesting that these projection neurons encode a specific subset of cognitive behaviors. Compared to the general non-identified neuronal population in the PFC, frontostriatal neurons showed selective engagement during periods of inhibitory control. Our results demonstrate a role for corticostriatal neurons in inhibitory control and possibly suggest that distinct domains of cognitive control over behavior are encoded by specific projection neuron populations.

INTRODUCTION

Cognitive control of behavior is a highly valued skill in society and from an early age people are trained to improve it in school and other institutions. The ability to inhibit behavior until conditions are appropriate (i.e. proactive inhibitory control) and stay focused (i.e. attention) are determinant factors of success in goal-directed behavior. Deficits in inhibitory control and attention are hallmark symptoms in a wide range of psychiatric and neurological disorders, ranging from schizophrenia, compulsivity and addiction disorders to cognitive decline and Alzheimer's disease[5,10,62]. Yet, how the brain organizes inhibitory control and attention is incompletely understood.

Efferent projections from the prefrontal cortex (PFC) to subcortical brain areas play an important role in inhibitory control and attention[1,5,209]. A major brain area receiving input from the PFC is the dorsomedial striatum (DMS) of the basal ganglia[60,92,210]. In human and non-human primates, dorsolateral PFC and DMS activity and connectivity strength is positively associated with periods of inhibitory control and attention[211,212]. Consistently, in rodents, optogenetic, chemogenetic and lesion-mediated impairment of the dorsal medial PFC (mPFC) - the rodent homologue of the dorsolateral and medial PFC[32,41,55,158] - or DMS[94,96] results in impaired inhibitory control and attention. The functional coupling of the dorsal mPFC and DMS is further supported by electrophysiological recordings of neuronal activity and local field potentials, showing synchronized activity in both brain areas during a delay period in which inhibitory control and attention are most needed[53,213,214]. It has been suggested that mPFC projection neurons directly control DMS activity[3,5,55], where glutamatergic input from mPFC terminals can shift the activity balance between the direct and indirect pathway[104,215,216]. This in turn could control the initiation and inhibition of actions or which attentional state is associated with the upcoming behavior. However, a causal demonstration of frontostriatal PFC projection neurons in inhibitory control and attention is still lacking.

A subgroup of dorsal mPFC pyramidal neurons and DMS medium spiny neurons (MSNs) show delay period-related persistent activation or silencing of firing rate, by which a smaller change in activity predicted impaired inhibitory control and

attention[19,20,41,53]. Moreover, dissociable task-relevant information and activity dynamics of mPFC neurons has been linked to projection neuron identity[57,64,65,68,217], suggesting that frontostriatal projection neurons display unique task-relevant activity. Therefore, we hypothesize that mPFC frontostriatal projections neurons encode inhibitory control and attention by the amplitude of persistent changes in firing rate.

To directly test this, we selectively silenced frontostriatal neurons that project from the dorsal mPFC to the DMS in freely moving rats in a self-paced, homecage-based, inhibitory control and attention task. We used sessions with a variable delay period and stimulus duration to specifically challenge inhibitory control and attentional control, respectively[17]. To investigate whether frontostriatal projection neurons encode inhibitory control and attention, we wirelessly recorded unit activity of optogenetically-identified mPFC neurons. To test if this encoding was unique within the mPFC we compared the activity of frontostriatal neurons to the general mPFC pyramidal neuron population. We found that silencing frontostriatal neurons only resulted in inhibitory control deficits, measured as an increase in premature responses. These frontostriatal neurons showed predominantly persistent activation or silencing during inhibitory control, and a reduced and advanced onset of change in activity in these neurons are associated with prematurely expressed responses in the task. Within the mPFC neuronal population, a larger fraction of frontostriatal projection neurons showed task-engagement with persistent changes in firing rate. Together, these findings demonstrate the role of frontostriatal projection neurons in behavioral inhibition.

RESULTS

INHIBITORY CONTROL AND ATTENTION BEHAVIOR

To quantitatively test inhibitory control and attention performance, we trained rats in a self-paced, homecage-based version[23,193] of the 5-choice serial reaction time task (5-CSRTT)[17]. Rats were trained to withhold a behavioral response during a delay period (also called 'intertrial interval') while attending to five holes for stimulus lights (cue) until a stimulus was presented randomly in one of them (**Figure 1A**). A correct response, i.e. a nose poke in the lit hole during a limited

hold period, was rewarded by a food pellet and a subsequent eat interval, after which the animal initiated the next trial with a second nose poke in the food magazine. A premature response during the delay period was interpreted as failed inhibitory control and was followed by a 5 s timeout period, during which the next trial could not be initiated. Incorrect responses to the stimulus light and omission of responses were also followed by a timeout period and were interpreted as impaired attention (**Figure 1B**). In the homecage-based version of the 5-CSRTT, trials could only be initiated by the animal during the first 2.5 h of the dark phase, when animals were most active193. Animals reached criterion performance within a week[193], after which they continued with cognitively challenging test sessions. In these sessions, task difficulty was increased by randomly varying the delay duration or stimulus duration, to probe either inhibitory control or attention, respectively[17]. Randomly varying delays between 5.0, 7.5 or 12.5 s (in 'inhibitory control sessions') resulted in more premature responses at longer delays (**Figure 1C**), as well as a decrease in accuracy of responding (**Figure 1D**) and no change in omissions (**Figure 1E**). Still, the animals maintained a high level of accuracy during longer delays, indicating that they successfully learned the task contingencies and did not base their response strategy on the 5 s delay time interval. Randomly varying stimulus durations between 1.0, 0.5 or 0.2 s (in 'attention sessions') did not affect premature responses (**Figure 1F**), but resulted in a sharp decrease in accuracy (**Figure 1G**) and increase of omissions (**Figure 1H**) at shorter stimulus durations. Traditionally the 5-CSRTT has a maximum of 100 trials per session, making statistical power low for sparser trial types such as premature responses[20,21]. Our semi-automated testing in a homecage-based environment allowed long sessions up to 2.5 h, resulting in a large number of trials per session providing higher statistical power (inhibitory control sessions, 420 ± 13 trials, attention sessions, 507 ± 14 trials, mean ± SEM).

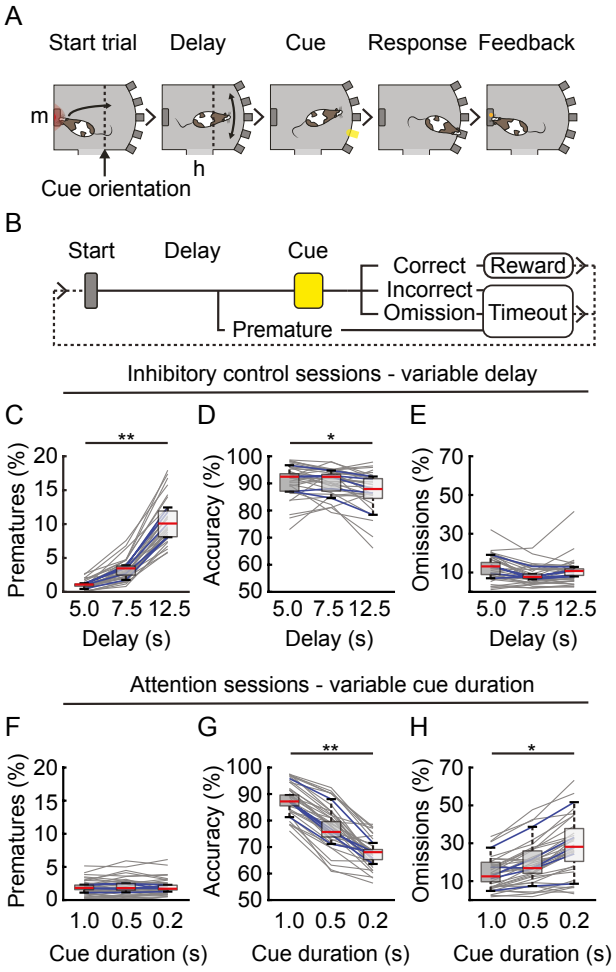

Figure 1. *Inhibitory control and attention behavior.*
(**A**) Cartoon representation of the task. Trial initiation, stimulus (cue) hole orientation, delay period, response, reward collection, (m) food magazine, (h) homecage. (**B**) Schematic lay-out of the task with response and feedback options. (**C–E**) Behavioral outcome of trials during inhibitory control sessions with randomly varied delay durations (n = 5 rats used for electrophysiology, 30 sessions). (**C**) Premature responses (Fr = 10.0, *** $p < 0.001$; post hoc, delay 5.0 s vs 12.5 s, $p = 0.0047$). (**D**) Accuracy of responding (Fr = 7.6, * $p < 0.05$; post hoc test delay 5.0 s vs 12.5 s, $p = 0.0343$). (**E**) Omissions (Fr = 3.6, $p = 0.18$). (**F–H**) Behavioral outcome of trials during attention sessions with randomly varied stimulus durations (n = 5 rats used for electrophysiology, 33 sessions). (**F**) Premature responses (Fr = 1.2, $p > 0.69$). (**G**) Accuracy of responding (Fr = 10.0, *** $p < 0.001$; post hoc, stimulus duration 1.0 s vs 0.2 s, $p = 0.0047$). (**H**) Omissions (Fr = 8.4, ** $p < 0.01$; post hoc, stimulus duration 1.0 s vs 0.2 s, $p = 0.0133$). (C–H) Friedman's ANOVA with Dun's post hoc test. Blue line, session mean per animal. Grey line, individual session. Boxplots: center line, median; box edges, 1st and 3th quartile; whiskers, data range without outliers.

FRONTOSTRIATAL NEURONS ARE REQUIRED FOR INHIBITORY CONTROL

To determine whether frontostriatal neurons are involved in inhibitory control and attention, we inhibited these mPFC projection neurons using DREADD (designer receptors exclusively activated by designer drugs)-mediated inactivation[218]. To target frontostriatal neurons, we simultaneously injected retrograde canine adenovirus type 2 carrying Cre recombinase (CAV2-Cre) in the DMS and Cre-dependent AAV-DIO-hM4D(Gi)-mCherry virus in the dorsal mPFC (**Figure 2A**). This resulted in viral expression in the dorsal mPFC region where striatal projection neurons are located[10] (**Figure 2B** and **S1**). Following recovery and 5-CSRTT training, animals (n = 10) received a systemic injection of Clozapine-N-Oxide (CNO), using a balanced design, 30 min before onset of the dark phase and initiation of the inhibitory control or attention 5-CSRTT test session. CNO induced a dose-dependent increase in premature responses during inhibitory control sessions (**Figure 2C**). Under these task conditions, we observed no effects on accuracy (**Figure 2D**) and omissions (**Figure 2E**). No changes in motor-related or motivation-related response latencies were observed (**Table S1**). No effects of CNO were observed during the attention sessions on premature responses (**Figure 2F**), accuracy (**Figure 2G**), omissions (**Figure 2H**) or other parameters (**Table S1**). To exclude the possibility that CNO or its metabolite clozapine confounded our results[219], we included a control group (n = 12 rats) that expressed eYFP only and no DREADD receptor. No effects of CNO in these control animals were observed (**Table S1**). These results show that frontostriatal neurons are necessary for maintaining inhibitory control over responding, as revealed only during the longest delay trials when inhibitory control is mostly challenged, and not for attention.

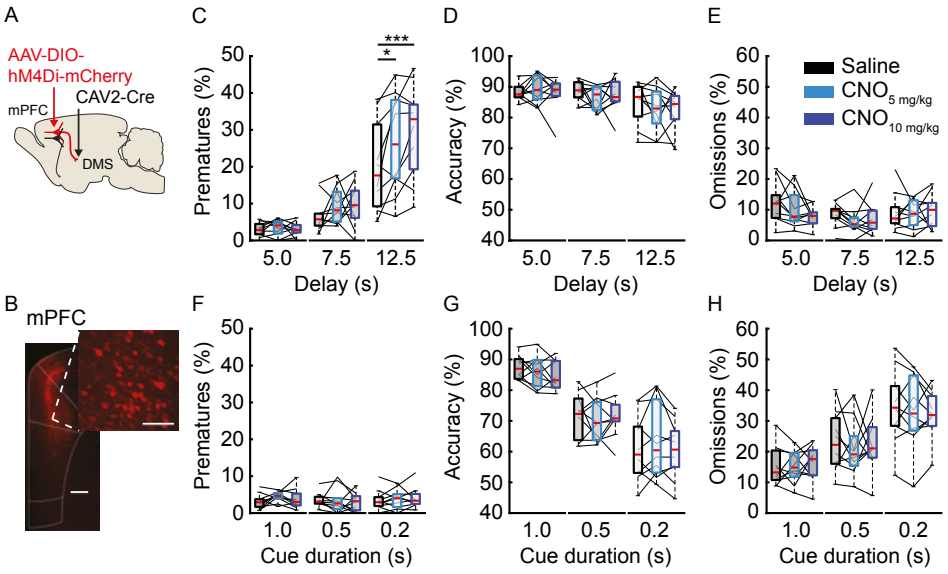

Figure 2. *Frontostriatal neurons are required for inhibitory control.*
(**A**) Schematic of virus injection locations. (**B**) Confocal images of mCherry expression in mPFC. Scale bar, 500 and 100 μm. (**C–E**) Behavioral response data for inhibitory control sessions with randomly varied delay durations with different doses of CNO (0, 5 and 10 mg/kg, 10 rats, 10 sessions). (**C**) Premature responses ($F_{[4,84]} = 2.63$, $p < 0.05$, post hoc, delay 12.5 s, CNO 0 vs 5 mg/kg: $t(9) = 2.30$, * $p = 0.047$, $d = 0.51$, power = 20.5%. CNO 0 vs 10 mg/kg: $t(9) = 3.85$, *** $p = 0.0039$, $d = 0.80$, power = 43%. (**D**) Accuracy ($F_{[4,84]} = 1.76$, $p = 0.15$). (**E**) Omissions ($F_{[4,84]} = 2.97$, $p < 0.05$, post hoc, $p > 0.05$). (**F–H**) Behavioral data for the variable stimulus duration sessions with different doses of CNO (0, 5 and 10 mg/kg, n = 10 rats, 10 sessions). (**F**) Premature responses ($F_{[4,84]} = 2.03$, $p = 0.1$). (**G**) Accuracy ($F_{[4,84]} = 1.94$, $p = 0.11$). (**H**) Omissions ($F_{[4,84]} = 0.99$, $p = 0.42$). (C–H) Three-way mixed repeated-measures ANOVA, dose x group x delay interaction with post hoc Wilcoxon rank-sum tests or t-tests, with Benjamini-Hochberg FDR correction. Boxplots: center line, median; box edges, 1st and 3th quartile; whiskers, data range without outliers. See also Figure S1 and Table S1.

WIRELESS RECORDINGS OF OPTOGENETICALLY-IDENTIFIED FRONTOSTRIATAL PROJECTION NEURONS

To determine the activity of frontostriatal projection neurons during 5-CSRTT performance we used wireless single-unit electrophysiological recordings combined with optogenetic identification[220,221] in freely moving, untethered rats. We injected CAV2-Cre in the DMS, but now a Cre-dependent virus carrying the light-sensitive opsin Channelrhodopsin (ChR2) attached to eYFP in the mPFC (**Figure 3A**). This resulted in viral expression in the dorsal mPFC and corresponding axonal labeling in the DMS (**Figure 3B**). Simultaneously, we implanted an optrode across the layers of the mPFC, containing a 4 shank, 64-electrode silicon probe combined with an optic fiber, glued on to a moveable drive (**Figure 3A**). This allowed wireless recording of single-unit activity in the mPFC while allowing to optogenetically identify ChR2-tagged frontostriatal neurons after each session. We recorded spiking activity from well-separated single-units during inhibitory control (543 units, 5 rats and 30 sessions) and attention sessions (n = 540 units, 5 rats, 33 sessions). Each animal was recorded in both session types after which the optrode was lowered by approximately 205 μm to a new location. All recordings were pooled and broad-spiking putative pyramidal neurons were separated from narrow-spiking putative interneurons (**Figure 3C**, broad-spiking, n = 932, narrow-spiking, n = 132, unclassified, n = 19) based on the spike-waveform shape features 'peak-to-trough-time' and 'half-peak-time'[20,222,223]. Only spiking activity of broad-spiking, putative pyramidal neurons was analyzed. Following each recording session, frontostriatal projection neurons were identified based on activation by brief pulses of blue light (2, 5 or 10 ms, 500 pulses, 5 Hz). We defined a significant increase in spiking using the stimulus-associated spike latency test (SALT[220], $p < 0.01$) and peak z-score > 1.65. Units were accepted as optogenetically-identified when they had a light-induced mean first spike latency < 7 ms, jitter < 3.5 ms, reliability > 0.03 and Pearson's waveform correlation > 0.8 (**Figure 3D** and **3E; Figure S2A–S2F**). An additional 4 neurons (n = 3 for inhibitory control sessions, n = 1 for attention sessions) were included that were stably recorded over two session types but where optogenetic identification was positive in only one of the two session types (**Figure S2G–S2J**), likely due to light delivery failure. In total, 44 broad-spiking frontostriatal neurons were identified in inhibitory control

sessions (recorded in 17/30 sessions, 5 rats) and 51 broad-spiking frontostriatal neurons in attention sessions (**Figure 3E**, recorded in 20/33 sessions, 5 rats, with 4 having optogenetically identified neurons).

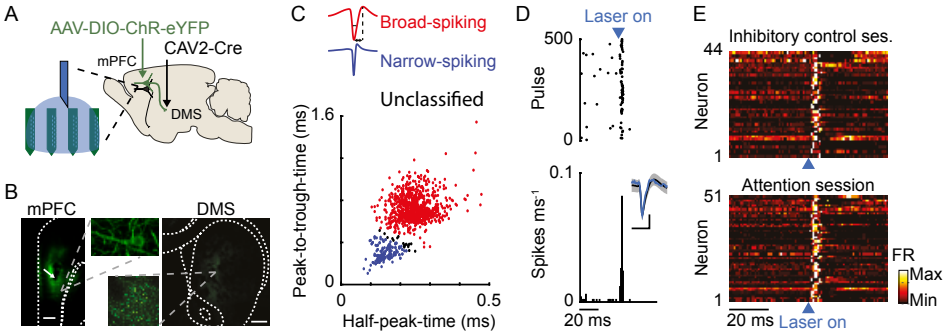

Figure 3. *Wireless recordings of optogenetically-identified frontostriatal projection neurons.*
(**A**) Schematic of virus injection and optrode locations. (**B**) Confocal images of eYFP expression in mPFC and DMS. Arrow, post hoc electrolytic lesion. Scale bar, 500 μm. (**C**) Single-unit separation (5 rats, 33 sessions) in to broad-spiking (red, n = 932 neurons), narrow-spiking (blue, n = 132 neurons), and unclassified (black, n = 19 neurons, Gaussian mixture model, posterior probability > 0.85). (**D**) Light-triggered activation of an optogenetically-identified neuron. Top, raster plot, bottom, peri-stimulus time histogram (PSTH) aligned to laser onset. Inset, spike waveform (behavior, black ± grey, mean ± SD; light-triggered, mean, blue). Scale bar, 1 ms by 50 μV. (**E**) Light-triggered activation of all optogenetically-identified neurons for inhibitory control (recorded in 17/30 sessions, 5 rats) and attention sessions (recorded in 20/33 sessions, 5 rats). Activity is normalized to peak. Colors indicate maximum and minimum activity. See also Figure S2.

PERSISTENT DELAY-PERIOD ACTIVITY OF FRONTOSTRIATAL PROJECTION NEURONS

Previous studies have shown that mPFC neurons with broad-spiking profiles are persistently activated or silenced during the delay period, where a reduced amplitude in firing rate predicted premature responses[19–21,41,55]. Moreover, DREADD-mediated inhibition (**Figure 2**) showed that activity of frontostriatal neurons is necessary for inhibitory control. We therefore hypothesized that frontostriatal neurons would be persistently activated or silenced during the delay period, before cue presentation. Since mPFC neurons change firing rate upon orientation towards the stimulus holes (cue orientation) rather than at trial start[21], we used video monitoring of the animals during the task to determine the exact time point

of stimulus hole orientation (**Figure 1A**). Analysis of spiking activity of the 44 optogenetically-identified broad-spiking units revealed three broad categories of activity patterns that occurred during the delay period before stimulus onset: persistently activated units (**Figure 4A**), non-activated units (**Figure 4B**) and persistently silenced units (**Figure 4C**). These persistent changes were present for all delay durations (**Figure 4D–F**), suggesting that mPFC frontostriatal projection neurons are involved in inhibitory control rather than timing-related activity[50]. To quantify the changes in firing rate during the delay period, we made a trial-based paired comparison per neuron of the activity relative to baseline during time windows at three moments in the task: (i) 1 s after trial start, (ii) 2 s after stimulus orientation and (iii) 2 s before stimulus onset (**Figure 4G** and **4H**). More frontostriatal projection neurons had significantly different firing rate following stimulus orientation compared to after trial start and maintained this activity throughout the delay period. Neurons were therefore categorized into "persistently activated", "non-activated" or "persistently silenced" based on a change in firing rate in both time bins: 'after stimulus orientation' (time bin 2) and 'before stimulus onset' (time bin 3). Neurons were categorized as "persistently activated" or "persistently silenced" if the direction of change compared to baseline in both time bins 2 and 3 was positive or negative, respectively. Units with a significant firing rate change in only one or none of the time bins were categorized as "non-activated" (**Figure 4G**). A total of 73% (32/44) of frontostriatal projection neurons showed persistent changes in activity with 32% (14/44) persistently activated and 41% (18/44) persistently silenced (**Figure 4H** and **4I**). During attention sessions we also found frontostriatal projection neurons with persistent changes in activity throughout the delay period (**Figure 5A–C**). Of those 74% (38/51) with persistent changes in firing activity, 35% (18/51) were activated, 39% (20/51) silenced, while 26% (13/51) were not persistently activated or silenced (**Figure 5D–F**). Together, this demonstrates that frontostriatal neurons show persistent changes in firing rate in the delay period, independent of the session type and delay duration.

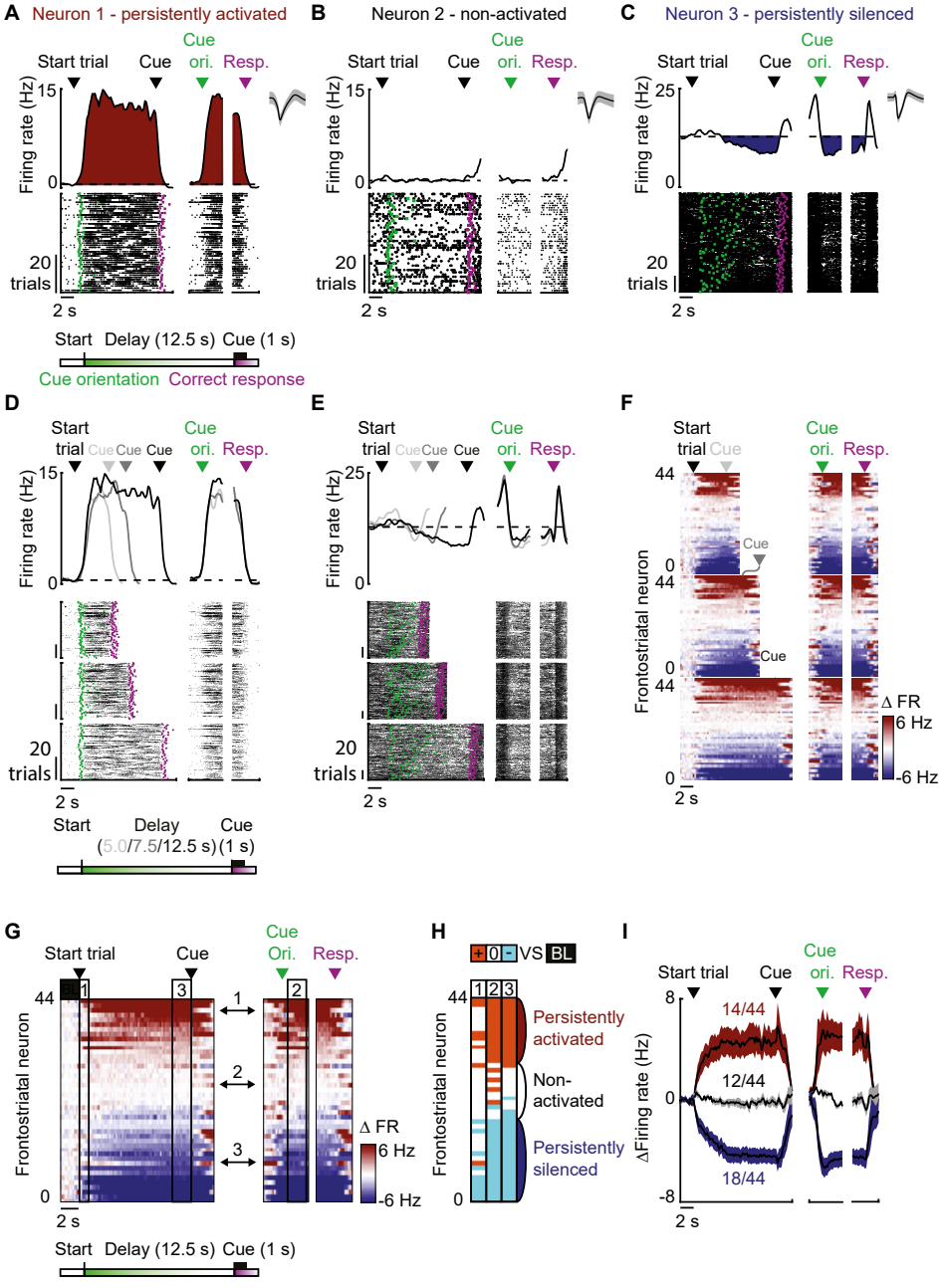
A Neuron 1 - persistently activated
B Neuron 2 - non-activated
C Neuron 3 - persistently silenced
Start trial
Cue
Cue ori.
Resp.
Firing rate (Hz)
20 trials
2 s
Start Delay (12.5 s) Cue (1 s)
Cue orientation Correct response
D
E
F
Start trial Cue Cue Cue
Start Delay (5.0/7.5/12.5 s) Cue (1 s)
Frontostriatal neuron
Δ FR
6 Hz
-6 Hz
G
Cue Ori.
Start Delay (12.5 s) Cue (1 s)
H
+ 0 - VS BL
Persistently activated
Non-activated
Persistently silenced
I
ΔFiring rate (Hz)
14/44
12/44
18/44

Figure 4. *Persistent delay-period activity of frontostriatal neurons in inhibitory control sessions.* (**A–C**) Activity of example frontostriatal projection neurons during correct trials with the longest delay of the inhibitory control sessions. (**A**) Persistently activated neuron. Top, peri-event time histogram (PETH), bottom, spike raster plot. Dotted line, baseline activity (BL, 0 – 2 before trial start). Red, activity above BL. Green, stimulus orientation moment, purple, response. Spike waveform, mean ± SD. (**B**) Non-activated neuron, plotted as in (A). (**C**) Persistently silenced neuron, plotted as in (A) but with blue to indicate activity below BL. (**D–F**) Activity of all frontostriatal projection neurons across delay durations (top - bottom, grey - black, short - long delay). (**D, E**) Activity of example neuron 1 and 3, plotted as in (A-C). (**F**) Δ Firing rate over all delays. (**G**) Δ Firing rate for correct trials during the longest wait time. Arrows, location of example neuron 1, 2 and 3. Window 1) 0 - 1 s after trial start, 2) 0.6 - 2.6 s after the stimulus orientation moment, 3) 2 - 0 s before the stimulus (5 rats, 17 sessions). (**H**) Activity categories. Colors indicate change in firing rate from BL with activated (orange), no change (white) and silenced (cyan). Wilcoxon signed-rank over Δ firing rate of all correct trials per neuron, $p < 0.05$. (**I**) Δ Firing rate per activity category. Data presented as mean ± SEM. Colormaps, Δ firing rate from BL, clipped at +6 Hz and -6 Hz. Neurons sorted on activity category and Δ firing rate in window 3.

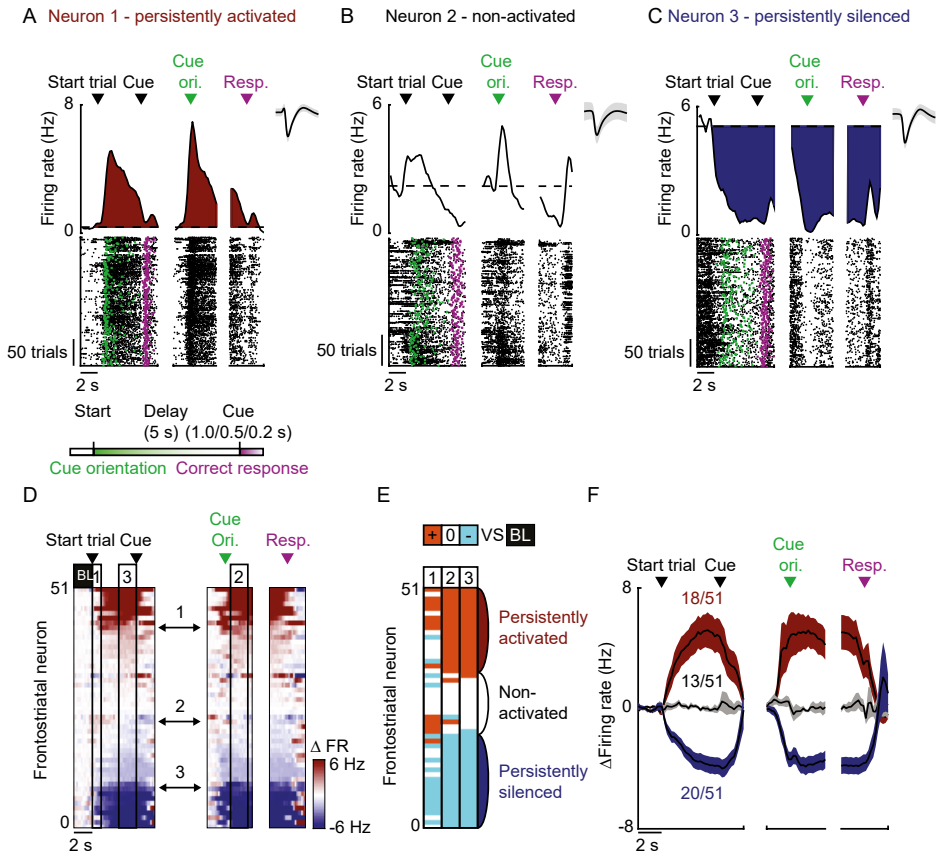

Figure 5. *Persistent delay-period activity of frontostriatal neurons in attention sessions.*
(**A–C**) Activity of frontostriatal projection neurons during all correct trials of the attention sessions. (**A**) Persistently activated neuron. Top, peri-event time histogram (PETH), bottom, spike raster plot. Dotted line, baseline (BL, 0 – 2 before trial start) activity). Red, activity above BL. Green, cue orientation moment, purple, response. Spike waveform, mean ± SD. (**B**) Non-activated neuron, plotted as in (A). (**C**) Persistently silenced neuron, plotted as in (A) but with blue to indicate activity below BL. (**D**) Δ Firing rate for all correct trials during attention sessions. Arrows, location of example neuron 1, 2 and 3. Window 1) 0 - 1 s after trial start, 2) 0.6 - 2.6 s after the cue orientation moment, 3) 2 - 0 s before the cue (4 rats, 20 sessions). (**E**) Activity categories. Colors indicate change in firing rate from BL with activated (orange), no change (white) and silenced (cyan). Wilcoxon signed-rank over Δ firing rate of all correct trials per neuron, $p < 0.05$. (**F**) Δ Firing rate per activity category. Data presented as mean ± SEM. Colormaps, Δ firing rate from BL, clipped at +6 Hz and -6 Hz. Neurons sorted on activity category and Δ firing rate in window 3.

FRONTOSTRIATAL PROJECTION NEURONS ARE SPECIALIZED IN PERSISTENT DELAY-PERIOD ACTIVITY

To test whether frontostriatal projection neurons in the dorsal mPFC showed specialized activity patterns compared to the overall broad-spiking mPFC neuronal population, we compared the fraction of neurons that was persistently activated, non-activated and persistently silenced for the frontostriatal projection neuron group to the neighboring non-optogenetically-identified broad-spiking neurons. Although complete exclusion of frontostriatal neurons from the non-identified group was impossible, to minimize inclusion of these neurons in the non-identified group, we excluded units from sessions without optogenetically-identified neurons or units that only partially met the optogenetic identification criteria. Non-identified neurons recorded in correct trials (280 neurons, 5 rats, 17 sessions) with the longest delays had persistently activated, non-activated and persistently silenced activity profiles (**Figure 6A**), but with different fractions of the population than identified frontostriatal projection neurons (**Figure 6B** left vs. right). We quantified this difference by comparing the fraction of neurons falling in each activity category between the frontostriatal and non-identified group. The frontostriatal projection neuron group showed a higher fraction of persistently activated (frontostriatal, 32%, 14/44, vs. non-identified, 19%, 52/280) and silenced units (frontostriatal, 41%, 18/44, vs. non-identified, 21%, 60/280) at the cost of the non-activated category (frontostriatal, 27%, 12/44, vs. non-identified, 60%, 168/280, **Figure 6C**). We repeated the comparison of fractions of groups during the attention sessions and found that frontostriatal neurons (n = 51, 20 sessions, 4 rats), compared to non-identified neurons (n = 258, 20 sessions, 4 rats), also showed a larger fraction of persistently activated neurons and a lower fraction of non-activated neurons, but no difference between persistently silenced neurons (**Figure S3**).

Neurons in superficial layers (I and II/III) and deep layers (V and VI) of the mPFC are known to show distinct task-related activity[223–225]. Frontostriatal projection neurons have been reported to be primarily located in deep layers V and VI[60], while superficial mPFC neurons mostly project to other cortical and subcortical areas. Therefore, a potential sampling bias could explain the difference in specialization between frontostriatal and non-frontostriatal neurons. The recording location

of frontostriatal and non-identified neurons did, however, not show a bias for recording depth (superficial layers 0 – 600 µm vs. deep layers 600 – 1400 µm from pia[60]), as nearly all neurons were recorded in deep layers (**Figure S4**). Together, this shows that frontostriatal neurons, compared to neighboring broad-spiking neurons, are differentially engaged during periods of inhibitory control, with persistent changes in firing rate as dominant pattern.

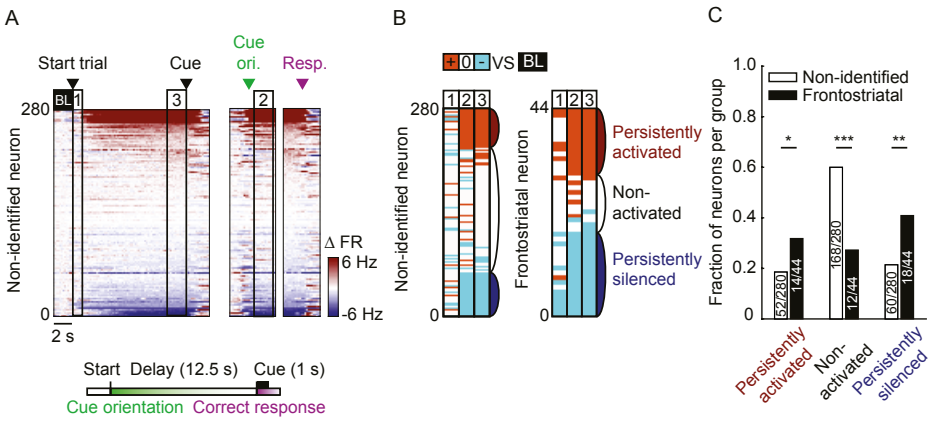

Figure 6. *Frontostriatal neurons are specialized in persistent delay-period activity.*
(**A**) Δ Firing rate for non-identified neurons (n = 258 neurons, 20 sessions, 5 rats) during the longest delay trials in the inhibitory control sessions. Colors indicate Δ firing rate (FR) from BL (2 – 0 s before trial start) clipped at +6 Hz and -6 Hz. Window 1) 0 – 1 s after trial start, 2) 0.6 – 2.6 s after stimulus orientation and 3) 2 – 0 s before the stimulus. (**B**) Activity categories for non-identified (left, same as Figure 4H) and frontostriatal (right). Colors indicate change in firing rate from BL with activated (orange), no change (white) and silenced (cyan). Wilcoxon signed-rank over Δ firing rate of all correct trials per neuron, $p < 0.05$. (**C**) Fraction of neurons per group (non-identified and frontostriatal) that are persistently activated ($X^2(1) = 4.114$, * $p = 0.043$), non-activated ($X^2(1) = 7.895$, ** $p = 0.005$) and persistently silenced ($X^2(1) = 16.495$, *** $p = 0.0005$). Neurons sorted on activity category and Δ firing rate in window 3. See also Figure S3 and S4.

ACTIVITY OF FRONTOSTRIATAL NEURONS PREDICT SUCCESSFUL INHIBITORY CONTROL OF BEHAVIOR

It has previously been suggested that the strength of inhibitory control of an animal could be reflected by the amount of change in firing rate by mPFC neurons during behavioral inhibition[41]. It was also found that early in a premature response trial, animals were faster to orient themselves toward the stimulus holes following trial start[21], which may suggest that animals experience an error in timing of initiation of behavioral control. We therefore tested whether frontostriatal projec-

tion neurons show firing patterns that are associated with reduced behavioral control and altered timing of initiation of behavioral control, as reflected in reduced changes in amplitude of persistent firing rate and advanced start of firing rate change in premature trials compared to correct response trials. Indeed, we observed persistently activated (**Figure 7A**) and persistently silenced (**Figure 7B**) neurons that showed reduced changes in firing rate compared to baseline in premature response trials compared to correct response trials. We then calculated the change in firing rate per trial for each neuron after stimulus orientation and before a response compared to baseline and took the mean over all trials. Combined, persistently activated and silenced neurons had reduced changes in firing rate in premature trials compared to correct trials, both following stimulus orientation and before the response was made (**Figure 7C**). Behaviorally, animals oriented toward the stimulus holes at an earlier time point in premature response trials compared to correct trials (**Figure 7D** and **7E**, 1268 correct trials, 743 premature trials, 17 sessions, 5 rats), indicating altered timing of initiation of inhibitory control that was followed by failed inhibitory control. Similar to the advanced onset of stimulus orientation behavior, the moment of change in firing rate after the baseline period was also advanced in premature trials compared correct trials (**Figure 7F** and **7H**, 1921 correct trials, 907 premature trials, 17 sessions, 5 rats). A fraction of trials failed to reach significant activation or silencing between the trial start and response. This failure rate was higher for premature trials compared to correct trials (**Figure 7I**). Considering that silencing frontostriatal projection neuron activity using DREADDs did not result in changes in attentional performance, we expected that these neurons would not encode attentional errors. Indeed, combined persistently activated and silenced frontostriatal neurons did not show a difference in firing rate between incorrect and omission trials compared to correct trials, both immediately after stimulus orientation and just before stimulus onset (**Figure S5**). Together, these results show that failed inhibitory control, but not attention, is correlated to a reduced change in firing rate of mPFC frontostriatal projection neurons, combined with an earlier onset of persistent changes in firing rate (**Figure 7J**).

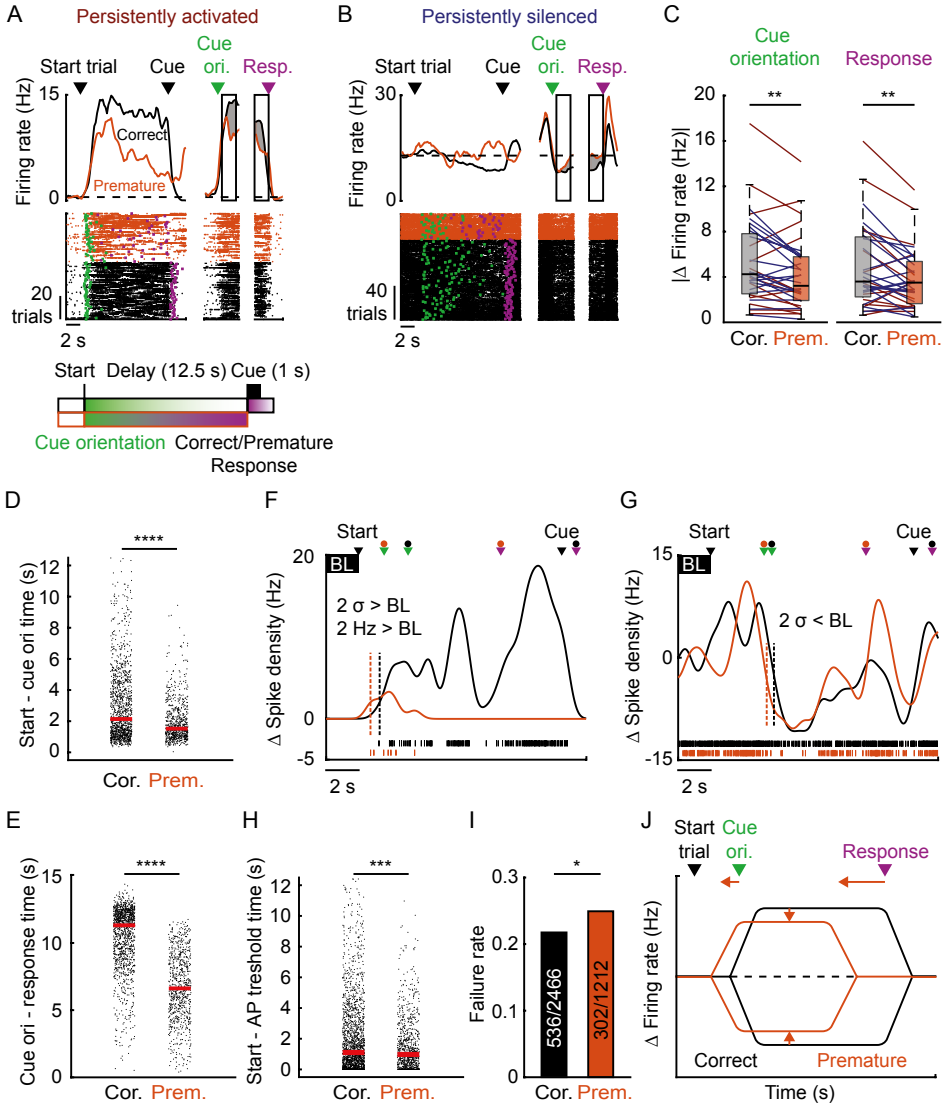

Figure 7. *Activity of frontostriatal neurons predicts successful inhibitory control of behavior.*
(**A** and **B**) Activity of persistently changed frontostriatal projection neurons during correct (black) and premature (orange) trials. (**A**) Persistently activated neuron. Top, PETH, bottom, spike raster plot. Green, stimulus orientation moment, purple, response, dotted line, baseline activity. Windows, 0.6 - 2.6 s after the stimulus orientation moment and 2 – 0 s before the response. Grey, difference between correct and premature. (**B**) Persistently silenced neuron, plotted as in (A). (**C**) Absolute change in firing rate for persistently activated (red) and silenced (blue) neurons after stimulus orientation ($Z = 2.749$, ** $p = 0.0088$) and before response ($Z = 2.618$, ** $p = 0.0088$, Wilcoxon signed-rank test, Benjamini–Hochberg FDR-corrected). Data point, session mean. (**D** and **E**)

Time between behavioral events (n = 1268 correct trials, n = 743 premature trials, 17 sessions, 5 rats). (**D**) Trial start to stimulus orientation (Z = 8.802, **** p < 0.0001). (**E**) Stimulus orientation and response (Z = 27.445, **** p < 0.0001). (**F-I**) Trial-based firing rate measurements for correct and premature trials (n = 1921 correct trials, n = 907 premature trials, 17 sessions, 5 rats). (**F**) Persistently activated neuron. Lines, Δ Spike density function from BL with Gaussian kernel (σ, 400 ms). Bottom, spike raster plot. Dotted line, first time point above AP threshold (2σ > BL and 2 Hz > BL, σ = standard deviation). Green and purple arrows indicate cue orientation and response moment, respectively, for premature (orange dot) and correct (black dot) trials. (**G**) Persistently silenced neuron, plotted as in (F). Dotted line, first time point below AP threshold (2σ < BL). (**H**) Time between start of trial and crossing of AP threshold (Z = 3.370, *** p = 0.0007). (**I**) Fraction of trials that failed to cross the AP threshold ($X^2(1) = 4.676$, * p = 0.03). (**J**) Schematic of the main differences between correct and premature trials. Orange arrows indicate the direction of change in premature response trials compared to correct response trials. All data for the longest delay trials of the inhibitory control sessions. (D, E and H) Wilcoxon rank-sum test, p < 0.05. Red line, median. Boxplots: center line, median; box edges, 1st and 3th quartile; whiskers, data range without outliers. See also Figure S5.

DISCUSSION

In this study we tested whether dorsal mPFC projection neurons that target the medial dorsal striatum encode inhibitory control and attention, using chemogenetic silencing and wireless extracellular single-unit recordings of identified corticostriatal mPFC projection neurons. Our results provide direct evidence that these frontostriatal neurons (i) are required for inhibitory control and not attention, (ii) are highly task engaged within the mPFC, showing predominantly persistent delay period-related activation and silencing in firing rate, and (iii) encode inhibitory control, where the amplitude and onset of change in activity are correlated to premature response behavior. Together, these results demonstrate a role of frontostriatal projection neurons in regulating proactive inhibitory control.

Previous work in humans, macaques and rodents has linked the PFC and DMS with proactive inhibition of behavioral responses until these are appropriate[5,19–21,41,53,55]. Neuroimaging studies in humans show that the dorsolateral PFC and the medial striatum are activated while proactively withholding a response in a go/no-go paradigm with high working memory demand[54,226–228]. These activity changes have been suggested to reflect a rule selective (i.e. “stop left”) engagement of a frontostriatal pathway to inhibit a behavioral response[5]. More specifically, it is proposed that these frontostriatal projection neurons engage the direct and indirect pathway of the striatum, eventually resulting in inhibition of a neuronal ensemble of a specific response in the motor cortex[5]. Anatomical studies show dense

innervation of the medial dorsal striatum by the dorsal PFC, strongly supporting a functional coupling between these regions[60,211,229]. Primate and rodent experiments have provided insight into how this frontostriatal pathway regulates proactive inhibitory control. Both mPFC and DMS neurons show persistent changes in firing rate, either by increased or decreased activity during the delay period before a response[19–21,41,53–55]. Moreover, a lower amplitude in activity of mPFC neurons was correlated to prematurely expressed responses, further supporting the role of persistent changes in firing rate as mechanism for inhibitory control[41,55]. Thus far, the exact role of the frontostriatal pathway in inhibitory control remains unknown. Our results support the hypothesis that the frontostriatal pathway is required for inhibitory control and that the amplitude of persistent changes in activity predict a failure of inhibitory control. However, to directly link the firing rate of frontostriatal neurons to inhibitory control, a more temporally and cell-type specific manipulation is required. An approach using silencing and activating opsins specifically in persistently activated or silenced neurons, respectively, would allow this.

Effects of DREADD-mediated inhibition of frontostriatal neurons were only present when the task difficulty was increased using longer, variable delay periods, but not during the standard delay period or variable stimulus duration sessions. This implies that frontostriatal neurons are engaged only under sufficiently challenging conditions. Alternatively, the standard 5 s delay condition might not be sensitive enough due to the low number of premature trials to reveal an effect on premature responses.

Neurons in the mPFC show a highly heterogeneous activity profile during cognitive control. Subpopulations of mPFC neurons have been shown to encode differential task information and activity dynamics[19,64,65,220,230]. Projection-specific identity of neurons successfully predicts task-involvement[64–66], such as, striatum-projecting PFC neurons that represent decision value[68,217] and thalamic-projecting PFC neurons that encode working memory and attention[56,57]. Given the role of the mPFC and DMS in inhibitory control and the unique task-relevant contribution of projection-specific neurons we expected that the subgroups of persistently activated or silenced mPFC neurons would mainly be composed of frontostriatal

projection neurons. Previous work in the 5-CSRTT showed that, collectively, CAMKII-expressing putative pyramidal neurons in the dorsal mPFC are required for attentional control[158]. We observed that, in comparison to neighboring non-tagged putative pyramidal neurons, frontostriatal neurons showed a higher fraction of delay period engagement. Together, this might suggest that selective populations of long-range-projecting pyramidal neurons within the PFC contribute differentially to the organization of goal-directed behavior[68,220]. The differences in the fractions of persistently activated, silenced and non-activated neurons we observe between the frontostriatal projections neurons and neighboring non-identified broad-spiking neurons are probably even an underestimation. The non-identified group likely contains false negatives due to limited viral transduction efficiency[231] and stringent optogenetic identification criteria. Future experiments directly comparing the role of projection-specific mPFC neurons can provide evidence for the dissociable roles of mPFC projection neurons in cognitive control.

Optogenetic inhibition of dorsal mPFC pyramidal neurons results in decreased attention in the 5-CSRTT[158]. Moreover, lesion, disconnection, optogenetic or chemogenetic manipulations in either the mPFC or the striatum were found to modulate attention suggesting that dorsal frontostriatal neurons regulate attentional control[32,39,94,96,158]. We here report the first direct manipulation of frontostriatal neurons in an attentional task and observe no clear effects on attention. This might suggest that DMS-projecting dorsal mPFC neurons are not involved in attentional control. Previous work was based on projection unspecific approaches that could potentially influence the activity of non-projection-specific neurons. It is therefore possible that attention is regulated by other mPFC pyramidal neurons. It has for example been shown that mPFC projections to the visual thalamic reticular nucleus, visual cortex and claustrum regulate attention[131,232]. However, to exclude the possibility of a role of frontostriatal neurons in attentional control more experiments need to be performed using projection-specific approaches in different attentional paradigms.

The mPFC contains two types of striatal projection neurons: pyramidal tract (PT) and intratelencephalic (IT) neurons, with each different physiological and

anatomical properties[233–235]. PT neurons are located in L5b, project to the ipsilateral striatum and brain stem, but can collateralize to many other structures. PT neurons have been suggested to suppress movement through the indirect pathway[235]. IT neurons are located in L5/6, project to both the ipsilateral and contralateral striatum and are thought to be involved in action execution through innervation of the direct pathway[235]. Possibly, persistently activated neurons are PT neurons, whereas persistently silenced neurons are IT neurons, but this is unclear and warrants further investigation.

Persistent changes in neuronal activity have also been linked to estimation of time intervals[53,55], by which the amplitude and ramping angle of firing rate positively correlates with estimated time interval[236]. Moreover, earlier onset of the stimulus orientation moment during premature responses has been reported in the 5-CSRTT without a shorter stimulus orientation to response time, suggesting that animals use a time estimation strategy only, with an advanced onset of trial engagement accounting for premature responses[21]. A failure in time estimation could contribute to the lower changes in firing rate of frontostriatal projections neurons during premature responses that we observed. However, our observations of a high level of performance during the longest delay trials, a lack of correlation between the response times during premature trials and amplitude of change in persistent activity (data not shown) and persistent changes in activity of frontostriatal neuron activity over all delay durations, collectively suggest that the dominant behavioral strategy is waiting for stimulus onset.

Inhibitory control is likely regulated through converging activity of functionally specialized brain areas. For example, both PFC projection neurons to the ventral striatum and ventral striatal inhibitory neurons have also been linked to inhibitory control[192], which might be more involved in motivational aspects of inhibitory control. Moreover, neuromodulators such as dopamine, serotonin and acetylcholine have been linked to inhibitory control and likely play an important role in regulating activity of frontostriatal neurons[5,62]. Striatum-projecting mPFC neurons also are known to have collaterals to downstream brain areas, including

the amygdala, the superior colliculus and ventral striatum[60,194]. Our cell soma-targeted experimental approach allows the possibility that axon collaterals regulate inhibitory control. However, the reported fraction of neurons that have collaterals is relatively low and likely has a limited contribution to our behavioral results[60,194].

METHODS

SUBJECTS

All experimental procedures were in accordance with the European and Dutch law and approved by the animal ethical care committee of the VU University and VU University Medical Centre. For electrophysiology experiments, 5 rats were used, for DREADD-inhibition experiments, 12 rats were used and for the eYFP only DREADD control group, 12 rats were used. All rats were outbred males from Janvier Labs, France. Upon arrival (~6-8 weeks of age) animals were housed in pairs under a 12-h light/dark cycle with lights off at 7 PM. After surgery (at ~10 weeks of age) animals were housed individually for electrophysiology experiments. After two weeks rats were moved to the experimental facility under a reversed 12-h light/dark cycle with light off at 12 AM. About two weeks after arriving in the experimental facility animals started training in the task. Food and water was available ad libitum until a week before training, at which they were food restricted to 85% of free feeding body weight.

SURGERIES

Pre-operative injections of Baytril (5 mg/kg, s.c.), Rymadil (Carprofen, 5 mg/kg, s.c.), Temgesic (buprenorphine, 0.05 mg/kg, s.c.) and Lidocaine (xylocaine, s.c. on periost) were administered. During surgery, isoflurane was administered (4% induction/1.8-2.2% maintenance on oxygen and air) through a nose-piece. The eyes were protected with ointment and every hour saline (1 mL, s.c.) was administered to prevent dehydration during surgery. Rats were placed in a stereotactic device (Kopf Instruments) and an incision was made in the skin above the skull, the periost removed and the skull cleaned using H_2O_2. Virus injections and optrode implantation were done in one surgery for electrophysiology experiments. Post-operative carprofen was administered for two days. Animals were allowed to recover minimally for one week before being moved to the experimental facility. For all brain coordinates the Paxinos and Watson rat brain atlas was used[237]. Viral injections were made using a Nanoject II injector (Drummond Scientific). A waiting period of minimally 6 weeks was implemented between surgery and testing for all animals to ensure proper viral expression.

To target frontostriatal neurons for single-unit electrophysiology, injections of a retrograde CAV2-Cre virus (Montpellier Vector Platform[238,239]) were made in the DMS (unilaterally, 3 rats right, 2 rats left AP 1.44; ML 2.78; DV 4.47 mm from bregma at a 10° angle, 8 injections of 69nL at a titre of 1.25*10^12 VM/mL). After making a craniotomy above the mPFC, two times 7 * 69nL of an rAAV5-Ef1a-DIO-hchR2(H134R)-eYFP virus (UNC GTC VECTOR CORE, at a titre of ~7*10^12) was injected on the ipsilateral side in the dorsal mPFC (AP 2.76; ML 1.1 mm from bregma; DV 2.5 and 1.5 mm from brain surface at a 5° angle). The pipette was lowered slowly to the injection locations with at least 1 min between each injection, a 5 min delay when moving to a next injection depth (dorsal mPFC) and a 15 min delay after the final injection, to allow for diffusion of the virus. Finally, the pipette was retracted slowly to prevent tissue damage.

To selectively express DREADD receptors in DMS-projecting prefrontal neurons, 7 injections of 69 nL of CAV2-Cre were made bilaterally in the DMS, with a titre of 1.25*10^12 VM/mL using the abovementioned coordinates. Additionally, either the DREADD receptor (AAV5-EF1α-DIO-hM4D(Gi)-mCherry, UZH, Switzerland, 0.483 µl, 3.6*10^12 VM/mL) or the eYFP protein only (AAV5-EF1α-DIO-eYFP, UPenn, USA, 0.483 µl, 4.2*10^12 VM/mL) was expressed with a bilateral infusion in the mPFC (AP 2.76; ML 1.3 and DV 2.9 mm from bregma at a 10° angle).

An optrode (see below) containing a silicon probe, optic fiber and moveable drive was implanted in a coronal plane above the viral injection site at DV coordinates between 1.2 and 1.5 mm from brain surface at a 5° angle and fixed to the skull using dental cement (3M RelyX Unicem 2) and 7 stainless steel screws (0.7 mm, Jeveka). A stainless steel reference wire was attached to the screw above the cerebellum. The ferrule of the optic fiber was protected using a metal sleeve (1,25mm, Prizmatix LTD) which was embedded in dental cement. Movable components within the dental cement and metal sleeve were protected using vaseline.

BEHAVIORAL SETUP

Rats were housed, trained and tested individually in a CombiCage[193]. Upon arrival in the experimental facility, rats were first given restricted access to only the

homecage. After a habituation period of two days the homecage was connected to an operant chamber (Med-Associates Inc., St. Albans, Vt, USA) with a tube, allowing free movement between the homecage and operant box. Rats were given minimally a week to acclimatize before the start of training. Most food was earned in the form of pellets (Dustless Precision Pellets, grain-based for electrophysiology experiments and training stages for DREADD experiments and purified for DREADD testing stages, F0165 or F0021, 45 mg, Bio-Serve, USA) in the task, however, occasionally animals did not earn enough food and were fed extra regular chow through an automatic feeding system above the homecage, 1.5 h after task completion. At the moment when the lights in the facility switched off (12 AM), rats could initiate trials at their own pace for a maximum duration of 2.5 h for both training and testing, after which they had to wait for the next day. Timestamps of nose-poke responses in the five stimulus holes and magazine port were recorded using IR beams. Custom-made Med Associates scripts were used to control the operant chambers and record behavioral data.

VIDEO RECORDING

During electrophysiology experiments head movement was tracked using an overhead infrared camera (25Hz, Panasonic WV-CP500 with CCTV lens 2.8-12mm F1.4 1/3" CS) and a blue LED on the wireless headstage with background infrared light. The stimulus orientation moment was defined using video analysis as the moment after trial start when the tracking LED crossed a boundary at 10 cm from the stimulus lights, using Bonsai software[240].

BEHAVIORAL TRAINING

As previously described in Bruinsma et al. (2019), there were 9 training stages during which rats progressively learned to withhold responding during a delay period (also called "intertrial interval" or "ITI") until a correct nose poke response could be made in one of five randomly lit stimulus holes. Briefly, in stage 1 50 semi-randomly timed pellet drop in the food magazine; in stage 2 50 trials of all stimulus lights on after a 5 s delay until nose poke; in stages 3-9 one stimulus hole was lit after a 5 s delay with gradual reduction in stimulus duration from 16 s to 1 s over stages and a response period (limited hold) of 2 s when the stimulus light

was switched off. Also, from stage 3 onwards trial availability was limited from 24 h to 2.5 h. Animals proceeded to the next stage when a they performed better than 80% accuracy in the last 20 trials and below 20% omissions for more than 200 correct trials in that particular stage. Animals were trained on stage 9 until they all reached more than 80% accuracy and below 40% omissions per session before proceeding with testing.

BEHAVIORAL TESTING

To challenge inhibitory control and attention, respectively, two versions of the protocol were used[193]: (i) in the inhibitory control sessions the delay to stimulus onset was randomly varied between 5, 7.5 and 12.5 s while the stimulus duration remained at 1 s, (ii) In the attention sessions the stimulus onset was randomly varied between 0.2, 0.5 and 1.0 s while the delay remained 5 s. Animals were tested on one session type per day. In the electrophysiology experiments, rats were typically recorded 4-7 days a week with alternating inhibitory control and attention protocols, whenever possible, and were trained on standard 5 s delay with 1 s stimulus duration sessions on no recording days. DREADD experiments were performed in weeks during which animals were subjected to inhibitory control or attention sessions every other day with standard training sessions in between. Testing with CNO was only done in inhibitory control and attention sessions.

CHEMOGENETIC SILENCING

Clozapine N-oxide (CNO) dihydrochloride (Hello Bio, UK) was dissolved in 0.9% saline and injected intraperitoneally 30 min before the start of a session. Solutions were freshly prepared on each test day and doses were administered using a balanced Latin square design. Animals received either 0, 5 or 10 mg/kg CNO, based on previously published studies in rats[194,241].

SINGLE-UNIT ELECTROPHYSIOLOGY

Extracellular single-unit activity was recorded using a chronic 4-shank, 64-channel silicon probe (P-type, shanks spaced 250 µm apart and electrodes 25 µm apart and organized in a vertical space of 200 µm, Cambridge Neurotech, UK) in combination with an optic fiber (100 µm diameter with an angled tip at ~0.5 mm above

the electrodes, Doric Lenses) to allow for optogenetic activation, glued on to a moveable nano-Drive (Cambridge Neurotech). This allowed recording of multiple locations within the dorsal mPFC. The optrode was lowered by approximately 205 μm in between recording locations. Analog signals were acquired using a 64-channel wireless headstage and receiver (Triangle BioSystems International, Durham, NC) with a gain of 800, bandpass filtered between 0.8 Hz and 7 kHz and digitized at 30003.0003 Hz using a National Instruments DAQ USB-6363 in combination with Neurorighter software242,243. Spike detection and clustering was done per shank using Klusta (version 3.0.16) and manual curation using the Kwik-gui interface[244]. A common median reference was applied before spike detection using the channels on the other shanks.

OPTOGENETIC IDENTIFICATION

After every test session we connected the rat to a diode-pumped laser (473 nm, Shanghai Laser and Optics Century Co, China) and applied different light stimulation protocols until reliable optogenetic identification was achieved: 500 pulses (2, 5 or 10 ms) at 5 Hz at 100% or 75% laser power, triggered by a master-9 (A.M.P.I, Israel).

HISTOLOGY

For histology, rats were anesthetized with isoflurane For histology, rats were anesthetized with isoflurane and Dormitol (100 mg kg-1) and transcardially perfused (~100 mL NaCl and 200 – 400 mL 4% paraformaldehyde (PFA, pH 7.3)). To determine electrode locations, microlesions were made using an anodal electrical current. Brains were collected and fixed in 4% PFA for at least 24 h before further processing. Coronal sections were made at 50 μm in 0.05M PB using a vibratome, mounted on glass slides with 2% Mowiol and cover slipped. Probe placement was verified visually with an Olympus BX51 microscope using a 4X air or 40X oil objective. Verification of viral expression for electrophysiology experiments was done using a confocal microscope (Nikon, 10X air or 40X oil objective, excitation wavelength, 488 nm, bandpass filter, 505 – 550 nm) and further processed in ImageJ (NIH, USA) to adjust contrast and brightness. Expression of the DREADD receptor was verified by staining for mCherry with a rabbit anti-RFP (Rockland, 1:1000) primary antibody and with a Alexa Fluor 546 donkey anti-rabbit (Thermo

Fisher Scientific, 1:400) as secondary antibody. Briefly, 50 µm sections were rinsed in PBS with 0.25% Triton X. Subsequently, sections were incubated for 3 h with blocking solution (PBS, 0.3% Triton X and 5% normal goat serum). Incubation with the primary antibody in blocking solution was done overnight, at 4° C. Afterwards, the sections were washed three times with PBS and incubated with the secondary antibody for 2 h at room temperature in blocking solution. Confocal images were acquired as described above and further processed in ImageJ[245]. For the DREADD validation experiments, a regions of interest (ROI) including the area of virus expression was selected in ImageJ. The area of the ROI was calculated and the numbers of cell bodies within the ROI were counted.

STATISTICAL ANALYSIS

Statistical analysis was performed in Matlab (Mathworks), unless otherwise stated. No statistical tests were done to determine sample size, but our sample sizes are similar to or larger than previously reported sample sizes[39,68,246]. Friedman's ANOVA (reported as Fr) with a Dun's post hoc test, a paired Wilcoxon signed-rank (reported as Z) or unpaired Wilcoxon rank-sum test (reported as Z) was used for non-parametric testing. Normality of the data was checked using D'Agostino-Pearsons omnibus normality test. To compare fractions a Chi-square test was used (reported as X2(df)).

For DREADD experiments a three-way mixed repeated-measures ANOVA (reported as F) with post hoc t-tests or Wilcoxon signed-rank tests (reported as t(df) = t-value, p = p-value, d = cohen's d, power = statistical power), with Benjamini-Hochberg false discovery rate (FDR) correction[247]. Normality of the data was checked using a Shapiro-Wilk test. A two-sample F-test was performed to test if the groups displayed equal variances across conditions. Post hoc testing, and correction for multiple comparisons, was done with t-tests and Wilcoxon signed-rank tests with Benjamini-Hochberg false discovery rate (FDR) correction[247], respectively.

Boxplots: center line, median; box edges, 1st and 3th quartile; whiskers, data range without outliers. Statistical significance was set at $p < 0.05$, unless otherwise stated. Details of statistical tests can be found in the figure legends and results sections.

BEHAVIORAL ANALYSIS

Behavioral performance was calculated as follows:

$$Premature\ responses\ (\%) = \frac{Premature\ response\ trials}{All\ trials} * 100$$

$$Accuracy\ (\%) = \frac{Correct\ response\ trials}{Correct + incorrect\ response\ trials} * 100$$

$$Omissions\ (\%) = \frac{Omission\ of\ response\ trials}{All\ completed\ trials} * 100$$

"All trials" contains correct, incorrect, premature and omission of response trials. "All completed trials" contains correct, incorrect and omission of response trials. For Figure 1 data was analyzed in Graphpad Prism (Graphpad Software, Inc.).

For DREADD experiments (**Figure 2 and Table S1**) trials with a magazine latency > 10 s were excluded from the behavioral analyses[23,193]. Effects of CNO were compared between the control and DREADD group with a three-way mixed repeated-measures ANOVA with dose, stimulus duration and delay as within-subject factors and the experimental group as between-subjects factor. As several behavioral parameters were not dependent on trial type, such as started number of trials, two-way mixed repeated measures ANOVAs with dose as within-subject factor and group as between-subject factor were employed.

SPIKE SORTING

A spike was detected if it crossed a threshold of 4.5 times the standard deviation above the background noise. Spike clusters were accepted as single-unit if they met the following quality criteria[223,248]: Isolation distance > 40, L-ratio < 1.5, inter-spike intervals below 1.5 ms < 0.25%. Moreover, the PCA of clusters were visually inspected on waveform stability over time and cross-correlograms were visually inspected to avoid duplicate neurons.

SPIKE WAVEFORM SEPARATION

Single units were separated in broad-spiking and narrow-spiking neurons using a Gaussian mixture model based clustering approach (Sigma was set to diagonal and shared covariance to false in the fitgmdist function) using the spike waveform features "half-peak-time" and "peak-to-through time"[20,222,223]. Neurons with a posterior probability > 0.85 of belonging to a broad- or narrow-spiking cluster were included, otherwise they were unclassified and removed from analysis.

OPTOGENETIC IDENTIFICATION CRITERIA

The first spikes within 10 ms after laser onset were compared to the 40 ms before laser onset using 1 ms bin sizes. Frontostriatal projection neurons were regarded as optogenetically-identified based on activation by brief pulses of blue light. Significant light-induced activation was determined with the stimulus-associated spike latency test[220] (SALT, $p < 0.01$) and peak z-score > 1.65. To prevent network-related activation and opsin-induced spike waveform distortion from contaminating optogenetic identification we added the following criteria: a light-induced mean first spike latency < 7 ms, jitter < 3.5 ms, reliability > 0.03 and Pearson's waveform correlation > 0.8[220,246]. An additional 4 neurons (n = 3 for inhibitory control sessions, n = 1 for attention sessions) were included that were stably recorded over two session types but in which optogenetic identification was positive in only one of the two session types, likely due to light delivery failure.

NEURON IDENTIFICATION OVER CONSECUTIVE DAYS

Single units were reliably tracked across consecutive days using the following criteria: recorded on the same depth, maximal difference in peak waveform channel position of one, Pearson's average waveform correlation on peak channel > 0.95, Pearson's correlation of interspike interval distributions (1 ms bins) between 0 and 50 ms > 0.8 and peri-event histogram correlation from 1 s before to 3 s after stimulus orientation > 0.5.

ANALYSIS OF FIRING RATE AND NEURON CATEGORIES

Peri event time histograms (PETHs) were made by taking the mean firing rate over trials using 200 ms bins. For display purposes, trial-averaged PETHs were

smoothed with a 600ms moving average. To determine if a neuron changed its activity in the task, trial-based paired comparisons in firing rate were made between the baseline period and different phases in the task using a Wilcoxon signed-rank test ($p < 0.05$). This was done for both frontostriatal neurons and non-identified neurons without multiple comparisons correction. Baseline-corrected (Δ) firing rate was calculated by subtracting the baseline firing rate per trial and taking the mean over trials. Neuron-averaged Δ firing rates between correct and errors (premature, incorrect and omissions) were compared using Wilcoxon signed rank tests ($p < 0.05$) after testing for normality using D'Agostino-Pearsons omnibus normality test in Graphpad Prism. Spike density functions were calculated by convolving spikes with a Gaussian kernel (σ, 400 ms).

EXCLUSION CRITERIA

For comparisons between frontostriatal neurons and neurons recorded in the same session we excluded all neurons that were not recorded in a same session as optogenetically-identified neurons or only had a significant SALT ($p < 0.01$) without other optogenetic identification criteria. For comparisons in firing rates for electrophysiology experiments, omission trials were removed during which the rat did not cross the stimulus orientation line. These were regarded as trials that were accidentally started, yet without task engagement. Also trials were removed of which video monitoring was unreliable. Two animals with no expression or only unilateral expression of the DREADD receptor were excluded from analysis, resulting in 10 animals for analysis.

SUPPLEMENTARY FIGURES AND TABLES

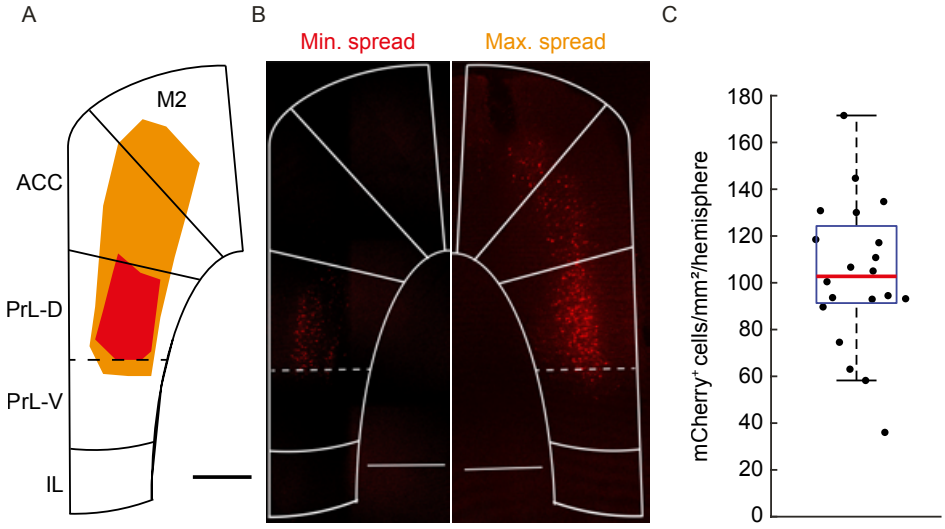

Figure S1. *DREADD virus spread in the dorsal mPFC. Related to Figure 2.*
(**A**) Schematic of the minimal and maximal spread of the hM4D(Gi)-mCherry virus in the dorsal mPFC. M2, secondary motor cortex, ACC, anterior cingulate cortex, Pr-D, dorsal prelimbic cortex, Pr-V, ventral prelimbic cortex, IL, infralimbic cortex. (**B**) Example confocal images of the minimal and maximal hM4D(Gi)-mCherry virus spread from two animals. (**C**) Number of mCherry-positive DREADD neurons (n = 20 hemispheres, 10 rats). Boxplots: center line, median; box edges, 1st and 3th quartile; whiskers, data range without outliers, cross, outlier. Scale bars, 1 mm.

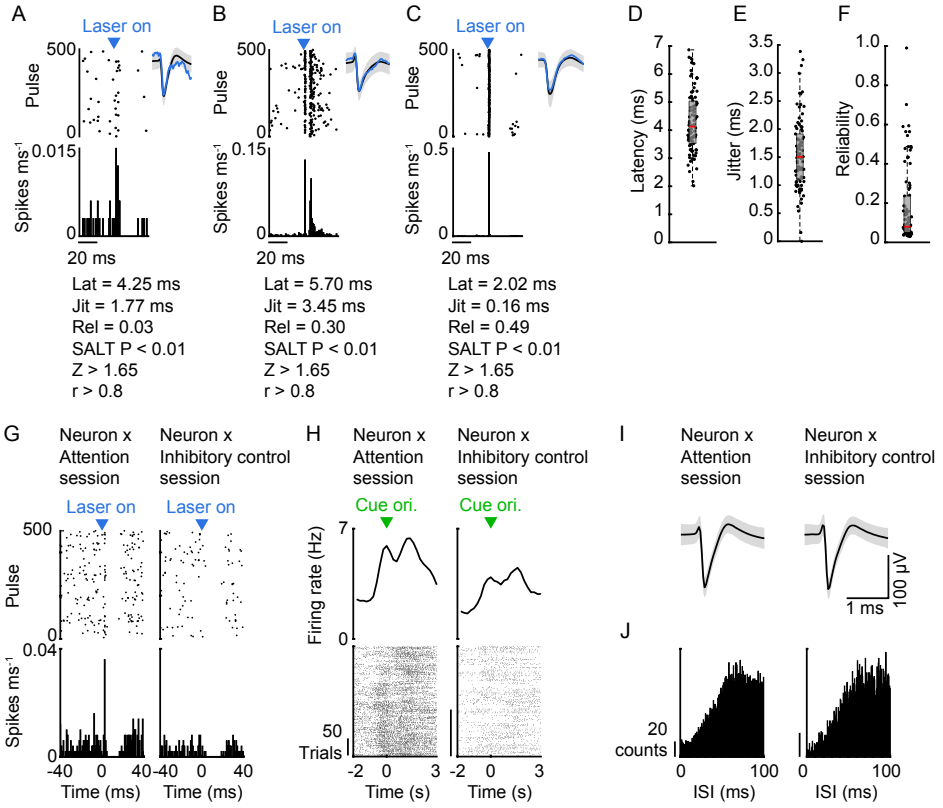

Figure S2. *Optogenetic identification of frontostriatal projection neurons. Related to Figure 3.*
(**A-C**) Optogenetic identification sessions from three example neurons. Top, raster plot, bottom PSTH, right, average waveform (black ± grey, plotted as mean ± SD) and average light triggered waveform (blue). (**A**) Lowest reliability example. (**B**) High jitter example due to second peak within 10 ms. Boxplot, median ± 1st and 3d quartile, dots, individual data points. (**C**) Low latency, low jitter and high reliability example. First spike latency (**D**), jitter (**E**) and reliability (**F**) of all optogenetically-identified neurons. (**G-J**) Criteria to identify same neuron over two days with same recording location. Used to include four neurons recorded over two session types where only one met the optogenetic identification criteria (see example in (**G**)). Pearson's correlation between the (**H**) PETHs aligned to cue orientation > 0.5, (**I**) average waveforms > 0.95 and (J) the ISI distribution between 0 - 100 ms > 0.7.

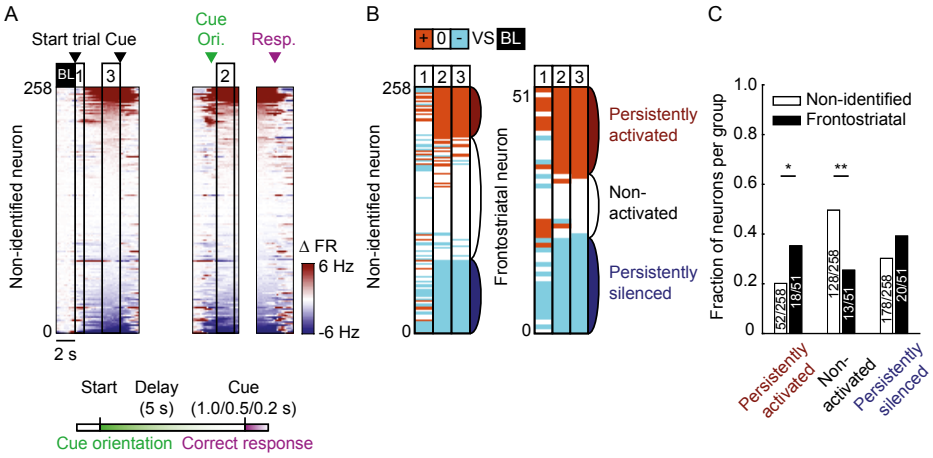

Figure S3. *Frontostriatal projections neurons within the frontal cortex are specialized in persistent delay activity, measured in attention sessions. Related to Figure 6.*

(**A**) Δ Firing rate for non-identified neurons during all correct trials of the attention sessions. Colors indicate Δ firing rate (FR) from BL (2 - 0 s before trial start) clipped at +6 Hz and -6 Hz. Window 1) 0 - 1 s after trial start, 2) 0.6 - 2.6 s after cue orientation and 3) 2 - 0 s before the cue. (**B**) Activity categories for non-identified (left) and frontostriatal (right). Colors indicate change in firing rate from BL with activated (orange), no change (white) and silenced (cyan). Wilcoxon signed-rank over Δ firing rate of all correct trials per neuron, $p < 0.05$. (**C**) Fraction of neurons per group (non-identified and frontostriatal) that are persistently activated ($X^2(1) = 5.570$, * $p = 0.0183$), non-activated ($X^2(1) = 9.9874$, ** $p = 0.0016$) and persistently silenced ($X^2(1) = 1.5876$, $p = 0.2078$). Neurons sorted on activity category and Δ firing rate in window 3.

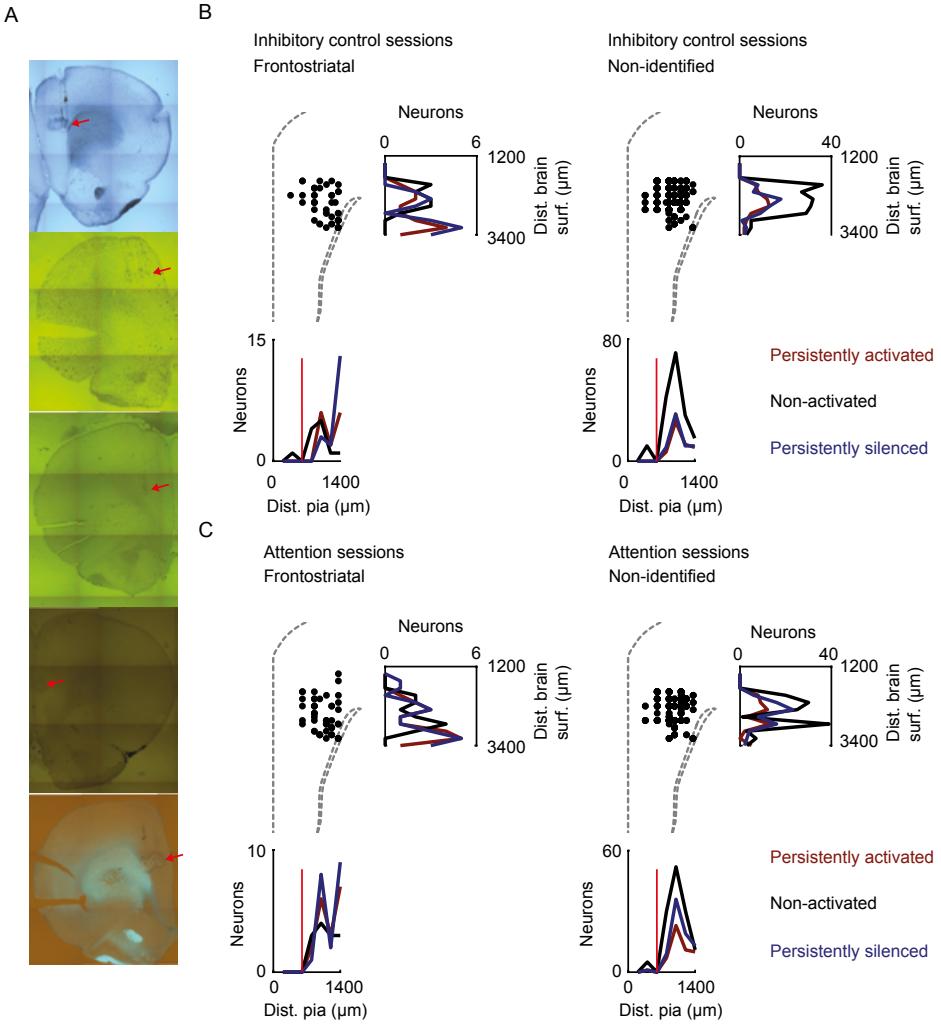

Figure S4. *Single-unit recording locations for neurons groups and activity categories. Related to Figure 6.* (**A**) Histological verification of recording location (red arrow). (**B**) Recording locations of frontostriatal neurons (left) and non-identified neurons (right) during inhibitory control sessions. (**C**) Recording locations of frontostriatal neurons (left) and non-identified neurons (right) during the attention sessions. Each dot represent the estimated recording location of a sessions after visual inspection of the post-hoc electrolytic marking. Red, persistently activated neurons, black, non-activated neurons and blue, persistently silenced neurons. Vertical red line, separation between superficial and deep cortical layers at 600 µm from pia.

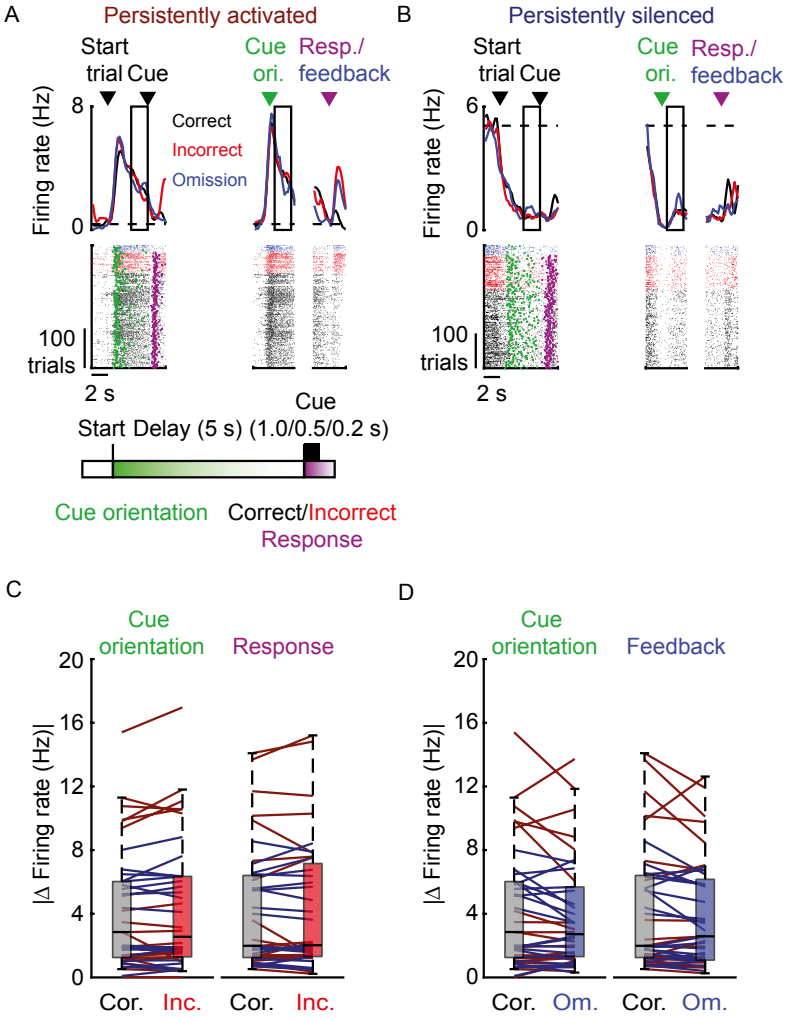

Figure S5. *Similar activity of frontostriatal projection neurons during correct, incorrect and omissions trials in attention sessions. Related to Figure 7.*

(**A** and **B**) Activity of persistently changed frontostriatal projection neurons during all correct (black), incorrect (bright red) and omission (blue) trials. (**A**) Persistently activated neuron. Top, PETH, bottom, spike raster plot. Green, cue orientation moment, purple, response, dotted line, baseline activity. Window, 0.6 - 2.6 s after the cue orientation moment and 2 - 0 s before the cue. Grey, difference between correct and premature. (**B**) Persistently silenced neuron, plotted as in (A). (**C** and **D**) Absolute Δ firing rate for persistently activated (dark red lines) and silenced (dark blue lines) neurons. (**C**) Correct vs. incorrect trials in window after cue orientation ($Z = -0.7759$, $p = 0.8756$) and before response ($Z = 0.0941$, $p = 0.9250$). (**D**) Correct vs. omission trials in window after cue orientation ($Z = 1.6605$, $p = 0.0968$) and before response ($Z = 1.9692$, $p = 0.0968$). (C and D) Wilcoxon signed-rank test, $p < 0.05$, Benjamini–Hochberg FDR corrected. Data points, session mean. Boxplots: center line, median; box edges, 1st and 3th quartile; whiskers, data range without outliers.

	Delay/ cue duration (s)	DREADD (n = 10)			eYFP only (n = 12)		
		Saline	CNO 5 mg/kg	CNO 10 mg/kg	Saline	CNO 5 mg/kg	CNO 10 mg/kg
Premature responses (%)	**5**	2.88 ± 1.91	3.47 ± 2.30	3.05 ± 1.92	4.00 ± 2.92	3.92 ± 2.20	3.09 ± 2.54
	7.5	6.99 ± 4.69	9.40 ± 4.72	9.70 ± 6.06	9.21 ± 6.80	11.29 ± 5.53	8.88 ± 3.85
	12.5	19.80 ± 12.07	26.38 ± 13.84*	29.74 ± 12.64*	27.21 ± 16.29	28.15 ± 14.38	24.83 ± 13.62
Accuracy (%)	**5**	88.09 ± 2.56	89.38 ± 4.54	87.99 ± 5.44	89.94 ± 6.17	89.13 ± 5.56	91.53 ± 4.85
	7.5	88.56 ± 3.62	86.46 ± 4.00	87.33 ± 5.39	88.62 ± 8.05	88.16 ± 7.39	88.85 ± 7.49
	12.5	84.85 ± 6.80	82.84 ± 7.29	82.03 ± 6.94	80.90 ± 9.80	83.86 ± 9.13	83.36 ± 9.69
Omissions (%)	**5**	12.35 ± 6.23	10.06 ± 5.97	7.97 ± 3.27	7.18 ± 3.96	9.25 ± 4.72	8.31 ±5.41
	7.5	8.54 ± 3.77	6.38 ± 4.37	7.22 ± 5.10	6.46 ± 2.89	5.97 ± 2.32	6.99 ± 5.30
	12.5	9.13 ± 6.12	8.80 ± 4.56	9.71 ± 5.45	8.05 ± 5.72	7.11 ± 4.59	6.54 ± 2.87
Correct response latency (s)	**5**	1.26 ± 0.16	1.21 ± 0.22	1.16 ± 0.12	1.10 ± 0.15	1.12 ± 0.18	1.11 ± 0.20
	7.5	1.19 ± 0.17	1.13 ± 0.16	1.14 ± 0.12	1.07 ± 0.18	1.04 ± 0.17	1.05 ± 0.17
	12.5	1.15 ± 0.14	1.13 ± 0.16	1.11 ± 0.12	1.07 ± 0.15	1.05 ± 0.18	1.02 ± 0.17
Premature response latency (s)	**5**	3.64 ± 0.55	3.41 ± 0.51	3.51 ± 0.61	3.50 ± 0.59	3.75 ± 0.56	3.37 ± 0.42
	7.5	5.51 ± 0.75	5.32 ± 0.53	5.52 ± 0.45	5.39 ± 0.47	5.41 ± 0.58	5.39 ± 0.50
	12.5	8.18 ± 0.68	8.35 ± 0.71	8.62 ± 0.47	8.33 ± 0.64	8.32 ± 0.83	8.61 ± 0.84
Number of started trials	**All delays**	400.20 ± 58.69	399.50 ± 79.56	416.60 ± 55.97	433.08 ± 53.41	442.08 ± 33.32	430.08 ± 46.57
Magazine latency (s)	**All delays**	2.15 ± 0.36	2.04 ± 0.38	2.03 ± 0.37	2.24 ± 0.28	2.28 ± 0.35	2.30 ± 0.34
Perseverative responses on target (%)	**All delays**	2.98 ± 2.21	2.91 ± 1.66	3.04 ± 1.11	3.12 ± 1.55	2.99 ± 1.48	2.82 ± 1.22

Premature responses (%)	**1**	3.12 ± 2.06	4.44 ± 1.42	3.81 ± 2.68	4.24 ± 2.44	4.25 ± 3.85	4.00 ± 2.70
	0.5	3.49 ± 1.88	3.33 ± 3.29	2.92 ± 2.37	4.03 ± 3.02	4.42 ± 3.56	4.66 ± 3.21
	0.2	3.50 ± 2.69	3.79 ± 2.56	3.99 ± 2.80	4.51 ± 3.17	4.04 ± 3.59	3.03 ± 2.00
Accuracy (%)	**1**	87.38 ± 3.82	85.94 ± 5.06	84.97 ± 4.73	90.02 ± 5.00	89.52 ± 6.11	88.78 ± 4.66
	0.5	70.94 ± 7.11	69.72 ± 6.91	70.89 ± 7.00	78.13 ± 4.93	77.12 ± 6.05	77.60 ± 6.74
	0.2	60.73 ± 10.44	63.13 ± 12.06	60.02 ± 9.29	65.13 ± 4.87	64.49 ± 6.43	68.24 ± 8.03
Omissions (%)	**1**	15.20 ± 6.41	15.07 ± 5.24	16.13 ± 5.91	6.80 ± 4.56	7.54 ± 5.28	7.32 ± 3.55
	0.5	22.73 ± 9.42	20.42 ± 8.72	21.81 ± 8.90	11.44 ± 6.77	8.55 ± 5.31	11.83 ± 6.07
	0.2	33.78 ± 11.88	32.41 ± 11.69	31.65 ± 7.55	17.73 ± 6.37	17.42 ± 9.51	20.10 ± 7.15
Correct response latency (s)	**1**	1.32 ± 0.15	1.29 ± 0.16	1.27 ± 0.19	1.09 ± 0.15	1.10 ± 0.14	1.10 ± 0.12
	0.5	1.09 ± 0.13	1.06 ± 0.14	1.08 ± 0.17	0.94 ± 0.14	0.94 ± 0.09	0.96 ± 0.10
	0.2	0.99 ± 0.16	0.93 ± 0.15	0.94 ± 0.13	0.86 ± 0.15	0.85 ± 0.12	0.89 ± 0.08
Number of started trials	**Cue**	432.3 ± 84.11	416 ± 107.95	431.7 ± 75.71	517.25 ± 48.07	509.42 ± 37.65	505.25 ± 42.98
Magazine latency (s)	**Cue**	2.17 ± 0.35	2.14 ± 0.34	2.21 ± 0.42	2.46 ± 0.29	2.43 ± 0.31	2.54 ± 0.33
Perseverative responses on target (%)	**Cue**	1.41 ± 0.75	2.22 ± 1.40	2.16 ± 1.38	3.09 ± 1.50	2.89 ± 1.27	2.99 ± 0.81

Supplementary Table S1. *Effects of DREADD-mediated inhibition of frontostriatal projection neurons on task parameters.*

Summary of behavioral parameters from inhibitory control and attention sessions. Post-hoc tests are Benjamini–Hochberg FDR-corrected. DREADD group, n = 10 rats, eYFP only group, n = 12 rats. Data expressed as mean ± SD. Significant difference compared to saline condition indicated in bold and "*".

CHAPTER 6

Discussion

SYNOPSIS

So, what happens within our prefrontal cortex if we drive our car and listen to our favorite neuroscience professor in class? Within this thesis I focus on the role of specific neurons within the medial prefrontal cortex, namely pyramidal neurons and subcortically-projecting neurons, in inhibitory control and attention. In **chapter two** I describe that the medial prefrontal cortex (mPFC) is not a homogeneous brain area but has a functional dorsoventral axis. Pyramidal neurons in the dorsal mPFC are required to sustain attention (i.e. focus on traffic) during the entire delay period that we exert cognitive control, whereas ventral mPFC pyramidal neurons are required for both inhibitory control and attention at the end of the delay near the detection of a sensory event (i.e. focus on the lecture and don't interrupt the professor with your burning questions but wait until the lecture is over). **Chapter three** takes a side-step (but a very important one) to improve the behavioral paradigm used to study inhibitory control and attention in rats, the 5-choice serial reaction time task (5-CSRTT). By making the 5-CSRTT homecage-based using the CombiCage, self-paced, and introducing variable conditions (i.e. when a right turn is coming or how briefly we see the road sign), we were able to i) drastically reduce training time and experimenter interference time, ii) increase the numbers of trials per session and iii) increase experimental throughput while improving inhibitory control and attentional read-outs.

The mPFC is a highly heterogenous brain area that requires constant communication with different functionally specialized downstream brain areas in order to correctly regulate inhibitory control and attention. In **chapter four** I narrow my scope to the role of subsets mPFC neurons in inhibitory control and attention, specifically long-range, topographically-projecting, putative pyramidal neurons to the mediodorsal thalamus and striatum, along the dorsoventral axis of the mPFC. I describe that distinct subsets of mPFC-projecting neurons carry different information in support of inhibitory control that can deviate from what generalized manipulations of pre- or post-synaptic brain areas would suggest. Finally in **chapter five** I make the last focusing step and describe that individual mPFC to the dorsomedial striatum projection neurons are involved inhibitory control with persistent changes in activity. See **figure 1** for a schematic overview of the main findings regarding the mPFC in cognitive control.

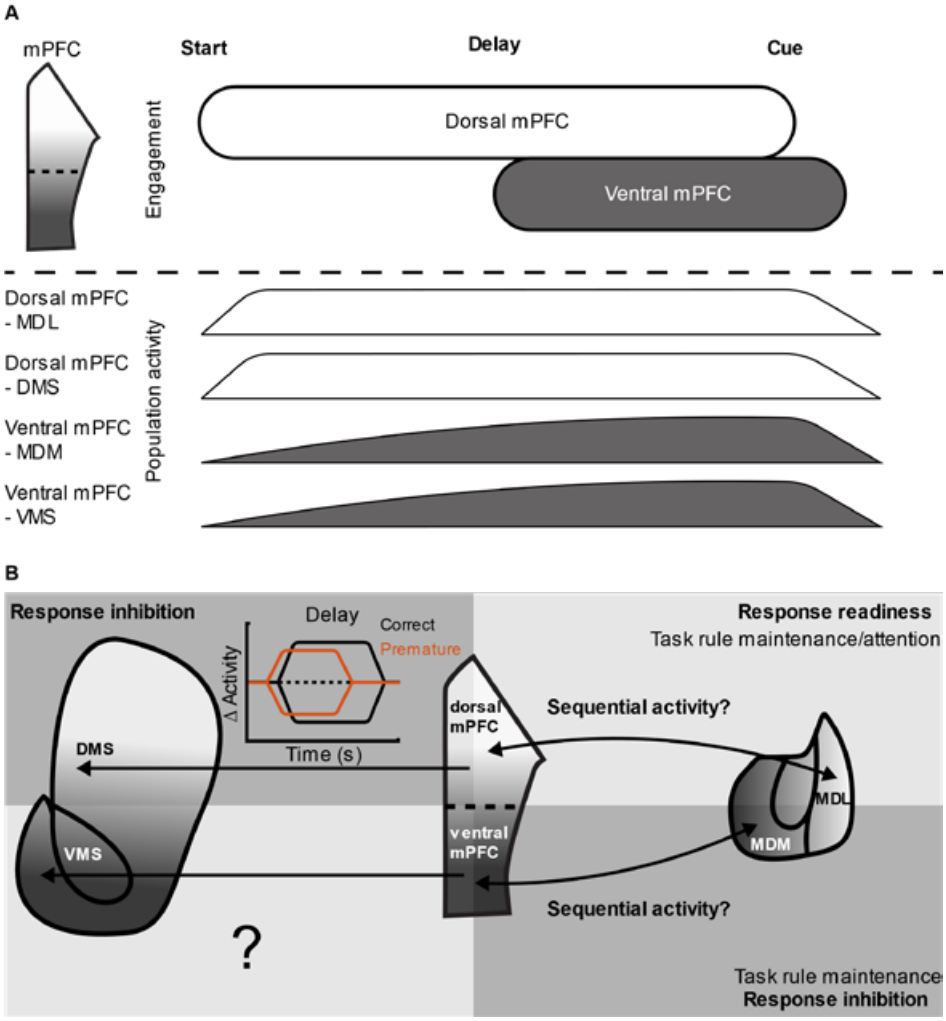

Figure 1. *Schematic overview of the main findings within this thesis on pyramidal output neurons across the dorsoventral axis of the mPFC in cognitive control.*

(**A**) Temporal engagement, as measured by behavioral effects after optogenetic inhibition of CAMKII-expressing putative pyramidal neurons (top), or measured as specific projection neuron absolute population activity (bottom), along the dorsoventral axis of the mPFC during a stimulus free delay period. (**B**) mPFC projection-neuron specific role in cognitive control, with a focus on behavioral control and attention. Proposed neuronal encoding mechanisms are indicated.

THE MPFC ALONG THE DORSOVENTRAL AXIS

Our results support the idea that the mPFC can be divided in a functional dorsoventral axis[37]. Studies of attention performance in animals with lesions of the dorsal or ventral mPFC have suggested that the this region might be more involved in sensori-motor integration and attentional control, whereas the ventral mPFC integrates limbic-emotional information and is more involved in inhibitory control, or 'waiting impulsivity'[7,20,31,32,38–40], although functional overlap between the dorsal and ventral mPFC has also been reported in other cue detection paradigms[31,40,41]. Different encoding mechanisms have been suggested in support of inhibitory control and attention, where persistent changes in firing activity throughout the delay period has been most extensively investigated[19–21,53]. The dorsoventral axis in encoding mechanisms remains, however, poorly understood as most studies investigating neuronal activity are performed in the dorsal mPFC. Nonetheless, there are indications that dorsal and ventral mPFC neurons differentially encode cognitive control, with the dorsal mPFC being more proactively involved over longer periods before cue detection and the ventral mPFC around cue detection and integration[41]. In chapter 2, using optogenetically-mediated inhibition of CaMKII-expressing pyramidal neurons in an inhibitory control and attention paradigm, we demonstrate two important observations. First, the dorsal mPFC neurons are required over seconds long periods across the whole delay duration, whereas the ventral mPFC neurons are only required around the cue presentation period. Second, pyramidal neurons of the dorsal mPFC are more involved in attentional control, whereas ventral mPFC neurons are more involved in inhibitory control. The differential temporal engagement of the dorsal and ventral mPFC is in line with recent experiments that showed a functional gradient from dorsal to ventral mPFC neurons in proactive to reactive behavioral control, using both single-unit electrophysiology and optogenetic manipulation[41]. Taken together, it becomes clear that the dorsal mPFC is involved in planning and temporal integration of contextual information, whereas the ventral mPFC is more reactively involved around the moment when planning needs to be translated in to action. Our results also indicate that the dorsal mPFC is involved in attentional control, whereas the ventral mPFC is involved in both attentional control and inhibitory control. Although the role of the dorsal mPFC in attentional control

and the ventral mPFC in inhibitory control is in line with lesion studies in the 5-CSRTT[7,20,31,32,38–40,42], studies using a paradigm where animals had to actively press a lever until a cue was presented also indicated a role for the dorsal mPFC in inhibitory control[41,53]. Possibly, the standard version of the 5-CSRTT that we used was not challenging enough for control of response inhibition because animals were trained and tested only on a fixed delay of 5 seconds, allowing the rat to precisely predict when a stimulus was presented. Indeed, randomly varying the delay duration in CombiCage 5-CSRTT used in chapter 4 and 5 resulted in a delay dependent increase in premature responses and the role of specific projection neurons was only present during the longer delay durations. Future experiments silencing the total population of dorsal or ventral mPFC pyramidal neurons using the variable longer delay session of the CombiCage 5-CSRTT can show if possible effects of over training animals on a fixed delay length confounded our findings in chapter 2.

THE RECIPROCAL FRONTOTHALAMIC CIRCUIT

The dorsal and ventral mPFC are highly interconnected with the MDL and MDM, respectively, forming reciprocal loops[72,249]. These loops are important for cognitive cognitive control, possibly by keeping task information online within the mPFC[56,57,63,76,79]. MD lesions result in both inhibitory control and attention deficits as measured in the 5-CSRTT[77]. However, we still poorly understand the properties of dorsoventral topographical mPFC connectivity with the MD, as most studies are focused on the dorsal mPFC-to-MDL connections only[56,57,249]. In chapter 4 we investigated the roles of dorsal and ventral mPFC projections to the MDL and MDM, respectively, in inhibitory control and attention. We show a dissociable and seemingly opposite role for MDL and MDM-projecting mPFC neurons, not in attention behavior as measured in accuracy of responding, but in response control as measured in premature responses and omissions. DREADD-mediated inhibition of topographically-projecting mPFC neurons to the MDL or MDM resulted in a delay-dependent decrease in premature responding combined with a delay-independent increase in omissions or a delay dependent increase in premature responding, respectively. One could interpret this in line with the role of topographical mPFC-MD reciprocal loops in sustaining task-relevant information within the mPFC and with a role of both the dorsal and ventral

mPFC in behavioral contol, albeit with a differential role of the dorsal and ventral mPFC region. Lowering task-relevant information content in the dorsal mPFC, by DREADD-mediated inhibition of MDL-projecting dorsal mPFC neurons, results in a weaker information trace that represents "GO" (i.e. 'prepare for cue detection') memory trace and instructs downstream brain areas which behavior needs to be prepared, resulting in both a general increase in omissions and delay dependent decrease in premature responding. The same principle might hold for the ventral mPFC-to-MDM loop, only here ventral mPFC rule information functions as a response break or "STOP" memory trace, which is released by DREADD-mediated inhibition. Based on the role of the dorsal mPFC in attentional control, however, one would also expect a decrease in response accuracy after DREADD-mediated inhibition. Additionally, the deficits observed after DREAD-mediated inhibition of MDL-projecting dorsal mPFC neurons, could also be an attention deficit, where a disruption in sustained attention resulted in a response readiness signal, where cue detection accuracy remained unchanged in both variable delay and variable cue conditions. Likely, deficits in accuracy of responding, as reported by studies using non-projection specific interference, was the result of projections to other brain areas than the MD, such as the visual thalamic reticular nucleus, visual cortex and claustrum[131,232]. It remains, however, possible that our DREADD-mediated inhibition was not powerful enough to reliably silence axonal output from all the projection neurons in the mPFC that were required for attentional control. Future experiments using stronger manipulations, such as with optogenetics[119,250], might have more behavioral impact. Moreover, optogenetics also provides a more temporally precise resolution than DREADDs, allowing the investigation of when MD-projecting mPFC are required. Using population-based bulk calcium imaging we showed that MDL-projecting dorsal mPFC neurons are more involved at the start of the delay phase, compared to MDM-projecting ventral mPFC neurons. This is in line with the proactive role of the dorsal mPFC in integrating information over the whole delay period and the reactive role of the ventral mPFC around the response period[41,158]. However, using temporally imprecise DREADD manipulations we are unable to rule out that the observed delay period changes in calcium signal reflect a causal involvement in behavior.

At the receiving end of the MD-projecting mPFC neurons are the MD relay neurons. The electrophysiological properties of MD relay neurons are important factors in how information from the mPFC, but also other brain areas, is received, processed and sent to other brain areas. In addition to differential functionality and activity dynamics of topographically-projecting MDL and MDM mPFC neurons, we show that there are differences in basic electrophysiological properties of post-synaptic, reciprocally connected, MDL and MDM neurons. While there is sparse evidence that MD relay neurons differ along the mediolateral axis in morphology[85], this is, to my knowledge, the first demonstration that MDL and MDM neurons, that are reciprocally connected to the mPFC, differ in electrophysiological properties. MDM relay neurons have a higher input resistance, slower membrane time constant and are require less input current to elicit APs, compared to MDL neurons. At the same time the MDL and MDM both receive facilitation synaptic input from the mPFC. Combined with the differences in functionality and activity dynamics along the dorsoventral axis of topographical input from mPFC to the MD, this suggests that these pathways should be seen as separate information streams in cognitive control, albeit both might still support task-relevant information within the mPFC[56,249]. However, differences in basic electrophysiological properties of post-synaptic MD neurons could simply be a homeostatic compensation for the quantity of input they receive[251], whereas qualitatively they could still have the same integrative properties. Future experiments can provide insight into the integrative properties of MDL and MDM neurons. For example, MD relay neurons have prominent subthreshold membrane resonances that allow preferential integration of input on their resonance frequency[252], or neuromodulators, such as dopamine, might differentially impact their functionality[69]. Moreover, precise in-vivo measurements of firing activity from MD-projecting mPFC neurons or mPFC-projecting MD neurons, will provide further insight in to what type of input comes from the mPFC and how this is integrated. This can, for example, be achieved using optogenetic identification of MD-projecting mPFC neurons in rats tested in the CombiCage 5-CSRTT, using an exact replica of the wireless single-unit electrophysiology and optogenetics experimental setup used in chapter 5. Additionally, this approach can directly test if MD-projecting mPFC neurons encode behavior through sequential activity, persistent changes in activity or

other encoding mechanisms, as there are no direct measurements of activity of these projection neurons. Moreover, MD relay neurons have a tonic and bursting firing mode, depending on the membrane potential[69,88]. It has been suggested that the bursting mode is used as a "wake-up call" for the cortex[69]. However, how the tonic and burst firing mode influence mPFC-MD interactions is poorly understood. Possibly, L5 dorsal mPFC input neurons at the start of a delay period provide a strong, but depressing, driver input on to MD relay neurons, causing a burst of action potentials in hyperpolarized MD relay neurons. In turn, this burst is reciprocally fed back on to mPFC neurons, resulting in weaker, but facilitating, modulator like input from L6 mPFC to MD neurons that are now in a depolarized tonic firing mode. Combined, this allows sustained activity of the mPFC-MD loop, and rule representation within the mPFC, until a bottom-up sensory signal shifts the activity in favor of a new task-relevant PFC rule. The respective role of L5 and L6 MD-projecting mPFC neurons remains largely unknown. The recent development of cortical layer-specific driver lines could greatly contribute to our understanding of the relative contribution of L5 and L6 neurons in cognitive control[253]. Alternatively, one could specifically target these layers using retrograde injections in specific collateral targets, such as L5 mPFC-MD neurons projecting to the pons[249].

THE FRONTOSTRIATAL CIRCUIT

We provide direct projection specific evidence for the role of dorsal mPFC projection neurons to the DMS in inhibitory control. The dorsal mPFC to the DMS has been associated with both inhibitory control and attention related deficits in the 5-CSRTT and other cue detection paradigms, whereas the ventral mPFC to the VMS has been most closely associated with inhibitory control[53,94,96,205,254]. However, direct projection neuron-based evidence was lacking. Here, we provide evidence that dorsal mPFC-DMS projections neurons are involved in inhibitory control, whereas ventral mPFC-VMS neurons do not show a role in either inhibitory control or attention measures in the 5-CSRTT. The role of DMS-projecting dorsal mPFC neurons in inhibitory control is in line with the prediction that this pathway is involved in response inhibition[5,8]. The lack of effects of DMS-projecting dorsal mPFC neurons in attentional control or VMS-projecting in inhibitory control and attentional measures can be interpreted in a lack of functional relevance for this behavior. There is, however, ample evidence that the dorsal mPFC to DMS circuit is involved in attention, where both functional impairment and disconnection studies of the dorsal mPFC and DMS show a role in attention in the 5-CSRTT[96,209,255]. Moreover, functional impairment and disconnection studies of the ventral mPFC and VMS also suggest a role in inhibitory control[10,205]. In order to provide more evidence for our reported lack of behavioral relevance of these mPFC to striatum-projecting neurons in attention or inhibitory control, several additional experiments are required using different inhibitory control and attentional paradigms, such as the divided attention task[131] or the response preparation task[41] where projection specific activity is disrupted using DREADD-mediated inhibition, or preferably optogenetic inhibition. Alternatively, the behavioral effects observed in previous studies, using non-projection specific lesions, resulted from damage to input or output from other brain areas. In line with this, we did find a clear role for ventral mPFC to MDM in inhibitory control. Moreover, other brain regions where the ventral mPFC projects to, including for example, the amygdala[60] have also been implicated in inhibitory control in the 5-CSRTT[256]. Moreover, the dorsal mPFC also projects to different brain regions that have been implicated in attention control such as the claustrum, thalamic reticular nucleus and visual cortex[131,232], which could account for the observed attentional effects after brain lesions.

Whereas the dorsal and ventral striatum are seen as separate information streams, how the output neurons of the dorsal and ventral striatum, the MSNs, integrate mPFC input from the dorsal and ventral mPFC remains poorly understood. In addition to the functional differences between the dorsal and ventral mPFC to striatum pathways, we provide evidence that the MSNs of the DMS and VMS receive differential synaptic input, with VMS MSNs receiving more depressing synaptic input compared to the DMS MSNs, while no differences in basic electrophysiological properties were observed. Higher synaptic facilitation possibly allows for sustained innervation of MSNs in the DMS, allowing seconds long excitation, throughout the delay period, of MSN ensembles encoding a specific behavioral repertoire, while depressing input on to VMS MSNs might allow for stronger, but shorter, excitation of neurons required only around to cue period in adaptive behavior. In support of this idea, the strong persistent delay-period activation of DMS-projecting mPFC is clear from both the single-unit electrophysiology and fiber photometry studies, especially compared to fiber photometry signal strength in VMS-projecting ventral mPFC neurons.

Cortical input to MSNs of the striatum have been hypothesized to provide contextual input for upcoming behavior[5]. Synaptic input to direct and indirect pathway MSNs from persistently activated and silenced PFC neurons could shift the balance of the DMS pathway activity to control behavior. Both D1 and D2-dopamine receptor expressing MSNs from the direct and indirect pathway, respectively, have been hypothesized to represent motor information (i.e. “nose poke”) and form interconnected ensembles that compete for activity[98–101]. Computational modeling work shows that synaptic input from the mPFC to MSNs can shift this balance[104], potentially in favor of the indirect pathway during inhibitory control. We hypothesize that persistently activated and persistently silenced frontostriatal projection neurons preferentially innervate the indirect and direct pathway, respectively. During correct inhibitory control the balance between direct and indirect pathway activity would then shift in favor of the indirect pathway, resulting in motor inhibition. Consequently, impaired inhibitory control, e.g. during premature response trials in the 5-CSRTT, could be caused by a failure in the shift of balance (i.e. lower changes in firing rate) towards the indirect pathway, while maintaining

higher direct pathway activity and maintaining the drive to execute behavior. Whereas striatal-projecting mPFC neurons have been shown to innervate both D1 and D2-receptor-containing MSNs[102], it remains to be tested if persistently activated and persistently silenced neurons show a preference for either type. Although topological dmPFC to DMS innervation patterns have been reported[210], organizational principles in selective targeting of MSN subtypes by frontostriatal neurons remain unknown.

A possible driver of delay period neural activity within the mPFC is dopamine. Dopamine has been extensively linked to behavioral control and, moreover, the mPFC and striatum both contain D1-expressing and D2-expressing neurons[257]. Recent work demonstrated that the dorsal mPFC mainly contain D1-expressing neurons, whereas the ventral mPFC mainly contain D2-expressing neurons[258]. D1-expressing dorsal mPFC neurons have been linked to inhibitory control and temporal organization of behavior[259], suggesting that the dorsal mPFC neurons we manipulated and recorded from are predominantly D1-expressing neurons. In addition, D1 receptor activation results in faster modulation of the network whereas D2 receptor activation results in slower modulation[257]. Dopaminergic input from the VTA is suggested to be active throughout the delay period, allowing it to maintain persistent activity throughout the delay. Dorsal mPFC neurons also project to the VTA and receive input from the VTA, possibly allowing it to sustain activity[257]. The role of dopamine input in persistent activity within the mPFC and behavioral control can be investigated using an experimental set-up as in chapter 5 where frontostriatal neurons are optogenetically identified and recorded using single-unit electrophysiology, while at the same time dopamine axons within the mPFC can be selectively silenced using a red shifted inhibitory opsin[260].

A FUTURE FOR CELL TYPING

The brain consists of many different cell types based on various criteria. In order to understand how groups of neurons can form a functional entity that can exert cognitive control, we need to classify groups of neurons based on similar functional properties. Classically this has been done on morphological properties[261], but newer methods allow characterization on electrophysiological characteristics[262], a

combination of methods[263] or genetic make-up using RNAseq in combination with projection area[189]. Understanding how functional groups of neurons contribute to cognitive control will hopeful provide insight in to different diseases that affect these particular groups of neurons[264], and, importantly, can allow precise targeting of these neurons for therapeutic interventions. We use projection area as cell-type feature, which generally can correlate to transcriptomics profile, morphology and firing patterns, but how well this correlates to function remains relatively unknown. We demonstrate within the mPFC that putative pyramidal projection neurons can be divided in to functionally separate groups of neurons depending on projection area. However, it is known that striatal and thalamic-projecting mPFC neurons have additional characteristics that allow further characterization in sub-classes and which need to be linked to in-vivo firing rate and behavioral function in order to fully understand the role of these pathways.

An important step for clinical relevance of our projection-specific results is the translation to humans. Although there are strong indications using methods such as functional MRI that the frontostriatal and frontothalamic pathways are involved in inhibitory control and attention, and are disturbed during several disease states[5,10], it is essential that more detailed projection-specific neuronal activity recordings can be performed in humans. It remains, however, extremely challenging to perform reliable in-vivo neuronal activity recordings of single neurons in humans as these are usually acquired as a byproduct of electrode placement for human surgical interventions[265]. Recent electrode developments and modeling approaches, however, may provide a valuable start at unraveling cell-type identity in behaving humans. The development of higher channel count and density electrode arrays, such as the neuropixel probe[266], provides a higher spatial resolution extracellular spike waveform sign of individual neurons. Together with recent advances in cell-typing based on extracellular waveform features[267,268], this could allow more detailed investigation in to how cell-types within the human brain contribute to behavior. For example, modeling of bio-realistic human neurons in combination with the use of the heart rate-induced movements of the extracellular electrode, implanted in human patients, has recently achieved the separation of two types of spiny pyramidal neurons[269]. To further understand the morpho-elec-

tric properties of individual cell types, a 'ground truth' dataset should be made of positively optogenetically identified neurons that are recorded using high density extracellular electrodes[270].

FUTURE AVENUES

We have demonstrated differential roles of separate groups of projection neurons within the mPFC in cognitive control. Undoubtedly, this is only a small link in the the chain that is required for cognitive control, as many other neural circuits are likely involved. Moreover, we don't know which language, or code, neurons use to exert cognitive control. These are only two future avenues. As always in science - the more we know the more we don't know.

Therefore, below I will provide several open questions regarding the underlying circuits of cognitive control, including inhibitory control and attention.

- *How do topographically-projecting mPFC to MD neurons encode cognitive control?*
- *Through which neuromodulators, synaptic input or local network mechanisms is persistent delay period activity of DMS-projecting mPFC neurons sustained?*
- *What are the characteristics, such as the transcriptomic profile, of persistently activated and silenced neurons?*
- *How are behavioral control, attention, working memory and other cognitive control domains related?*
- *How do different projection neurons communicate within the mPFC?*
- *What are the roles of other cognitive control linked brain areas and neuromodulators such as the amygdala, hippocampus, dopamine, serotonin and how do they affect the mPFC in inhibitory control and attention?*
- *How does information flow between the dorsal and ventral mPFC?*
- *How do projection specific neurons learn?*
- *Can we replicate our findings in humans?*

Answering these questions will provide important steps towards the ultimate goal: understanding the role of the frontal cortex in orchestrating cognitive control over behavior in health and disease.

REFERENCES

1. Miller, E. K. & Cohen, J. D. An integrative theory of prefrontal cortex function. Annu. Revi 24, 167–202 (2001).
2. Euston, D. R., Gruber, A. J. & McNaughton, B. L. The role of medial prefrontal cortex in memory and decision making. Neuron 76, 1057–1070 (2012).
3. Alexander, W. H. & Brown, J. W. Medial prefrontal cortex as an action-outcome predictor. Nat. Neurosci. 14, 1338–1344 (2011).
4. Dalley, J. W., Everitt, B. J. & Robbins, T. W. Impulsivity, compulsivity, and top-down cognitive control. Neuron 69, 680–94 (2011).
5. Aron, A. R. From reactive to proactive and selective control: developing a richer model for stopping inappropriate responses. Biol. Psychiatry 69, e55–e68 (2011).
6. Botvinick, M. & Braver, T. Motivation and cognitive control: from behavior to neural mechanism. Annu. Rev. Psychol. 66, 83–113 (2015).
7. Dalley, J. W., Cardinal, R. N. & Robbins, T. W. Prefrontal executive and cognitive functions in rodents: neural and neurochemical substrates. Neurosci. Biobehav. Rev. 28, 771–784 (2004).
8. Eagle, D. M. & Baunez, C. Is there an inhibitory-response-control system in the rat? Evidence from anatomical and pharmacological studies of behavioral inhibition. Neurosci. Biobehav. Rev. 34, 50–72 (2010).
9. Dambacher, F. et al. Out of control: Evidence for anterior insula involvement in motor impulsivity and reactive aggression. Soc. Cogn. Affect. Neurosci. 10, 508–516 (2013).
10. Dalley, J. W. & Robbins, T. W. Fractionating impulsivity: neuropsychiatric implications. Nat. Rev. Neurosci. 18, 158–171 (2017).
11. Fiebelkorn, I. C. & Kastner, S. A Rhythmic theory of attention. Trends Cogn. Sci. 23, 87–101 (2019).
12. Buschman, T. J. & Kastner, S. from behavior to neural dynamics: an integrated theory of attention. Neuron 88, 127–144 (2015).
13. Laurent, A. et al. Attentional deficits in patients with schizophrenia and in their non-psychotic first-degree relatives. Psychiatry Res. 89, 147–159 (1999).
14. Marvel, C. L. & Paradiso, S. Cognitive and neurological impairment in mood disorders. Psychiatr. Clin. North Am. 27, 19–36 (2004).
15. Porter, R., Bourke, C. & Gallagher, P. Neuropsychological impairment in major depression: its nature, origin and clinical significance. Aust. N. Z. J. Psychiatry 41, 115–128 (2007).
16. Huang-Pollock, C. L., Karalunas, S. L., Tam, H. & Moore, A. N. Evaluating vigilance deficits in ADHD: a meta-analysis of CPT performance. J. Abnorm. Psychol. 121, 360–371 (2012).
17. Bari, A., Dalley, J. W. & Robbins, T. W. The application of the 5-choice serial reaction time task for the assessment of visual attentional processes and impulse control in rats. Nat. Protoc. 3, 759–67 (2008).
18. Lustig, C., Kozak, R., Sarter, M., Young, J. W. & Robbins, T. W. CNTRICS final animal model task selection: control of attention. Neurosci. Biobehav. Rev. 37, 2099–2110 (2013).
19. Totah, N. K. B., Kim, Y. B., Homayoun, H. & Moghaddam, B. Anterior cingulate neurons represent errors and preparatory attention within the same behavioral sequence. J. Neurosci. 29, 6418–6426 (2009).
20. Kim, H., Ährlund-Richter, S., Wang, X., Deisseroth, K. & Carlén, M. Prefrontal parvalbumin neurons in control of attention. Cell 164, 208–218 (2016).
21. Donnelly, N. A., Paulsen, O., Robbins, T. W. & Dalley, J. W. Ramping single unit activity in the medial prefrontal cortex and ventral striatum reflects the onset of waiting but not imminent impulsive actions. Eur. J. Neurosci. 41, 1524–1537 (2015).
22. Poddar, R., Kawai, R. & Ölveczky, B. P. A fully automated high-throughput training system for rodents. PLoS One 8, 1–10 (2013).
23. Remmelink, E., Chau, U., Smit, A. B., Verhage, M. & Loos, M. A one-week 5-choice serial reaction time task to measure impulsivity and attention in adult and adolescent mice. Sci. Rep. 7, 42519 (2017).

24. Pezzulo, G. & Cisek, P. navigating the affordance landscape: feedback control as a process model of behavior and cognition. Trends Cogn. Sci. 20, 414–424 (2016).
25. Buschman, T. J. & Miller, E. K. Top-down versus bottom-up control of attention in the prefrontal and posterior parietal cortices. Science (80-.). 315, 1860–1864 (2007).
26. Sharpe, M. J. et al. An integrated model of action selection: distinct modes of cortical control of striatal decision making. Annu. Rev. Psychol. 70, 53–76 (2019).
27. S.R. Heilbronner. Circuit based cortico-striatal homologies between rat and primate. 80, 509–521 (2017).
28. Carlén, M. What constitutes the prefrontal cortex? Science (80-.). 358, 478–482 (2017).
29. Laubach, M., Amarante, L. M., Swanson, K. & White, S. R. What, if anything, is rodent prefrontal cortex? Eneuro 5, ENEURO.0315-18.2018 (2018).
30. Broersen, L. M. & Uylings, H. B. M. Visual attention task performance in Wistar and Lister Hooded rats: response inhibition deficits after medial prefrontal cortex lesions. Neuroscience 94, 47–57 (1999).
31. Muir, J. L., Everitt, B. J. & Robbins, T. W. The cerebral cortex of the rat and visual attentional function: dissociable effects of mediofrontal, cingulate, anterior dorsolateral, and parietal cortex lesions on a five-choice serial reaction time task. Cereb. Cortex 6, 470–481 (1996).
32. Passetti, F., Chudasama, Y. & Robbins, T. W. The frontal cortex of the rat and visual attentional performance: dissociable functions of distinct medial prefrontal subregions. Cereb. Cortex 12, 1254–1268 (2002).
33. Chudasama, Y., Baunez, C. & Robbins, T. W. Functional disconnection of the medial prefrontal cortex and subthalamic nucleus in attentional performance: evidence for corticosubthalamic interaction. J. Neurosci. 23, 5477–5485 (2003).
34. Maddux, J.-M. & Holland, P. C. Effects of dorsal or ventral medial prefrontal cortical lesions on five-choice serial reaction time performance in rats. Behav. Brain Res. 221, 63–74 (2011).
35. Pezze, M., McGarrity, S., Mason, R., Fone, K. C. & Bast, T. Too little and too much: hypoactivation and disinhibition of medial prefrontal cortex cause attentional deficits. J. Neurosci. 34, 7931–7946 (2014).
36. Pezze, M. a., Dalley, J. W. & Robbins, T. W. Remediation of attentional dysfunction in rats with lesions of the medial prefrontal cortex by intra-accumbens administration of the dopamine D 2/3 receptor antagonist sulpiride. Psychopharmacology (Berl). 202, 307–313 (2009).
37. Heidbreder, C. a. & Groenewegen, H. J. The medial prefrontal cortex in the rat: Evidence for a dorsoventral distinction based upon functional and anatomical characteristics. Neurosci. Biobehav. Rev. 27, 555–579 (2003).
38. Chudasama, Y. et al. Dissociable aspects of performance on the 5-choice serial reaction time task following lesions of the dorsal anterior cingulate, infralimbic and orbitofrontal cortex in the rat: differential effects on selectivity, impulsivity and compulsivity. Behav. Brain Res. 146, 105–119 (2003).
39. Koike, H. et al. Chemogenetic inactivation of dorsal anterior cingulate cortex neurons disrupts attentional behavior in mouse. Neuropsychopharmacology 41, 1014–1023 (2016).
40. Pehrson, A. L., Bondi, C. O., Totah, N. K. B. & Moghaddam, B. The influence of NMDA and GABAA receptors and glutamic acid decarboxylase (GAD) activity on attention. Psychopharmacology (Berl). 225, 31–39 (2013).
41. Hardung, S. et al. A functional gradient in the rodent prefrontal cortex supports behavioral inhibition. Curr. Biol. 27, 549–555 (2017).
42. Murphy, E. R. et al. Impulsive behaviour induced by both NMDA receptor antagonism and GABAA receptor activation in rat ventromedial prefrontal cortex. Psychopharmacology (Berl). 219, 401–410 (2012).
43. Moorman, D. E. & Aston-Jones, G. Prefrontal neurons encode context-based response execution and inhibition in reward seeking and extinction. Proc. Natl. Acad. Sci. 112, 9472–9477 (2015).

44. Caballero, J. P., Scarpa, G. B., Remage-Healey, L. & Moorman, D. E. Differential effects of dorsal and ventral medial prefrontal cortex inactivation during natural reward seeking, extinction, and cue-induced reinstatement. eNeuro 6, (2019).
45. Lundqvist, M., Herman, P. & Miller, E. K. Working memory: delay activity, yes! persistent activity? maybe not. J. Neurosci. 38, 7013–7019 (2018).
46. Masataka, N. H. and W. Prefrontal and cingulate unit activity during timing behavior in the monkey. Brain Res. 171, 213–224 (1979).
47. Prut, Y. et al. Spatiotemporal structure of cortical activity: properties and behavioral relevance. J. Neurophysiol. 79, 2857–2874 (1998).
48. Rajan, K., Harvey, C. D. D. & Tank, D. W. W. Recurrent network models of sequence generation and memory. Neuron 90, 128–142 (2016).
49. Luczak, A., McNaughton, B. L. & Harris, K. D. Packet-based communication in the cortex. Nat. Rev. Neurosci. 16, 745–755 (2015).
50. Paton, J. J. & Buonomano, D. V. The neural basis of timing: distributed mechanisms for diverse functions. Neuron 98, 687–705 (2018).
51. Harris, K. D. & Thiele, A. Cortical state and attention. Nat. Rev. Neurosci. 12, 509–523 (2011).
52. Ainsworth, M. et al. Rates and rhythms: a synergistic view of frequency and temporal coding in neuronal networks. Neuron 75, 572–583 (2012).
53. Emmons, E. B. et al. Rodent medial frontal control of temporal processing in the dorsomedial striatum. J. Neurosci. 37, 8718–8733 (2017).
54. Funahashi, S., Chafee, M. V. & Goldman-Rakic, P. S. Prefrontal neuronal activity in rhesus monkeys performing a delayed anti-saccade task. Nature 365, 753–756 (1993).
55. Narayanan, N. S. & Laubach, M. Top-down control of motor cortex ensembles by dorsomedial prefrontal cortex. Neuron 52, 921–931 (2006).
56. Schmitt, L. I. et al. Thalamic amplification of cortical connectivity sustains attentional control. Nature 545, 219–223 (2017).
57. Bolkan, S. S. et al. Thalamic projections sustain prefrontal activity during working memory maintenance. Nat. Neurosci. 20, 987–996 (2017).
58. Dudchenko, P. A. An overview of the tasks used to test working memory in rodents. Neurosci. Biobehav. Rev. 28, 699–709 (2004).
59. Tang, C., Herikstad, R., Parthasarathy, A., Libedinsky, C. & Yen, S.-C. Independent activity subspaces for working memory and motor preparation in the lateral prefrontal cortex. bioRxiv الجديد الجا, 756072 (2019).
60. Gabbott, P. L. a, Warner, T. a., Jays, P. R. L., Salway, P. & Busby, S. J. Prefrontal cortex in the rat: projections to subcortical autonomic, motor, and limbic centers. J. Comp. Neurol. 492, 145–177 (2005).
61. R. P. Vertes, S. B. L. and W. B. H. Limbic circuitry of the midline thalamus. Neurosci. Biobehav. Rev. 54, 89–107 (2015).
62. Parnaudeau, S., Bolkan, S. S. & Kellendonk, C. The mediodorsal thalamus: an essential partner of the prefrontal cortex for cognition. Biol. Psychiatry 1–9 (2017). doi:10.1016/j.biopsych.2017.11.008
63. Mitchell, A. S. Neuroscience and biobehavioral reviews the mediodorsal thalamus as a higher order thalamic relay nucleus important for learning and decision-making. Neurosci. Biobehav. Rev. 54, 76–88 (2015).
64. Kim, C. K. et al. Molecular and circuit-dynamical identification of top-down neural mechanisms for restraint of reward seeking. Cell 170, 1013–1027 (2017).
65. Otis, J. M. et al. Prefrontal cortex output circuits guide reward seeking through divergent cue encoding. Nature 543, 103–107 (2017).
66. Ye, L. et al. Wiring and molecular features of prefrontal ensembles representing distinct experiences. Cell 165, 1776–1788 (2016).
67. Bari, B. A. et al. Stable representations of decision variables for flexible behavior. Neuron 103, 922-933.e7 (2019).

68. Hirokawa, J., Vaughan, A., Masset, P., Ott, T. & Kepecs, A. Frontal cortex neuron types categorically encode single decision variables. Nature 576, 446–451 (2019).
69. Sherman, S. M. & Guillery, R. W. Exploring the thalamus and its role in cortical function. exploring the thalamus and its role in cortical function (2006). doi:10.7551/mitpress/2940.001.0001
70. Collins, D. P., Anastasiades, P. G., Marlin, J. J. & Carter, A. G. Reciprocal circuits linking the prefrontal cortex with dorsal and ventral thalamic nuclei. Neuron 98, 366-379.e4 (2018).
71. Kuramoto, E. et al. Individual mediodorsal thalamic neurons project to multiple areas of the rat prefrontal cortex: a single neuron-tracing study using virus vectors. J. Comp. Neurol. 525, 166–185 (2017).
72. Alcaraz, F., Marchand, A. R., Courtand, G., Coutureau, E. & Wolff, M. Parallel inputs from the mediodorsal thalamus to the prefrontal cortex in the rat. Eur. J. Neurosci. 44, 1972–1986 (2016).
73. Mitchell, A. S. & Chakraborty, S. What does the mediodorsal thalamus do? Front. Syst. Neurosci. 7, 37 (2013).
74. Parnaudeau, S. et al. Mediodorsal thalamus hypofunction impairs flexible goal-directed behavior. Bps 77, 1–9 (2014).
75. Rikhye, R. V., Gilra, A. & Halassa, M. M. Thalamic regulation of switching between cortical representations enables cognitive flexibility. Nat. Neurosci. 21, 1753–1763 (2018).
76. Alcaraz, F. et al. Thalamocortical and corticothalamic pathways differentially contribute to goal-directed behaviors in the rat. Elife 7, 1–17 (2018).
77. Chudasama, Y. & Muir, J. L. Visual attention in the rat: a role for the prelimbic cortex and thalamic nuclei? Behav. Neurosci. 115, 417–428 (2001).
78. Mitchell, A. S., Browning, P. G. F. & Baxter, M. G. Neurotoxic lesions of the medial mediodorsal nucleus of the thalamus disrupt reinforcer devaluation effects in rhesus monkeys. J. Neurosci. 27, 11289–11295 (2007).
79. Parnaudeau, S. et al. Inhibition of mediodorsal thalamus disrupts thalamofrontal connectivity and cognition. Neuron 77, 1151–1162 (2013).
80. Ferguson, B. R. & Gao, W. J. Thalamic control of cognition and social behavior via regulation of gamma-aminobutyric acidergic signaling and excitation/inhibition balance in the medial prefrontal cortex. Biol. Psychiatry 83, 657–669 (2018).
81. Pergola, G. et al. The regulatory role of the human mediodorsal thalamus. Trends Cogn. Sci. 22, 1011–1025 (2018).
82. Sherman, S. M. Thalamus plays a central role in ongoing cortical functioning. Nat. Neurosci. 19, 533–541 (2016).
83. Delevich, K., Tucciarone, J., Huang, Z. J. & Li, X. B. The mediodorsal thalamus drives feedforward inhibition in the anterior cingulate cortex via parvalbumin interneurons. 35, 5743–5753 (2015).
84. Kuroda, M., Yokofujita, J., Oda, S. & Price, J. L. Synaptic relationships between axon terminals from the mediodorsal thalamic nucleus and γ-aminobutyric acidergic cortical cells in the prelimbic cortex of the rat. J. Comp. Neurol. 477, 220–234 (2004).
85. Kuroda, M., Yokofujita, J. & Murakami, K. An ultrastructural study of the neural circuit between the prefrontal cortex and the mediodorsal nucleus of the thalamus. Prog. Neurobiol. 54, 417–458 (1998).
86. Jones, E. G. The thalamic matrix and thalamocortical synchrony. Trends Neurosci. 24, 595–601 (2001).
87. Halassa, M. M. & Sherman, S. M. Thalamocortical circuit motifs: a general framework. Neuron 103, 762–770 (2019).
88. Zeldenrust, F., Wadman, W. J. & Englitz, B. Neural coding with bursts—current state and future perspectives. Front. Comput. Neurosci. 12, 1–14 (2018).
89. Zeldenrust, F., Chameau, P. & Wadman, W. J. Spike and burst coding in thalamocortical relay cells. PLoS Computational Biology 14, (2018).

90. Vertes, R. P. Differential projections of the infralimbic and prelimbic cortex in the rat. Synapse 51, 32–58 (2004).
91. Klaus, A., Alves da Silva, J. & Costa, R. M. What, if, and when to move: basal ganglia circuits and self-paced action initiation. Annu. Rev. Neurosci. 42, 459–483 (2019).
92. Hunnicutt, B. J. et al. A comprehensive excitatory input map of the striatum reveals novel functional organization. Elife 5, 1–32 (2016).
93. Voorn, P., Vanderschuren, L. J. M. J., Groenewegen, H. J., Robbins, T. W. & Pennartz, C. M. a. Putting a spin on the dorsal-ventral divide of the striatum. Trends Neurosci. 27, 468–474 (2004).
94. Rogers, R. D., Baunez, C., Everitt, B. J. & Robbins, T. W. Lesions of the medial and lateral striatum in the rat produce differential deficits in attentional performance. Behav. Neurosci. 115, 799–811 (2001).
95. Christakou, A., Robbins, T. W. & Everitt, B. J. Prefrontal cortical-ventral striatal interactions involved in affective modulation of attentional performance: implications for corticostriatal circuit function. J. Neurosci. 24, 773–780 (2004).
96. Christakou, a, Robbins, T. W. & Everitt, B. J. Functional disconnection of a prefrontal cortical-dorsal striatal system disrupts choice reaction time performance: implications for attentional function. Behav. Neurosci. 115, 812–825 (2001).
97. Kreitzer, A. C. & Malenka, R. C. Striatal plasticity and basal ganglia circuit function. Neuron 60, 543–554 (2008).
98. Barbera, G. et al. Spatially compact neural clusters in the dorsal striatum encode locomotion relevant information. Neuron 92, 202–213 (2016).
99. Cui, G. et al. Concurrent activation of striatal direct and indirect pathways during action initiation. Nature 494, 238–242 (2013).
100. Kravitz, A. V et al. Control of basal ganglia circuitry. Nature 466, 622–626 (2010).
101. Sippy, T., Lapray, D., Crochet, S. & Petersen, C. C. H. Cell-type-specific sensorimotor processing in striatal projection neurons during goal-directed behavior. Neuron 88, 298–305 (2015).
102. Wall, N. R., DeLaParra, M., Callaway, E. M. & Kreitzer, A. C. Differential innervation of direct- and indirect-pathway striatal projection neurons. Neuron 79, 347–360 (2013).
103. Guo, Q. et al. Whole-brain mapping of inputs to projection neurons and cholinergic interneurons in the dorsal striatum. PLoS One 10, 1–15 (2015).
104. Ardid, S. et al. Biased competition in the absence of input bias revealed through corticostriatal computation. Proc. Natl. Acad. Sci. U. S. A. 116, 8564–8569 (2019).
105. Carter, A. G., Soler-Llavina, G. J. & Sabatini, B. L. Timing and location of synaptic inputs determine modes of subthreshold integration in striatal medium spiny neurons. J. Neurosci. 27, 8967–8977 (2007).
106. Kupchik, Y. M. et al. Not valid for accumbens projections. 18, 1230–1232 (2016).
107. Suska, A., Lee, B. R., Huang, Y. H., Dong, Y. & Schluter, O. M. Selective presynaptic enhancement of the prefrontal cortex to nucleus accumbens pathway by cocaine. Proc. Natl. Acad. Sci. 110, 713–718 (2013).
108. Al-muhtasib, N., Forcelli, P. A. & Vicini, S. Differential electrophysiological properties of D1 and D2 spiny projection neurons in the mouse nucleus accumbens core. Physiol. Rep. 6, (2018).
109. Olton, D. S., Wenk, G. L., Church, R. M. & Meck, W. H. Attention and the frontal cortex as examined by simultaneous temporal processing. Neuropsychologia 26, 307–318 (1988).
110. Granon, S., Hardouin, J., Courtière, A. & Poucet, B. Evidence for the involvement of the rat prefrontal cortex in sustained attention. Q. J. Exp. Psychol. Sect. B Comp. Physiol. Psychol. 51, 219–233 (1998).
111. Robbins, T. W. The 5-choice serial reaction time task: behavioural pharmacology and functional neurochemistry. Psychopharmacology (Berl). 163, 362–80 (2002).
112. Kahn, J. B. et al. Medial prefrontal lesions in mice impair sustained attention but spare

maintenance of information in working memory. Learn. Mem. 19, 513–517 (2012).
113. Chudasama, Y., Bussey, T. J. & Muir, J. L. Effects of selective thalamic and prelimbic cortex lesions on two types of visual discrimination and reversal learning. Eur. J. Neurosci. 14, 1009–1020 (2001).
114. Totah, N. K. B., Kim, Y. & Moghaddam, B. Distinct prestimulus and poststimulus activation of VTA neurons correlates with stimulus detection. J. Neurophysiol. 110, 75–85 (2013).
115. Cho, K. K. A. et al. Gamma rhythms link prefrontal interneuron dysfunction with cognitive inflexibility in Dlx5/6+/– Mice. Neuron 85, 1332–1343 (2015).
116. Riga, D. et al. Optogenetic dissection of medial prefrontal cortex circuitry. Front. Syst. Neurosci. 8, 1–19 (2014).
117. Douglas, R. J. & Martin, K. A. C. Neuronal circuits of the neocortex. Annu. Rev. Neurosci. 27, 419–451 (2004).
118. Parnaudeau, S. et al. Mediodorsal thalamus hypofunction impairs flexible goal-directed behavior. Biol. Psychiatry 77, 445–453 (2015).
119. Yizhar, O., Fenno, L. E., Davidson, T. J., Mogri, M. & Deisseroth, K. Optogenetics in neural systems. Neuron 71, 9–34 (2011).
120. Cassaday, H. J. From attention to memory along the dorsal-ventral axis of the medial prefrontal cortex: some methodological considerations. Front. Syst. Neurosci. 8, 1–24 (2014).
121. Romanski, L. M. et al. Dual streams of auditory afferents target multiple domains in the primate prefrontal cortex. Nat. Neurosci. 2, 1131–1136 (1999).
122. Hayton, S. J., Lovett-Barron, M., Dumont, E. C. & Olmstead, M. C. Target-specific encoding of response inhibition: Increased contribution of AMPA to NMDA receptors at excitatory synapses in the prefrontal cortex. J. Neurosci. 30, 11493–11500 (2010).
123. Totah, N. K. B., Jackson, M. E. & Moghaddam, B. Preparatory attention relies on dynamic interactions between prelimbic cortex and anterior cingulate cortex. Cereb. Cortex 23, 729–738 (2013).
124. Kassam, S. M., Herman, P. M., Goodfellow, N. M., Alves, N. C. & Lambe, E. K. Developmental excitation of corticothalamic neurons by nicotinic acetylcholine receptors. J. Neurosci. 28, 8756–8764 (2008).
125. Proulx, E., Piva, M., Tian, M. K., Bailey, C. D. C. & Lambe, E. K. Nicotinic acetylcholine receptors in attention circuitry: the role of layer VI neurons of prefrontal cortex. Cell. Mol. Life Sci. 71, 1225–1244 (2014).
126. Thomson, A. M. Neocortical layer 6, a review. Front. Neuroanat. 4, 1–14 (2010).
127. Pragay, E. B., Mirsky, A. F. & Nakamura, R. K. Attention-related unit activity in the frontal association cortex during a go/no-go visual discrimination task. Exp. Neurol. 96, 481–500 (1987).
128. Risterucci, C., Terramorsi, D., Nieoullon, A. & Amalric, M. Excitotoxic lesions of the prelimbic-infralimbic areas of the rodent prefrontal cortex disrupt motor preparatory processes. Eur. J. Neurosci. 17, 1498–1508 (2003).
129. Moore, T., Armstrong, K. M. & Fallah, M. Visuomotor origins of covert spatial attention. Neuron 40, 671–683 (2003).
130. Rodgers, C. C. & DeWeese, M. R. Neural correlates of task switching in prefrontal cortex and primary auditory cortex in a novel stimulus selection task for rodents. Neuron 82, 1157–1170 (2014).
131. Wimmer, R. D. et al. Thalamic control of sensory selection in divided attention. Nature 526, 705–709 (2015).
132. Killcross, S. & Coutureau, E. Coordination of actions and habits in the medial prefrontal cortex of rats. Cereb. Cortex 13, 400–408 (2003).
133. Smith, K. S., Virkud, a., Deisseroth, K. & Graybiel, a. M. Reversible online control of habitual behavior by optogenetic perturbation of medial prefrontal cortex. Proc. Natl. Acad. Sci. (2012). doi:10.1073/pnas.1216264109
134. Feja, M. & Koch, M. Ventral medial prefrontal cortex inactivation impairs impulse control but

does not affect delay-discounting in rats. Behav. Brain Res. 264, 230–239 (2014).
135. Sesack, S. R., Deutch, A. Y., Roth, R. H. & Bunney, B. S. Topographical organization of the efferent projections of the medial prefrontal cortex in the rat: an anterograde tract-tracing study with Phaseolus Vulgaris Leucoagglutinin. J. Comp. Neurol. 290, 213–242 (1989).
136. Zhang, S. et al. Long-range and local circuits for top-down modulation of visual cortex processing. Science (80-.). 345, 660–665 (2014).
137. Park, J., Wood, J., Bondi, C., Arco, A. Del & Moghaddam, B. Anxiety evokes hypofrontality and disrupts rule-relevant encoding by dorsomedial prefrontal cortex neurons. J. Neurosci. 36, 3322–3335 (2016).
138. Delatour, B. & Gisquet-Verrier, P. Involvement of the dorsal anterior cingulate cortex in temporal behavioral sequencing: subregional analysis of the medial prefrontal cortex in rat. Behav. Brain Res. 126, 105–114 (2001).
139. Gisquet-Verrier, P. & Delatour, B. The role of the rat prelimbic/infralimbic cortex in working memory: Not involved in the short-term maintenance but in monitoring and processing functions. Neuroscience 141, 585–596 (2006).
140. Gourley, S. L. & Taylor, J. R. Going and stopping: dichotomies in behavioral control by the prefrontal cortex. Nat. Neurosci. 19, 656–664 (2016).
141. Adhikari, A. et al. Basomedial amygdala mediates top-down control of anxiety and fear. Nature 527, 179–185 (2015).
142. van Aerde, K. I., Heistek, T. S. & Mansvelder, H. D. Prelimbic and infralimbic prefrontal cortex interact during fast network oscillations. PLoS One 3, 1–7 (2008).
143. Pezze, M., McGarrity, S., Mason, R., Fone, K. C. & Bast, T. Too little and too much: hypoactivation and disinhibition of medial prefrontal cortex cause attentional deficits. J. Neurosci. 34, 7931–7946 (2014).
144. Paine, T. a, Slipp, L. E. & Carlezon, W. a. Schizophrenia-like attentional deficits following blockade of prefrontal cortex GABAA receptors. Neuropsychopharmacology 36, 1703–1713 (2011).
145. Kaping, D., Vinck, M., Hutchison, R. M., Everling, S. & Womelsdorf, T. Specific contributions of ventromedial, anterior cingulate, and lateral prefrontal cortex for attentional selection and stimulus valuation. PLoS Biol. 9, (2011).
146. Petrides, M. Dissociable roles of mid-dorsolateral prefrontal and anterior inferotemporal cortex visual working memory. J. Neurosci. 20, 7496–7503 (2000).
147. Gruber, A. J., Hussain, R. J. & O'Donnell, P. The nucleus accumbens: a switchboard for goal-directed behaviors. PLoS One 4, (2009).
148. Semenova, S., Stolerman, I. P. & Markou, A. Chronic nicotine administration improves attention while nicotine withdrawal induces performance deficits in the 5-choice serial reaction time task in rats. Pharmacol. Biochem. Behav. 87, 360–368 (2007).
149. Pinto, L. et al. Fast modulation of visual perception by basal forebrain cholinergic neurons. Nat. Neurosci. 16, 1857–1863 (2013).
150. Castellanos, F. X. & Tannock, R. Neuroscience of attention-deficit/hyperactivity disorder: the search for endophenotypes. Nat. Rev. Neurosci. 3, 617–628 (2002).
151. Luck, S. J. & Gold, J. M. The construct of attention in schizophrenia. Biol. Psychiatry 64, 34–39 (2008).
152. Blondeau, C. & Dellu-Hagedorn, F. Dimensional analysis of ADHD subtypes in rats. Biol. Psychiatry 61, 1340–1350 (2007).
153. Bhandari, J., Daya, R. & Mishra, R. K. Improvements and important considerations for the 5-choice serial reaction time task-An effective measurement of visual attention in rats. J. Neurosci. Methods 270, 17–29 (2016).
154. Bohacek, J. & Daniel, J. M. Increased daily handling of ovariectomized rats enhances performance on a radial-maze task and obscures effects of estradiol replacement. Horm. Behav. 52, 237–243 (2007).
155. Sorge, R. E. et al. Olfactory exposure to males, including men, causes stress and related

analgesia in rodents. Nat. Methods 11, 629–632 (2014).
156. Deutsch-Feldman, M., Picetti, R., Seip-Cammack, K., Zhou, Y. & Kreek, M. J. Effects of handling and vehicle injections on adrenocorticotropic and corticosterone concentrations in Sprague-Dawley compared with Lewis rats. J Am Assoc Lab Anim Sci 54, 35–39 (2015).
157. Sänger, J., Bechtold, L., Schoofs, D., Blaszkewicz, M. & Wascher, E. The influence of acute stress on attention mechanisms and its electrophysiological correlates. Front. Behav. Neurosci. 8, 353 (2014).
158. Luchicchi, A. et al. Sustained attentional states require distinct temporal involvement of the dorsal and ventral medial prefrontal cortex. Front. Neural Circuits 10, 70 (2016).
159. Pattij, T. et al. Strain specificity and cholinergic modulation of visuospatial attention in three inbred mouse strains. Genes, Brain Behav. 6, 579–587 (2007).
160. Hodges, D. B., Lindner, M. D., Hogan, J. B., Jones, K. M. & Markus, E. J. Scopolamine induced deficits in a battery of rat cognitive tests: comparisons of sensitivity and specificity. Behav. Pharmacol. 20, 237–251 (2009).
161. Lyeth, B. G. et al. Postinjury scopolamine administration in experimental traumatic brain injury. Brain Res. 569, 281–286 (1992).
162. Granon, S. et al. Enhanced and impaired attentional performance after infusion of D1 dopaminergic receptor agents into rat prefrontal cortex. J. Neurosci. 20, 1208–1215 (2000).
163. Hahn, B., Shoaib, M. & Stolerman, I. P. Nicotine-induced enhancement of attention in the five-choice serial reaction time task: the influence of task demands. Psychopharmacology (Berl). 162, 129–137 (2002).
164. Loos, M. et al. Sheltering behavior and locomotor activity in 11 genetically diverse common inbred mouse strains using home-cage monitoring. PLoS One 9, 1–9 (2014).
165. Rivalan, M., Munawar, H., Fuchs, A. & Winter, Y. An automated, experimenter-free method for the standardised, operant cognitive testing of rats. PLoS One 12, 1–19 (2017).
166. Locke, E. A. Toward a theory of task motivation and incentives. Organ. Behav. Hum. Perform. 3, 157–189 (1968).
167. Young, J. W., Jentsch, J. D., Bussey, T. J., Wallace, T. L. & Hutcheson, D. M. Consideration of species differences in developing novel molecules as cognition enhancers. Neurosci. Biobehav. Rev. 37, 2181–2193 (2013).
168. Cope, Z. A. et al. Premature responses in the five-choice serial reaction time task reflect rodents' temporal strategies: evidence from no-light and pharmacological challenges. Psychopharmacology (Berl). 233, 3513–3525 (2016).
169. Saund, J., Dautan, D., Rostron, C., Urcelay, G. P. & Gerdjikov, T. V. Thalamic inputs to dorsomedial striatum are involved in inhibitory control: evidence from the five-choice serial reaction time task in rats. Psychopharmacology (Berl). 234, 2399–2407 (2017).
170. Schippers, M. C. et al. Deep brain stimulation of the nucleus accumbens core affects trait impulsivity in a baseline-dependent manner. Front. Behav. Neurosci. 11, 52 (2017).
171. Counotte, D. S. et al. Lasting synaptic changes underlie attention deficits caused by nicotine exposure during adolescence. Nat. Neurosci. 14, 417–9 (2011).
172. Jones, D. N. C. & Higgins, G. A. Effect of scopolamine on visual attention in rats. Psychopharmacology (Berl). 120, 142–149 (1995).
173. Mirza, N. R. & Stolerman, I. P. The role of nicotinic and muscarinic acetylcholine receptors in attention. Psychopharmacology (Berl). 148, 243–250 (2000).
174. Jäkälä, P. et al. The effects of p-chlorophenylalanine-induced serotinin synthesis inhibition and muscarinic blockade on the performance of rats in a 5-choice serial reaction time task. Behav. Brain Res. 51, 29–40 (1992).
175. Higgs, S., Deacon, R. M. J. & Rawlins, J. N. P. Effects of scopolamine on a novel choice serial reaction time task. Eur. J. Neurosci. 12, 1781–1788 (2000).
176. Mirza, N. R. & Bright, J. L. Nicotine-induced enhancements in the five-choice serial reaction time task in rats are strain-dependent. Psychopharmacology (Berl). 154, 8–12 (2001).
177. Jog, M. S., Kubota, Y., Connolly, C. I., Hillegaart, V. & Graybiel, A. M. Building neural

representations of Habits. Science (80-.). (1999).
178. Yin, H. H. & Knowlton, B. J. The role of the basal ganglia in habit formation. Nat. Rev. Neurosci. 7, 464–476 (2006).
179. Smith, K. S. & Graybiel, A. M. Habit formation. Dialogues Clin Neurosci 18, 33–43 (2016).
180. Serra, M. et al. Social isolation-induced decreases in both the abundance of neuroactive steroids and GABA(A) receptor function in rat brain. J. Neurochem. 75, 732–740 (2000).
181. Weiss, I. C., Pryce, C. R., Jongen-Rêlo, A. L., Nanz-Bahr, N. I. & Feldon, J. Effect of social isolation on stress-related behavioural and neuroendocrine state in the rat. Behav. Brain Res. 152, 279–295 (2004).
182. Weintraub, A., Singaravelu, J. & Bhatnagar, S. Enduring and sex-specific effects of adolescent social isolation in rats on adult stress reactivity. Brain Res. 1343, 83–92 (2010).
183. Kirkpatrick, K., Marshall, A. T., Clarke, J. & Cain, M. E. Environmental rearing effects on impulsivity and reward sensitivity. Behav. Neurosci. 127, 712–724 (2013).
184. Wang, M. Z., Marshall, A. T. & Kirkpatrick, K. Differential effects of social and novelty enrichment on individual differences in impulsivity and behavioral flexibility. Behav. Brain Res. 327, 54–64 (2017).
185. Riga, D. et al. Hippocampal extracellular matrix alterations contribute to cognitive impairment associated with a chronic depressive-like state in rats. Sci. Transl. Med. 9, eaai8753 (2017).
186. Benjamini, Y. & Hochberg, Y. Controlling the false discovery rate: a practical and powerful approach to multiple testing. J. R. Stat. Soc. B 57, 289–300 (1995).
187. Harris, J. A. et al. Hierarchical organization of cortical and thalamic connectivity. Nature 575, 195–202 (2019).
188. Groenewegen, H. J. Organization of the afferent connections of the mediodorsal thalamic nucleus in the rat, related to the mediodorsal-prefrontal topography. Neuroscience 24, 379–431 (1988).
189. Tasic, B. et al. Shared and distinct transcriptomic cell types across neocortical areas. Nature 563, 72–78 (2018).
190. Kupferschmidt, D. A., Juczewski, K., Cui, G., Johnson, K. A. & Lovinger, D. M. Parallel, but dissociable, processing in discrete corticostriatal inputs encodes skill learning. Neuron 96, 476-489.e5 (2017).
191. Bolkan, S. S. et al. Thalamic projections sustain prefrontal activity during working memory maintenance. Nat. Neurosci. 20, 987–996 (2017).
192. Pisansky, M. T. et al. Nucleus accumbens fast-spiking interneurons constrain impulsive action. Biol. Psychiatry 86, 836–847 (2019).
193. Bruinsma, B. et al. An automated home-cage-based 5-choice serial reaction time task for rapid assessment of attention and impulsivity in rats. Psychopharmacology (Berl). (2019). 236, 2015-2026.
194. Hart, G., Bradfield, L. A., Fok, S. Y., Chieng, B. & Balleine, B. W. The bilateral prefronto-striatal pathway is necessary for learning new goal-directed actions. Curr. Biol. 28, 2218–2229 (2018).
195. Murugan, M. et al. Combined social and spatial coding in a descending projection from the prefrontal cortex. Cell 171, 1663-1677.e16 (2017).
196. Lee, A. T., Vogt, D., Rubenstein, J. L. & Sohal, V. S. A class of GABAergic neurons in the prefrontal cortex sends long-range projections to the nucleus accumbens and elicits acute avoidance behavior. J. Neurosci. 34, 11519–11525 (2014).
197. Rock, C., Zurita, H., Wilson, C. & Apicella, A. J. An inhibitory corticostriatal pathway. Elife 5, 1–17 (2016).
198. Wolff, M. & Vann, S. D. The cognitive thalamus as a gateway to mental representations. J. Neurosci. 39, 3–14 (2019).
199. Marton, T. F., Seifikar, H., Luongo, F. J., Lee, A. T. & Sohal, V. S. Roles of prefrontal cortex and mediodorsal thalamus in task engagement and behavioral flexibility. J. Neurosci. 38,

2569–2578 (2018).
200. Ferenczi, E. A. et al. Prefrontal cortical regulation of brainwide circuit dynamics and reward-related behavior. Science (80-.). 351, aac9698–aac9698 (2016).
201. Agnoli, L. & Mainolfi, P. Striatum control different aspects of attentional performance in the five-choice serial reaction time task under a condition of increased activity of corticostriatal. Neuropsychopharmacology 38, 701–14 (2012).
202. Emmons, E. B., Kennedy, M., Kim, Y. & Narayanan, N. S. Corticostriatal stimulation compensates for medial frontal inactivation during interval timing. Sci. Rep. 9, (2019).
203. Ding, J., Peterson, J. D. & Surmeier, D. J. Corticostriatal and thalamostriatal synapses have distinctive properties. J. Neurosci. 28, 6483–6492 (2008).
204. Friedman, A. et al. A corticostriatal path targeting striosomes controls decision-making under conflict. Cell 161, 1320–1333 (2015).
205. Feja, M. & Koch, M. Frontostriatal systems comprising connections between ventral medial prefrontal cortex and nucleus accumbens subregions differentially regulate motor impulse control in rats. Psychopharmacology (Berl). 232, 1291–1302 (2015).
206. Belin-Rauscent, A. et al. From impulses to maladaptive actions: the insula is a neurobiological gate for the development of compulsive behavior. Mol. Psychiatry 21, 491–499 (2016).
207. Abela, A. R., Dougherty, S. D., Fagen, E. D., Hill, C. J. R. & Chudasama, Y. Inhibitory Control deficits in rats with ventral hippocampal lesions. Cereb. Cortex 23, 1396–1409 (2013).
208. Lerner, T. N. et al. Intact-brain analyses reveal distinct information carried by SNc dopamine subcircuits. Cell 162, 635–647 (2015).
209. Dalley, J. W., Everitt, B. J. & Robbins, T. W. Impulsivity, compulsivity, and top-down cognitive control. Neuron 69, 680–694 (2011).
210. Friedman, A. et al. A corticostriatal path targeting striosomes controls decision-making under conflict. Cell 161, 1320–1333 (2015).
211. Marquand, A. F., Haak, K. V. & Beckmann, C. F. Functional corticostriatal connection topographies predict goal-directed behaviour in humans. Nat. Hum. Behav. 1, 1–23 (2017).
212. Adnan Majid, D. S., Cai, W., Corey-Bloom, J. & Aron, A. R. Proactive selective response suppression is implemented via the basal ganglia. J. Neurosci. 33, 13259–13269 (2013).
213. Bissonette, G. B. & Roesch, M. R. Neural correlates of rules and conflict in medial prefrontal cortex during decision and feedback epochs. Front. Behav. Neurosci. 9, 1–14 (2015).
214. Bissonette, G. B. & Roesch, M. R. Neurophysiology of rule switching in the corticostriatal circuit. Neuroscience 345, 64–76 (2017).
215. Wei, W., Rubin, J. E. & Wang, X. J. Role of the indirect pathway of the basal ganglia in perceptual decision making. J. Neurosci. 35, 4052–4064 (2015).
216. Dunovan, K., Lynch, B., Molesworth, T. & Verstynen, T. Competing basal ganglia pathways determine the difference between stopping and deciding not to go. Elife 4, 1–24 (2015).
217. Bari, B. A. et al. Stable representations of decision variables for flexible behavior. Neuron 103, 922-933.e7 (2019).
218. Armbruster, B. N., Li, X., Pausch, M. H., Herlitze, S. & Roth, B. L. Evolving the lock to fit the key to create a family of G protein-coupled receptors potently activated by an inert ligand. Proc. Natl. Acad. Sci. U. S. A. 104, 5163–5168 (2007).
219. Gomez, J. L. et al. Chemogenetics revealed: DREADD occupancy and activation via converted clozapine. Science (80-.). 357, 503–507 (2017).
220. Kvitsiani, D. et al. Distinct behavioural and network correlates of two interneuron types in prefrontal cortex. Nature 498, 363–366 (2013).
221. Lima, S. Q., Hromádka, T., Znamenskiy, P. & Zador, A. M. PINP: a new method of tagging neuronal populations for identification during in vivo electrophysiological recording. PLoS One 4, e6099 (2009).
222. Barthó, P. et al. Characterization of neocortical principal cells and interneurons by network interactions and extracellular features. J. Neurophysiol. 92, 600–608 (2004).
223. de Haan, R. et al. Neural representation of motor output, context and behavioral adaptation in

rat medial prefrontal cortex during learned behavior. Front. Neural Circuits 12, 1–17 (2018).
224. Kamigaki and Dan. Delay activity of specific prefrontal interneuron subtypes modulates memory-guided behavior. Nat. Neurosci. 52, 566–584 (2017).
225. Pinto, L. & Dan, Y. Cell-type-specific activity in prefrontal cortex during goal-directed behavior. Neuron 87, 437–451 (2015).
226. Chikazoe, J. et al. Functional dissociation in right inferior frontal cortex during performance of go/no-go task. Cereb. Cortex 19, 146–152 (2009).
227. Mostofsky, S. H. & Simmonds, D. J. Response inhibition and response selection: two sides of the same coin. J. Cogn. Neurosci. 20, 751–761 (2008).
228. Jahfari, S., Stinear, C. M., Claffey, M., Verbruggen, F. & Aron, A. R. Responding with restraint: what are the neurocognitive mechanisms? J. Cogn. Neurosci. 22, 1479–1492 (2010).
229. Alexander, G. Parallel organization of functionally segregated circuits linking basal ganglia and cortex. Annu. Rev. Neurosci. 9, 357–381 (1986).
230. Allen, W. E. et al. Global representations of goal-directed behavior in distinct cell types of mouse neocortex. Neuron 94, 891-907.e6 (2017).
231. Tervo, D. G. R. et al. A designer AAV variant permits efficient retrograde access to projection neurons. Neuron 92, 372–382 (2016).
232. White, M. G. et al. Anterior cingulate cortex input to the claustrum is required for top-down action control. Cell Rep. 22, 84–95 (2018).
233. Lei, W., Jiao, Y., Del Mar, N. & Reiner, A. Evidence for differential cortical input to direct pathway versus indirect pathway striatal projection neurons in rats. J. Neurosci. 24, 8289–8299 (2004).
234. Reiner, A. et al. Corticostriatal projection neurons – dichotomous types and dichotomous functions. Front. Neuroanat. 4, 1–15 (2011).
235. Shepherd, G. M. G. Corticostriatal connectivity and its role in disease. Nat. Rev. Neurosci. 14, 278–291 (2013).
236. Narayanan, N. S. Ramping activity is a cortical mechanism of temporal control of action. Curr. Opin. Behav. Sci. 8, 226–230 (2016).
237. Paxinos, G and Watson, C. The rat brain in stereotaxis coordinates. (Elsevier Inc, 2007).
238. Hnasko, T. S. et al. Cre recombinase-mediated restoration of nigrostriatal dopamine in dopamine-deficient mice reverses hypophagia and bradykinesia. Proc. Natl. Acad. Sci. U. S. A. 103, 8858–8863 (2006).
239. Kremer, E. J., Boutin, S., Chillon, M. & Danos, O. Canine adenovirus vectors: an alternative for adenovirus-mediated gene transfer. J. Virol. 74, 505–512 (2000).
240. Lopes, G. et al. Bonsai: an event-based framework for processing and controlling data streams. Front. Neuroinform. 9, 1–14 (2015).
241. Panoz-Brown, D. et al. Replay of episodic memories in the rat. Curr. Biol. 28, 1628-1634.e7 (2018).
242. Rolston, J. D., Gross, R. E. & Potter, S. M. A low-cost multielectrode system for data acquisition enabling real-time closed-loop processing with rapid recovery from stimulation artifacts. Front. Neuroeng. 2, 1–17 (2009).
243. Newman, J. P. et al. Closed-loop, multichannel experimentation using the open-source NeuroRighter electrophysiology platform. Front. Neural Circuits 6, 1–35 (2012).
244. Rossant, C. et al. Spike sorting for large, dense electrode arrays. Nat. Neurosci. 19, 634–641 (2016).
245. Schneider, C. A., Rasband, W. S. & Eliceiri, K. W. NIH Image to ImageJ: 25 years of image analysis. Nat. Methods 9, 671–675 (2012).
246. Burgos-Robles, A. et al. Amygdala inputs to prefrontal cortex guide behavior amid conflicting cues of reward and punishment. Nat. Neurosci. 20, 824–835 (2017).
247. Benjamini, Y. & Hochberg, Y. Controlling the false discovery rate: a practical and powerful approach to multiple testing. J. R. Stat. Soc. B 57, 289–300 (1995).
248. Schmitzer-Torbert, N., Jackson, J., Henze, D., Harris, K. & Redish, a. D. Quantitative

measures of cluster quality for use in extracellular recordings. Neuroscience 131, 1–11 (2005).
249. Collins, D. P., Anastasiades, P. G., Marlin, J. J. & Carter, A. G. Reciprocal circuits linking the prefrontal cortex with dorsal and ventral thalamic nuclei. Neuron 98, 366-379.e4 (2018).
250. Klapoetke, N. C. et al. Independent optical excitation of distinct neural populations. Nat. Methods 11, 338–346 (2014).
251. Turrigiano, G. Homeostatic synaptic plasticity: local and global mechanisms for stabilizing neuronal function. Cold Spring Harb. Perspect. Biol. 4, 1–17 (2012).
252. Hutcheon, B. & Yarom, Y. Resonance, oscillation and the intrinsic frequency preferences of neurons. Trends Neurosci. 23, 216–222 (2000).
253. Daigle, T. L. et al. A suite of transgenic driver and reporter mouse lines with enhanced brain-cell-type targeting and functionality. Cell 174, 465-480.e22 (2018).
254. Donnelly, N. a. et al. Oscillatory activity in the medial prefrontal cortex and nucleus accumbens correlates with impulsivity and reward outcome. PLoS One 9, e111300 (2014).
255. Luchicchi, A., Bloem, B., Viaña, J. N. M., Mansvelder, H. D. & Role, L. W. Illuminating the role of cholinergic signaling in circuits of attention and emotionally salient behaviors. Front. Synaptic Neurosci. 6, 1–10 (2014).
256. Yin, F. et al. The basolateral amygdala regulation of complex cognitive behaviours in the five-choice serial reaction time task. Psychopharmacology (Berl). 236, 3135–3146 (2019).
257. Ott, T. & Nieder, A. Dopamine and cognitive control in prefrontal cortex. Trends Cogn. Sci. 23, 213–234 (2019).
258. Green, S. M., Nathani, S., Zimmerman, J., Fireman, D. & Urs, N. M. Retrograde labeling illuminates distinct topographical organization of D1 and D2 receptor-positive neurons in the prefrontal cortex of mice. (2020).
259. Kim, Y. C. & Narayanan, N. S. Prefrontal D1 dopamine-receptor neurons and delta resonance in interval timing. Cereb. Cortex 29, 2051–2060 (2019).
260. Chuong, A. S. et al. Noninvasive optical inhibition with a red-shifted microbial rhodopsin. Nat. Neurosci. 17, 1123–1129 (2014).
261. Sotelo, C. Viewing the brain through the master hand of Ramon y Cajal. Nat. Rev. Neurosci. 4, 71–77 (2003).
262. Gouwens, N. W. et al. Classification of electrophysiological and morphological neuron types in the mouse visual cortex. Nat. Neurosci. 22, 1182–1195 (2019).
263. Gouwens, N. W. et al. Toward an integrated classification of cell types: morphoelectric and transcriptomic characterization of individual gabaergic cortical neurons. SSRN Electron. J. (2020). doi:10.2139/ssrn.3544405
264. Nagy, C. et al. Single-nucleus transcriptomics of the prefrontal cortex in major depressive disorder implicates oligodendrocyte precursor cells and excitatory neurons. Nat. Neurosci. 1–11 (2020). doi:10.1038/s41593-020-0621-y
265. Mansvelder, H. D., Verhoog, M. B. & Goriounova, N. A. Synaptic plasticity in human cortical circuits: cellular mechanisms of learning and memory in the human brain? Curr. Opin. Neurobiol. 54, 186–193 (2019).
266. Jun, J. J. et al. Fully integrated silicon probes for high-density recording of neural activity. Nature 551, 232–236 (2017).
267. Jia, X. et al. High-density extracellular probes reveal dendritic backpropagation and facilitate neuron classification. J. Neurophysiol. 121, 1831–1847 (2019).
268. Trainito, C., von Nicolai, C., Miller, E. K. & Siegel, M. Extracellular spike waveform dissociates four functionally distinct cell classes in primate cortex. Curr. Biol. 29, 2973-2982.e5 (2019).
269. Mosher, C. P. et al. Cellular classes in the human brain revealed in vivo by heartbeat-related modulation of the extracellular action potential waveform. Cell Rep. 30, 3536-3551.e6 (2020).
270. Petersen, P. CellExplorer: a graphical user interface and standardized pipeline for visualizing and characterizing single neuron features. (2020).

ENGLISH SUMMARY

Cognitive control allows us to direct our behavior in line with our internal goals. This is a crucial ability to be successful in society. Two forms of cognitive control are proactive inhibitory control (i.e. the ability to suppress behavior until appropriate to execute) and attention (i.e. de ability to be alert and filter out important environmental sensory information). Inhibitory control and attention are both dependent on the prefrontal cortex (PFC). It is thought that the PFC learns to represent the 'rules' of the environment (e.g. action-outcome associations) and provide an instructive signal to downstream brain areas how to act in line with your current goal. This instructive signal is primarily provided by so called pyramidal shaped neurons, called pyramidal neurons, which extend far in to the brain. These pyramidal neurons communicate with other brain areas using short electrical signals, called action potentials. De PFC contains a range of different pyramidal neuron types, with extensions (called axons) to all different kinds of brain areas. The PFC can also be functionally and anatomically divided along a vertical axis (or dorsoventral axis), where the dorsal and ventral part contribute differentially to cognitive control. How the different pyramidal projections neurons across the dorsoventral axis of the PFC are involved in inhibitory control and attention is poorly understood. In my thesis we use very precise, projection-neuron specific, techniques to investigate the role of projection neurons in the medial region of the PFC (mPFC) in inhibitory control and attention using rats. In chapter 1 I introduce all scientific concepts that are used within this thesis.

We start by investigating the role of the entire pyramidal neuron population across the dorsoventral axis of the mPFC in inhibitory control and attention (chapter 2). We do this using rats that are performing in a behavioral task that measures inhibitory control and attention, called the 5-choice serial reaction time task (5-CSRTT). In this behavioral task rats have to wait until one of five stimulus lights in a random position in a curved wall is presented. Then they have to respond to the lit stimulus hole in order to earn a food reward. Sometimes the rat fails to wait and responds prematurely. This is seen as a failure of inhibitory control. Sometimes the rat fails to respond in to correct hole and respond to the incorrect hole or omits a response at all. This is seen as a failure in attention. The

cycle of waiting and responding can be repeated up to hundreds of times per day and when average over the day provides an indication of how well the rat can exert inhibitory control and attention. We show that along the dorsoventral axis pyramidal neurons contribute differentially to inhibitory control and attention on different times during the task. Using light-sensitive proteins (optogenetics) we impaired the activity of pyramidal neurons temporarily during execution of the 5-CSRTT. We show that dorsal mPFC pyramidal neurons are involved in attention on a long timescale, seconds before the stimulus light is presented until a response is made. De ventral mPFC pyramidal neurons are involved in both inhibitory control and attention, but on a shorter timescale just before the presentation of the stimulus light. Because we used a fixed delay time between the start of the trial and presentation of the stimulus and a relatively long time of stimulus presentation, it remains possible that the rat knows exactly when he has to respond and how much attention is required. Thereby, the rats likely only needed a low level of inhibitory control and attention, resulting in an impaired ability to detect behavioral impairments.

Therefore, in chapter 3, we introduced a homecage-based version (CombiCage) of the 5-CSRTT where we had sessions with variable longer delay to stimulus times and variable shorter stimulus presentation times. Making the delay period variably longer resulted in increased premature responses and making the stimulus presentation period variably shorter resulted in more errors in detecting the stimulus light. Because we made the 5-CSRTT homecage-based, we could also make the training semi-automatic and self-paced, resulting in minimal intervention from the experimenter. This lead to a big improvement in training times in comparison to the conventional way of training, as used in chapter 2. Moreover, the rats could do many more repetitions of the task, resulting in larger statistical power.

In chapter 4 we used the improved CombiCage 5-CSRTT to investigate the role of different projection neurons across the dorsoventral axis of the mPFC in inhibitory control and attention. We looked at a two relatively large groups of projection neurons to different brain regions that are involved in inhibitory control and attention, the striatum and mediodorsal thalamus (MD). It remains unknown how

these topographically projection neurons across the dorsoventral axis to subregions of the striatum and MD are involved in inhibitory control and attention. Possibly, the role of the mPFC in inhibitory control and attention can be attributed to projection neurons to other brain regions than the striatum and MD. Using projection-specific impairment of neuronal activity in the 5-CSRTT with chemogenetics, we investigated their contribution to inhibitory control and attention. When and how these projection neurons were active, we measured using fiber photometry. To investigate what type of neurons within the subregions of the striatum and MD, that receive topographical input from the dorsal or ventral mPFC, and what type of synaptic input they receive, we used patch-clamp electrophysiology in brain slices. We found that disturbing the activity of projection neurons from the dorsal mPFC to the lateral MD, lead to fewer premature responses and more omission of responses. This indicates that this pathway is involved in keeping a working memory trace about the general task-rules active within the mPFC, and not so much inhibitory control or attention. Otherwise, disturbing the activity of ventral mPFC to medial MD projection neurons resulted in an increase in premature responses. This indicates that this pathway is involved in inhibitory control and functions as a break on behavior. Disturbing the activity of dorsal mPFC projection neurons to the dorsomedial striatum resulted in more premature responses. This indicates that this pathways is also involved in inhibitory control and acts as a brake on behavior. Only projections from the ventral mPFC to the ventromedial striatum had a role in behavior. Recordings of the activity of these four projection populations during the 5-CSRTT showed that both dorsal mPFC projection neuron groups were longer engaged during the delay period, before the presentation of the stimulus light, than both ventral mPFC projection neuron groups. Moreover, the activity was also linked to the behavioral performance. Neurons within the striatal and MD subregions, that received input from the respective dorsal or ventral mPFC projection neurons, also showed differential electrophysiological properties. Together, this indicates that cognitive control, and specifically inhibitory control and attention, are differentially regulated by specific dorsoventrally organized mPFC pathways.

In chapter 5 we look with even greater detail how dorsal mPFC projection neurons to the dorsomedial striatum are involved in inhibitory control. Measurements of the activity of single neurons, using *in-vivo* electrophysiology in combination with optogenetic identification, showed how activity of these projection neurons is linked to inhibitory control in the CombiCage 5-CSRTT. During the delay period, while waiting for the presentation of a stimulus light, about half of these frontostriatal projection neurons is persistently activated, while about the other half is persistently silenced, and a small fraction is non-responding. Compared to neighboring non-optogenetically identified neurons, this activity pattern was unique, indicating that this group was specifically involved in inhibitory control using persistent changes in firing rate. When the activity of these frontostriatal projection neurons during the delay period was compared between correct and premature trials, we observed that during premature trials the change in activity was lower for both persistently activated and silenced neurons. This indicates that dorsomedial striatum projection neurons from the dorsal mPFC are specifically involved in inhibitory control by means of persistent changes in activity.

In conclusion, we show that cognitive control, and specifically inhibitory control and attention, are regulated by different types of projection neurons across the dorsoventral axis of the rat mPFC, that topographically project to the striatum or MD. In chapter 6 I discuss how this fits in the literature.

NEDERLANDSE SAMENVATTING

Met cognitieve controle kunnen we ons gedrag sturen zodat dit overeenkomt met ons interne doel of drijfveer. Dit is een cruciale vaardigheid in het dagelijks leven. Twee vormen van cognitieve controle zijn proactieve motor impuls controle (i.e. de mogelijkheid om impulsieve acties te onderdrukken) en aandacht (i.e. de mogelijkheid om alert te zijn en belangrijke relevante sensorische informatie uit de omgeving te filteren). Impuls controle en aandacht zijn beide afhankelijk van de prefrontale cortex (PFC). Het wordt gedacht dat de PFC de regels van de omgeving leert (bijvoorbeeld actie-uitkomst associaties) en andere lager liggende hersengebieden instrueert hoe het best gehandeld moet worden gebaseerd op je huidige doel. Dit instructieve signaal van de PFC wordt voornamelijk gegeven door zogenoemde piramidaal vormige cellen genaamd piramidaalneuronen die lange uitlopers (axonen) hebben door de hersenen. Deze piramidaalneuronen communiceren met andere hersengebieden met behulp van zeer korte elektrische stroompjes, de zogenaamde actiepotentialen. De PFC bevat een groot scala aan verschillende type projectieneuronen, welke axonen hebben naar verschillende doelgebieden in de hersenen die ieder hun eigen functie hebben in cognitieve controle. De PFC kan functioneel en anatomische verdeeld worden over een verticale as, waarbij de bovenste en onderste gedeeltes een andere bijdrage aan cognitieve controle leveren. Hoe verschillende projectieneuronen over deze verticale as van de PFC betrokken zijn bij impuls controle en attentie is nog onbekend. In mijn proefschrift gebruiken we zeer precieze projectieneuron-specifieke technieken om, met behulp van ratten, de bijdrage van projectieneuronen in het mediale deel van de PFC (mPFC) in impuls controle en aandacht te onderzoeken. De wetenschappelijke concepten en technieken die worden gebruikt binnen dit proefschrift worden geïntroduceerd in hoofdstuk 1.

We beginnen met het onderzoeken wat de rol is van de algehele populatie pyramidaalneuronen (waar alle subtypes van projectieneuronen onder vallen) over de verticale as van de mPFC, in impuls controle en aandacht (hoofdstuk 2). Dit doen we met behulp van ratten in een gedragstaak die zowel impuls controle als aandacht meet. Deze taak heet de 5-choice serial reaction time task (5-CSRTT). Bij het starten van deze taak moeten ratten wachten tot een van vijf lampjes in een willekeurig gat in de muur aan gaat. De rat moet daar op reageren door met zijn

snuit in het gat te gaan. Een correcte reactie op het lampje dat aan is gegaan wordt beloond met voedsel. Soms kan de rat niet wachten en reageert hij al voordat een lampje is aangegaan, dit is een premature response, en wordt gezien als impulsief gedrag. Soms reageert de rat door met zijn neus in het foute gat te gaan of reageert hij helemaal niet. Dit wordt gezien als een gevolg van verminderde aandacht. Deze gedragscyclus van wachten en reageren op een lampje kunnen ze wel honderden keren per dag herhalen waardoor je gemiddeld genomen over al deze herhalingen een goed idee krijgt van de mate van impuls controle en aandacht van de rat. We laten zien dat over de verticale as van de mPFC piramidaalneuronen op verschillende momenten in gedrag en bij ander soort gedrag betrokken zijn. Met behulp van lichtgevoelige eiwitten (optogenetica) kunnen we heel precies de elektrische activiteit van de pyramidaalneuronen tijdelijk verstoren tijdens de 5-CSRTT. Hiermee laten we zien dat het bovenste deel van de pyramidaalneuronen in de mPFC betrokken zijn bij aandacht op een langdurig tijdsschaal, namelijk vanaf enkele seconden voordat het lampje aan gaat tot de reactie. Het onderste deel van de pyramidaalneuronen binnen de mPFC zijn meer betrokken rond de reactie op het lampje, en beïnvloeden zowel impuls controle en aandacht, en zijn meer betrokken rond de reactie op het lampje. Omdat we een vaste wachttijd tot het lampje aan gaat en relatief lange duur dat het lampje aan is gebruiken, is het mogelijk dat de rat precies weet wanneer hij moet reageren en hoeveel aandacht hij nodig heeft. Hierdoor heeft de rat mogelijk weinig impuls controle en aandacht nodig en meet de taak mogelijk niet precies genoeg het gedrag van interesse.

Daarom hebben we in hoofdstuk 3 een thuiskooi (of CombiCage) versie van de 5-CSRTT geïntroduceerd met gedragssessies met een variabele wachttijd of een variabele tijd dat het lampje aan is. Het variabel verlengen van de wachttijd tot presentatie van het lampje leidde tot meer premature reacties en het variabel korter schijnen van het lampje leidde tot meer fouten in detecteren van het lampje. Omdat we een thuiskooi versie van de 5-CSRTT hebben gemaakt, kunnen we de rat halfautomatisch trainen, op hun eigen tempo, met minimale interventie van de onderzoekers. Dit leidde tot een grote winst in trainingstijd ten opzichte van de conventionele manier van trainen en bovendien deed de rat veel meer herhalingen van de taak zodat de statistische kracht van de taak sterk toenam.

In hoofdstuk 4 gebruiken we de verbeterde CombiCage versie van 5-CSRTT om de rol van verschillende projectieneuronen over de verticale as van de mPFC in impuls controle en aandacht te onderzoeken. Hierbij kijken we naar twee relatief grote groepen pyramidaalneuronen binnen de mPFC die, georganiseerd over een as, naar specifieke gebieden in de hersenen projecteren die beiden betrokken zijn bij impuls controle en aandacht. Namelijk, het striatum en de mediaal dorsale thalamus (MD). Echter, is het is nog onbekend of en hoe deze projectieneuronen over de verticale as van de mPFC naar sub gebieden binnen het striatum en de MD betrokken zijn bij impuls controle en aandacht. Mogelijk is de rol van de mPFC bij impuls controle en aandacht niet toe te schijrven aan deze striatum en MD projectieneuronen, maar aan neuronen die naar andere gebieden projecteren. Met projectieneuron-specifieke verstoring van de activiteit tijdens de taak, door de techniek chemogenetica toe te passen, kunnen we de betrokkenheid van de projecties aantonen in impuls controle en aandacht. Wanneer en hoe deze projectieneuronen elektrisch actief zijn, en dus een signaal versturen naar het striatum of MD, meten we met behulp van fiber photometry. Om te achterhalen wat voor type neuronen binnen de sub gebieden in het striatum of MD, die input krijgen van het bovenste of onderste deel van de mPFC, en wat voor informatie ze krijgen van de mPFC, gebruiken we patch-clamp elektrofysiologie in hersenplakjes. We vinden dat het verstoren van de activiteit van de projectieneuronen uit de bovenste deel van de mPFC naar het laterale deel van de MD leidt tot minder premature reacties en meer gebrek aan reacties. Dit duidt er op dat deze verbinding mogelijk betrokken is bij een algemene functie van het in werkgeheugen houden van de regels in de taak, en niet specifiek impuls controle of aandacht. Anderzijds, het verstoren van de activiteit van de neuronen uit het onderste deel van de mPFC, die projecteren naar het mediale deel van de MD, resulteert in meer premature reacties. Dit duidt er op dat deze verbinding betrokken is bij impuls controle en functioneert als rem op gedrag. Verstoring van de activiteit van de verbindingen tussen het bovenste deel van de mPFC naar het mediale deel van het dorsale striatum leidt tot meer premature responses. Dit duidt er op dat ook deze verbindingen betrokken zijn bij impuls controle en functioneren als rem op gedrag. Alleen de verbindingen tussen onderste deel van de mPFC naar de onderste deel van het mediale striatum leken geen bijdrage aan gedrag te leveren. Metingen van de activiteit van deze vier

subtypes projectieneuronen tijdens de 5-CSRTT lieten zien dat beide subtypes projectieneuronen in het bovenste deel van de mPFC langer actief waren tijdens de wachttijd voor dat een lampje aan ging, dan de subtypes projectieneuronen in het onderste deel van de mPFC. Bovendien was de mate van activiteit gekoppeld aan de uitvoering van gedrag. Neuronen binnen sub gebieden van het striatum en MD, die input krijgen van het bovenste of onderste deel van de mPFC, hadden ook andere elektrische eigenschappen. Samen duidt dit er op dat cognitieve controle, en specifiek impuls controle en aandacht, gereguleerd wordt door verschillende types neuronale banen die georganiseerd zijn over de verticale as van de mPFC.

In hoofdstuk 5 kijken we met nog meer detail naar hoe projectieneuronen van het bovenste deel van de mPFC naar het mediaal dorsale striatum betrokken zijn bij impuls controle. Met metingen van de activiteit op het niveau van individuele neuronen, met behulp van in-vivo elektrofysiologie en optogenetische identificatie, laten we zien hoe activiteit van deze neuronen gekoppeld is aan impuls controle in de CombiCage 5-CSRTT. Tijdens de wachttijd, voordat een lampje aan gaat, wordt ongeveer de helft van de projectieneuronen actief en ongeveer de andere helft juist minder actief. Ten opzichte van de in de buurt liggende niet-dorsaal striatum-projecterende projectieneuronen is deze activiteit uniek, wat er op duidt dat deze projectieneuron groep uniek betrokken is bij impuls controle. Wanneer de activiteit van deze neuronen tijdens de wachttijd tussen correcte reacties en premature reacties vergeleken werd zagen we dat de verandering in activiteit minder was voor zowel geactiveerde als minder geactiveerde neuronen. Dit duidt er op dat pyramidaalneuronen uit het bovenste deel van de mPFC naar de mediale deel van de dorsale striatum, uniek betrokken zijn bij impuls controle door middel van een balans in langdurige activatie en inactivatie.

Samenvattend laten we zien dat cognitieve controle, en in specifiek impuls controle en aandacht, gereguleerd wordt door verschillende subtypes pyramidaal-neuronen over de verticale as van de rat mPFC, die projecteren subgebieden van striatum en MD. In hoofdstuk 6 bespreek ik hoe dit past in de huidige literatuur.

DANKWOORD/ACKNOWLEDGEMENTS

Dit proefschrift voelt als een resultaat van een leerzaam en leuk proces van vallen, opstaan, er lering uit trekken en weer door gaan. De goede afloop is grotendeels te danken aan de steun en het vertrouwen van vrienden en collega's in mijn omgeving die ik graag wil bedanken.

Natuurlijk moet ik beginnen met de mede **Optoboys, Bastiaan en Sybren**. We begonnen alle drie bijna gelijk - nog nat achter de wetenschappelijke oren - aan dit avontuur. We hadden de mazzel dat we op hetzelfde project zaten: uitvogelen hoe de mPFC projectieneuronen bij gedrag betrokken waren. De vele buurman en buurman achtige situaties in de bouwmarkt of timmerend aan de CombiCages zal ik altijd blijven koesteren. Bovendien hebben we samen nog prachtige papers kunnen publiceren, hadden we een drukbezochte poster op de FENS in Berlijn en hebben we een dijk van een gedragstaak afgeleverd. **Bastiaan**, van jouw humor, kijk op het leven, conceptuele inzicht, kennis van de literatuur en experimentele vaardigheden kan ik nog veel leren en waren een zeer waardevolle toevoeging aan het team. Samen hebben we veel tijd doorgebracht en van alles meegemaakt. Zo hebben we uren zitten zwoegen op het fabriceren van kleine onderdeeltjes die direct door de ratten weer kapot werden gemaakt en hebben we tijdens een lunch-pauze gesprint over de campus voor een paar agenten uit om een crimineel staande te houden. **Sybren**, onze social butterfly, gecombineerd met technisch inzicht en schijnbaar onuitputtelijke energie en veerkracht. Je hebt de unieke gave om elk moment op te leuken door over een random tv programma, je nieuwe kikkervisjes of natuurlijk sporten te beginnen. Blijf dit vooral doen! Ik hoop dat we in de toekomst nog vele kilometers kunnen fietsen. Heren, heel veel dank voor de afgelopen jaren!

De samenstelling van dit team is te danken aan jou, **Huib**. Gedurende al die jaren heb je mij altijd veel vrijheid en vertrouwen gegeven om uitdagende experimenten te doen, ook al was deze vrijheid naar mijn idee niet altijd vanzelfsprekend. Je gaf me bijvoorbeeld de mogelijkheid om zelf een draadloze in-vivo elektrofysiologie en opgenetische identificatie opstelling op te bouwen voor niet vergevingsgezinde ratten en vele probes te implanteren, voordat er überhaupt een zinnig resultaat uit kwam. Maar, deze vrijheid wist je altijd perfect af te wisselen door de nodige

sturing op de juiste momenten, zoals een draadloze opstelling aanschaffen en nog net op tijd een patch project starten voordat het te laat was. Hierdoor heb ik uiteindelijk meerdere projecten succesvol kunnen afronden. Hiernaast houd je altijd een heerlijk ongedwongen en open sfeer in het lab. Kortom, je hebt voor mij de ideale wetenschappelijke speeltuin gecreëerd en daarvoor ben ik je heel dankbaar.

Tommy, je opgewekte, warme persoonlijkheid en enthousiasme maakte het altijd erg leuk om bij je langs te komen. We konden zowel goed over wetenschap, en vooral gedragswerk, alsook het leven daar buiten praten. Zo zijn we zelfs een keer naar de bios geweest! Ondanks dat mijn werk vaak niet jou gebied van expertise was heb ik toch veel aan je scherpe input gehad. Dank voor alles!

Antonio, aan de grondslag van mijn proefschrift ligt jouw solide basis. Je hebt mij de fijne kneepjes van het vak geleerd, waaronder hoe je moet handelen in noodsituaties na gebeten te worden door een rat. Bovendien ben je een erg fijn persoon om mee te werken en te BBQen. Dank daar voor! In deze lijn moet ik ook **Ouissame** bedanken die veel belangrijk werk vroeg in het project heeft gedaan. Samen met **Chris Kortleven** maakten jullie de overstap naar het verre Amersfoort een stuk aangenamer.

Roel, als wetenschappelijke grote broer was je vaak een stapje voor op mij. Hierdoor heb ik erg veel van je kunnen leren. Ook was je een goede vriend om de tegenslagen mee weg te drinken, maar vooral ook om de mooie dingen te vieren zoals werk retreats in Frankrijk, boottochtjes, fietsen, borrels, papers, ONWARs en nieuw nageslacht. Veel dank en laten we dit vooral blijven doen!

Een aantal zeer belangrijke pijlers van het lab hebben de nodige kennis en enthousiasme op mij kunnen overdragen. **Marcel**, zonder jouw ervaring in de in-vivo elektrofysiologie had dit project waarschijnlijk nooit van de grond gekomen, dank voor je steun en enthousiasme! **Tim H.**, zonder jouw hulp was het patch gedeelte van mijn project ook nooit gelukt. Bovendien was je een vaste deelnemer aan alle leuke activiteiten die we met het lab deden. Veel dank! **Hans**, ik heb dankbaar gebruik kunnen maken van jou eindeloze kennis en liefde voor het vak. Na elk gesprek liep ik weer wijzer weg. Veel dank! **Jaap**, naast je uitstekende volleybal en

borrel skills heb je vooral op het einde voor mij veel druk kunnen wegnemen door te helpen met experimenten, dank! **Anton**, dank voor je kennis van operaties en in-vivo elektrofysiologie. **Anna**, dank voor het samen organiseren van de beste lab uitjes, organisatorische kwaliteiten en je altijd fijne aanwezigheid! Daarnaast heb ik uitgebreid gebruik kunnen maken van (bijna) de leukste plek van de VU, de werkplaats. **Tinco, Rogier, Rob van de G., Dick, Peter, Lex, Rob, Niek, Jurriaan en andere werkplaatsers**, enorm bedankt! **Yvar** en **Dustin**, jullie hebben vanaf het begin mij veel bij kunnen brengen over het doen van experimenten met proefdieren. Dank voor het leuke samenwerken!

Aan dit proefschrift gaan meerdere studentprojecten vooraf, **Saartje, Antonieta, Judith, Sanne, Emma, Rachel, Soraya, Jeroen** en **Lotte**, dank voor jullie harde en enthausiaste werk met Bastiaan, Sybren of mij.

Rogier Min, je bent een rode draad in mijn wetenschappelijke carrière. Zonder jou had ik deze PhD ook niet gehad. Veel dank voor je steun en vertrouwen!

De VU en het VUmc zijn een mengelmoes van erg leuke mensen die het dagelijks werk zo veel leuker maken. **Joshua en Amber**, dank voor jullie vriendschap, fietstripjes, vakanties en nog veel te veel om op de noemen. **Madi**, dank voor je vriendschap, altijd positieve aanwezigheid en het delen van lief en leed sinds het prille begin van mijn project. **Tim K.** dank voor je humor, soms norsigheid, muzikaliteit, creativiteit en vriendschap! **INF band, Tim, Amber en Joshua**, ik heb altijd erg genoten van onze studio sessies, dank voor de vrolijke noot! **Alle sportieve mensen**, dank voor het fietsen, volleyballen, hardlopen etc.! **Laurens**, dank voor je koffies en zeer gewaardeerde steun in de wetenschap en daar buiten. **Nathan**, I very much appreciate our mountainbike trips and your insights as senior scientist, let's keep that going! **Chris de Kock**, dank voor je positiviteit en het uitlenen van Roel! **Mohit**, thanks for the bike adventures and keeping the science real! **Thijs, Ioannis, Adrian, Djai, René, Ayoub, Jean, Sarah, Eelke, Arthur, Rhiannon, Klaus, Suman, Simon, Johnny, Sonja, Natalia, Hemanth, Romy** and all other CNCR members, thanks!

Dank **Lianne** voor onze vriendschap. Het is altijd fijn om even met jou bij te babbelen over wetenschap en van alles en nog wat. **Ellen, Koen, Stephen, Scott, Minha, Dylan, Romy, Laurens, Marta, Tim, Serena and Tessa**, thanks for accepting me as one of you and all the fun times after study hours! Dan mijn Amsterdamse generatiegenoten van system neuroscientists, **Koen, Bastijn, Julien, Matthijs, Esther en Fran**. Erg leuk om te zien hoe iedereen ontwikkeld. Dank voor de gezelligheid en de troubleshoot sessies!

Before my PhD, I had the pleasure to work and grow under the supervision of excellent scientists who each taught me valuable (scientific) lessons, **Harm Krugers, Stephan Michel, Wilbert Zwart, Sanne Schagen** and **Hadi Saiepour,** thank you!

Many thanks to the reading committee, **Judith Homberg, Fransesco Battaglia, Cyriel Pennartz, Christiaan Levelt, Frank Meye** and **Pieter Roelfsema**, for your time and scientific insights.

Voor al mijn vrienden buiten de wetenschap en familie, dank voor de vriendschap, feesten, borrels, spelletjes spelen, city trips en steun, ook al ben ik veel te vaak aan het werk!

Atie, Jan, Floor, Emma, **opa en oma**, dank voor de fijne opvoeding waarbij creativiteit en nieuwsgierigheid centraal stonden. Extra dank aan Emma voor het maken van de cover design en de opmaak van dit proefschrift! **Neeltje**, dank voor je eeuwige steun, liefde en begrip. Al vanaf de eerste dag van psychobiologie zijn we samen dit wetenschappelijke avontuur samen aan gegaan en zo zullen we de toekomstige avonturen ook samen aan gaan. **Jippe**, jouw komst heeft de laatste periode van mijn PhD ongvergetelijk gemaakt. Ik kijk er naar uit om je later de schoonheid van de wetenschap, natuur en het leven te laten zien.

LIST OF PUBLICATIONS

Terra, H.*, Bruinsma, B.*, de Kloet, S.F., van der Roest, M., Pattij, T., and Mansvelder, H.D. (2020). Prefrontal cortical projection neurons targeting dorsomedial striatum control behavioral inhibition. Current Biology.

de Kloet, S.F.*, Bruinsma, B.*, **Terra, H.***, Heistek, T.S., Passchier, E.M.J., van den Berg, A.S., Luchicchi, A., Min, R., Pattij, T., Mansvelder, H.D. Bi-directional command of cognitive control by distinct prefrontal cortical output neurons to thalamus and striatum. In preparation.

Bruinsma, B.*, **Terra, H.***, de Kloet, S.F.*, Luchicchi, A., Timmerman, A.J., Remmelink, E., Loos, M., Pattij, T., and Mansvelder, H.D. (2019). An automated home-cage-based 5-choice serial reaction time task for rapid assessment of attention and impulsivity in rats. Psychopharmacology (Berl). 236, 2015-2026.

Luchicchi, A., Mnie-Filali, O.*, **Terra, H.***, Bruinsma, B.*, de Kloet, S.F.*, Obermayer, J., Heistek, T.S., de Haan, R., de Kock, C.P.J., Deisseroth, K., et al. (2016). Sustained attentional states require distinct temporal involvement of the dorsal and ventral medial prefrontal cortex. Front. Neural Circuits 10, 70.

Vosko, A., van Diepen, H., Kuljis, D., Chiu, A.M., Heyer, D., **Terra, H.**, Carpenter, E., Michel, S., Meijer, J.H., and Colwell, C.S. (2015). Role of vasoactive intestinal peptide in the light input to the circadian system. Eur. J. Neurosci. 42(2): 1839–1848.

Struik, R.F., Marchant, N.J., de Haan, R., **Terra, H.**, van Mourik, Y., Schetters, D., Carr, M.R., van der Roest, M., Heistek, T.S., and De Vries, T.J. (2019). Dorsomedial prefrontal cortex neurons encode nicotine-cue associations. Neuropsychopharmacology 44, 2011–2021.

Zwart, W., **Terra, H.**, Linn, S.C., and Schagen, S.B. (2015). Cognitive effects of endocrine therapy for breast cancer: keep calm and carry on? Nat. Rev. Clin. Oncol. 12, 597–606.

* Equal contribution

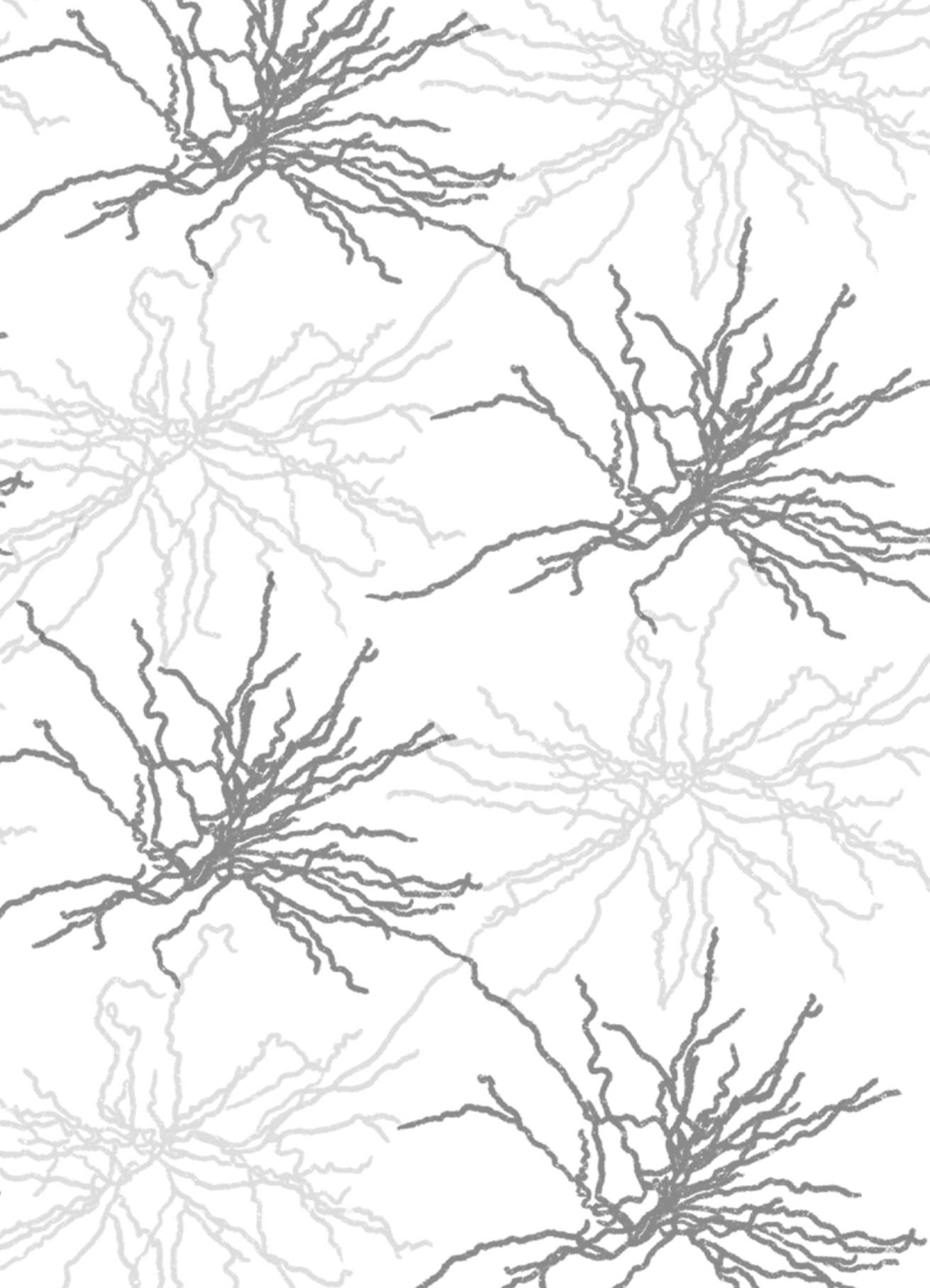

Huub (1989) was born and raised just above Amsterdam, in a little town called Krommenie. A book about how a man mistook his wife for a hat sparked his fascination for the brain. In 2007 he moved to the city to study the brain at the University of Amsterdam. In 2014 he moved across the city to pursue a PhD at the Vrije Universiteit. Here he studied how the brain controls behavior.

> *very impressive piece of work...*
> **Reviewer 1**

> *WEHHH EH-eh-ehh!*
> **Jippe**

> *Stop spike sorting and clean the kitchen.*
> **Neeltje**

> *This is so disappointing...*
> **Reviewer 2**

> *Worthy of a Nobel Prize.*
> **Reviewer 3**